CARTILAGE AND LABRUM MECHANICS IN THE NORMAL AND PATHOMORPHOLOGIC HUMAN HIP

by

Corinne Reid Henak

A dissertation submitted to the faculty of
The University of Utah
in partial fulfillment of the requirements for the degree of

Doctor of Philosophy

Department of Bioengineering

The University of Utah

August 2013

The University of Utah Graduate School

STATEMENT OF DISSERTATION APPROVAL

The dissertation of **Corinne Reid Henak**

has been approved by the following supervisory committee members:

Jeffrey A. Weiss	, Chair	**5-28-2013** Date Approved
Andrew E. Anderson	, Member	**5-28-2013** Date Approved
Kent N. Bachus	, Member	**5-28-2013** Date Approved
Richard D. Rabbitt	, Member	**5-28-2013** Date Approved
Christopher L. Peters	, Member	**6-3-2013** Date Approved

and by **Patrick A. Tresco**, Chair of the Department of **Bioengineering**

and by Donna M. White, Interim Dean of The Graduate School.

ABSTRACT

While the healthy hip provides decades of pain free articulation, the cartilage and labrum may degenerate during the process of osteoarthritis (OA). Most hip OA is caused by subtle pathomorphologies, including acetabular dysplasia and acetabular retroversion. The link between pathomorphology and OA is thought to be mechanical, but the mechanics have not been quantified. The aim of this dissertation was to provide insight into the pathogenesis of hip OA via finite element (FE) modeling. The objectives were two-fold: to validate a subject-specific modeling protocol for a series of specimens and assess the effects of assumptions on model predictions, and to use the modeling protocol to evaluate soft tissue mechanics in pathomorphologic hips in comparison to normal hips. For the first objective, FE predictions of contact stress and contact area were directly validated for five cadaveric specimens, and the specimen- and region-specific hyperelastic material behavior of cartilage was determined. FE predictions of contact stress and contact area were in good agreement with experimental results, and were relatively insensitive to the assumed cartilage constitutive model. There were distinct regional differences in the hyperelastic material behavior of human hip cartilage, with stiffer lateral than medial cartilage and stiffer acetabular than femoral cartilage. In order to investigate the mechanical link between pathomorphology and hip OA, FE models of ten hips with normal morphology, ten hips with acetabular dysplasia and ten hips with acetabular retroversion were generated. FE models of dysplastic acetabula demonstrated

the importance of the acetabular labrum in load support in the dysplastic hip. FE models of retroverted acetabula demonstrated distinct superomedial contact patterns in comparison to distributed contact patterns in the normal hip. Finally, the effects of cartilage constitutive model on predictions of transchondral maximum shear stress and first principal strain were evaluated. In contrast to contact stress and contact area, maximum shear stress and first principal strain were sensitive to the cartilage constitutive model. Overall, this dissertation provides novel insights into the contact mechanics of pathomorphologic hips that may be important in the pathogenesis of OA, as well as the technical foundation for studies evaluating additional mechanical variables in the human hip.

To my husband, family and friends: thank you for your encouragement and support.

TABLE OF CONTENTS

LIST OF FIGURES

LIST OF SYMBOLS

Symbol	
E	Young's modulus
G	Shear modulus
K	Bulk modulus
ν	Poisson's ratio
C_1, C_3,C_4,C_5,λ^*	Coefficients in the transversely isotropic constitutive model
W	Strain energy
μ	Coefficient in the neo-Hookean constitutive model
C_1, C_2, E_0	Coefficients in the Veronda Westmann constitutive model
ξ, β	Coefficients in the ellipsoidal fiber distribution constitutive model
J	Jacobian
λ	Stretch
σ	Uniaxial Cauchy stress
,	First and second deviatoric invariants
τ_{max}	Cauchy maximum shear stress
E_1	Green-Lagrange first principal strain

LIST OF ABBREVIATIONS

Abbreviation	
FE	Finite element
FEA	Finite element analysis
OA	Osteoarthritis
GAG	Glycosaminoglycan
PG	Proteoglycan
ECM	Extracellular matrix
CT	Computed tomography
MRI	Magnetic resonance imaging
LCEA, CEA	Lateral center edge angle
ACEA	Anterior centere edge angle
PAO	Periacetabular osteotomy
IRB	Institutional Review Board
EFD	Ellipsoidal fiber distribution
VW	Veronda Westmann
nH	neo-Hookean
DEA	Discrete element analysis
BW	Body weight
A-P	Anteroposterior
BMI	Body mass index
WH, WHS	Heel strike during walking
WM, WMS	Midstance during walking
DH, DHS	Heel strike during stair descent
AH, AHS	Heel strike during stair ascent

ACKNOWLEDGEMENTS

I am indebted to many people for their participation in my education and their involvement in my dissertation research. My undergraduate advisors, Drs. Peter Laz, Paul Rullkoetter and Joseph Langenderfer, provided the opportunity for me to discover the joy of research and to develop skills that provided a solid foundation for my graduate studies.

I am indebted to my PhD advisor, Dr. Jeffrey Weiss, for providing an excellent combination of freedom and guidance that allowed me to develop independence and expertise as a researcher. Dr. Christopher Peters provided clinical perspective and thereby context for this research. I am indebted to Dr. Andrew Anderson for his active participation in this research, his support of my endeavors, and his career and life advice. The other members of my committee, Drs. Richard Rabbitt and Kent Bachus, provided support and feedback on this research, as well as active guidance for my development as a scientist. Dr. Benjamin Ellis supported my endeavors and Steve Maas developed and refined the computational tools necessary for this research. I am grateful to members of the Musculoskeletal Research Laboratories and the Orthopedic Research Laboratory at the University of Utah for many conversations on biomechanics, which have greatly enhanced my education.

Finally, I am grateful for financial support for this research that was provided by the National Institutes of Health Grants R01AR053344 and R01GM083925.

CHAPTER 1

INTRODUCTION

Motivation

Articular cartilage is a soft tissue at the ends of long bones that functions as a load-bearing surface for decades in healthy joints. Cartilage is a highly hydrated tissue, with healthy cartilage comprised of approximately 80% fluid and 20% solid [1]. The solid phase of cartilage consists primarily of the extracellular matrix, which is made up of proteins (primarily type II collagen) and proteoglycans with glycosaminoglycan side chains, and a small volume fraction of chondrocytes [1]. Collagen and proteoglycans are responsible for the mechanical behavior of cartilage while chondrocytes are responsible for the metabolic behavior of cartilage [2-6]. The relative composition and orientation of these components varies within joints, across joints within species, across species and through the depth of the cartilage [7-13]. This gives rise to complex material behavior in articular cartilage. Cartilage is able to withstand decades of loading in healthy joints. Unfortunately, cartilage can be damaged via several processes, including osteoarthritis (OA). In OA, cartilage damage is initiated by altered mechanical loading, and is then advanced by a combination of altered mechanics and altered metabolism [2, 14-17]. Once cartilage has begun to degenerate, the process is difficult to stop or reverse and will ultimately lead to the total loss of articular cartilage that characterizes end-stage OA [1,

18]. Although mechanics are known to be important in the pathogenesis of OA, the specific causes of the onset and progression of OA are not fully understood at either the joint or the tissue level.

In addition to articular cartilage, some diarthroidial joints have fibrocartilagenous structures within the joint space. These fibrocartilagenous articular structures may also have a role in the onset and progression of OA. For example, the fibrocartilagenous meniscus in the knee is important for dissipating load and providing stability. Accelerated knee OA occurs when the meniscus is removed or damaged [19-22]. The acetabular labrum in the hip forms a ring around the acetabulum and has a composition and structure similar to the meniscus in the knee [23-28]. The labrum has been implicated as part of the continuum of joint degeneration that ultimately leads to OA in the hip [29-34].

Hip OA affects 10% of the population and is primarily the result of pathomophology [35-37]. The hip is a large load bearing joint, which is approximated as a ball and socket joint, with the femoral head acting as the ball and the acetabulum acting as the socket. However, there are certain abnormalities that alter the bony morphology of the hip joint and thus predispose it to OA. While pathomophology can occur on either the acetabular or the femoral side of the joint, the focus of this dissertation will be on those occurring on the acetabular side of the joint. One such pathomorphology is acetabular dysplasia. In acetabular dysplasia, the acetabulum is shallow, which results in decreased area for load transfer across the hip joint in comparison to the normal hip. Acetabular dysplasia is also characterized by flatter acetabula and more elliptical femoral heads [38-41]. Acetabular dysplasia is thought to cause approximately 20% of all hip

OA [42]. Another acetabular pathomophology is acetabular retroversion. The retroverted acetabulum is characterized by opening more posteriorly than the normal acetabulum [43]. Acetabular retroversion is not well understood, but radiographic signs of retroversion have been found in a greater percentage of patients with hip OA than those without hip OA, which has led to the understanding that acetabular retroversion causes OA [44-47]. Although both acetabular dysplasia and acetabular retroversion are thought to cause OA via altered mechanics when compared to the normal hip, this causation has not been systematically established.

Although mechanics cannot be measured directly in vivo, computational methods can be used to predict them in an attempt to understand the pathogenesis of OA. One computational method that can be used is finite element (FE) analysis. In FE analysis, the governing system of equations is the equations of motion, conservation laws and constitutive models. FE analysis uses basis functions with compact support to approximate a solution to the system of equations at each point in the continuum, which has been discretized into finite elements. Because FE analysis is an approximate technique, verification, validation and parameter studies must be completed prior to acceptance of the results [48-50].

Previous research has used the FE method to study of hip joint mechanics. These studies have provided interesting insights, demonstrating the intersubject variability in the normal population, some effects of hip pathomorphology and the effects of geometric modeling assumptions on model results [51-54]. However, these studies have two primary sets of limitations. Previous studies of hip mechanics using the FE method have employed simplified cartilage constitutive equations, specifically linear or quasilinear

elasticity. Studies evaluating the effects of bony pathology have used models with idealized geometry or have omitted the acetabular labrum, which may provide inaccurate predictions [51, 52, 54]. The only model validation previously completed was for a single specimen [55]. While this study addressed certain modeling assumptions, questions remain regarding the effects of modeling assumptions on model validation and the ability of the subject-specific modeling to produce valid results across subject-specific geometry. Additionally, the mechanics of the dysplastic and retroverted hip have not been fully quantified, but can be addressed via FE modeling.

Research Goals

The overall objective of this research was two-fold: to validate a subject-specific modeling protocol for a series of specimens and to assess the effects of modeling assumptions on model predictions; and to use the subject-specific modeling protocol to evaluate cartilage mechanics in subjects with acetabular dysplasia and with acetabular retroversion. An understanding of the validity of FE predictions and the effects of cartilage constitutive assumption on model predictions can inform the use and interpretation of FE analysis applied to live subjects. While certain pathomorphologies are implicated in early onset hip OA, the precise mechanical causes are unknown. Therefore, this dissertation will quantify mechanics that may cause OA in patient populations. The topics of this dissertation will address the following hypotheses:

(1) FE model predictions will compare well, both qualitatively and quantitatively, with experimental measures of contact stress and contact area. Further, FE model validation of contact stress and contact area will be insensitive to cartilage constitutive assumptions.

(2) The assumed labral constitutive model and the location of the chondrolabral boundary will affect FE predictions of cartilage and labrum contact mechanics in the human hip.

(3) The acetabular labrum will be an important load-bearing structure in the dysplastic hip, but not in the normal hip.

(4) Cartilage contact mechanics in the retroverted hip will be quantitatively different than in the normal hip.

(5) Cartilage constitutive assumptions will affect FE predictions of results other than contact stress and contact area, specifically maximum shear stress and first principal strain.

Summary of Chapters

This dissertation focuses on validation, parameter studies and subject-specific FE modeling of the human hip joint. Chapter 2 provides the necessary background for the reader across several topics pertinent to this dissertation. Cartilage structure and the resulting mechanics are discussed in order to provide context for the selection of cartilage constitutive models. Classes of constitutive models that are applicable to cartilage are briefly reviewed. Following background at the tissue level, the anatomy of the normal and the pathomorphologic human hip joint are reviewed. OA is reviewed in order to ground the reader in this disease in general as well as in OA of the human hip specifically. Finally, the background chapter closes with a review of computational modeling with an emphasis on FE modeling. Technical background is presented, including motivation for model validation and the importance of parameter studies. Previous applications of FE modeling to the human hip are reviewed.

Chapter 3 addresses the need for model validation and sensitivity studies across a series of specimens for providing confidence in model predictions. Additionally, this chapter assesses the influence of the assumed cartilage constitutive behavior on model predictions of contact stress and contact area. Five male cadaveric specimens underwent experimental loading wherein contact pressure and contact area were measured using pressure-sensitive film. Region- and specimen-specific cartilage material behavior was characterized using cartilage samples from the contralateral joint. Specimen-specific FE models were generated of each specimen, with various cartilage constitutive descriptions. Experimentally measured contact mechanics and FE predicted contact mechanics were compared. This study indicated good agreement between experimental and computational results. This study also demonstrated the relative insensitivity of the predicted cartilage contact stress and contact area to the assumed cartilage constitutive model. Overall, the findings of this study provide confidence in predicting subject-specific cartilage contact stress and contact area in the human hip using average cartilage material coefficients.

Chapter 4 focuses on assessing the effects of modeling assumptions for the acetabular labrum. In particular, this study evaluated the effects of the assumed labrum constitutive model and the location of the chondrolabral boundary on subject-specific predictions of labral mechanics in one hip with normal anatomy and one hip with acetabular dysplasia. In this study, it was found that the percentage of the total load transferred across the joint that was transferred through the acetabular labrum was sensitive to the assumed labral constitutive model, as well as to the assumed chondrolabral boundary. Based on this sensitivity study, suggestions are made regarding

a conservative placement of the chondrolabral boundary and a constitutive model that captures the main structural features of the labrum for subject-specific FE modeling of the hip with the acetabular labrum.

Contact mechanics in hips with acetabular dysplasia are the focus of Chapter 5. The findings from the first two studies informed the development of subject-specific FE models of hips with acetabular dysplasia and hips with normal bony anatomy. In this chapter, twenty subjects were recruited for subject-specific finite element modeling. Ten subjects had normal hip morphology and no history of hip pain. Ten subjects were being seen in the clinic for hip pain secondary to acetabular dysplasia. CT arthrography was used to capture subject-specific joint geometry, from which subject-specific FE models were generated. Differences in cartilage and labrum mechanics were evaluated between the two groups. This study found distinct differences in labral mechanics between the two groups. Specifically, the labrum in the dysplastic hips supported a significantly larger portion of the load and had larger superior labral contact areas than in normal hips. However, there were minimal differences in cartilage contact mechanics between normal and dysplastic hips. This study provides quantitative evidence regarding the importance of the labrum as a load-bearing structure in dysplastic hips.

Contact mechanics in hips with acetabular retroversion, a second patient population at risk of hip OA, are the focus of Chapter 6. Ten subjects with hip pain secondary to acetabular retroversion were recruited. CT arthrography was used to capture subject-specific geometry and subject-specific FE models were built. Cartilage contact mechanics in the retroverted hips were compared to cartilage contact mechanics in normal hips. This study revealed superomedial contact in the retroverted hips in

comparison to distributed contact in normal hips. Because hips with acetabular retroversion are not currently well understood, this study provides unique first insight into the alterations in cartilage stress and contact area in this patient population.

The effects of modeling assumptions on predictions of transchondral first principal strain and maximum shear stress are the focus of Chapter 7. This study used the specimen-specific FE models produced in Chapter 3. Nearly-linear, material nonlinear and tension-compression nonlinear cartilage constitutive models were used to predict maximum shear stress and first principal strain at the articular surface, at the osteochondral interface and transchondrally. In contrast to the minimal effect of the assumed cartilage constitutive model on predictions of contact stress and contact area, this study demonstrated that the assumed constitutive model causes significant differences in predictions of cartilage maximum shear stress and first principal strain. This study provides the necessary modeling requirements for predicting these variables, which may be important for the pathogenesis of osteoarthritis, in future subject-specific modeling studies.

The significance of this work is discussed in Chapter 8, which also outlines future directions that have yet to be explored.

References

[1] Buckwalter, J. A., Mankin, H. J., and Grodzinsky, A. J., 2005, "Articular Cartilage and Osteoarthritis," Instr Course Lect, 54, pp. 465-480.

[2] Arokoski, J. P., Jurvelin, J. S., Vaatainen, U., and Helminen, H. J., 2000, "Normal and Pathological Adaptations of Articular Cartilage to Joint Loading," Scand J Med Sci Sports, **10**(4), pp. 186-198.

[3] Bhosale, A. M., and Richardson, J. B., 2008, "Articular Cartilage: Structure, Injuries and Review of Management," Br Med Bull, 87, pp. 77-95.

[4] Cohen, N. P., Foster, R. J., and Mow, V. C., 1998, "Composition and Dynamics of Articular Cartilage: Structure, Function, and Maintaining Healthy State," J Orthop Sports Phys Ther, **28**(4), pp. 203-215.

[5] Poole, A. R., Kojima, T., Yasuda, T., Mwale, F., Kobayashi, M., and Laverty, S., 2001, "Composition and Structure of Articular Cartilage: A Template for Tissue Repair," Clin Orthop Relat Res (391 Suppl), pp. S26-33.

[6] Schmidt, T. A., and Sah, R. L., 2007, "Effect of Synovial Fluid on Boundary Lubrication of Articular Cartilage," Osteoarthritis Cartilage, **15**(1), pp. 35-47.

[7] Buckley, M. R., Gleghorn, J. P., Bonassar, L. J., and Cohen, I., 2008, "Mapping the Depth Dependence of Shear Properties in Articular Cartilage," J Biomech, **41**(11), pp. 2430-2437.

[8] Chen, A. C., Bae, W. C., Schinagl, R. M., and Sah, R. L., 2001, "Depth- and Strain-Dependent Mechanical and Electromechanical Properties of Full-Thickness Bovine Articular Cartilage in Confined Compression," J Biomech, **34**(1), pp. 1-12.

[9] Maroudas, A., Bayliss, M. T., and Venn, M. F., 1980, "Further Studies on the Composition of Human Femoral Head Cartilage," Ann Rheum Dis, **39**(5), pp. 514-523.

[10] Mow, V., Gu, W., and Chen, F., 2005, "Structure and Function of Articular Cartilage and Meniscus," Basic Orthopaedic Biomechanics and Mechano-Biology, V. Mow, and R. Huiskes, eds., Lippincott, Philadephia, pp. 181-258.

[11] Mow, V. C., and Guo, X. E., 2002, "Mechano-Electrochemical Properties of Articular Cartilage: Their Inhomogeneities and Anisotropies," Annu Rev Biomed Eng, **4**(1), pp. 175-209.

[12] Schinagl, R. M., Gurskis, D., Chen, A. C., and Sah, R. L., 1997, "Depth-Dependent Confined Compression Modulus of Full-Thickness Bovine Articular Cartilage," J Orthop Res, **15**(4), pp. 499-506.

[13] Setton, L. A., Zhu, W., and Mow, V. C., 1993, "The Biphasic Poroviscoelastic Behavior of Articular Cartilage: Role of the Surface Zone in Governing the Compressive Behavior," J Biomech, **26**(4-5), pp. 581-592.

[14] Adatia, A., Rainsford, K. D., and Kean, W. F., 2012, "Osteoarthritis of the Knee and Hip. Part I: Aetiology and Pathogenesis as a Basis for Pharmacotherapy," J Pharm Pharmacol, **64**(5), pp. 617-625.

[15] Buckwalter, J. A., Saltzman, C., and Brown, T., 2004, "The Impact of Osteoarthritis: Implications for Research," Clin Orthop Relat Res (427 Suppl), pp. S6-15.

[16] de Lange-Brokaar, B. J., Ioan-Facsinay, A., van Osch, G. J., Zuurmond, A. M., Schoones, J., Toes, R. E., Huizinga, T. W., and Kloppenburg, M., 2012, "Synovial Inflammation, Immune Cells and their Cytokines in Osteoarthritis: A Review," Osteoarthritis Cartilage, **20**(12), pp. 1484-1499.

[17] Gupta, K. B., Duryea, J., and Weissman, B. N., 2004, "Radiographic Evaluation of Osteoarthritis," Radiol Clin North Am, **42**(1), pp. 11-41, v.

[18] Goldring, M. B., 2012, "Articular Cartilage Degradation in Osteoarthritis," H S S J, **8**(1), pp. 7-9.

[19] Crema, M. D., Roemer, F. W., Felson, D. T., Englund, M., Wang, K., Jarraya, M., Nevitt, M. C., Marra, M. D., Torner, J. C., Lewis, C. E., and Guermazi, A., 2012, "Factors Associated with Meniscal Extrusion in Knees with or at Risk for Osteoarthritis: The Multicenter Osteoarthritis Study," Radiology, **264**(2), pp. 494-503.

[20] Jeong, H. J., Lee, S. H., and Ko, C. S., 2012, "Meniscectomy," Knee Surg Relat Res, **24**(3), pp. 129-136.

[21] Knoop, J., Dekker, J., Klein, J. P., van der Leeden, M., van der Esch, M., Reiding, D., Voorneman, R. E., Gerritsen, M., Roorda, L. D., Steultjens, M. P., and Lems, W. F., 2012, "Biomechanical Factors and Physical Examination Findings in Osteoarthritis of the Knee: Associations with Tissue Abnormalities Assessed by Conventional Radiography and High Resolution 3.0 Tesla Magnetic Resonance Imaging," Arthritis Res Ther, **14**(5), p. R212.

[22] Tucker, B., Khan, W., Al-Rashid, M., and Al-Khateeb, H., 2012, "Tissue Engineering for the Meniscus: A Review of the Literature," Open Orthop J, 6, pp. 348-351.

[23] Czerny, C., Hofmann, S., Urban, M., Tschauner, C., Neuhold, A., Pretterklieber, M., Recht, M. P., and Kramer, J., 1999, "MR Arthrography of the Adult Acetabular Capsular-Labral Complex: Correlation with Surgery and Anatomy," Am J Roentgenol, **173**(2), pp. 345-349.

[24] Keene, G. S., and Villar, R. N., 1994, "Arthroscopic Anatomy of the Hip: An In Vivo Study," Arthroscopy, **10**(4), pp. 392-399.

[25] Lecouvet, F. E., Vande Berg, B. C., Malghem, J., Lebon, C. J., Moysan, P., Jamart, J., and Maldague, B. E., 1996, "MR Imaging of the Acetabular Labrum: Variations in 200 Asymptomatic Hips," Am J Roentgenol, **167**(4), pp. 1025-1028.

[26] Petersen, W., Petersen, F., and Tillmann, B., 2003, "Structure and Vascularization of the Acetabular Labrum with Regard to the Pathogenesis and Healing of Labral Lesions," Arch Orthop Trauma Surg, **123**(6), pp. 283-288.

[27] Seldes, R. M., Tan, V., Hunt, J., Katz, M., Winiarsky, R., and Fitzgerald, R. H., Jr., 2001, "Anatomy, Histologic Features, and Vascularity of the Adult Acetabular Labrum," Clin Orthop Relat Res (382), pp. 232-240.

[28] Won, Y. Y., Chung, I. H., Chung, N. S., and Song, K. H., 2003, "Morphological Study on the Acetabular Labrum," Yonsei Med J, **44**(5), pp. 855-862.

[29] Fujii, M., Nakashima, Y., Jingushi, S., Yamamoto, T., Noguchi, Y., Suenaga, E., and Iwamoto, Y., 2009, "Intraarticular Findings in Symptomatic Developmental Dysplasia of the Hip," J Pediatr Orthop, **29**(1), pp. 9-13.

[30] Klaue, K., Durnin, C. W., and Ganz, R., 1991, "The Acetabular Rim Syndrome. A Clinical Presentation of Dysplasia of the Hip," J Bone Joint Surg Br, **73**(3), pp. 423-429.

[31] Leunig, M., Podeszwa, D., Beck, M., Werlen, S., and Ganz, R., 2004, "Magnetic Resonance Arthrography of Labral Disorders in Hips with Dysplasia and Impingement," Clin Orthop Relat Res (418), pp. 74-80.

[32] McCarthy, J., Noble, P., Aluisio, F. V., Schuck, M., Wright, J., and Lee, J. A., 2003, "Anatomy, Pathologic Features, and Treatment of Acetabular Labral Tears," Clin Orthop Relat Res (406), pp. 38-47.

[33] Peelle, M. W., Della Rocca, G. J., Maloney, W. J., Curry, M. C., and Clohisy, J. C., 2005, "Acetabular and Femoral Radiographic Abnormalities Associated with Labral Tears," Clin Orthop Relat Res, 441, pp. 327-333.

[34] Wenger, D. E., Kendell, K. R., Miner, M. R., and Trousdale, R. T., 2004, "Acetabular Labral Tears Rarely Occur in the Absence of Bony Abnormalities," Clin Orthop Relat Res (426), pp. 145-150.

[35] Gosvig, K. K., Jacobsen, S., Sonne-Holm, S., Palm, H., and Troelsen, A., 2010, "Prevalence of Malformations of the Hip Joint and their Relationship to Sex, Groin Pain, and Risk of Osteoarthritis: A Population-Based Survey," J Bone Joint Surg Am, **92**(5), pp. 1162-1169.

[36] Harris-Hayes, M., and Royer, N. K., 2011, "Relationship of Acetabular Dysplasia and Femoroacetabular Impingement to Hip Osteoarthritis: A Focused Review," P M R, **3**(11), pp. 1055-1067 e1051.

[37] Murray, R. O., 1965, "The Aetiology of Primary Osteoarthritis of the Hip," The British Journal Of Radiology, **38**(455), pp. 810-824.

[38] Clohisy, J. C., Nunley, R. M., Carlisle, J. C., and Schoenecker, P. L., 2009, "Incidence and Characteristics of Femoral Deformities in the Dysplastic Hip," Clin Orthop Relat Res, **467**(1), pp. 128-134.

[39] Noble, P. C., Kamaric, E., Sugano, N., Matsubara, M., Harada, Y., Ohzono, K., and Paravic, V., 2003, "Three-Dimensional Shape of the Dysplastic Femur: Implications for THR," Clin Orthop Relat Res (417), pp. 27-40.

[40] Steppacher, S. D., Tannast, M., Werlen, S., and Siebenrock, K. A., 2008, "Femoral Morphology Differs Between Deficient and Excessive Acetabular Coverage," Clin Orthop Relat Res, **466**(4), pp. 782-790.

[41] Sugano, N., Noble, P. C., Kamaric, E., Salama, J. K., Ochi, T., and Tullos, H. S., 1998, "The Morphology of the Femur in Developmental Dysplasia of the Hip," J Bone Joint Surg Br, **80**(4), pp. 711-719.

[42] Solomon, L., 1976, "Patterns of Osteoarthritis of the Hip," J Bone Joint Surg Br, **58**(2), pp. 176-183.

[43] Reynolds, D., Lucas, J., and Klaue, K., 1999, "Retroversion of the Acetabulum. A Cause of Hip Pain," J Bone Joint Surg Br, **81**(2), pp. 281-288.

[44] Ezoe, M., Naito, M., and Inoue, T., 2006, "The Prevalence of Acetabular Retroversion Among Various Disorders of the Hip," J Bone Joint Surg Am, **88**(2), pp. 372-379.

[45] Giori, N. J., and Trousdale, R. T., 2003, "Acetabular Retroversion is Associated with Osteoarthritis of the Hip," Clin Orthop Relat Res (417), pp. 263-269.

[46] Kim, W. Y., Hutchinson, C. E., Andrew, J. G., and Allen, P. D., 2006, "The Relationship Between Acetabular Retroversion and Osteoarthritis of the Hip," J Bone Joint Surg Br, **88**(6), pp. 727-729.

[47] Sierra, R. J., 2013, "The Management of Acetabular Retroversion with Reverse Periacetabular Osteotomy," Instr Course Lect, 62, pp. 305-313.

[48] 2006, "ASME V&V 10-2006 Guide for Verification and Validation in Computational Solid Mechanics," ASME Standards.

[49] Anderson, A. E., Ellis, B. J., and Weiss, J. A., 2007, "Verification, Validation and Sensitivity Studies in Computational Biomechanics," Comput Methods Biomech Biomed Engin, **10**(3), pp. 171-184.

[50] Henninger, H. B., Reese, S. P., Anderson, A. E., and Weiss, J. A., 2010, "Validation of Computational Models in Biomechanics," Proc Inst Mech Eng H, **224**(7), pp. 801-812.

[51] Anderson, A. E., Ellis, B. J., Maas, S. A., and Weiss, J. A., 2010, "Effects of Idealized Joint Geometry on Finite Element Predictions of Cartilage Contact Stresses in the Hip," J Biomech, **43**(7), pp. 1351-1357.

[52] Chegini, S., Beck, M., and Ferguson, S. J., 2009, "The Effects of Impingement and Dysplasia on Stress Distributions in the Hip Joint During Sitting and Walking: A Finite Element Analysis," J Orthop Res, **27**(2), pp. 195-201.

[53] Harris, M. D., Anderson, A. E., Henak, C. R., Ellis, B. J., Peters, C. L., and Weiss, J. A., 2012, "Finite Element Prediction of Cartilage Contact Stresses in Normal Human Hips," J Orthop Res, **30**(7), pp. 1133-1139.

[54] Russell, M. E., Shivanna, K. H., Grosland, N. M., and Pedersen, D. R., 2006, "Cartilage Contact Pressure Elevations in Dysplastic Hips: A Chronic Overload Model," J Orthop Surg Res, 1, pp. 6-6.

[55] Anderson, A. E., Ellis, B. J., Maas, S. A., Peters, C. L., and Weiss, J. A., 2008, "Validation of Finite Element Predictions of Cartilage Contact Pressure in the Human Hip Joint," J Biomech Eng, **130**(5), pp. 051008-051008.

CHAPTER 2

BACKGROUND

Cartilage

Cartilage Structure and Function

Articular cartilage is a highly hydrated tissue, with a solid matrix composed primarily of type II collagen, proteoglycans (PGs) with glycosaminoglycan (GAG) side chains and chondrocytes. By weight, normal articular cartilage is ~70-85% interstitial fluid [1-4]. The solid portion of cartilage consists of the extracellular matrix (ECM) and the chondrocytes. By dry weight, cartilage ECM is composed of ~60% collagen, 25-30% PGs and 15-20% noncollagenous proteins and glycoproteins [1]. Chondrocytes comprise approximately 1-5% of the total volume of adult human cartilage, a relatively sparse cell density in comparison to other tissues [1, 3, 5, 6]. Because cartilage is neither vascularized nor enervated, chondrocytes are responsible for all metabolic activity in cartilage [3]. Each of the components of the ECM, as well as the interstitial fluid, govern specific mechanical behaviors of articular cartilage, while the chondrocytes drive cartilage metabolism [7].

Interstitial fluid in articular cartilage has important mechanical roles, including creating swelling pressures, supporting load and maintaining cartilage lubrication. Interstitial fluid is composed of a solvent phase (water), multiple charged ions and

possibly other solutes. The main free ions in cartilage are sodium (Na^+) and chlorine (Cl^-) [2]. Other free ions that can be found in interstitial fluid are calcium (Ca^{2+}) and potassium (K^+) [2]. These ions are free to move within the cartilage and therefore create an osmotic balance with the fixed negative charges of the ECM. Interstital fluid supports large portions of the load transferred across diarthroidial joints under fast loading [8, 9]. Because cartilage is so highly hydrated, it takes a finite amount of time for interstitial fluid to exude following the application of load. Therefore, under nearly-instantaneous loading, fluid does not have time to move within the ECM and supports the vast majority of the applied load [10-12]. Interstitial fluid and the load supported by the fluid also contribute to the low coefficient of friction in healthy cartilage (~0.01-0.02) [8, 13, 14].

Type II collagen is the main collagen type in cartilage, with types IX, IX, VI and X also present in smaller amounts [1, 3, 4]. Type II collagen is made up of three α_1 (II) chains, and accounts for 90-95% of all collagen in cartilage [1, 3-5]. Type II collagen is considered primarily responsible for the strength of cartilage under tensile and shear deformation [3-5, 10]. Collagen fibrils in cartilage are approximately 20 nm in diameter in the superficial zone, and increase in size up to 70 to 120 nm in the deep zone [5]. Other types of collagen found in cartilage serve a variety of functions. Types IX and XI collagen bind covalently to type II collagen [1]. These collagen types may help stabilize the ECM by creating interfibrillar connections [1, 3]. Additionally, type IX collagen may be important in fibril assembly [3, 5]. Type VI collagen is primarily found in the pericellular matrix immediately adjacent to chondrocytes and is therefore thought to help chondrocytes attach to the ECM [1, 3, 5]. Type X collagen has a role in tissue

mineralization and is primarily found in the calcified zone near the subchondral bone in healthy cartilage [1, 3].

PGs are protein polysaccharide molecules with GAG side chains [3, 15]. There are two types of PG in cartilage: large, aggregating PGs (aggrecans) and small leucine-rich repeat PGs (e.g., biglycan, decorin and fibromodulin) [3, 15]. The main GAG side chains in cartilage are chondroitin sulfate, keratin sulfate, dermatan sulfate and hyaluronan [1, 3]. Type IX collagen is also often considered a PG because it behaves like one [1]. PGs and GAGs are primarily responsible for the compressive strength of cartilage under fast loading, the permeability under slow loading and maintaining tissue hydration [3, 5, 10, 15].

Interactions between ECM constituents are also important in the behavior of cartilage. For example, the swelling behavior of cartilage is controlled by the interactions between the PGs, whose negatively charged sulfate and carboxylate groups create a Donnan effect, and the collagen network, which resists ECM expansion [3, 5].

There are three distinct zones in articular cartilage, wherein the constituent percentages and orientations vary. The superficial zone is the 10-20% nearest the articular surface [2]. In the superficial zone, collagen is oriented primarily in the plane of the articular surface [4, 5]. GAG content is the lowest in the superficial zone and increases through the cartilage depth [5, 6]. Chondrocytes in the superficial zone are somewhat flattened and are aligned approximately parallel to the articular surface [5]. The middle zone is the next ~40-60% [2]. This portion of cartilage makes up the bulk of the material and thereby the bulk of the material behavior. In the middle zone, collagen is oriented approximately randomly and chondrocytes are more rounded than in the

superficial zone [4, 5]. The deep zone of cartilage is the bottom ~30% [2]. Collagen is orientated approximately perpendicular to the osteochondral interface in the deep zone. Chondrocytes in the deep zone express the hyertrophic phenotype and synthesize type X collagen [5]. Below the deep zone is the calcified cartilage, which is sometimes considered a fourth zone in cartilage [3, 4].

Chondrocytes, the cell type in articular cartilage, are responsible for all metabolic activity of cartilage but make minimal contribution to mechanics. While each individual chondrocyte has a high metabolic output, the relatively sparse chondrocyte density results in a relatively low intrinsic ability of cartilage to heal [3, 6, 7]. In healthy cartilage, chondrocytes maintain cartilage homeostasis by producing both ECM constituents and enzymes that break down the ECM [3].

Overall, cartilage structure and function is governed by complex interactions between the ECM components, the interstitial fluid and the metabolic activity of the chondrocytes (Figure 2.1).

Cartilage Mechanics and Constitutive Modeling

Cartilage mechanics are complex in response to the complex structure that governs them (Figure 2.1). Cartilage behavior is rate- and time-dependent as a result of both the fluid-solid interactions and the intrinsic viscoelasticity of the solid phase [16-19]. Cartilage behavior is nonlinear: the solid matrix exhibits material nonlinearity in the stress-strain response and the tissue exhibits strain-dependent permeability and diffusivity [20-24]. Further, the response of cartilage to tensile loading is much stiffer than that to compressive loading, a phenomenon referred to as tension-compression nonlinearity [20].

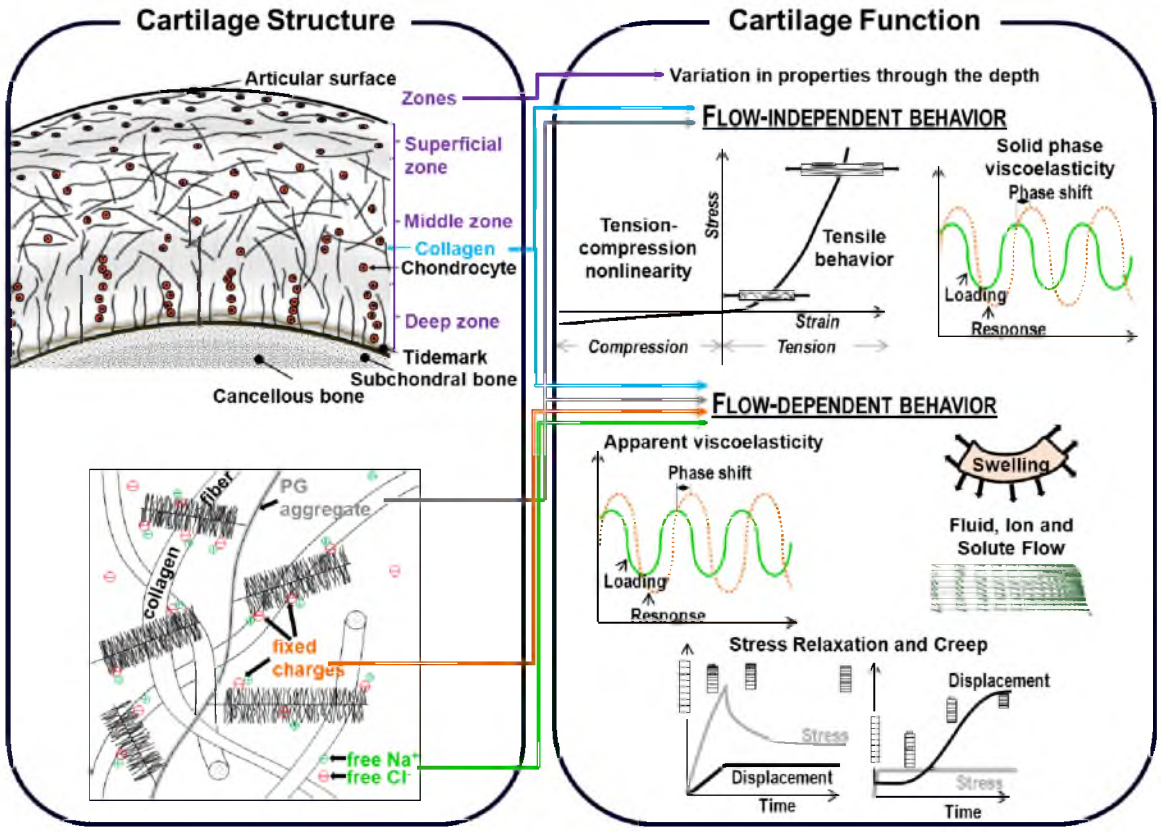

Figure 2.1: Schematic of cartilage structure and function. Left – cartilage structure and components. Right – complex cartilage function that arises from features of cartilage structure.

Cartilage properties are spatially inhomogeneous and vary between joints and species. Variations in cartilage properties through the depth of the cartilage arise from the zonal organization of cartilage [25-30]. Cartilage behavior varies between joints within species and between species within joints, indicating that using the constitutive behavior from the species of interest may be important in accurately predicting cartilage mechanics [20, 31-35]. Spatial inhomogeneity in material behavior also occurs within joints [31, 32].

There are three types of constitutive models that are applicable for articular cartilage: elastic, viscoelastic and multiphasic. Each of these types of constitutive models has many subfamilies that can capture a variety of specific behaviors. Elastic constitutive

models are those in which there is a one-to-one correspondence between stress and strain. These constitutive models are the most straightforward to understand, the most straightforward to fit to experimental data and the least computationally expensive when implemented into a finite element solver. Hyperelastic constitutive models are a subset of elastic constitutive models wherein a strain energy function exists. The stress can then be obtained from the derivative of the strain energy function. The advantage of hyperelastic constitutive models in general is that they are indifferent to rotations and thus are suitable for large deformations [36]. Elastic constitutive models are suitable for capturing cartilage behavior in the limits of fast and slow loading [37]. Under fast loading, the fluid has not had time to exude from the cartilage matrix. In this case, the cartilage behavior of the fluid and solid together may be approximated as an incompressible elastic material. Under slow loading, all fluid has exuded from the cartilage matrix. In this case, the elastic model describes the behavior of the drained solid matrix.

Viscoelastic constitutive models allow for energy dissipation, and phenomenologically capture the time- and rate-dependent behavior of cartilage. Viscoelasticity is suitable for loading rates that do not fit within the very fast or very slow loading that is suitable for elastic behavior, but when separating fluid and solid behavior is not of interest. Several continuum viscoelastic representations have been developed and used for cartilage [38-41].

Multiphasic constitutive models represent cartilage as multiple phases, including a solid phase, a fluid phase, and possibly ion or solute phases. Multiphasic materials are appropriate for use in predictions of cartilage mechanics when interactions between

solids and fluids, the movement of solutes, solid versus fluid phase stresses and the movement of fluids are of interest. Multiphasic materials have a long history of development and use for representing the behavior of articular cartilage [2, 4, 19, 21-24, 26, 42-58].

The salient features of cartilage behavior to capture with a constitutive model depend on the required level of accuracy and the desired computational model outputs. The appropriate constitutive model should be selected that captures the cartilage behavior of interest but is also tractable in terms of available coefficients and computational efficiency [59, 60].

Hip Joint Anatomy and Pathology

Hip Joint Anatomy

The hip joint is the articulation between the hemipelvis and the femur (Figure 2.2). The hemipelvis is comprised of the ilium, the ischium and the pubis, which fuse in the acetabulum. The hip joint is grossly approximated as a ball and socket joint, wherein the femoral head is the ball and the acetabulum is the socket. The acetabulum and the femur are covered with layers of articular cartilage. In the acetabulum, the cartilage is approximately horseshoe-shaped. Femoral cartilage covers the entire femoral head, and is therefore approximately spherical. The hip joint is an important weight-bearing joint.

In addition to cartilage in the articular space, the acetabular labrum is a fibrocartilagenous ring attached to the acetabular rim. The labrum is approximately triangular in structure, although minor morphological variations exist [61-64]. The dimensions of the labrum vary by anatomical position from 4.0-5.5 mm wide at the base of the labrum and from 3.8-6.4 mm high from the acetabular rim to the tip of the labrum

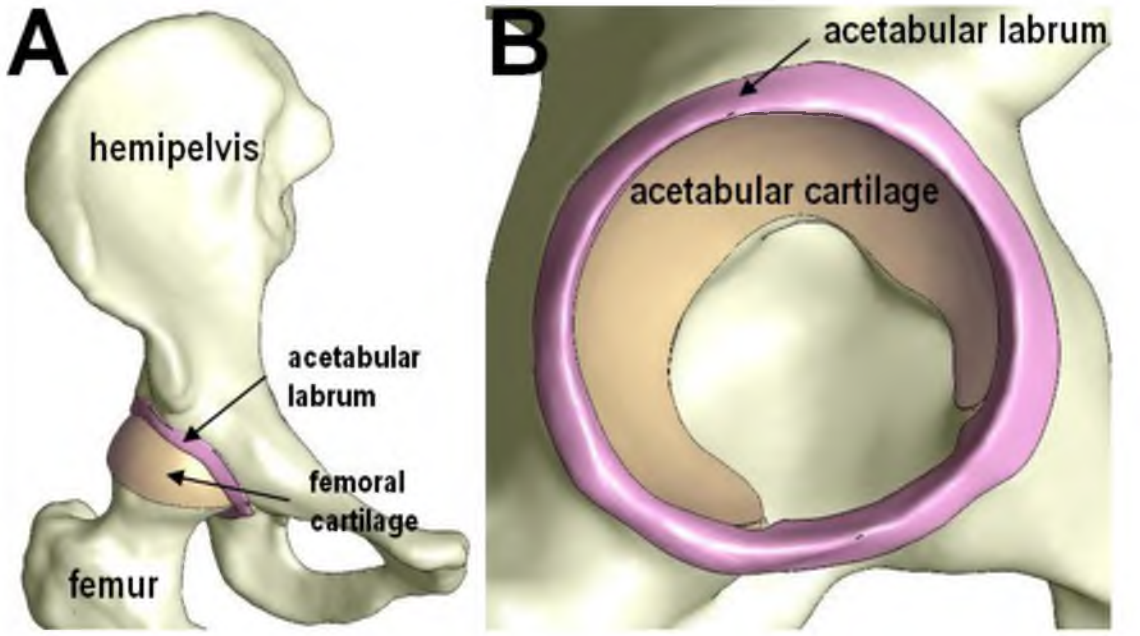

Figure 2.2: Schematic of the human hip joint. A – the whole joint, including both bones, the articular cartilage and the acetabular labrum. B – the acetabulum, highlighting the acetabular cartilage and acetabular labrum.

[65]. The labrum is the thickest at the base of the labrum in the anterior acetabulum and the tallest in the superior acetabulum [65]. The labrum is a continuation of the acetabular articular surface through the chondrolabral junction. Occasionally, a sulcus is present, which is a minor gap in the chondrolabral junction [61, 62, 66-69]. In addition to its attachment to the cartilage, the labrum attaches to the bony acetabular rim and to the hip capsule [65, 70]. Three distinct layers have been found in the acetabular labrum [66]. Circumferential bundles of types I collagen make up the inner layer, which is the most substantial [66]. In addition to type I collagen, type II collagen was found in the outer layers of the acetabular labrum [66]. Type III collagen is also present in all layers of the labrum [66]. Vascularization of the acetabular labrum is limited to the peripheral regions, indicating that the labrum, like cartilage, has a limited capacity to heal when damaged intra-articularly [66].

The mechanical and metabolic behavior of acetabular labrum has been the subject of limited study. The tensile and compressive properties of bovine labrum were evaluated under uniaxial load [71]. Mechanical behavior of the human labrum has been evaluated in two studies. Using tissue from patients undergoing hip surgery, the tensile properties of human acetabular labrum were obtained [72]. Because this tissue was from patients undergoing surgery, it is unlikely that the results represent the material behavior of healthy labrum. A second study evaluated the tensile and compressive behavior of the human labrum and reported mean moduli [73]. The metabolic activity of the labrum has been the subject of a single study, which demonstrated high expression of type I collagen genes and low expression of type II collagen genes in isolated labrum cells [74]. While the labrum is often compared to the meniscus because they are both fibrocartilagenous intra-articular structures, higher levels of type II collagen genes are expressed by labrum cells than by meniscus cells [74].

Acetabular Dysplasia

Acetabular dysplasia is characterized by a shallow acetabular socket, which results in undercoverage of the femoral head (Figure 2.3). Screening for acetabular dysplasia is part of most newborn examinations [75, 76]. While these screening procedures catch the majority of children with gross acetabular dysplasia, more mild forms may be missed and persist into adolescence or adulthood [75]. Acetabular dysplasia that presents during adulthood is the focus of this dissertation.

The prevalence of adult radiographic acetabular dysplasia is approximately 1-14%, depending on the radiographic criteria used for diagnosis and the ethnicity of subjects [76-79]. Acetabular dysplasia occurs at a higher rate in females than in males

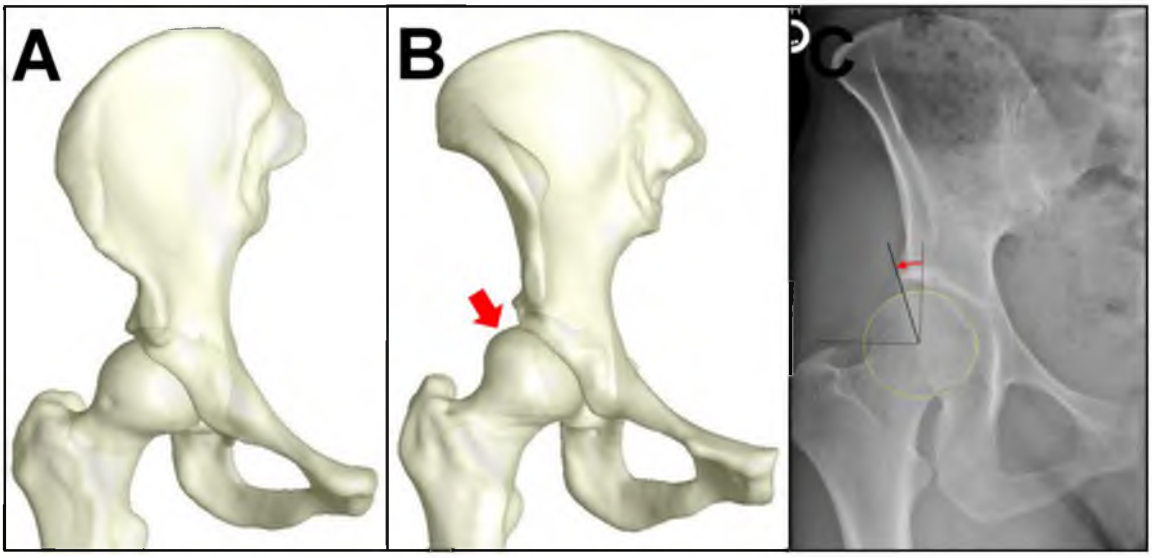

Figure 2.3: Characteristics of acetabular dysplasia. A – anteroposterior projection of the normal hip. B – anteroposterior projection of the dyplastic hip. The red arrow highlights the undercovered femoral head. C – anteroposterior radiograph of the dysplastic hip showing the center-edge angle. The femoral head is fit to a circle (yellow). The angle between vertical and the lateral edge of the acetabular sourcil is the center edge angle (red).

[76, 80]. Environmental factors, including breech presentation and high birth also increase the risk of acetabular dysplasia [76, 80]. Additionally, there appears to be a strong genetic component to acetabular dysplasia, with a family history of dysplasia increasing a subject's risk of having a diagnosis of dysplasia [76, 80, 81]. Acetabular dysplasia is more commonly found in both monozygotic twins than in both dizygotic twins [81]. Using a large, multigenerational family, Feldman et al. were able to establish that the mode of inheritance from this family was autosomal dominant with variable expression [82]. The authors discussed the likelihood that variable expression was caused by the contribution of environmental factors [82].

Adult acetabular dysplasia is typically diagnosed radiographically [75, 83, 84]. The most common measurements used to diagnose acetabular dysplasia include the

lateral center-edge angle (LCEA), the anterior center-edge angle (ACEA), the Sharp's angle and the acetabular index [75, 83]. Each of these measurements provides information regarding the acetabular morphology in isolation or the relationship between the acetabulum and the femur. The LCEA is measured on anteroposterior radiographs (Figure 2.3C). This angle was first described by Wiberg in 1939 [85]. The LCEA characterizes the lateral coverage of the femoral head by the acetabulum [83, 86]. To obtain the LCEA, the center of the femoral head is found by approximating the femoral head with a circle. The vertical axis relative to the patient's position in the radiograph is then found. To do this, a line is drawn between the most distal points of the two ischial tuberosities to create the horizontal axis. The vertical axis is then created as a line that is perpendicular to the horizontal line. For reference, the vertical axis is placed through the center of the femoral head. The LCEA is then the angle between vertical and the lateral edge of the acetabular sourcil [87]. The cutoff angle below which acetabular dysplasia is diagnosed varies depending on the study, and is usually either 20° or 25° [77, 86]. The ACEA is measured on false profile radiographs and characterizes the anterior coverage of the femoral head by the acetabulum [86]. The ACEA is measured using similar methods to the LCEA, albeit in a different radiographic view. This angle and radiographic view were first described by Lequesne and de Sèze in 1961 [75]. ACEA less than 20° are considered dysplastic [86]. The Sharp's angle measures the orientation of the acetabulum in the anteroposterior projection, without reference to the femur [88]. The Sharp's angle is the angle between horizontal and a line that goes through the distal teardrop and the lateral edge of the sourcil [88]. This angle was first described by Sharp in 1961 [88]. Angles below 42° were described as normal, angles from 42°-47° were described as

questionable and angles above 47° indicated dysplasia [88]. The acetabular index, also known as the acetabular inclination or Tönnis angle, measures the orientation of the acetabular sourcil in the anteroposterior projection without reference to the femur. This angle is the angle between horizontal and a line connecting the medial and lateral points on the sourcil [86, 89]. Acetabular indices greater than 10° indicate acetabular dysplasia [86]. Advanced imaging, including volumetric computed tomography (CT) and magnetic resonance imaging (MRI) with or without contrast agent in the joint, can also be used in the diagnosis of acetabular dysplasia to evaluate three-dimensional bony morphology and the integrity of the articular soft tissue [75, 84].

Clinical exams and history are used in conjunction with radiographic diagnosis to pinpoint the cause of hip pain as acetabular dysplasia. When evaluating a patient's history, known risk factors including family history of dysplasia and breech presentation should be evaluated [75]. Previous surgical history should also be obtained [84]. Any functional limitations should be discussed with the patient, as patients with acetabular dysplasia may have pain or discomfort with weight-bearing activities [75, 84]. Patient gait should be evaluated, as weak abductors may result in a Trendelenburg gait [75]. Trendelenburg gait, as first described by Trendelenburg in 1895, is the pattern of a dropped contralateral pelvis when in single leg stance, which is accompanied by lateral trunk movement towards the weight-bearing leg [90]. Patients with acetabular dysplasia may present with pain when placed in hip flexion, adduction and internal rotation (the impingement exam) due to lesions on the acetabular rim [75, 91]. However, patients with dysplasia most often have a full range of hip motion [84].

The acetabular labrum is frequently damaged or altered in patients with acetabular dysplasia. Labral tears rarely occur without underlying bony abnormality and are often found in hips with acetabular dysplasia [84, 92-97]. The labrum in dysplastic hips is also typically hypertrophic [91, 98-100]. Labral pathology can result in paralabral cysts and the acetabular rim syndrome [91].

Although acetabular dysplasia is characterized and diagnosed by the acetabular morphology, the femoral morphology may also be abnormal. Femoral anteversion, the rotation of the proximal femur, is increased in dysplastic hips compared to normal hips [101, 102]. The femurs in hips with acetabular dysplasia have shorter femoral necks with decreased head-neck offset [102-104]. The femoral head in hips with acetabular dysplasia are more elliptical and less spherical than in normal hips [88, 103, 104].

Acetabular Retroversion

Acetabular retroversion is characterized by a retroverted acetabular socket. In the normal hip, the acetabular socket opens anteriorly and laterally. In the hip with acetabular retroversion, the acetabular socket opens more posteriorly [105, 106]. This may create anterior overcoverage, posterior undercoverage or some combination of anterior overcoverage and posterior undercoverage [107, 108]. Acetabular retroversion is described as a possible cause of pincer femoroacetabular impingment via anterior overcoverage [109, 110]. Because acetabular retroversion in the native hip was first described in 1999, less information is available regarding the causes and effects of acetabular retroversion than regarding acetabular dysplasia [105, 111].

The prevalence of acetabular retroversion in the normal population has been reported at 5-48%, depending on the criteria used and subjects evaluated [112-116].

Acetabular retroversion, as diagnosed by the crossover sign, is more common in males than in females [114]. Even in the normal population, males have lower acetabular anteversion than females [115, 117]. While a genetic component to femororacetabular impingement has been suggested [118], hereditability of acetabular retroversion in particular has not been established [119]. However, hip development in general results from unknown combination of genes and environment [119]. Therefore, it is likely that acetabular retroversion results from genetic and environmental risk factors that have yet to be identified.

Retroversion is most commonly diagnosed via the presence of the crossover sign on plane film radiographs (Figure 2.4) [110, 120]. The crossover sign indicates the relationship between the anterior and posterior rims of the acetabulum, and thus describes the acetabular morphology in isolation. In the normal hip, the anterior acetabulum is medial to the posterior acetabulum over the whole joint in the anteroposterior projection. In the hip with acetabular retroversion, the anterior acetabulum is lateral to the posterior acetabulum near the top of the socket. Moving down from the top of the socket, projections of the anterior and posterior acetabular rims cross in the retroverted hip, creating the crossover sign [105]. The posterior wall sign can also be used to evaluate the relative coverage of the femoral head by the acetabular socket in acetabular retroversion [120]. In the normal hip, the center of the femoral head lies medial to or in line with the projection of the posterior acetabular rim in the anteroposterior plane. The posterior wall sign is present when the center of the femoral head is lateral to the projection of the posterior acetabular rim [105]. Because of the sensitivity of plane film radiographic diagnosis of acetabular retroversion to minor perturbations in patient position during

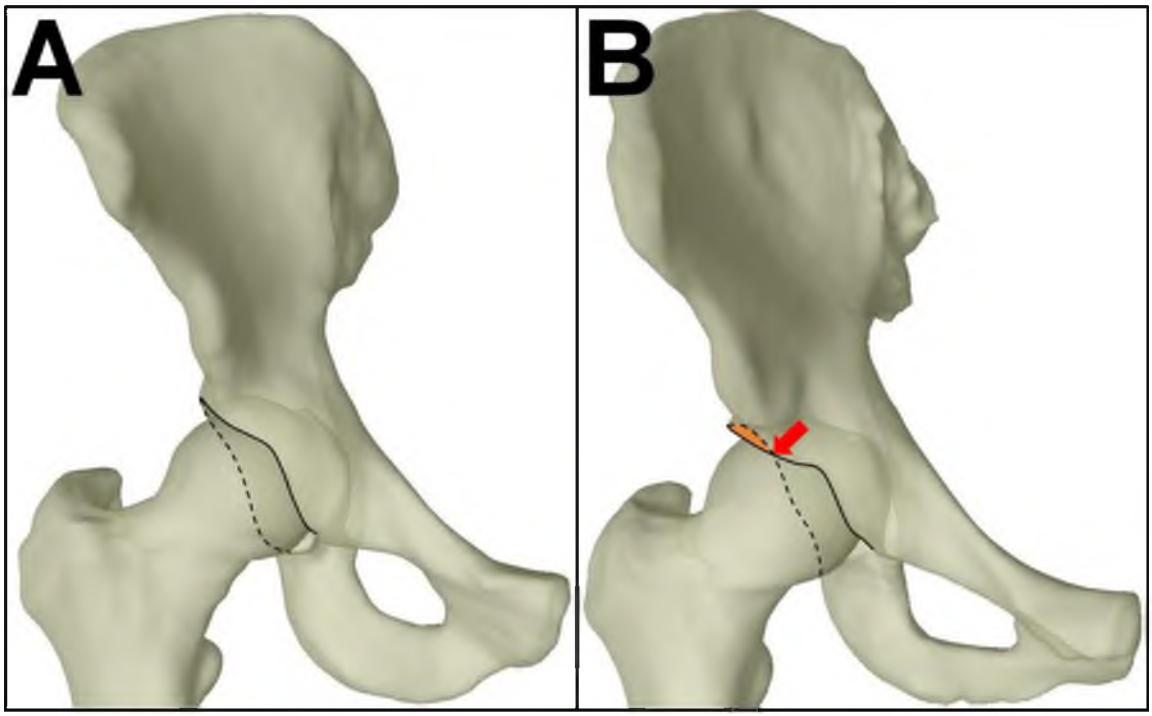

Figure 2.4: Characteristics of acetabular retroversion. The anterior acetabular rim is outlined in a solid line and the posterior acetabular rim is outlined in a dashed line. A – anteroposterior projection of a normal hip. The anterior rim lies medial to the posterior rim. B – anteroposterior projection of a retroverted hip. The anterior acetabular rim lies medial to the posterior acetabular rim at the superior acetabulum (orange region). As the lines progress distally, they cross, creating the cross-over sign (red arrow).

imaging, volumetric image data are also useful for the accurate diagnosis of acetabular retroversion [105, 110, 121-124]. Although acetabular retroversion is defined as an independent acetabular morphology, it also occurs in combination with acetabular dysplasia. Approximately 17-18% of patients with acetabular dysplasia have acetabular retroversion [112, 125, 126].

Clinical exams and patient history are important in the diagnosis of acetabular retroversion [84, 127]. As with acetabular dysplasia, diagnosis of acetabular retroversion should include information regarding the patient's history and information regarding that activities elicit pain [106]. Activities associated with hip flexion and sports, including

sitting, pivoting and running, often cause pain in hips with acetabular retroversion [128-130]. Patients with retroversion are frequently aware of their limited ranges of motion, which can be confirmed via clinical exam [110]. The impingement exam, which places the hip in flexion, abduction and internal rotation, can be used to determine whether acetabular retroversion is causing femoroacetabular impingement [120]. Pain during the impingement exam indicates femoroacetabular impingement.

Osteoarthritis

What is Osteoarthritis?

Osteoarthritis (OA) is the symptomatic loss of articular cartilage in diarthrodial joints, accompanied by changes to the joint synovium and bone [10, 131-134]. OA is initiated by mechanical overload and sustained by an abnormal mechanical and metabolic environment. While it was initially thought that cartilage was the main driver in OA, recent evidence indicates that inflammation of all tissues in and around the joint are important factors [1, 133, 135-137]. OA is characterized by persistent joint pain and stiffness, and often presents during clinical exam via decreased mobility [131, 132, 136]. In the hip, pain associated with OA occurs in the lateral and anterior thigh and groin [131].

OA affects approximately 27 million adults in the US [132]. Globally, 10% of the population over 60 has OA [138]. The prevalence of hip OA is estimated at 9.5% of males and 11.2% of females [79]. The lifetime risk of developing hip OA is 1 in 4, which is lower than the 1 in 2 lifetime risk of knee OA, yet still a significant burden [139, 140].

OA is diagnosed through a combination of patient history, clinical exam and radiographic exam [1, 132, 141, 142]. The hallmark of radiographic OA is cartilage loss, as indicated radiographically by joint space narrowing [131, 137, 143]. Asymmetric joint space narrowing indicates regional cartilage loss. In the hip, asymmetric cartilage loss often causes superior or medial migration of the femoral head [131]. Bony features characteristic of OA include the formation of osteophytes, subchondral cysts and subchondral sclerosis, which are all visible on radiographs [131, 134, 136, 143]. In the hip, bony changes also include femoral head remodeling and thickening in the cortical bone of the femoral neck [131].

Cartilage undergoes a series of changes before the dramatic wearing away seen in the final stages of OA. In early degeneration, the water content in cartilage is increased [1, 10, 134]. This may be in part due to damage to the cartilage matrix, which impairs the ability of the matrix to resist swelling forces [144-146]. Chondrocytes change during OA, undergoing proliferation and a phenotypic change to hypertrophy [1, 131, 136]. In healthy cartilage, chondrocytes are able to maintain the cartilage matrix by a combination of ECM creation and degradation. However, during the OA process, chondrocytes are unable to maintain this homeostasis and instead may contribute to matrix degeneration [137]. Cartilage PGs undergo changes in composition early in OA, including decreased concentration, decreased length and decreased aggregation [1, 134]. Following increased water content and PG changes, the matrix undergoes surface fibrillation and cracking [1, 10, 146]. Once the matrix has degenerated beyond the reparative capabilities of the chondrocytes, cartilage degeneration proceeds to full thickness cartilage loss and OA [1, 147]. The process of degeneration in OA is slow, which makes the onset of OA difficult

to capture [136]. Therefore, evaluation of the mechanical causes of OA relies on experimental and computational methods as complements to clinical studies.

Mechanical Causes of OA at the Tissue Level

At the tissue level, loading of cartilage explants provides insight into the potential mechanical causes of OA in a controlled manner. In cartilage explants, the structure of the native tissue is maintained and chondrocytes are able to achieve steady-state matrix turnover [144, 148]. Therefore, the use of cartilage explants to study the metabolic response of cartilage likely mimics the in vivo response fairly closely, while allowing more controlled loading regimes in order to isolate the effects of specific stimuli [144, 148]. The results of loading are evaluated using markers of gross structural changes and metabolic changes. Damage to the cartilage matrix can be assessed using microscopy, and sometimes even gross visual inspection. Changes to cartilage metabolism have been evaluated using several different techniques. The incorporation of radiolabeled proline and sulfate can be tracked in order to evaluate the synthesis of proteins and GAGs, respectively [149, 150]. Changes in the synthesis of matrix metalloproteinases, which degrade the cartilage extracellular matrix, can be evaluated [151, 152]. Additionally, the effect of loading on chondrocytes can be evaluated by determining the number of live and dead chondrocytes following loading [153-156]. Combinations of these outputs have been used to provide insight into the effects of specific loading regimes on the response of cartilage at the tissue level. There are three common loading regimes that have been applied to explants for understanding the mechanical causes of OA: compression, shear and high-rate impact.

The effects of compressive loading vary based on whether the load is static or dynamic. Static loading is generally detrimental to cartilage, inducing decreased GAG and protein synthesis and increased proteinase synthesis [144, 148-150, 157]. Dynamic compression causes a complex series of changes to protein and GAG synthesis, chondrocyte viability, physical integrity of the cartilage and cartilage mechanical properties depending on the frequency and level of loading [144, 148, 149, 157]. GAG and protein synthesis increases at low levels of compressive load and high levels of loading frequency [150, 152, 158-161]. The locations of GAG and protein synthesis vary depending on the frequency, suggesting that compression-induced fluid flow is an important cause of the changes in metabolism [158, 159]. When low levels of compressive loading are applied at slow rates, there is no change in protein or GAG synthesis [150, 161]. However, when high levels of compressive loading are applied at slow rates, synthesis of both protein and GAG can be inhibited [153, 162, 163]. In addition to affecting the metabolism of the cartilage matrix constituents, dynamic compression can upregulate the synthesis of proteinases [151, 152, 164, 165]. Chondrocyte apoptosis can occur during dynamic loading, with a general increase in the number of apoptotic cells with increasing strain rate and increasing load levels [153-156, 165-167]. Following higher levels of compression, the mechanical properties of cartilage may also be altered [153, 154, 156, 168, 169]. Understanding the specific mechanical cues that cause changes in cartilage following compressive loading is complicated by inhomogenous stress fields, fluid flow induced by compression and zonal variations in cartilage material properties [155, 156, 165, 168]. However, the overall picture is that the responses of cartilage to dynamic compression are complex and include both reparative

and damaging changes in metabolism, as well as gross changes to the cartilage matrix, while static compression is detrimental to cartilage.

Shear loading is a unique loading regime because it produces an isochoric deformation and therefore, no fluid flow is induced. Shear loading tends to increase the synthesis of proteoglycans and cartilage matrix proteins [149]. In bovine calf explants, shear loading increased both protein synthesis and proteoglycan synthesis for shear strain amplitudes of 3% and loading frequencies of 0.01-1.0 Hz [170-172]. When evaluated over time, aggrecan synthesis increased after just 1 hour, while all protein expression increased by 24 hours [170, 173]. At higher frequencies, 90,000 cycles of shear loading can cause decreases in both the loss and storage moduli [174]. Together, these results indicate the capacity for shear loading to cause a chondroprotective response or damage, depending on the frequency and magnitude of loading.

Impact injury loading is primarily focused on understanding the causes of posttraumatic OA. Impact injury occurs at high loading rates, and is most frequently achieved through a metal indenter on the cartilage surface. However, in terms of application to in vivo situations, it is important to note that metal-on-cartilage impact damage is distinct from cartilage-on-cartilage impact damage [175]. Although impact injury is almost always detrimental to cartilage, the extent of the damage and the magnitude of the change depend on the loading regime. Specifically, the time to peak load, peak stress, peak strain, energy of impact, number of impacts and time following impact can all affect the measured metabolic response of the tissue [176, 177]. Impact injury can cause changes in biomechanical properties, changes in the integrity of the cartilage extracellular matrix, changes in metabolic activity and decreased cell viability or

increased chondrocyte apoptosis [144, 148, 149, 167]. The location and extent of changes to cell viability in cartilage explants depend on the loading level. High energy impact causes larger numbers of apoptotic chondrocytes and more extensive matrix damage than low energy impact causes [167, 178, 179]. When the location of decreased chondrocyte viability was evaluated in porcine and bovine explants, it was found that all changes were limited to the superficial and middle zones [180, 181]. This indicates that the zonal variation in cartilage properties may be an important variable in mediating cartilage response to injurious loading. The number of viable cells also decreased with increasing time following impact [181]. The effect of increasing strain rate in bovine calf cartilage has demonstrated that with an increasing rate of impact, there is decreased cell viability, decreased compressive stiffness, decreased shear stiffness and a decreased reparative metabolic response of the tissue [153]. As with other loading regimes, the results from impact studies are difficult to translate directly to the pathogenesis of OA in humans. However, the dependency on loading parameters, as well as evidence suggesting the importance of the zonal organization of cartilage, may have important implications for the onset of OA.

In conclusion, investigations into the mechanical effects on cartilage in the tissue level indicate strong dose-dependency. These studies provide valuable starting points for the selection of mechanical variables that may be relevant to the onset of OA when using computational modeling. However, there are some limitations inherent in many of the previous studies. First, most studies are limited to animal tissue. While there are many similarities in the behavior of articular cartilage across species, differences in the response, and particularly in the precise levels of load that elicit a response, may exist.

Second, many of the studies report results for which it is difficult to decouple multiple mechanical cues. For example, many loading regimes include both matrix deformation and induced fluid and solute flow. Even during shear loading, where fluid flow is not induced, it is unlikely that the stress and strain fields within the explants are homogeneous due to inhomogeneity in the cartilage material behavior with depth. Therefore, these previous studies serve as a starting point for selecting relevant variables to report in FE models, but do not provide specific thresholds above which damage occurs. Overall, previous work indicates the role of mechanical forces in OA, but there remains a need for improved understanding of the thresholds that result in the initiation and progression of OA [182].

Causes of Hip OA

The causes of hip OA are multifactorial and are still the topic of debate. Historically, OA was distinguished between primary and secondary. Primary OA was that for which there was no predisposing factor; a disease of old age [134, 183]. Secondary OA was that for which there was a known risk factor [134]. In 1965, Murray suggested that almost all cases that had been previously diagnosed as primary hip OA were actually sequelae from subtle pathomorphology [184]. Since then, there has been rigorous debate regarding the effects of pathomorphology, including acetabular dysplasia and acetabular retroversion, on the development of hip OA [185]. In addition to pathomorphology, long-term increased loading via heavy-lifting, standing at work and obesity are implicated as causes of secondary hip OA [138, 186, 187]. Genetic factors may be important in the pathogenesis of hip OA [183]. Although there are many potential causes of hip OA, hip OA secondary to acetabular dysplasia and acetabular retroversion motivate this research.

The signs of OA secondary to hip pathomorphology in the young patient are distinct from the cartilage thinning and radiographic joint space narrowing that are typically observed in OA in the older patient. Early-stage degeneration in subjects with hip pathomorphology is characterized by focal damage rather than global cartilage thinning. Specifically, focal cartilage loss near the periphery of the acetabulum, labral tearing, labral fibrillation, cartilage delamination and cysts near the periphery of the acetabulum are observed in early stage OA resulting from hip pathomorphology [91-94, 96-99, 109, 111, 188-191]. These distinct signs of early OA in the young patient with hip pathomorphology motivate research aimed at understanding a potentially distinct pathway to OA in pathomorphologic hips.

Acetabular dysplasia is one of the more commonly recognized causes of secondary hip OA. Murray identified dysplasia as one of the causes of OA when he suggested that almost all primary hip OA is actually secondary [184]. Shortly afterwards, Solomon found that 20% of hip OA may be caused by mild acetabular dysplasia [192]. Since then, many studies have confirmed the findings that mild acetabular dysplasia causes OA [91, 139, 193-196]. Although two studies have found that OA is not secondary to acetabular dysplasia in men and in Chinese men [197, 198], the general consensus remains that acetabular dysplasia causes hip OA. Early damage in acetabular dysplasia includes labral tearing and hypertrophy, focal cartilage lesions and bone cysts near the acetabular rim [91, 93, 94, 96-99, 189].

Acetabular retroversion is clinically accepted as a cause of OA, although there is considerably less evidence than in the case of acetabular dysplasia [106]. The prevalence of radiographic measurements of retroversion is increased in patients with OA. In two

separate series of radiographs, 20% of subjects with OA also had a crossover sign, compared to 5-6% of subjects without OA [112, 113]. Another study found that hips with retroversion had smaller mean joint space, an indication of OA, than those without retroversion had [199]. Early damage in acetabular retroversion includes labral tears, as well as cartilage lesions in the posterior and peripheral acetabulum [97, 98, 113, 190, 191].

The clinical understanding that altered mechanics cause OA in acetabular dysplasia and acetabular retroversion informs current surgical interventions. These surgical interventions are designed and practiced with the aim of reducing elevated stresses [120, 200]. One of the more common surgeries for treating abnormal acetabular morphology in the adult is periacetabular osteotomy (PAO), wherein the acetabular socket is cut free from the pelvis and reoriented. PAO was developed in 1983 to treat adult acetabular dysplasia and is the preferred treatment for acetabular dysplasia at many institutions [84, 201-203]. Medium- and long-term follow-up data demonstrate the efficacy of PAO for treating acetabular dysplasia in selected patients [203-209]. The preferred surgical treatment for acetabular retroversion varies by clinic, radiographic and clinical picture of the patient, and coexisting deformities. In some cases, PAO or reverse PAO is performed [106, 111, 120]. Alternatively, if diagnosis has demonstrated that anterior femoroacetabular impingement is causing problems secondary to acetabular retroversion, the anterior rim may be debrided [106, 120]. Two short-term studies have demonstrated good outcomes for the treatment of acetabular retroversion [120, 130]. Long-term follow-up data are unavailable for surgeries correcting acetabular retroversion at this time.

Computational Modeling

The role of Modeling in Understanding the Pathogenesis of OA

Although there is substantial evidence linking altered cartilage mechanics to the onset and progression of OA, mechanics are difficult or impossible to measure directly in vivo. Cartilage contact stress and contact area can be measured using pressure-sensitive film and thin film transducers, but these technologies require the joint space to be opened. Pressure-sensitive film has been used to measure joint mechanics in the rabbit while the animal was still alive [210], but is not appropriate for use in humans. Strain measurements can be made in vivo using technologies such as magnetic resonance elastography and displacement-encoded imaging [211]. However, these techniques are limited by their long scanning times and have not yet been widely adapted in whole joint analysis.

The desire to understand cartilage mechanics coupled with the limitations of in vivo measurement has led to the adoption of computational modeling to predict cartilage mechanics. There are several types of computational models, all of which approximate solutions to systems of equations that do not have exact solutions. The most common computational models for predicting joint mechanics are discrete element analysis (DEA) and finite element analysis (FEA). Multiscale modeling is a budding field in joint mechanics, and has been used in limited studies. Each of these methods has advantages and limitations. DEA uses discrete elements, such as springs and dashpots, to represent deformable structures [212, 213]. DEA is limited to predictions at the articular contact surface, but requires the least computational time and is therefore valuable for large cohort studies [214-217]. In FEA, a continuous structure is discretized into finite

elements that have basis functions with compact support. The primary advantage of FEA over DEA is the ability of FEA to predict stress and strain at every point in the continuum. Multiscale modeling concurrently produces stress and strain across multiple physical scales [218, 219]. The term multiscale modeling has also been used to indicate modeling wherein stresses or strains from a macroscale model are used as boundary conditions for a microscale model. While multiscale modeling provides more information than continuum-level FEA, it is also more computationally expensive and has thus far only been used to evaluate cartilage mechanics in a few studies [220-225].

Verification, Validation and Parametric Analysis

Because computational models generate approximate solutions to systems of equations, verification, validation and parameter studies are important for generating confidence in model predictions. Verification is the process of ensuring that the equations being solved are being solved correctly [226-228]. This process is primarily completed during software development. Verification is completed by comparing a subset of problems with analytical solutions against the analytical solutions and by comparing model predictions against those produced by existing code. When new constitutive models are implemented, verification consists of comparing predictions with the new implementations with analytical solutions. Mesh convergence analysis, wherein the mesh resolution is increased until the solution does not change as a result of the discretization, is also part of verification.

As a complement to model verification, model validation is the process of ensuring that the equations being solved match the physical reality that is being modeled [226-228]. Model validation can be either direct or indirect. In direct validation, there is

a one-to-one comparison between the computational model and an experimental set-up, with the experimental results serving as the gold standard. In indirect validation, computational results are compared to experimental results, but the comparison is not one-to-one. For example, computational results may be compared to published experimental results. Direct validation is the preferred method of model validation because it is the more rigorous method and thus provides the greatest insight into the reliability of model predictions [229]. However, direct validation is challenging and expensive; therefore indirect validation is more frequently employed.

An additional consideration in model validation is the choice of the variable being compared between computational and experimental set-ups. Ideally, the variables selected for model validation are the same variables that the model is intended to predict. For example, if a model is intended to predict cartilage contact stress, than using cartilage contact stress for direct model validation is the most appropriate choice. Conversely, using joint kinematics to validate a model developed to predict contact stress is not appropriate. Unfortunately, it is often not possible to validate all outputs that a model is designed to predict. Therefore, as a practical matter, model validation should be undertaken with as many of the variables of interest as possible. Variables that cannot be validated should be predicted with caution, after parameter studies have been completed.

Previous model validation of whole joint models has focused on contact stress and contact area. At the hip, a single cadaveric specimen was used for model validation of contact stress and contact area [230]. At the ankle, two specimens were used for model validation [231]. At the knee, a single specimen was used for model validation [232]. All of these validation studies focused on contact stress and contact area, both because

these variables are experimentally measureable and because of the potential relevancy of these variables to joint degeneration.

As the final piece of generating confidence in model predictions, parametric analysis is the systematic evaluation of the effects of model inputs on model outputs. The aim of parametric analysis is to assess model sensitivity to perturbations in inputs, many of which are assumed or have inherent uncertainty (e.g., material coefficients, which are often determined experimentally). Because parametric analysis is used to evaluate model sensitivity, they have also been called sensitivity studies. To complete parametric analysis, model inputs are perturbed individually to assess the effects of each input independently. Although parHmetric analysis can be completed on a single model, using a series of models provides the benefit of being able to statistically evaluate the effects of model inputs.

FEA of the Human Hip Joint

Predictions of contact mechanics in the human hip have been made previously using FEA. These previous studies have included model validation, assessment of normal hips and assessment of pathomorphologic hips. A single hip joint model was directly validated and modeling assumptions were evaluated via parameter studies. For this model, a one-to-one comparison was made between experimental measurements using pressure-sensitive film and FEA predictions. Experimental and FEA results were in good qualitative and quantitative agreement. The magnitude of contact stress was compared pixel-wise between the experimental and FEA results, resulting in an RMS error in contact stress of approximately 30% [230]. In addition to direct validation, this model was used to assess the effects of model inputs on FEA predictions using parameter

studies. Cartilage was assumed to be neo-Hookean hyperelastic and both the effects of changes in the shear modulus and the effects of changes in the bulk modulus were assessed. These changes had a minimal effect on results, altering the RMS error in contact stress by ~7%. The effects of the representation of the bone were also assessed. Using rigid bones rather than deformable bones altered the RMS error in contact stress by ~30%. Conversely, using just the cortical shell rather than the cortical shell and the trabecular bone only altered the RMS error in contact stress by ~3% [230]. FEA predictions that assumed idealized geometry rather than specimen-specific geometry caused inaccurate model predictions, both in terms of stress pattern and stress magnitude [233, 234]. Overall, the effects of many modeling assumptions on the prediction of contact mechanics in the human hip have been rigorously evaluated, which allows for confident predictions of these variables in the human hip.

FEA of normal hips has provided insight into contact patterns and contact stresses in this population. Harris et al. employed the validated modeling protocol described above to predict cartilage contact stress and contact area in ten subjects without pathomorphology or hip pain. This study demonstrated large intersubject variability in contact pattern and contact stress even in a population of normal hips [235]. This study was designed to provide baseline data for the comparison of abnormal mechanics in pathologic hips.

FEA of pathologic populations suggests that hips with bony pathology experience altered cartilage mechanics. In a series of subjects who had undergone closed reduction for dysplasia at infancy, Russell et al. used FEA to predict cartilage contact mechanics during the walking gait cycle. Patients were separated into asymptomatic and

symptomatic groups and were also compared to a single normal subject. Contact area was larger in the normal hip than in the asymptomatic subjects, while peak pressure was smaller. Although contact areas were not different between asymptomatic and symptomatic subjects, peak pressure on the femoral head was larger in symptomatic subjects than in asymptomatic subjects. Overall, this study found altered cartilage mechanics in residual dysplasia compared to the normal hip, as well as altered cartilage mechanics depending on the severity and resulting symptoms in residual dysplasia [236]. Using idealized model geometry, Chegini et al. evaluated the effects of deficient acetabula characteristic of dysplasia and found that dysplasia caused localized stresses on the lateral acetabular rim [237]. Together, previous FEA studies of normal and pathomorphologic hips provide insight into the variable contact patterns in normal hips, as well as the elevations and lateral shift in contact stress in the dysplastic hip.

References

[1] Buckwalter, J. A., Mankin, H. J., and Grodzinsky, A. J., 2005, "Articular Cartilage and Osteoarthritis," Instr Course Lect, 54, pp. 465-480.

[2] Mow, V., Gu, W., and Chen, F., 2005, "Structure and Function of Articular Cartilage and Meniscus," Basic Orthopaedic Biomechanics and Mechano-Biology, V. Mow, and R. Huiskes, eds., Lippincott, Philadephia, pp. 181-258.

[3] Bhosale, A. M., and Richardson, J. B., 2008, "Articular Cartilage: Structure, Injuries and Review of Management," Br Med Bull, 87, pp. 77-95.

[4] Cohen, N. P., Foster, R. J., and Mow, V. C., 1998, "Composition and Dynamics of Articular Cartilage: Structure, Function, and Maintaining Healthy State," J Orthop Sports Phys Ther, **28**(4), pp. 203-215.

[5] Poole, A. R., Kojima, T., Yasuda, T., Mwale, F., Kobayashi, M., and Laverty, S., 2001, "Composition and Structure of Articular Cartilage: A Template for Tissue Repair," Clin Orthop Relat Res (391 Suppl), pp. S26-33.

[6] Malda, J., de Grauw, J. C., Benders, K. E., Kik, M. J., van de Lest, C. H., Creemers, L. B., Dhert, W. J., and van Weeren, P. R., 2013, "Of Mice, Men and Elephants: The Relation Between Articular Cartilage Thickness and Body Mass," PLoS One, **8**(2), p. e57683.

[7] Minas, T., 2012, "A Primer in Cartilage Repair," J Bone Joint Surg Br, 94(11 Suppl A), pp. 141-146.

[8] Ateshian, G. A., 2009, "The Role of Interstitial Fluid Pressurization in Articular Cartilage Lubrication," J Biomech, **42**(9), pp. 1163-1176.

[9] Krishnan, R., Kopacz, M., and Ateshian, G. A., 2004, "Experimental Verification of the Role of Interstitial Fluid Pressurization in Cartilage Lubrication," J Orthop Res, **22**(3), pp. 565-570.

[10] Arokoski, J. P., Jurvelin, J. S., Vaatainen, U., and Helminen, H. J., 2000, "Normal and Pathological Adaptations of Articular Cartilage to Joint Loading," Scand J Med Sci Sports, **10**(4), pp. 186-198.

[11] Ateshian, G. A., Ellis, B. J., and Weiss, J. A., 2007, "Equivalence Between Short-Time Biphasic and Incompressible Elastic Material Responses," J Biomech Eng, **129**(3), pp. 405-412.

[12] Wong, M., Ponticiello, M., Kovanen, V., and Jurvelin, J. S., 2000, "Volumetric Changes of Articular Cartilage During Stress Relaxation in Unconfined Compression," J Biomech, **33**(9), pp. 1049-1054.

[13] Caligaris, M., and Ateshian, G. A., 2008, "Effects of Sustained Interstitial Fluid Pressurization Under Migrating Contact Area, and Boundary Lubrication by Synovial Fluid, on Cartilage Friction," Osteoarthritis Cartilage, **16**(10), pp. 1220-1227.

[14] Schmidt, T. A., and Sah, R. L., 2007, "Effect of Synovial Fluid on Boundary Lubrication of Articular Cartilage," Osteoarthritis Cartilage, **15**(1), pp. 35-47.

[15] Roughley, P. J., 2006, "The Structure and Function of Cartilage Proteoglycans," Eur Cell Mater, 12, pp. 92-101.

[16] DiSilvestro, M. R., Zhu, Q., Wong, M., Jurvelin, J. S., and Suh, J. K., 2001, "Biphasic Poroviscoelastic Simulation of the Unconfined Compression of Articular Cartilage: I--Simultaneous Prediction of Reaction Force and Lateral Displacement," J Biomech Eng, **123**(2), pp. 191-197.

[17] Huang, C. Y., Soltz, M. A., Kopacz, M., Mow, V. C., and Ateshian, G. A., 2003, "Experimental Verification of the Roles of Intrinsic Matrix Viscoelasticity and Tension-Compression Nonlinearity in the Biphasic Response of Cartilage," J Biomech Eng, **125**(1), pp. 84-93.

[18] Mak, A. F., 1986, "The Apparent Viscoelastic Behavior of Articular Cartilage--The Contributions from the Intrinsic Matrix Viscoelasticity and Interstitial Fluid Flows," J Biomech Eng, **108**(2), pp. 123-130.

[19] Mow, V. C., Kuei, S. C., Lai, W. M., and Armstrong, C. G., 1980, "Biphasic Creep and Stress Relaxation of Articular Cartilage in Compression? Theory and Experiments," J Biomech Eng, **102**(1), pp. 73-84.

[20] Huang, C. Y., Stankiewicz, A., Ateshian, G. A., and Mow, V. C., 2005, "Anisotropy, Inhomogeneity, and Tension-Compression Nonlinearity of Human Glenohumeral Cartilage in Finite Deformation," J Biomech, **38**(4), pp. 799-809.

[21] Abazari, A., Elliott, J. A., McGann, L. E., and Thompson, R. B., 2012, "MR Spectroscopy Measurement of the Diffusion of Dimethyl Sulfoxide in Articular Cartilage and Comparison to Theoretical Predictions," Osteoarthritis Cartilage, **20**(9), pp. 1004-1010.

[22] Burstein, D., Gray, M. L., Hartman, A. L., Gipe, R., and Foy, B. D., 1993, "Diffusion of Small Solutes in Cartilage as Measured by Nuclear Magnetic Resonance (NMR) Spectroscopy and Imaging," J Orthop Res, **11**(4), pp. 465-478.

[23] Evans, R. C., and Quinn, T. M., 2005, "Solute Diffusivity Correlates with Mechanical Properties and Matrix Density of Compressed Articular Cartilage," Arch Biochem Biophys, **442**(1), pp. 1-10.

[24] Mauck, R. L., Hung, C. T., and Ateshian, G. A., 2003, "Modeling of Neutral Solute Transport in a Dynamically Loaded Porous Permeable Gel: Implications for

Articular Cartilage Biosynthesis and Tissue Engineering," J Biomech Eng, **125**(5), pp. 602-614.

[25] Buckley, M. R., Gleghorn, J. P., Bonassar, L. J., and Cohen, I., 2008, "Mapping the Depth Dependence of Shear Properties in Articular Cartilage," J Biomech, **41**(11), pp. 2430-2437.

[26] Chen, A. C., Bae, W. C., Schinagl, R. M., and Sah, R. L., 2001, "Depth- and Strain-Dependent Mechanical and Electromechanical Properties of Full-Thickness Bovine Articular Cartilage in Confined Compression," J Biomech, **34**(1), pp. 1-12.

[27] Maroudas, A., Bayliss, M. T., and Venn, M. F., 1980, "Further Studies on the Composition of Human Femoral Head Cartilage," Ann Rheum Dis, **39**(5), pp. 514-523.

[28] Mow, V. C., and Guo, X. E., 2002, "Mechano-Electrochemical Properties of Articular Cartilage: Their Inhomogeneities and Anisotropies," Annu Rev Biomed Eng, **4**(1), pp. 175-209.

[29] Schinagl, R. M., Gurskis, D., Chen, A. C., and Sah, R. L., 1997, "Depth-Dependent Confined Compression Modulus of Full-Thickness Bovine Articular Cartilage," J Orthop Res, **15**(4), pp. 499-506.

[30] Setton, L. A., Zhu, W., and Mow, V. C., 1993, "The Biphasic Poroviscoelastic Behavior of Articular Cartilage: Role of the Surface Zone in Governing the Compressive Behavior," J Biomech, **26**(4-5), pp. 581-592.

[31] Athanasiou, K. A., Agarwal, A., and Dzida, F. J., 1994, "Comparative Study of the Intrinsic Mechanical Properties of the Human Acetabular and Femoral Head Cartilage," J Orthop Res, **12**(3), pp. 340-349.

[32] Athanasiou, K. A., Agarwal, A., Muffoletto, A., Dzida, F. J., Constantinides, G., and Clem, M., 1995, "Biomechanical Properties of Hip Cartilage in Experimental Animal Models," Clin Orthop Relat Res (316), pp. 254-266.

[33] Demarteau, O., Pillet, L., Inaebnit, A., Borens, O., and Quinn, T. M., 2006, "Biomechanical Characterization and In Vitro Mechanical Injury of Elderly Human Femoral Head Cartilage: Comparison to Adult Bovine Humeral Head Cartilage," Osteoarthritis Cartilage, **14**(6), pp. 589-596.

[34] Shepherd, D. E., and Seedhom, B. B., 1999, "The 'Instantaneous' Compressive Modulus of Human Articular Cartilage in Joints of the Lower Limb," Rheumatology (Oxford), **38**(2), pp. 124-132.

[35] Treppo, S., Koepp, H., Quan, E. C., Cole, A. A., Kuettner, K. E., and Grodzinsky, A. J., 2000, "Comparison of Biomechanical and Biochemical Properties of Cartilage from Human Knee and Ankle Pairs," J Orthop Res, **18**(5), pp. 739-748.

[36] Holzapfel, G., 2000, *Nonlinear Solid Mechanics: A Continuum Approach for Engineering*, John Wiley & Sons Ltd, West Sussex.

[37] Taylor, Z. A., and Miller, K., 2006, "Constitutive Modeling of Cartilaginous Tissues: a Review," J Appl Biomech, **22**(3), pp. 212-229.

[38] Fung, Y. C., 1993, *Biomechanics: Mechanical Poperties of Living Tissues,* Springer-Verlag, New York.

[39] Keenan, K. E., Pal, S., Lindsey, D. P., Besier, T. F., and Beaupre, G. S., 2012, "A Viscoelastic Constitutive Model Can Accurately Represent Entire Creep Indentation Tests of Human Patella Cartilage," J Appl Biomech.

[40] Park, S., and Ateshian, G. A., 2006, "Dynamic Response of Immature Bovine Articular Cartilage in Tension and Compression, and Nonlinear Viscoelastic Modeling of the Tensile Response," J Biomech Eng, **128**(4), pp. 623-630.

[41] Thomas, G. C., Asanbaeva, A., Vena, P., Sah, R. L., and Klisch, S. M., 2009, "A Nonlinear Constituent Based Viscoelastic Model for Articular Cartilage and Analysis of Tissue Remodeling Due to Altered Glycosaminoglycan-Collagen Interactions," J Biomech Eng, **131**(10), p. 101002.

[42] Ateshian, G. A., Albro, M. B., Maas, S., and Weiss, J. A., 2011, "Finite Element Implementation of Mechanochemical Phenomena in Neutral Deformable Porous Media Under Finite Deformation," J Biomech Eng, **133**(8), p. 081005.

[43] Ateshian, G. A., Chahine, N. O., Basalo, I. M., and Hung, C. T., 2004, "The Correspondence Between Equilibrium Biphasic and Triphasic Material Properties in Mixture Models of Articular Cartilage," J Biomech, **37**(3), pp. 391-400.

[44] Ateshian, G. A., Warden, W. H., Kim, J. J., Grelsamer, R. P., and Mow, V. C., 1997, "Finite Deformation Biphasic Material Properties of Bovine Articular Cartilage from Confined Compression Experiments," J Biomech, **30**(11-12), pp. 1157-1164.

[45] DiSilvestro, M. R., and Suh, J. K., 2001, "A Cross-Validation of the Biphasic Poroviscoelastic Model of Articular Cartilage in Unconfined Compression, Indentation, and Confined Compression," J Biomech, **34**(4), pp. 519-525.

[46] DiSilvestro, M. R., Zhu, Q., and Suh, J. K., 2001, "Biphasic Poroviscoelastic Simulation of the Unconfined Compression of Articular Cartilage: II--Effect of Variable Strain Rates," J Biomech Eng, **123**(2), pp. 198-200.

[47] Fortin, M., Soulhat, J., Shirazi-Adl, A., Hunziker, E. B., and Buschmann, M. D., 2000, "Unconfined Compression of Articular Cartilage: Nonlinear Behavior and Comparison with a Fibril-Reinforced Biphasic Model," J Biomech Eng, **122**(2), pp. 189-195.

[48] Gu, W. Y., Lai, W. M., and Mow, V. C., 1998, "A Mixture Theory for Charged-Hydrated Soft Tissues Containing Multi-Electrolytes: Passive Transport and Swelling Behaviors," J Biomech Eng, **120**(2), pp. 169-180.

[49] Holmes, M. H., 1986, "Finite Deformation of Soft Tissue: Analysis of a Mixture Model in Uni-Axial Compression," J Biomech Eng, **108**(4), pp. 372-381.

[50] Holmes, M. H., and Mow, V. C., 1990, "The Nonlinear Characteristics of Soft Gels and Hydrated Connective Tissues in Ultrafiltration," J Biomech, **23**(11), pp. 1145-1156.

[51] Huyghe, J. M., and Janssen, J. D., 1997, "Quadriphasic Mechanics of Swelling Incompressible Porous Media," Int J Eng Sci, **35**(8), pp. 793-802.

[52] Lai, W. M., Hou, J. S., and Mow, V. C., 1991, "A Triphasic Theory for the Swelling and Deformation Behaviors of Articular Cartilage," J Biomech Eng, **113**(3), pp. 245-258.

[53] Lai, W. M., and Mow, V. C., 1980, "Drag-Induced Compression of Articular Cartilage During a Permeation Experiment," Biorheology, **17**(1-2), pp. 111-123.

[54] Lai, W. M., Mow, V. C., and Roth, V., 1981, "Effects of Nonlinear Strain-Dependent Permeability and Rate of Compression on the Stress Behavior of Articular Cartilage," J Biomech Eng, **103**(2), pp. 61-66.

[55] Li, G., Gil, J., Kanamori, A., and Woo, S. L., 1999, "A Validated Three-Dimensional Computational Model of a Human Knee Joint," J Biomech Eng, **121**(6), pp. 657-662.

[56] Li, L. P., Soulhat, J., Buschmann, M. D., and Shirazi-Adl, A., 1999, "Nonlinear Analysis of Cartilage in Unconfined Ramp Compression Using a Fibril Reinforced Poroelastic Model," Clin Biomech (Bristol, Avon), **14**(9), pp. 673-682.

[57] Sengers, B. G., Oomens, C. W., and Baaijens, F. P., 2004, "An Integrated Finite-Element Approach to Mechanics, Transport and Biosynthesis in Tissue Engineering," J Biomech Eng, **126**(1), pp. 82-91.

[58] Wilson, W., van Donkelaar, C. C., and Huyghe, J. M., 2005, "A Comparison Between Mechano-Electrochemical and Biphasic Swelling Theories for Soft Hydrated Tissues," J Biomech Eng, **127**(1), pp. 158-165.

[59] Huang, C. Y., Mow, V. C., and Ateshian, G. A., 2001, "The Role of Flow-Independent Viscoelasticity in the Biphasic Tensile and Compressive Responses of Articular Cartilage," J Biomech Eng, **123**(5), pp. 410-417.

[60] Pierce, D. M., Trobin, W., Trattnig, S., Bischof, H., and Holzapfel, G. A., 2009, "A Phenomenological Approach Toward Patient-Specific Computational Modeling of

Articular Cartilage Including Collagen Fiber Tracking," J Biomech Eng, **131**(9), p. 091006.

[61] Czerny, C., Hofmann, S., Urban, M., Tschauner, C., Neuhold, A., Pretterklieber, M., Recht, M. P., and Kramer, J., 1999, "MR Arthrography of the Adult Acetabular Capsular-Labral Complex: Correlation with Surgery and Anatomy," Am J Roentgenol, **173**(2), pp. 345-349.

[62] Keene, G. S., and Villar, R. N., 1994, "Arthroscopic Anatomy of the Hip: An in Vivo Study," Arthroscopy, **10**(4), pp. 392-399.

[63] Lecouvet, F. E., Vande Berg, B. C., Malghem, J., Lebon, C. J., Moysan, P., Jamart, J., and Maldague, B. E., 1996, "MR Imaging of the Acetabular Labrum: Variations in 200 Asymptomatic Hips," Am J Roentgenol, **167**(4), pp. 1025-1028.

[64] Won, Y. Y., Chung, I. H., Chung, N. S., and Song, K. H., 2003, "Morphological Study on the Acetabular Labrum," Yonsei Med J, **44**(5), pp. 855-862.

[65] Seldes, R. M., Tan, V., Hunt, J., Katz, M., Winiarsky, R., and Fitzgerald, R. H., Jr., 2001, "Anatomy, Histologic Features, and Vascularity of the Adult Acetabular Labrum," Clin Orthop Relat Res (382), pp. 232-240.

[66] Petersen, W., Petersen, F., and Tillmann, B., 2003, "Structure and Vascularization of the Acetabular Labrum with Regard to the Pathogenesis and Healing of Labral Lesions," Arch Orthop Trauma Surg, **123**(6), pp. 283-288.

[67] Dinauer, P. A., Murphy, K. P., and Carroll, J. F., 2004, "Sublabral Sulcus at the Posteroinferior Acetabulum: A Potential Pitfall in MR Arthrography Diagnosis of Acetabular Labral Tears," Am J Roentgenol, **183**(6), pp. 1745-1753.

[68] Saddik, D., Troupis, J., Tirman, P., O'Donnell, J., and Howells, R., 2006, "Prevalence and Location of Acetabular Sublabral Sulci at Hip Arthroscopy with Retrospective MRI Review," Am J Roentgenol, **187**(5), pp. W507-511.

[69] Studler, U., Kalberer, F., Leunig, M., Zanetti, M., Hodler, J., Dora, C., and Pfirrmann, C. W., 2008, "MR Arthrography of the Hip: Differentiation Between an Anterior Sublabral Recess as a Normal Variant and a Labral Tear," Radiology, **249**(3), pp. 947-954.

[70] Safran, M. R., 2010, "The Acetabular Labrum: Anatomic and Functional Characteristics and Rationale for Surgical Intervention," J Am Acad Orthop Surg, **18**(6), pp. 338-345.

[71] Ferguson, S. J., Bryant, J. T., and Ito, K., 2001, "The Material Properties of the Bovine Acetabular Labrum," J Orthop Res, **19**(5), pp. 887-896.

[72] Ishiko, T., Naito, M., and Moriyama, S., 2005, "Tensile Properties of the Human Acetabular Labrum-The First Report," J Orthop Res, **23**(6), pp. 1448-1453.

[73] Smith, C. D., Masouros, S., Hill, A. M., Amis, A. A., and Bull, A. M. J., 2009, "A Biomechanical Basis for Tears of the Human Acetabular Labrum," Br J Sports Med, **43**(8), pp. 574-578.

[74] Dhollander, A. A., Lambrecht, S., Verdonk, P. C., Audenaert, E. A., Almqvist, K. F., Pattyn, C., Verdonk, R., Elewaut, D., and Verbruggen, G., 2012, "First Insights into Human Acetabular Labrum Cell Metabolism," Osteoarthritis Cartilage, **20**(7), pp. 670-677.

[75] Bittersohl, B., Hosalkar, H. S., and Wenger, D. R., 2012, "Surgical Treatment of Hip Dysplasia in Children and Adolescents," Orthop Clin N Am, **43**(3), pp. 301-315.

[76] Dezateux, C., and Rosendahl, K., 2007, "Developmental Dysplasia of the Hip," Lancet, **369**(9572), pp. 1541-1552.

[77] Engesaeter, I. O., Laborie, L. B., Lehmann, T. G., Fevang, J. M., Lie, S. A., Engesaeter, L. B., and Rosendahl, K., 2013, "Prevalence of Radiographic Findings Associated with Hip Dysplasia in a Population-Based Cohort of 2081 19-Year-Old Norwegians," Bone Joint J, **95-B**(2), pp. 279-285.

[78] Inoue, K., Wicart, P., Kawasaki, T., Huang, J., Ushiyama, T., Hukuda, S., and Courpied, J., 2000, "Prevalence of Hip Osteoarthritis and Acetabular Dysplasia in French and Japanese Adults," Rheumatology (Oxford), **39**(7), pp. 745-748.

[79] Gosvig, K. K., Jacobsen, S., Sonne-Holm, S., Palm, H., and Troelsen, A., 2010, "Prevalence of Malformations of the Hip Joint and their Relationship to Sex, Groin Pain, and Risk of Osteoarthritis: A Population-Based Survey," J Bone Joint Surg Am, **92**(5), pp. 1162-1169.

[80] de Hundt, M., Vlemmix, F., Bais, J. M., Hutton, E. K., de Groot, C. J., Mol, B. W., and Kok, M., 2012, "Risk Factors for Developmental Dysplasia of the Hip: A Meta-Analysis," Eur J Obstet Gynecol Reprod Biol, **165**(1), pp. 8-17.

[81] Wilkinson, J. A., 1992, "Etiologic Factors in Congenital Displacement of the Hip and Myelodysplasia," Clin Orthop Relat Res (281), pp. 75-83.

[82] Feldman, G. J., Peters, C. L., Erickson, J. A., Hozack, B. A., Jaraha, R., and Parvizi, J., 2012, "Variable Expression and Incomplete Penetrance of Developmental Dysplasia of the Hip: Clinical Challenge in a 71-Member Multigeneration Family," J Arthroplasty, **27**(4), pp. 527-532.

[83] Wiberg, G., 1953, "Shelf Operation in Congenital Dysplasia of the Acetabulum and in Subluxation and Dislocation of the Hip," J Bone Joint Surg Am, **35-A**(1), pp. 65-80.

[84] Peters, C. L., and Erickson, J., 2006, "The Etiology and Treatment of Hip Pain in the Young Adult," J Bone Joint Surg Am, **88** Suppl 4, pp. 20-26.

[85] Wiberg, G., 1939, "Studies on Dysplastic Acetabula and Congenital Subluxation of the Hip Joint, with Special Reference to the Complication of Osteo-Arthritis.," Acta Chir Scand, **83**(Supplementum 58), pp. 1-135.

[86] Clohisy, J. C., Carlisle, J. C., Beaule, P. E., Kim, Y. J., Trousdale, R. T., Sierra, R. J., Leunig, M., Schoenecker, P. L., and Millis, M. B., 2008, "A Systematic Approach to the Plain Radiographic Evaluation of the Young Adult Hip," J Bone Joint Surg Am, **90** Suppl 4, pp. 47-66.

[87] Anderson, L. A., Gililland, J., Pelt, C., Linford, S., Stoddard, G. J., and Peters, C. L., 2011, "Center Edge Angle Measurement for Hip Preservation Surgery: Technique and Caveats," Orthopedics, **34**(2), p. 86.

[88] Sharp, I. K., 1961, "Acetabular Dysplasia the Acetabular Angle," J Bone Joint Surg Br, **43**(2), pp. 268-272.

[89] Tönnis, D., Legal, H., and Graf, R., 1987, *Congenital Dysplasia and Dislocation of the Hip in Children and Adults*, Springer-Verlag Berlin, Germany.

[90] Trendelenburg, F., 1998, "Trendelenburg's Test: 1895," Clin Orthop Relat Res (355), pp. 3-7.

[91] Klaue, K., Durnin, C. W., and Ganz, R., 1991, "The Acetabular Rim Syndrome. A Clinical Presentation of Dysplasia of the Hip," J Bone Joint Surg Br, **73**(3), pp. 423-429.

[92] Wenger, D. E., Kendell, K. R., Miner, M. R., and Trousdale, R. T., 2004, "Acetabular Labral Tears Rarely Occur in the Absence of Bony Abnormalities," Clin Orthop Relat Res (426), pp. 145-150.

[93] Dorrell, J. H., and Catterall, A., 1986, "The Torn Acetabular Labrum," J Bone Joint Surg Br, **68**(3), pp. 400-403.

[94] Fujii, M., Nakashima, Y., Jingushi, S., Yamamoto, T., Noguchi, Y., Suenaga, E., and Iwamoto, Y., 2009, "Intraarticular Findings in Symptomatic Developmental Dysplasia of the Hip," J Pediatr Orthop, **29**(1), pp. 9-13.

[95] Guevara, C. J., Pietrobon, R., Carothers, J. T., Olson, S. A., and Vail, T. P., 2006, "Comprehensive Morphologic Evaluation of the Hip in Patients with Symptomatic Labral Tear," Clin Orthop Relat Res, 453, pp. 277-285.

[96] McCarthy, J., Noble, P., Aluisio, F. V., Schuck, M., Wright, J., and Lee, J. A., 2003, "Anatomy, Pathologic Features, and Treatment of Acetabular Labral Tears," Clin Orthop Relat Res (406), pp. 38-47.

[97] Peelle, M. W., Della Rocca, G. J., Maloney, W. J., Curry, M. C., and Clohisy, J. C., 2005, "Acetabular and Femoral Radiographic Abnormalities Associated with Labral Tears," Clin Orthop Relat Res, 441, pp. 327-333.

[98] Groh, M. M., and Herrera, J., 2009, "A Comprehensive Review of Hip Labral Tears," Curr Rev Musculoskelet Med, **2**(2), pp. 105-117.

[99] Leunig, M., Podeszwa, D., Beck, M., Werlen, S., and Ganz, R., 2004, "Magnetic Resonance Arthrography of Labral Disorders in Hips with Dysplasia and Impingement," Clin Orthop Relat Res (418), pp. 74-80.

[100] Leunig, M., Werlen, S., Ungersbock, A., Ito, K., and Ganz, R., 1997, "Evaluation of the Acetabular Labrum by MR Arthrography," J Bone Joint Surg Br, **79**(2), pp. 230-234.

[101] Sugano, N., Noble, P. C., Kamaric, E., Salama, J. K., Ochi, T., and Tullos, H. S., 1998, "The Morphology of the Femur in Developmental Dysplasia of the Hip," J Bone Joint Surg Br, **80**(4), pp. 711-719.

[102] Noble, P. C., Kamaric, E., Sugano, N., Matsubara, M., Harada, Y., Ohzono, K., and Paravic, V., 2003, "Three-Dimensional Shape of the Dysplastic Femur: Implications for THR," Clin Orthop Relat Res (417), pp. 27-40.

[103] Steppacher, S. D., Tannast, M., Werlen, S., and Siebenrock, K. A., 2008, "Femoral Morphology Differs Between Deficient and Excessive Acetabular Coverage," Clin Orthop Relat Res, **466**(4), pp. 782-790.

[104] Clohisy, J. C., Nunley, R. M., Carlisle, J. C., and Schoenecker, P. L., 2009, "Incidence and Characteristics of Femoral Deformities in the Dysplastic Hip," Clin Orthop Relat Res, **467**(1), pp. 128-134.

[105] Reynolds, D., Lucas, J., and Klaue, K., 1999, "Retroversion of the Acetabulum. A Cause of Hip Pain," J Bone Joint Surg Br, **81**(2), pp. 281-288.

[106] Sierra, R. J., 2013, "The Management of Acetabular Retroversion with Reverse Periacetabular Osteotomy," Instr Course Lect, **62**, pp. 305-313.

[107] Dandachli, W., Islam, S. U., Liu, M., Richards, R., Hall-Craggs, M., and Witt, J., 2009, "Three-Dimensional CT Analysis to Determine Acetabular Retroversion and the Implications for the Management of Femoro-Acetabular Impingement," J Bone Joint Surg Br, **91**(8), pp. 1031-1036.

[108] Hansen, B. J., Harris, M. D., Anderson, L. A., Peters, C. L., Weiss, J. A., and Anderson, A. E., 2012, "Correlation Between Radiographic Measures of Acetabular Morphology with Three-Dimensional Femoral Head Coverage in Patients with Acetabular Retroversion," Acta Orthop, **83**(3), pp. 233-239.

[109] Ganz, R., Leunig, M., Leunig-Ganz, K., and Harris, W. H., 2008, "The Etiology of Osteoarthritis of the Hip: An Integrated Mechanical Concept," Clin Orthop Relat Res, **466**(2), pp. 264-272.

[110] Tannast, M., Siebenrock, K. A., and Anderson, S. E., 2007, "Femoroacetabular Impingement: Radiographic Diagnosis--What the Radiologist Should Know," Am J Roentgenol, **188**(6), pp. 1540-1552.

[111] Tonnis, D., and Heinecke, A., 1999, "Acetabular and Femoral Anteversion: Relationship with Osteoarthritis of the Hip," J Bone Joint Surg Am, **81**(12), pp. 1747-1770.

[112] Ezoe, M., Naito, M., and Inoue, T., 2006, "The Prevalence of Acetabular Retroversion Among Various Disorders of the Hip," J Bone Joint Surg Am, **88**(2), pp. 372-379.

[113] Giori, N. J., and Trousdale, R. T., 2003, "Acetabular Retroversion is Associated with Osteoarthritis of the Hip," Clin Orthop Relat Res (417), pp. 263-269.

[114] Laborie, L. B., Lehmann, T. G., Engesaeter, I. O., Eastwood, D. M., Engesaeter, L. B., and Rosendahl, K., 2011, "Prevalence of Radiographic Findings Thought to be Associated with Femoroacetabular Impingement in a Population-Based Cohort of 2081 Healthy Young Adults," Radiology, **260**(2), pp. 494-502.

[115] Perreira, A. C., Hunter, J. C., Laird, T., and Jamali, A. A., 2011, "Multilevel Measurement of Acetabular Version Using 3-D CT-Generated Models: Implications for Hip Preservation Surgery," Clin Orthop Relat Res, **469**(2), pp. 552-561.

[116] Werner, C. M., Copeland, C. E., Ruckstuhl, T., Stromberg, J., Seifert, B., and Turen, C. H., 2008, "Prevalence of Acetabular Dome Retroversion in a Mixed Race Adult Trauma Patient Population," Acta Orthop Belg, **74**(6), pp. 766-772.

[117] Cobb, J., Logishetty, K., Davda, K., and Iranpour, F., 2010, "Cams and Pincer Impingement are Distinct, Not Mixed: The Acetabular Pathomorphology of Femoroacetabular Impingement," Clin Orthop Relat Res, **468**(8), pp. 2143-2151.

[118] Pollard, T. C., Villar, R. N., Norton, M. R., Fern, E. D., Williams, M. R., Murray, D. W., and Carr, A. J., 2010, "Genetic Influences in the Aetiology of Femoroacetabular Impingement: A Sibling Study," J Bone Joint Surg Br, **92**(2), pp. 209-216.

[119] Hogervorst, T., Eilander, W., Fikkers, J. T., and Meulenbelt, I., 2012, "Hip Ontogenesis: How Evolution, Genes, and Load History Shape Hip Morphotype and Cartilotype," Clin Orthop Relat Res, **470**(12), pp. 3284-3296.

[120] Peters, C. L., Anderson, L. A., Erickson, J. A., Anderson, A. E., and Weiss, J. A., 2011, "An Algorithmic Approach to Surgical Decision Making in Acetabular Retroversion," Orthopedics, **34**(1), p. 10.

[121] Kakaty, D. K., Fischer, A. F., Hosalkar, H. S., Siebenrock, K. A., and Tannast, M., 2010, "The ischial spine sign: does pelvic tilt and rotation matter?," Clin Orthop Relat Res, **468**(3), pp. 769-774.

[122] Siebenrock, K. A., Kalbermatten, D. F., and Ganz, R., 2003, "Effect of Pelvic Tilt on Acetabular Retroversion: A Study of Pelves from Cadavers," Clin Orthop Relat Res (407), pp. 241-248.

[123] Zaltz, I., Kelly, B. T., Hetsroni, I., and Bedi, A., 2012, "The Crossover Sign Overestimates Acetabular Retroversion," Clin Orthop Relat Res.

[124] Bircher, M. D., 1999, "Retroversion of the Acetabulum," J Bone Joint Surg Br, **81**(4), pp. 743-744.

[125] Fujii, M., Nakashima, Y., Yamamoto, T., Mawatari, T., Motomura, G., Matsushita, A., Matsuda, S., Jingushi, S., and Iwamoto, Y., 2010, "Acetabular Retroversion in Developmental Dysplasia of the Hip," J Bone Joint Surg Am, **92**(4), pp. 895-903.

[126] Li, P. L., and Ganz, R., 2003, "Morphologic Features of Congenital Acetabular Dysplasia: One in Six is Retroverted," Clin Orthop Relat Res (416), pp. 245-253.

[127] Palmer, W. E., 2010, "Femoroacetabular Impingement: Caution is Warranted in Making Imaging-Based Assumptions and Diagnoses," Radiology, **257**(1), pp. 4-7.

[128] Clohisy, J. C., Knaus, E. R., Hunt, D. M., Lesher, J. M., Harris-Hayes, M., and Prather, H., 2009, "Clinical Presentation of Patients with Symptomatic Anterior Hip Impingement," Clin Orthop Relat Res, **467**(3), pp. 638-644.

[129] Lequesne, M., and Bellaiche, L., 2012, "Anterior Femoroacetabular Impingement: an Update," Joint Bone Spine, **79**(3), pp. 249-255.

[130] Siebenrock, K. A., Schoeniger, R., and Ganz, R., 2003, "Anterior Femoro-Acetabular Impingement Due to Acetabular Retroversion. Treatment with Periacetabular Osteotomy," J Bone Joint Surg Am, **85-A**(2), pp. 278-286.

[131] Gupta, K. B., Duryea, J., and Weissman, B. N., 2004, "Radiographic Evaluation of Osteoarthritis," Radiol Clin North Am, **42**(1), pp. 11-41, v.

[132] Buckwalter, J. A., Saltzman, C., and Brown, T., 2004, "The Impact of Osteoarthritis: Implications for Research," Clin Orthop Relat Res (427 Suppl), pp. S6-15.

[133] de Lange-Brokaar, B. J., Ioan-Facsinay, A., van Osch, G. J., Zuurmond, A. M., Schoones, J., Toes, R. E., Huizinga, T. W., and Kloppenburg, M., 2012, "Synovial Inflammation, Immune Cells and their Cytokines in Osteoarthritis: A Review," Osteoarthritis Cartilage, **20**(12), pp. 1484-1499.

[134] Adatia, A., Rainsford, K. D., and Kean, W. F., 2012, "Osteoarthritis of the Knee and Hip. Part I: Aetiology and Pathogenesis as a Basis for Pharmacotherapy," J Pharm Pharmacol, **64**(5), pp. 617-625.

[135] Berenbaum, F., 2013, "Osteoarthritis as an Inflammatory Disease (Osteoarthritis is Not Osteoarthrosis!)," Osteoarthritis Cartilage, **21**(1), pp. 16-21.

[136] Poole, A. R., 2012, "Osteoarthritis as a Whole Joint Disease," H S S J, **8**(1), pp. 4-6.

[137] van der Kraan, P. M., 2012, "Osteoarthritis Year 2012 in Review: Biology," Osteoarthritis Cartilage, **20**(12), pp. 1447-1450.

[138] Murphy, L., and Helmick, C. G., 2012, "The Impact of Osteoarthritis in the United States: A Population-Health Perspective," Am J Nurs, **112**(3 Suppl 1), pp. S13-19.

[139] Murphy, L. B., Helmick, C. G., Schwartz, T. A., Renner, J. B., Tudor, G., Koch, G. G., Dragomir, A. D., Kalsbeek, W. D., Luta, G., and Jordan, J. M., 2010, "One in Four People May Develop Symptomatic Hip Osteoarthritis in His or Her Lifetime," Osteoarthritis Cartilage, **18**(11), pp. 1372-1379.

[140] Murphy, L., Schwartz, T. A., Helmick, C. G., Renner, J. B., Tudor, G., Koch, G., Dragomir, A., Kalsbeek, W. D., Luta, G., and Jordan, J. M., 2008, "Lifetime Risk of Symptomatic Knee Osteoarthritis," Arthritis Rheum, **59**(9), pp. 1207-1213.

[141] Salaffi, F., Carotti, M., Stancati, A., and Grassi, W., 2003, "Radiographic Assessment of Osteoarthritis: Analysis of Disease Progression," Aging Clin Exp Res, **15**(5), pp. 391-404.

[142] Lawrence, R. C., Felson, D. T., Helmick, C. G., Arnold, L. M., Choi, H., Deyo, R. A., Gabriel, S., Hirsch, R., Hochberg, M. C., Hunder, G. G., Jordan, J. M., Katz, J. N., Kremers, H. M., and Wolfe, F., 2008, "Estimates of the Prevalence of Arthritis and Other Rheumatic Conditions in the United States. Part II," Arthritis Rheum, **58**(1), pp. 26-35.

[143] Hochberg, M. C., 2012, "Osteoarthritis Year 2012 in Review: Clinical," Osteoarthritis Cartilage, **20**(12), pp. 1465-1469.

[144] Guilak, F., Fermor, B., Keefe, F. J., Kraus, V. B., Olson, S. A., Pisetsky, D. S., Setton, L. A., and Weinberg, J. B., 2004, "The Role of Biomechanics and Inflammation in Cartilage Injury and Repair," Clin Orthop Relat Res (423), pp. 17-26.

[145] Setton, L. A., Elliott, D. M., and Mow, V. C., 1999, "Altered Mechanics of Cartilage with Osteoarthritis: Human Osteoarthritis and an Experimental Model of Joint Degeneration," Osteoarthritis Cartilage, **7**(1), pp. 2-14.

[146] Wilson, W., van Donkelaar, C. C., van Rietbergen, R., and Huiskes, R., 2005, "The Role of Computational Models in the Search for the Mechanical Behavior and Damage Mechanisms of Articular Cartilage," Med Eng Phys, **27**(10), pp. 810-826.

[147] Goldring, M. B., 2012, "Articular Cartilage Degradation in Osteoarthritis," H S S J, **8**(1), pp. 7-9.

[148] Guilak, F., 2011, "Biomechanical Factors in Osteoarthritis," Best Pract Res Clin Rheumatol, **25**(6), pp. 815-823.

[149] Grodzinsky, A. J., Levenston, M. E., Jin, M., and Frank, E. H., 2000, "Cartilage Tissue Remodeling in Response to Mechanical Forces," Annu Rev Biomed Eng, 2, pp. 691-713.

[150] Sah, R. L., Kim, Y. J., Doong, J. Y., Grodzinsky, A. J., Plaas, A. H., and Sandy, J. D., 1989, "Biosynthetic Response of Cartilage Explants to Dynamic Compression," J Orthop Res, **7**(5), pp. 619-636.

[151] Gosset, M., Berenbaum, F., Levy, A., Pigenet, A., Thirion, S., Cavadias, S., and Jacques, C., 2008, "Mechanical Stress and Prostaglandin E2 Synthesis in Cartilage," Biorheology, **45**(3-4), pp. 301-320.

[152] Gosset, M., Berenbaum, F., Levy, A., Pigenet, A., Thirion, S., Saffar, J. L., and Jacques, C., 2006, "Prostaglandin E2 Synthesis in Cartilage Explants Under Compression: mPGES-1 is a Mechanosensitive Gene," Arthritis Res Ther, **8**(4), p. R135.

[153] Kurz, B., Jin, M., Patwari, P., Cheng, D. M., Lark, M. W., and Grodzinsky, A. J., 2001, "Biosynthetic Response and Mechanical Properties of Articular Cartilage After Injurious Compression," J Orthop Res, **19**(6), pp. 1140-1146.

[154] Loening, A. M., James, I. E., Levenston, M. E., Badger, A. M., Frank, E. H., Kurz, B., Nuttall, M. E., Hung, H. H., Blake, S. M., Grodzinsky, A. J., and Lark, M. W., 2000, "Injurious Mechanical Compression of Bovine Articular Cartilage Induces Chondrocyte Apoptosis," Arch Biochem Biophys, **381**(2), pp. 205-212.

[155] Lucchinetti, E., Adams, C. S., Horton, W. E., Jr., and Torzilli, P. A., 2002, "Cartilage Viability After Repetitive Loading: A Preliminary Report," Osteoarthritis Cartilage, **10**(1), pp. 71-81.

[156] Thibault, M., Poole, A. R., and Buschmann, M. D., 2002, "Cyclic Compression of Cartilage/Bone Explants in Vitro Leads to Physical Weakening, Mechanical Breakdown of Collagen and Release of Matrix Fragments," J Orthop Res, **20**(6), pp. 1265-1273.

[157] Bader, D. L., Salter, D. M., and Chowdhury, T. T., 2011, "Biomechanical Influence of Cartilage Homeostasis in Health and Disease," Arthritis, 2011, p. 979032.

[158] Buschmann, M. D., Kim, Y. J., Wong, M., Frank, E., Hunziker, E. B., and Grodzinsky, A. J., 1999, "Stimulation of Aggrecan Synthesis in Cartilage Explants by Cyclic Loading is Localized to Regions of High Interstitial Fluid Flow," Arch Biochem Biophys, **366**(1), pp. 1-7.

[159] Kim, Y. J., Sah, R. L., Grodzinsky, A. J., Plaas, A. H., and Sandy, J. D., 1994, "Mechanical Regulation of Cartilage Biosynthetic Behavior: Physical Stimuli," Arch Biochem Biophys, **311**(1), pp. 1-12.

[160] Li, K. W., Williamson, A. K., Wang, A. S., and Sah, R. L., 2001, "Growth Responses of Cartilage to Static and Dynamic Compression," Clin Orthop Relat Res (391 Suppl), pp. S34-48.

[161] Parkkinen, J. J., Lammi, M. J., Helminen, H. J., and Tammi, M., 1992, "Local Stimulation of Proteoglycan Synthesis in Articular Cartilage Explants by Dynamic Compression In Vitro," J Orthop Res, **10**(5), pp. 610-620.

[162] Piscoya, J. L., Fermor, B., Kraus, V. B., Stabler, T. V., and Guilak, F., 2005, "The Influence of Mechanical Compression on the Induction of Osteoarthritis-Related Biomarkers in Articular Cartilage Explants," Osteoarthritis Cartilage, **13**(12), pp. 1092-1099.

[163] Torzilli, P. A., Grigiene, R., Huang, C., Friedman, S. M., Doty, S. B., Boskey, A. L., and Lust, G., 1997, "Characterization of Cartilage Metabolic Response to Static and Dynamic Stress Using a Mechanical Explant Test System," J Biomech, **30**(1), pp. 1-9.

[164] Fermor, B., Weinberg, J. B., Pisetsky, D. S., Misukonis, M. A., Banes, A. J., and Guilak, F., 2001, "The Effects of Static and Intermittent Compression on Nitric Oxide Production in Articular Cartilage Explants," J Orthop Res, **19**(4), pp. 729-737.

[165] Lin, P. M., Chen, C. T., and Torzilli, P. A., 2004, "Increased Stromelysin-1 (MMP-3), Proteoglycan Degradation (3B3- and 7D4) and Collagen Damage in Cyclically Load-Injured Articular Cartilage," Osteoarthritis Cartilage, **12**(6), pp. 485-496.

[166] Clements, K. M., Bee, Z. C., Crossingham, G. V., Adams, M. A., and Sharif, M., 2001, "How Severe Must Repetitive Loading be to Kill Chondrocytes in Articular Cartilage?," Osteoarthritis Cartilage, **9**(5), pp. 499-507.

[167] Quinn, T. M., Allen, R. G., Schalet, B. J., Perumbuli, P., and Hunziker, E. B., 2001, "Matrix and Cell Injury Due to Sub-Impact Loading of Adult Bovine Articular Cartilage Explants: Effects of Strain Rate and Peak Stress," J Orthop Res, **19**(2), pp. 242-249.

[168] Rolauffs, B., Muehleman, C., Li, J., Kurz, B., Kuettner, K. E., Frank, E., and Grodzinsky, A. J., 2010, "Vulnerability of the Superficial Zone of Immature Articular Cartilage to Compressive Injury," Arthritis Rheum, **62**(10), pp. 3016-3027.

[169] Chen, C. T., Burton-Wurster, N., Lust, G., Bank, R. A., and Tekoppele, J. M., 1999, "Compositional and Metabolic Changes in Damaged Cartilage are Peak-Stress, Stress-Rate, and Loading-Duration Dependent," J Orthop Res, **17**(6), pp. 870-879.

[170] Fitzgerald, J. B., Jin, M., and Grodzinsky, A. J., 2006, "Shear and Compression Differentially Regulate Clusters of Functionally Related Temporal Transcription Patterns in Cartilage Tissue," J Biol Chem, **281**(34), pp. 24095-24103.

[171] Jin, M., Frank, E. H., Quinn, T. M., Hunziker, E. B., and Grodzinsky, A. J., 2001, "Tissue Shear Deformation Stimulates Proteoglycan and Protein Biosynthesis in Bovine Cartilage Explants," Arch Biochem Biophys, **395**(1), pp. 41-48.

[172] Nugent, G. E., Aneloski, N. M., Schmidt, T. A., Schumacher, B. L., Voegtline, M. S., and Sah, R. L., 2006, "Dynamic Shear Stimulation of Bovine Cartilage Biosynthesis of Proteoglycan 4," Arthritis Rheum, **54**(6), pp. 1888-1896.

[173] Fitzgerald, J. B., Jin, M., Chai, D. H., Siparsky, P., Fanning, P., and Grodzinsky, A. J., 2008, "Shear- and Compression-Induced Chondrocyte Transcription Requires MAPK Activation in Cartilage Explants," J Biol Chem, **283**(11), pp. 6735-6743.

[174] Simon, W. H., Mak, A., and Spirt, A., 1990, "The Effect of Shear Fatigue on Bovine Articular Cartilage," J Orthop Res, **8**(1), pp. 86-93.

[175] Heiner, A. D., Smith, A. D., Goetz, J. E., Goreham-Voss, C. M., Judd, K. T., McKinley, T. O., and Martin, J. A., 2013, "Cartilage-on-Cartilage Versus Metal-on-Cartilage Impact Characteristics and Responses," J Orthop Res, **31**(6), pp. 887-893.

[176] Scott, C. C., and Athanasiou, K. A., 2006, "Mechanical Impact and Articular Cartilage," Crit Rev Biomed Eng, **34**(5), pp. 347-378.

[177] Sun, H. B., 2010, "Mechanical Loading, Cartilage Degradation, and Arthritis," Ann N Y Acad Sci, 1211, pp. 37-50.

[178] Borrelli, J., Jr., Tinsley, K., Ricci, W. M., Burns, M., Karl, I. E., and Hotchkiss, R., 2003, "Induction of Chondrocyte Apoptosis Following Impact Load," J Orthop Trauma, **17**(9), pp. 635-641.

[179] Leucht, F., Durselen, L., Hogrefe, C., Joos, H., Reichel, H., Schmitt, H., Ignatius, A., and Brenner, R. E., 2012, "Development of a New Biomechanically Defined Single Impact Rabbit Cartilage Trauma Model for In Vivo-Studies," J Invest Surg, **25**(4), pp. 235-241.

[180] Milentijevic, D., Helfet, D. L., and Torzilli, P. A., 2003, "Influence of Stress Magnitude on Water Loss and Chondrocyte Viability in Impacted Articular Cartilage," J Biomech Eng, **125**(5), pp. 594-601.

[181] Stolberg-Stolberg, J. A., Furman, B. D., William Garrigues, N., Lee, J., Pisetsky, D. S., Stearns, N. A., DeFrate, L. E., Guilak, F., and Olson, S. A., 2013, "Effects of Cartilage Impact with and without Fracture on Chondrocyte Viability and the Release of Inflammatory Markers," J Orthop Res.

[182] Buckwalter, J. A., 2012, "The Role of Mechanical Forces in the Initiation and Progression of Osteoarthritis," H S S J, **8**(1), pp. 37-38.

[183] Hoaglund, F. T., 2013, "Primary Osteoarthritis of the Hip: A Genetic Disease Caused by European Genetic Variants," J Bone Joint Surg Am, **95**(5), pp. 463-468.

[184] Murray, R. O., 1965, "The Aetiology of Primary Osteoarthritis of the Hip," The British Journal Of Radiology, **38**(455), pp. 810-824.

[185] Harris-Hayes, M., and Royer, N. K., 2011, "Relationship of Acetabular Dysplasia and Femoroacetabular Impingement to Hip Osteoarthritis: A Focused Review," P M R, **3**(11), pp. 1055-1067 e1051.

[186] Sulsky, S. I., Carlton, L., Bochmann, F., Ellegast, R., Glitsch, U., Hartmann, B., Pallapies, D., Seidel, D., and Sun, Y., 2012, "Epidemiological Evidence for Work Load as a Risk Factor for Osteoarthritis of the Hip: A Systematic Review," PLoS One, **7**(2), p. e31521.

[187] Holliday, K. L., McWilliams, D. F., Maciewicz, R. A., Muir, K. R., Zhang, W., and Doherty, M., 2011, "Lifetime Body Mass Index, Other Anthropometric Measures of Obesity and Risk of Knee or Hip Osteoarthritis in the GOAL Case-Control Study," Osteoarthritis Cartilage, **19**(1), pp. 37-43.

[188] Hartig-Andreasen, C., Soballe, K., and Troelsen, A., 2013, "The Role of the Acetabular Labrum in Hip Dysplasia. A Literature Overview," Acta Orthop, **84**(1), pp. 60-64.

[189] Stelzeneder, D., Mamisch, T. C., Kress, I., Domayer, S. E., Werlen, S., Bixby, S. D., Millis, M. B., and Kim, Y. J., 2012, "Patterns of Joint Damage Seen on MRI in Early Hip Osteoarthritis due to Structural Hip Deformities," Osteoarthritis Cartilage, **20**(7), pp. 661-669.

[190] Larson, C. M., 2010, "Arthroscopic Management of Pincer-Type Impingement," Sports Med Arthrosc, **18**(2), pp. 100-107.

[191] Beck, M., Kalhor, M., Leunig, M., and Ganz, R., 2005, "Hip Morphology Influences the Pattern of Damage to the Acetabular Cartilage: Femoroacetabular Impingement as a Cause of Early Osteoarthritis of the Hip," J Bone Joint Surg Br, **87**(7), pp. 1012-1018.

[192] Solomon, L., 1976, "Patterns of Osteoarthritis of the Hip," J Bone Joint Surg Br, **58**(2), pp. 176-183.

[193] Cooperman, D. R., Wallensten, R., and Stulberg, S. D., 1983, "Acetabular Dysplasia in the Adult," Clin Orthop Relat Res (175), pp. 79-85.

[194] Harris, W. H., 1986, "Etiology of Osteoarthritis of the Hip," Clin Orthop Relat Res (213), pp. 20-33.

[195] Jessel, R. H., Zurakowski, D., Zilkens, C., Burstein, D., Gray, M. L., and Kim, Y. J., 2009, "Radiographic and Patient Factors Associated with Pre-Radiographic Osteoarthritis in Hip Dysplasia," J Bone Joint Surg Am, **91**(5), pp. 1120-1129.

[196] McWilliams, D. F., Doherty, S. A., Jenkins, W. D., Maciewicz, R. A., Muir, K. R., Zhang, W., and Doherty, M., 2010, "Mild Acetabular Dysplasia and Risk of Osteoarthritis of the Hip: A Case Control Study," Ann Rheum Dis, **69**(10), pp. 1774-1778.

[197] Croft, P., Cooper, C., Wickham, C., and Coggon, D., 1991, "Osteoarthritis of the Hip and Acetabular Dysplasia," Ann Rheum Dis, **50**(5), pp. 308-310.

[198] Lau, E. M., Lin, F., Lam, D., Silman, A., and Croft, P., 1995, "Hip Osteoarthritis and Dysplasia in Chinese Men," Ann Rheum Dis, **54**(12), pp. 965-969.

[199] Kim, W. Y., Hutchinson, C. E., Andrew, J. G., and Allen, P. D., 2006, "The Relationship Between Acetabular Retroversion and Osteoarthritis of the Hip," J Bone Joint Surg Br, **88**(6), pp. 727-729.

[200] Millis, M. B., and Kim, Y. J., 2002, "Rationale of Osteotomy and Related Procedures for Hip Preservation: A Review," Clin Orthop Relat Res (405), pp. 108-121.

[201] Ganz, R., Klaue, K., Vinh, T. S., and Mast, J. W., 1988, "A New Periacetabular Osteotomy for the Treatment of Hip Dysplasias. Technique and Preliminary Results," Clin Orthop Relat Res (232), pp. 26-36.

[202] Murphy, S. B., Millis, M. B., and Hall, J. E., 1999, "Surgical Correction of Acetabular Dysplasia in the Adult. A Boston Experience," Clin Orthop Relat Res (363), pp. 38-44.

[203] Leunig, M., and Ganz, R., 2011, "Evolution of Technique and Indications for the Bernese Periacetabular Osteotomy," Bull NYU Hosp Jt Dis, **69** Suppl 1, pp. S42-46.

[204] Siebenrock, K. A., Scholl, E., Lottenbach, M., and Ganz, R., 1999, "Bernese Periacetabular Osteotomy," Clin Orthop Relat Res (363), pp. 9-20.

[205] Steppacher, S. D., Tannast, M., Ganz, R., and Siebenrock, K. A., 2008, "Mean 20-Year Followup of Bernese Periacetabular Osteotomy," Clin Orthop Relat Res, **466**(7), pp. 1633-1644.

[206] Matheney, T., Kim, Y. J., Zurakowski, D., Matero, C., and Millis, M., 2010, "Intermediate to Long-Term Results Following the Bernese Periacetabular Osteotomy and Predictors of Clinical Outcome: Surgical Technique," J Bone Joint Surg Am, **92** Suppl 1 Pt 2, pp. 115-129.

[207] Troelsen, A., Elmengaard, B., and Soballe, K., 2009, "Medium-Term Outcome of Periacetabular Osteotomy and Predictors of Conversion to Total Hip Replacement," J Bone Joint Surg Am, **91**(9), pp. 2169-2179.

[208] Garras, D. N., Crowder, T. T., and Olson, S. A., 2007, "Medium-Term Results of the Bernese Periacetabular Osteotomy in the Treatment of Symptomatic Developmental Dysplasia of the Hip," J Bone Joint Surg Br, **89**(6), pp. 721-724.

[209] Kralj, M., Mavcic, B., Antolic, V., Iglic, A., and Kralj-Iglic, V., 2005, "The Bernese Periacetabular Osteotomy: Clinical, Radiographic and Mechanical 7-15-Year Follow-Up of 26 Hips," Acta Orthop, **76**(6), pp. 833-840.

[210] Leumann, A., Fortuna, R., Leonard, T., Valderrabano, V., and Herzog, W., 2013, "Dynamic In Vivo Force Transfer in the Lapine Knee Loaded by Quadriceps Muscle Contraction," Clin Biomech (Bristol, Avon).

[211] Chan, D. D., Neu, C. P., and Hull, M. L., 2009, "Articular Cartilage Deformation Determined in an Intact Tibiofemoral Joint by Displacement-Encoded Imaging," Magn Reson Med, **61**(4), pp. 989-993.

[212] Akbar, M., Farahmand, F., Jafari, A., and Foumani, M. S., 2012, "A Detailed and Validated Three-Dimensional Dynamic Model of the Patellofemoral Joint," J Biomech Eng, **134**(4), p. 041005.

[213] Li, G., Sakamoto, M., and Chao, E. Y., 1997, "A Comparison of Different Methods in Predicting Static Pressure Distribution in Articulating Joints," J Biomech, **30**(6), pp. 635-638.

[214] Anderson, D. D., Iyer, K. S., Segal, N. A., Lynch, J. A., and Brown, T. D., 2010, "Implementation of Discrete Element Analysis for Subject-Specific, Population-Wide Investigations of Habitual Contact Stress Exposure," J Appl Biomech, **26**(2), pp. 215-223.

[215] Segal, N. A., Anderson, D. D., Iyer, K. S., Baker, J., Torner, J. C., Lynch, J. A., Felson, D. T., Lewis, C. E., and Brown, T. D., 2009, "Baseline Articular Contact Stress Levels Predict Incident Symptomatic Knee Osteoarthritis Development in the MOST Cohort," J Orthop Res, **27**(12), pp. 1562-1568.

[216] Segal, N. A., Kern, A. M., Anderson, D. D., Niu, J., Lynch, J., Guermazi, A., Torner, J. C., Brown, T. D., and Nevitt, M., 2012, "Elevated Tibiofemoral Articular Contact Stress Predicts Risk for Bone Marrow Lesions and Cartilage Damage at 30 Months," Osteoarthritis Cartilage, **20**(10), pp. 1120-1126.

[217] Abraham, C. L., Maas, S. A., Weiss, J. A., Ellis, B. J., Peters, C. L., and Anderson, A. E., 2013, "A New Discrete Element Analysis Method for Predicting Hip Joint Contact Stresses," J Biomech.

[218] Geers, M. G. D., Kouznetsova, V. G., and Brekelmans, W. A. M., 2010, "Multi-scale Computational Homogenization: Trends and Challenges," J Comput Appl Math, **234**(7), pp. 2175-2182.

[219] Yuan, Z., and Fish, J., 2008, "Toward Realization of Computational Homogenization in Practice," Int J Numer Meth Eng, **73**(3), pp. 361-380.

[220] Fernandez, J. W., Shim, V. B., and Hunter, P. J., 2012, "Integrating Degenerative Mechanisms in Bone and Cartilage: A Multiscale Approach," Conf Proc IEEE Eng Med Biol Soc, 2012, pp. 6616-6619.

[221] Guilak, F., and Mow, V. C., 2000, "The Mechanical Environment of the Chondrocyte: A Biphasic Finite Element Model of Cell-Matrix Interactions in Articular Cartilage," J Biomech, **33**(12), pp. 1663-1673.

[222] Halloran, J. P., Sibole, S., van Donkelaar, C. C., van Turnhout, M. C., Oomens, C. W., Weiss, J. A., Guilak, F., and Erdemir, A., 2012, "Multiscale Mechanics of Articular Cartilage: Potentials and Challenges of Coupling Musculoskeletal, Joint, and Microscale Computational Models," Ann Biomed Eng, **40**(11), pp. 2456-2474.

[223] Kim, E., Guilak, F., and Haider, M. A., 2008, "The Dynamic Mechanical Environment of the Chondrocyte: A Biphasic Finite Element Model of Cell-Matrix Interactions Under Cyclic Compressive Loading," J Biomech Eng, **130**(6), p. 061009.

[224] Kim, E., Guilak, F., and Haider, M. A., 2010, "An Axisymmetric Boundary Element Model for Determination of Articular Cartilage Pericellular Matrix Properties In Situ via Inverse Analysis of Chondron Deformation," J Biomech Eng, **132**(3), p. 031011.

[225] Sibole, S. C., and Erdemir, A., 2012, "Chondrocyte Deformations as a Function of Tibiofemoral Joint Loading Predicted by a Generalized High-Throughput Pipeline of Multi-Scale Simulations," PLoS One, **7**(5), p. e37538.

[226] 2006, "ASME V&V 10-2006 Guide for Verification and Validation in Computational Solid Mechanics," ASME Standards.

[227] Anderson, A. E., Ellis, B. J., and Weiss, J. A., 2007, "Verification, Validation and Sensitivity Studies in Computational Biomechanics," Comput Methods Biomech Biomed Engin, **10**(3), pp. 171-184.

[228] Henninger, H. B., Reese, S. P., Anderson, A. E., and Weiss, J. A., 2010, "Validation of Computational Models in Biomechanics," Proc Inst Mech Eng H, **224**(7), pp. 801-812.

[229] Henak, C. R., Anderson, A. E., and Weiss, J. A., 2013, "Subject-Specific Analysis of Joint Contact Mechanics: Application to the Study of Osteoarthritis and Surgical Planning," J Biomech Eng, **135**(2), p. 021003.

[230] Anderson, A. E., Ellis, B. J., Maas, S. A., Peters, C. L., and Weiss, J. A., 2008, "Validation of Finite Element Predictions of Cartilage Contact Pressure in the Human Hip Joint," J Biomech Eng, **130**(5), pp. 051008-051008.

[231] Anderson, D. D., Goldsworthy, J. K., Li, W., James Rudert, M., Tochigi, Y., and Brown, T. D., 2007, "Physical Validation of a Patient-Specific Contact Finite Element Model of the Ankle," J Biomech, **40**(8), pp. 1662-1669.

[232] Donahue, T. L., Hull, M. L., Rashid, M. M., and Jacobs, C. R., 2002, "A Finite Element Model of the Human Knee Joint for the Study of Tibio-Femoral Contact," J Biomech Eng, **124**(3), pp. 273-280.

[233] Anderson, A. E., Ellis, B. J., Maas, S. A., and Weiss, J. A., 2010, "Effects of Idealized Joint Geometry on Finite Element Predictions of Cartilage Contact Stresses in the Hip," J Biomech, **43**(7), pp. 1351-1357.

[234] Gu, D. Y., Dai, K. R., Hu, F., and Chen, Y. Z., 2010, "The Shape of the Acetabular Cartilage Surface and its Role in Hip Joint Contact Stress," Conf Proc IEEE Eng Med Biol Soc, 2010, pp. 3934-3937.

[235] Harris, M. D., Anderson, A. E., Henak, C. R., Ellis, B. J., Peters, C. L., and Weiss, J. A., 2012, "Finite Element Prediction of Cartilage Contact Stresses in Normal Human Hips," J Orthop Res, **30**(7), pp. 1133-1139.

[236] Russell, M. E., Shivanna, K. H., Grosland, N. M., and Pedersen, D. R., 2006, "Cartilage Contact Pressure Elevations in Dysplastic Hips: A Chronic Overload Model," J Orthop Surg Res, 1, pp. 6-6.

[237] Chegini, S., Beck, M., and Ferguson, S. J., 2009, "The Effects of Impingement and Dysplasia on Stress Distributions in the Hip Joint During Sitting and Walking: A Finite Element Analysis," J Orthop Res, **27**(2), pp. 195-201.

CHAPTER 3[1]

SPECIMEN-SPECIFIC PREDICTIONS OF CONTACT STRESS UNDER PHYSIOLOGICAL LOADING IN THE HUMAN HIP: VALIDATION AND SENSITIVITY STUDIES

Abstract

Hip osteoarthritis may be initiated and advanced by abnormal cartilage contact mechanics, and finite element (FE) modeling provides an approach with the potential to allow the study of this process. Previous FE models of the human hip have been limited by single-specimen validation and the use of quasilinear or linear elastic constitutive models of articular cartilage. The effects of the latter assumptions on model predictions are unknown, partially because data for the instantaneous behavior of healthy human hip cartilage are unavailable. The aims of this study were to develop and validate a series of specimen-specific FE models, to characterize the regional instantaneous response of healthy human hip cartilage in compression, and to assess the effects of material nonlinearity, inhomogeneity and specimen-specific material coefficients on FE predictions of cartilage contact stress and contact area. Five cadaveric specimens underwent experimental loading, cartilage material characterization and specimen-specific FE modeling. Cartilage in the FE models was represented by average neo-

[1]Reprinted from *Biomechanics and Modeling in Mechanobiology*, Henak CR, Kapron AL, Anderson AE, Ellis BJ, Maas SA, Weiss JA, "Specimen-Specific Predictions of Contact Stress under Physiological Loading in the Human Hip: Validation and Sensitivity Studies", 2013, with permission from Springer.

Hookean, average Veronda Westmann and specimen- and region-specific Veronda Westmann hyperelastic constitutive models. Experimental measurements and FE predictions compared well for all three cartilage representations, which was reflected in average RMS errors in contact stress of less than 25%. The instantaneous material behavior of healthy human hip cartilage varied spatially, with stiffer acetabular cartilage than femoral cartilage, and stiffer cartilage in lateral regions than in medial regions. The Veronda Westmann constitutive model with average material coefficients accurately predicted peak contact stress, average contact stress, contact area and contact patterns. The use of subject- and region-specific material coefficients did not increase the accuracy of FE model predictions. The neo-Hookean constitutive model underpredicted peak contact stress in areas of high stress. The results of this study support the use of average cartilage material coefficients in predictions of cartilage contact stress and contact area in the normal hip. The regional characterization of cartilage material behavior provides the necessary inputs for future computational studies investigating cartilage mechanics other than contact stress and area in the human hip. In the future, the results of this study can be applied to subject-specific models to understand how abnormal hip contact stress and contact area contribute to OA.

Introduction

One in four people develop hip osteoarthritis (OA) during their lifetimes [1]. Abnormal cartilage contact mechanics may predict the onset and progression of OA [2-4]. Altered mechanics may initiate OA through damage to the physical integrity of cartilage or by initiating changes in cartilage metabolism. For example, altered pressures

change the metabolism of cartilage explants [3, 5]. Additionally, high stresses cause cartilage fissuring during impact loading in vitro [6-10].

Finite element (FE) methods have predicted cartilage stresses in the hip because stresses cannot currently be measured in vivo. Previous FE models of the human hip have provided insight into the mechanics of normal and pathologic hips, using both subject-specific and idealized geometries [11-18]. Models have demonstrated intersubject variability in the normal population [15], the influence of subject-specific geometry [12] and altered mechanics in hips with bony pathology compared to normal hips [14, 16, 18]. Some of these studies are severely limited because little or no effort was made to validate the models. Others are limited because they are based on model validation of a single specimen. Furthermore, all of these previous studies have assumed spatially homogeneous, quasilinear or linear elastic cartilage constitutive behavior.

Confidence in FE predictions and the effects of modeling assumptions on those predictions can be evaluated via direct validation and parametric analysis, respectively. Direct validation is the process of comparing experimental results and computational predictions using identical (or nearly identical) boundary conditions, loading conditions and geometry [19-21]. Parametric analysis is the systematic evaluation of the effects of modeling assumptions on model predictions. One specimen-specific FE model of the human hip was validated [11], however, a series of hip models has not been validated. Validation using a series of specimens provides two advantages over validation using a single specimen. First, validation on a series of specimens demonstrates the predictive capabilities of the FE models across specimen-specific geometries and elucidates the

expected interspecimen variability. Second, statistical methods can determine the effect of model parameters when multiple specimens are modeled.

While it is known that cartilage material behavior includes material nonlinearity and spatial inhomogeneity, the effects of cartilage constitutive model on FE predictions of cartilage contact stress and contact area in the human hip are unknown. Cartilage material behavior is time- and rate-dependent, but nearly-incompressible elastic material behavior is an appropriate simplification under fast loading rates such as those experienced during physiological loading, including walking [22, 23]. Although advanced constitutive models have not been employed in the human hip, FE predictions in the human knee suggest that some of the more advanced features of cartilage constitutive behavior are unnecessarily complicated for predictions of contact mechanics [24, 25]. Even with these simplifications, previous FE models of the human hip have used cartilage behavior with coefficients from other joints or other animals because there are no data available regarding the instantaneous response of healthy human hip cartilage ('instantaneous' is used to indicate loading over ≤ 0.5 seconds) [11, 12, 14-16]. Biphasic and linear elastic analyses of hip cartilage suggests that behavior from other joints and other animals does not match the behavior of human hip cartilage [26-29]. Therefore, regional instantaneous material behavior of healthy human hip cartilage must first be characterized to investigate whether features of the assumed cartilage constitutive model affect FE predictions of hip contact stress and contact area. The required complexity and specificity of cartilage constitutive model can then be determined by comparing results obtained with the simplest hyperelastic constitutive model, neo-Hookean, to cartilage representations that capture material nonlinearity and spatial inhomogeneity.

Therefore, there were three objectives to this study: (1) to develop and validate a series of specimen-specific FE models by directly comparing FE predictions of contact stress and contact area to experimental measurements; (2) to characterize the regional instantaneous response of healthy human hip cartilage in compression using quasilinear and nonlinear constitutive models; and (3) to assess the effects of material nonlinearity, inhomogeneity and specimen-specific material coefficients on FE predictions of cartilage contact stress and contact area. These objectives were carried out with a focus on predictions of contact stress and contact area, which could be measured in vitro in this study on a subject-specific basis, and are often used in the interpretation of mechanical loading relevant to the development of OA [18, 30-33].

Methods

Contact stress and contact area in five normal male cadaveric hips were investigated using a combined experimental and computational protocol (40 ± 14 years old, weight 62.8 ± 13.8 kg, height 176.5 ± 8.9 cm) [11]. All specimens were screened for hip pathology with an anteroposterior radiograph and known medical history. Cartilage was macroscopically examined during dissection. No osteoarthritic changes or degenerative lesions were found.

Experimental Methods

All soft tissue except cartilage was dissected from each specimen. Registration blocks were attached to the hemipelvis and the femur [11, 34]. Volumetric CT scans were obtained of the fully dissected, disarticulated specimens (Siemens Somatom Emotion, 512 × 512 pixel acquisition matrix, 276-420 mm FOV, 0.7 mm slice thickness).

Scanner settings were based on our previous study that demonstrated less than 10% RMS error in cartilage thickness using CT [35]. Anatomical coordinate systems were established using bony landmarks and were digitized relative to the registration blocks with a Microscribe G2X or MLX digitizer (accuracy $\leq$ 0.23 mm, CNC Services, Inc., Amherst, VA) [11, 36]. The femur and pelvis were cemented into custom test fixtures that provided rotation about the internal/external, flexion/extension and abduction/adduction axes as well as translation to align the joint (Figure 3.1). Testing was completed using an MTS 858 with a 4 kN load cell (MTS Systems Corporation, Eden Prairie, MN). The entire loading system allowed for the femur to impart a non-vertical joint reaction force onto the acetabulum, as is experienced in vivo [11, 36].

Four physiological loading scenarios were tested based on instrumented implant and gait data: heel strike during walking, midstance during walking, heel strike during stair descent and heel strike during stair ascent [36]. Each position was achieved using an iterative process until all three kinematic angles were within ± 3 deg of the target positions.

Low range pressure sensitive film cut into rosette patterns was used to measure contact stress and contact area (Fuji Prescale®, Sensor Products, Inc., NJ) [11]. Pressure-sensitive film measures the pressure, or the stress normal to the film. Thus, the pressure measured by the film can best be interpreted as the contact stress on the articular surface of the femur. Rosettes were placed between two polyethylene sheets and secured over the femoral head prior to each trial. Three trials were captured for each loading scenario and one trial from each loading scenario was selected for further analysis. The resultant loads for the selected trials were 1560 ± 335 N, 1520 ± 327 N, 1723 ± 326 N and 1464 ±

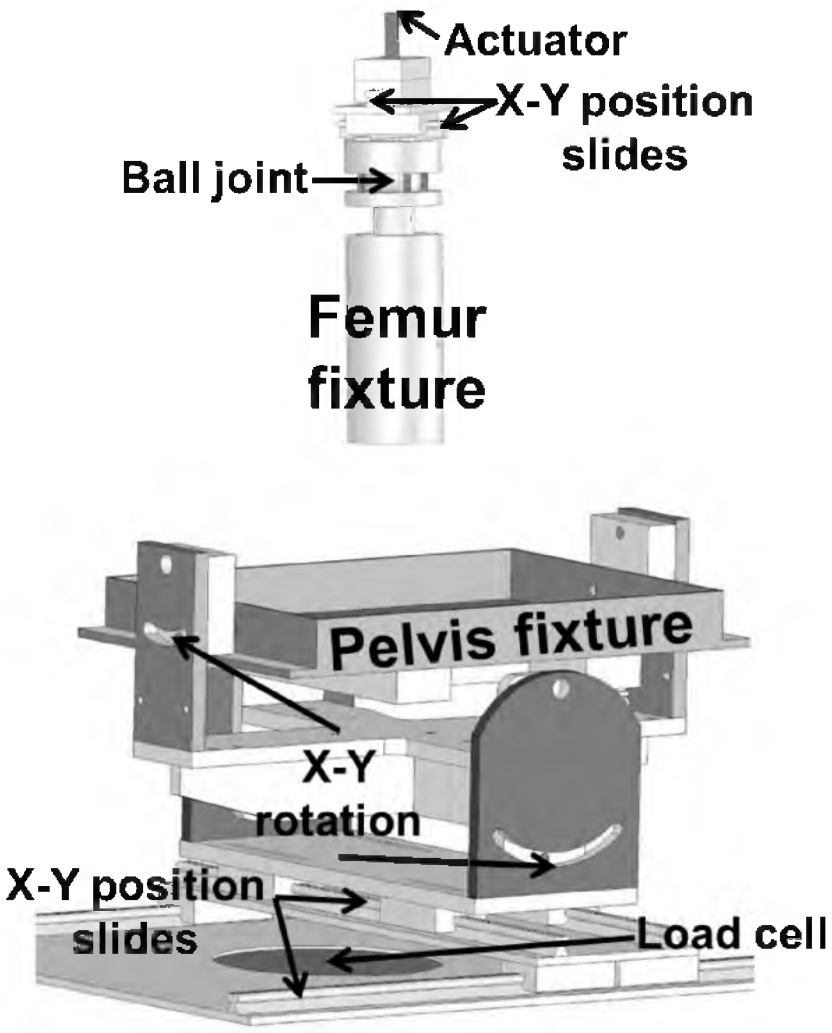

Figure 3.1: Fixture used to experimentally load specimens. The pelvis and femur were placed into anatomical positions and aligned prior to loading. Both the pelvis and the femur fixtures were able to translate and rotate to achieve the correct anatomical position.

284 N for heel strike during walking, midstance during walking, heel strike during stair descent and heel strike during stair ascent, respectively. Following each trial, the positions of the registration blocks and the pressure sensitive film rosettes were digitized.

To determine the correlation between pixel intensity and applied pressure, sections of unused pressure sensitive film were compressed between two flat platens layered with cellophane to a range of loads. All pressure sensitive film was scanned and converted to gray scale digital images for processing.

Cartilage Material Testing Methods

Unconfined compression testing was used to characterize the depth-averaged constitutive behavior of healthy human hip cartilage under fast loading rates, such as those applicable to the loading scenarios used during whole joint testing. On the day of soft tissue dissection, cartilage samples were harvested from nine regions on the femoral head and six regions on the acetabulum of the nontested joint of each specimen (Figure 3.2) [37]. One to two samples were obtained for each region. The number of samples was limited by the size and curvature of each anatomical region. A coring tool and scalpel excised each sample, which included the full cartilage thickness as well as some underlying subchondral bone. Samples were stored at -72°C until testing.

Each sample was sectioned serially using a microtome to remove subchondral bone and to create a deep surface parallel to the articular surface. Samples were then resized to 3.4 mm diameter cylinders and split in half along the long axis of the cylinder, resulting in two to four samples from each region. Sample height was measured three times using a resistance micrometer and measurements were averaged.

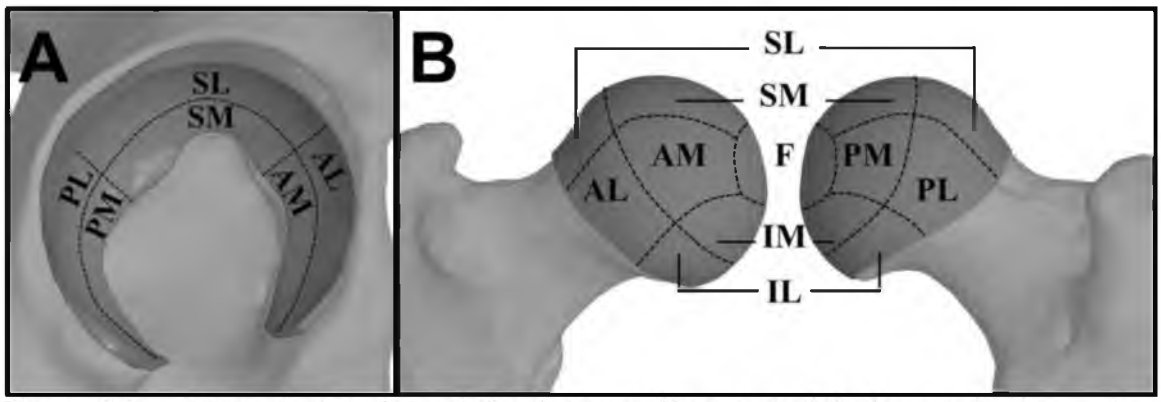

Figure 3.2: Anatomical regions defined for cartilage material characterization. A – acetabular cartilage. B – femoral cartilage. S = superior, P = posterior, A = anterior, I = inferior, M = medial, L = lateral and F = foveal.

Samples underwent unconfined compression testing between two glass slides. The custom test system consisted of a servo-controlled mechanical stage (Model MRV22, Tol-O-Matic, Hamel, MN), LVDT (Model ATA 2001, Schaevitz, Hampton, VA) and 10 lb load cell (LSB200, Futek Advanced Sensor Technology, Inc., Irvine, CA). A tare load of 58.9 ± 5.0 kPa was applied and held for 30 minutes, resulting in a stretch of 0.85 ± 0.08 [38-41]. The height of the sample following tare loading was determined from the position of the test system and was subsequently used as the reference height for loading.

After 30 minutes of tare loading, samples were compressed to a stretch ratio of 0.85 relative to the reference height over 1 second (15%/s). The loading rate was the approximate loading rate of walking [36], as well as a rate at which cartilage behavior is nearly-incompressible [22]. Cartilage testing was displacement driven, while load was measured. All testing was completed in a PBS bath at room temperature [40, 41].

Material coefficients for two hyperelastic constitutive models were fit to the experimental data. The neo-Hookean constitutive model represents a quasilinear relationship between stress and stretch. This model was selected because it is the simplest hyperelastic model, and therefore serves as a baseline. Further, previous hip FE models assumed neo-Hookean or linear elastic cartilage constitutive behavior and therefore this material model allows direct comparison with previous FE results [11-18]. In the Veronda Westmann model, stress is exponentially dependent on stretch [42]. This constitutive model was chosen to capture the material nonlinearity present in cartilage constitutive behavior, in contrast to the quasilinear neo-Hookean model.

For both constitutive models, a least squares fit minimized the difference between experimental and predicted stress-stretch curves to determine material coefficients

(SigmaPlot 11.0, Systat Software Inc., San Jose, CA). Uncoupled neo-Hookean strain energy was in the form [43]:

$$W = \frac{1}{2}\mu(\tilde{I}_1 - 3) + \frac{1}{2}K(\ln J)^2 \quad (1)$$

Here, μ is the shear modulus under infinitesimal strain, is the first deviatoric invariant, K is the bulk modulus and J is the determinant of the deformation gradient. For an incompressible material subjected to unconfined compression by a stretch ratio λ_3, the neo-Hookean Cauchy stress σ_{33} is:

$$\sigma_{33} = \frac{1}{2}\mu(\lambda_3^2 - \frac{1}{\lambda_3}) \quad (2)$$

Thus, μ was the coefficient that was determined by curve fitting in the neo-Hookean constitutive model. Veronda Westmann strain energy was in the form [42, 43]:

$$W = C_1(\exp[C_2(\tilde{I}_1 - 3)] - 1) - \frac{C_1C_2}{2}(\tilde{I}_2 - 3) + \frac{1}{2}K(\ln J)^2 \quad (3)$$

Here, is the second deviatoric invariant. For an incompressible material subjected to unconfined compression by a stretch ratio λ_3, the Veronda Westmann Cauchy stress σ_{33} is:

$$\sigma_{33} = C_1C_2[\left(2\lambda_3^2 - \frac{2}{\lambda_3}\right)\exp\left[C_2\left(\lambda_3^2 + \frac{2}{\lambda_3} - 3\right)\right] - \lambda_3 + \frac{1}{\lambda_3^2}] \quad (4)$$

The product C_1C_2 was defined as the Veronda Westmann modulus in the reference configuration and denoted E_0 for statistical comparisons between regions. The coefficients C_1 and C_2 were both determined by curve fitting the Veronda Westmann constitutive model to the data. For both constitutive models, the uniqueness of the best-fit material coefficients was verified by perturbing initial guesses.

The stretch ratio, λ_3, was derived from the applied crosshead displacement and the known sample height. Cauchy stress was derived from the measured load, initial cross-sectional area and stretch ratio, assuming material incompressibility [44].

Computational Methods

CT data were segmented using a combination of automated thresholding based on image intensity and manual segmentation methods in the Amira software (5.3, Visage Imaging, San Diego, CA) [11, 45]. Polygonal surfaces of the bone and cartilage were generated from the segmented data [11, 15, 16]. Cartilage surfaces were imported into TrueGrid (XYZ Scientific, Livermore, CA) to generate hexahedral FE meshes (Figure 3.3). Cortical bone surfaces were discretized into triangular shell elements with position-dependent thickness [45]. Cortical bone was represented as isotropic linear elastic (E = 17 GPa, ν = 0.29) [46]. Representation of the cortical bone was based on a previous validation study evaluating the effects of FE representation of bone on bone strain [45]. Mortar tied contact attached cartilage to bone, while mortar sliding contact governed the interaction between cartilage layers [47, 48]. All analyses were completed in NIKE3D [49].

FE models were generated with three different cartilage representations to determine the effects of cartilage material nonlinearity, inhomogeneity and specimen-specificity on FE predictions. The most specific cartilage representation used a Veronda Westmann constitutive model with specimen-specific regional material coefficients. To generate these models, a continuous heterogeneous distribution of the material coefficients was required. This was obtained using Laplace interpolation over the finite element mesh, with the material coefficients for each region serving as Dirichlet boundary conditions at

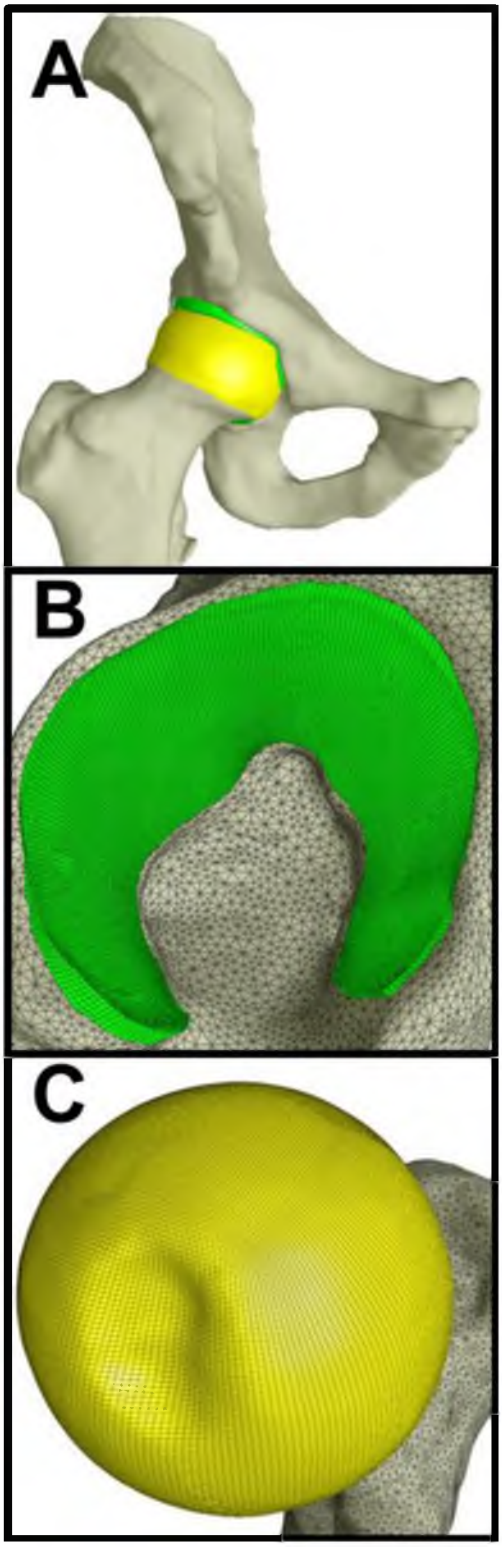

Figure 3.3: Representative FE model. Cortical bones are shown in white, femoral cartilage is shown in yellow and acetabular cartilage is shown in green. A – whole joint. B – acetabular cartilage. C – femoral cartilage.

the center of the region [50, 51]. Since the steady-state heat transfer equation is an example of Laplace's equation, the interpolation was performed using the heat transfer module in FEBio [51, 52]. The resulting continuous distribution was discretized into 25 specimen-specific sets of material coefficients on the femur and 25 specimen-specific sets of material coefficients on the acetabulum (this is referred to as "VW specific"). A second set of Veronda Westmann material coefficients were averaged across all specimens and regions (this is referred to as "VW average"). Similarly, neo-Hookean material coefficients were averaged across all specimens and regions (this is referred to as "nH average"). Bulk moduli were selected to enforce material near-incompressibility. The Veronda Westmann constitutive equation was implemented in NIKE3D and the implementation was verified by comparing the results of single element analyses with analytical solutions.

Boundary and loading conditions for the FE simulations were matched to experimental trials using the digitized data. Positions of the registration blocks segmented from CT data were aligned to their digitized experimental positions for each trial. Each model was run to the corresponding experimental load. For model validation, cartilage contact stress and cartilage contact area were obtained on the articular surface of the femoral cartilage. To compare the three methods for modeling cartilage, contact stress and contact area were obtained on the acetabular cartilage. All FE postprocessing was completed using PostView [53].

A mesh convergence study determined the appropriate number of elements through the cartilage thickness to achieve converged contact stress and contact area predictions. Cartilage meshes with three, four, five and six elements through the thickness were

generated for one specimen and analyzed with VW average cartilage. Overall mesh density was adjusted to maintain element aspect ratios and element Jacobians. Meshes were considered converged when the average change in contact stress and contact area across all four loading scenarios between subsequent meshes was less than 5%. Based on the results of the mesh convergence study, all further analyses were completed with five elements through the cartilage thickness.

Data and Statistical Methods

To validate the FE models, nodal contact stress results reported on the femoral head of the FE models were compared to experimental results from the matched trial. Intraclass correlation coefficients compared agreement between experimental and FE results for each of the four loading scenarios. A Bland-Altman analysis with an adjustment for clustered data compared the differences and tolerance intervals between experimental and FE results over all loading scenarios [54-56]. Finally, a pixel-wise calculation of RMS error between FE and experimental contact stress was completed in a custom program that we developed for a previous study [11] (Figure 3.4).

To investigate the influence of cartilage representation on FE predictions, FE nodal contact stress results from the three cartilage representations were compared in six regions of the acetabular cartilage (Figure 3.2). Contact stress and contact area were sampled on the articular surface of the acetabular cartilage. A pairwise comparison of results from each cartilage representation was completed using random effects linear regression that accounted for the nonindependence of data clustered within each specimen and loading scenario. Finner's procedure corrected the resulting *p*-values for

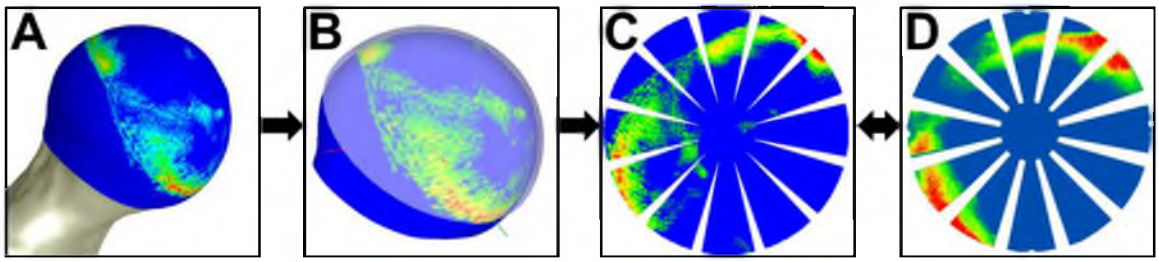

Figure 3.4: Process for comparing experimental and FE results pixel-wise. A – FE results are extracted from the articular surface of the femoral head. B – FE results are projected to a sphere and the experimental position of the pressure-sensitive film is overlaid. C – the spherical projection is mapped to a planar rosette, creating a simulated rosette with the same dimensions as the experimental rosette. D – the experimental rosette is used as the gold standard for pixel-wise comparison against the simulated rosette.

multiple comparisons [57].

Regional differences in FE results and cartilage material coefficients clustered within each specimen were also evaluated using random effects linear regression. FE results were compared pairwise between all six acetabular regions, as well as between lateral and medial regions. Material coefficients from six acetabular and nine femoral regions were pooled and compared between: all femoral versus all acetabular regions, all medial versus all lateral regions, medial versus lateral femoral regions and medial versus lateral acetabular regions. Additionally, all six acetabular regions and all nine femoral regions were compared pairwise. Finner's procedure corrected the resulting p-values for multiplicity [57]. Significance for all tests was set at $p \leq 0.05$.

Results

Experimental and computational results compared well for most specimens and loading scenarios (Figure 3.5). Interspecimen variability within each loading scenario was larger than interscenario variability within each specimen (Figure 3.5). Distinct contact patterns for each specimen were multicentric, banded or combinations of the

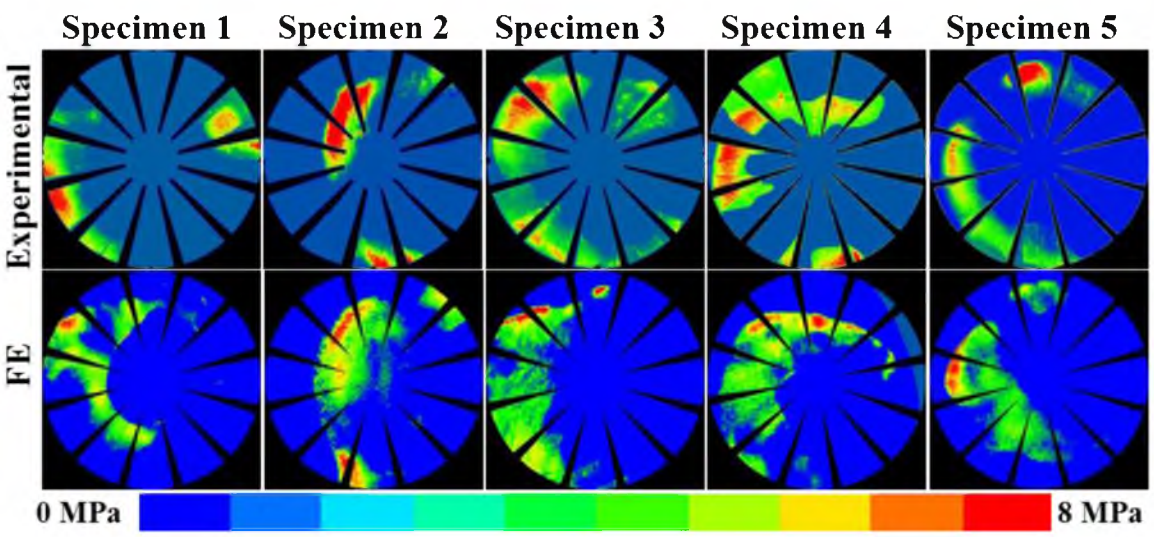

Figure 3.5: Comparisons between experimental and FE contact pressure for heel strike during stair descent in VW average models. Results compared well across specimen-specific geometry.

two. Qualitative differences between the three cartilage representations were nearly indistinguishable, which was reflected in minimal effects on RMS error in contact stress, minimal effects on contact stress differences and minimal effects on contact area differences (Figure 3.6). RMS error in contact stress was 23.8 ± 4.8%, 23.9 ± 4.8% and 23.3 ± 4.8% in the nH average, VW average and VW specific models, respectively. Experimental contact area was larger than FE predicted contact area with all cartilage representations (Figure 3.6A). Experimental peak contact stress was larger than FE predicted peak contact stress in the nH average models. Conversely, experimental peak contact stress was smaller than FE predicted peak contact stress in the VW average and VW specific models (Figure 3.6B). Experimental average contact stress was larger than FE predicted average contact stress with all cartilage representations (Figure 3.6C).

Cartilage material coefficients exhibited significant regional variation within the hip joint (Table 3.1). When the data were pooled, both μ and E_0 were larger in the acetabular

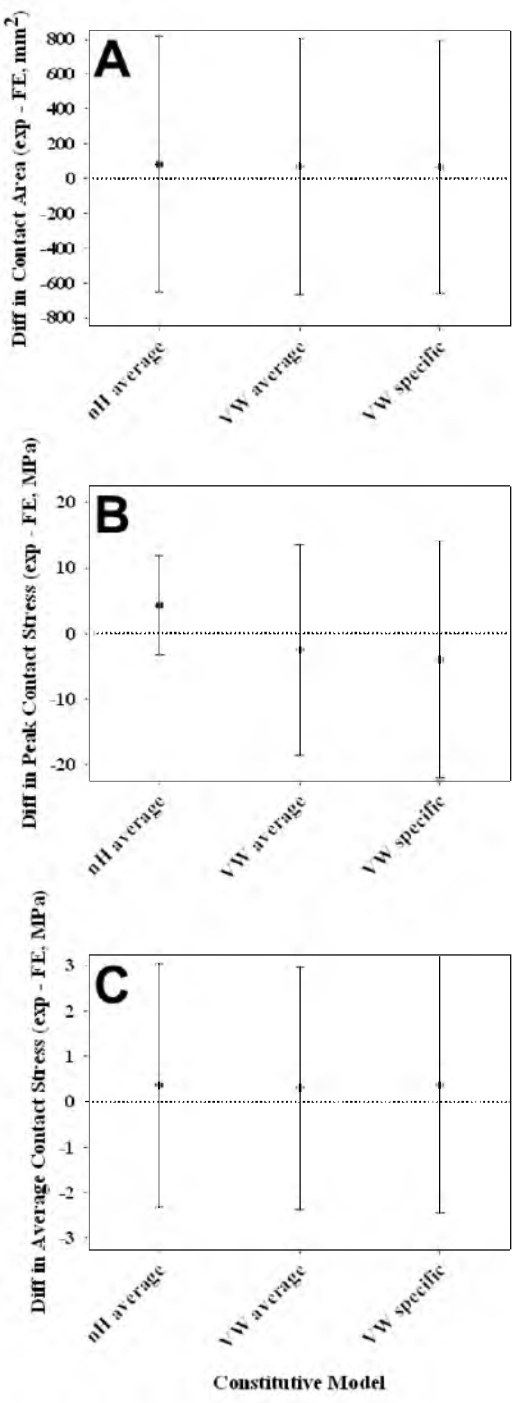

Figure 3.6: Comparisons of experimental and FE results show that validation metrics were insensitive to constitutive model. A – Bland-Altman analysis of contact area. B – Bland-Altman analysis of peak contact stress. C – Bland-Altman analysis of average contact stress. Differences were calculated by subtracting the FE predicted value from the experimentally measured value. Differences greater than zero indicate larger experimental results than FE predictions. Error bars = tolerance intervals corrected by the design effect.

Table 3.1 Constitutive model coefficients determined from curve fitting experimental Cauchy stress versus stretch data. Mean ± standard deviation are shown. Anatomical regions are shown in Figure 3.2. The pooled lateral, medial and whole regional coefficients were obtained by averaging across all samples.

Side	Region	neo-Hookean μ (MPa)	Veronda Westmann C_1 (MPa)	Veronda Westmann C_2 (no units)
Femur	AL	5.72 ± 2.74	0.30 ± 0.17	6.70 ± 1.51
	AM	4.06 ± 0.98	0.31 ± 0.27	5.87 ± 1.86
	SL	5.50 ± 1.52	0.34 ± 0.17	6.45 ± 2.13
	SM	3.46 ± 2.04	0.19 ± 0.18	8.40 ± 3.05
	PL	6.22 ± 2.32	0.38 ± 0.30	6.93 ± 2.33
	PM	4.74 ± 1.38	0.29 ± 0.08	6.98 ± 1.13
	IL	6.34 ± 0.74	0.48 ± 0.21	5.26 ± 0.94
	IM	3.92 ± 0.62	0.23 ± 0.18	7.23 ± 2.23
	F	4.98 ± 2.16	0.29 ± 0.17	6.34 ± 1.89
	Lateral	5.88 ± 2.10	0.36 ± 0.21	6.36 ± 1.42
	Medial	4.08 ± 1.52	0.26 ± 0.18	7.10 ± 2.68
	Whole	4.88 ± 2.02	0.30 ± 0.21	6.71 ± 2.27
Acetabulum	AL	9.34 ± 3.20	0.72 ± 0.37	5.31 ± 1.09
	AM	4.82 ± 1.12	0.22 ± 0.12	7.42 ± 1.51
	SL	6.54 ± 2.62	0.29 ± 0.16	7.31 ± 0.59
	SM	4.68 ± 0.58	0.26 ± 0.08	7.21 ± 0.94
	PL	7.96 ± 1.80	0.45 ± 0.10	6.13 ± 0.34
	PM	5.74 ± 1.78	0.31 ± 0.19	6.60 ± 1.09
	Lateral	7.74 ± 2.28	0.47 ± 0.27	6.33 ± 1.29
	Medial	5.04 ± 1.60	0.26 ± 0.15	7.20 ± 1.43
	Whole	6.44 ± 2.58	0.37 ± 0.25	6.69 ± 1.42
Both	Lateral	6.50 ± 2.54	0.40 ± 0.26	6.22 ± 1.48
	Medial	4.40 ± 1.56	0.28 ± 0.20	6.86 ± 2.44
	Whole	5.32 ± 2.32	0.34 ± 0.24	6.55 ± 2.07

cartilage than in the femoral cartilage, and larger in the lateral cartilage than in the medial cartilage. In the acetabulum, both μ and E_0 were larger in the AL region than in all other regions. Both μ and E_0 in the acetabulum were also larger in the PL region than in the PM and SM regions. In the SL region, μ was larger than in the SM region of the acetabulum. In the femur, both μ and E_0 were larger in the IL region than in the IM, PL, SM and AL regions. E_0 was also larger in the AM region than in the IM region in the femur. In the SM region, μ was smaller than in the SL, PM, PL and AL regions. In the PL region, μ was larger than in the AM region. In the SL region, μ was larger in than in the IM region in the femur. Although many of the regional differences were consistent for both constitutive models, the quasilinear behavior exhibited in the neo-Hookean constitutive model overpredicted stress at stretch values near unity and underpredicted stress at smaller stretch values (Figure 3.7).

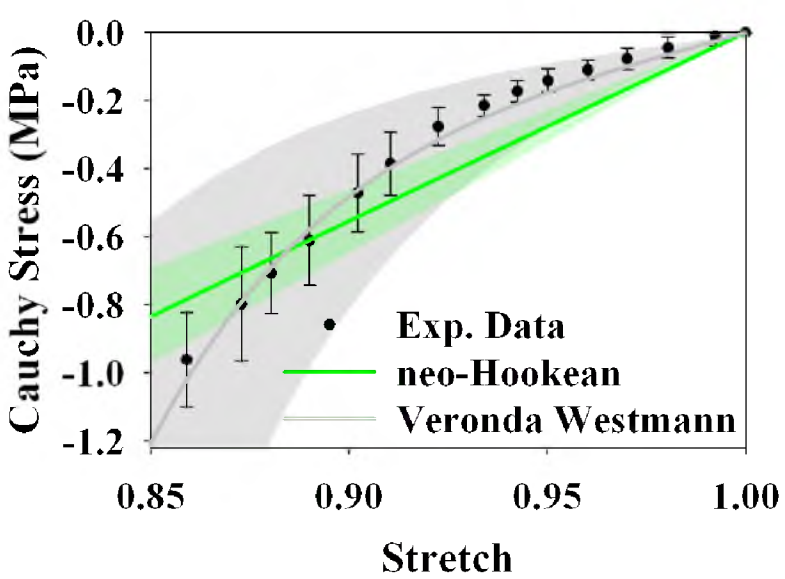

Figure 3.7: Experimental Cauchy stress versus stretch curve for one specimen in the femoral SM region. Error bars = standard deviation. Solid lines for each fit represent the response with average coefficients, shaded areas = standard deviation. The neo-Hookean constitutive model overpredicted stress magnitudes at stretch values near unity and underpredicted stress magnitudes at smaller stress values. The Veronda Westmann constitutive model captured cartilage material nonlinearity.

When comparing model predictions within each region between FE models, nH average models predicted lower peak contact stress than both VW average and VW specific models in some regions (Figure 3.8B). However, there were no significant differences in average contact stress or in contact area between the three cartilage representations (Figures 3.8A and 3.8C). There were no significant differences in FE results between VW average and VW specific models (Figure 3.8).

Peak contact stress, average contact stress and contact area varied by region, with higher values in several of the lateral regions (Figure 3.9). For all three cartilage representations, peak contact stress, average contact stress and contact area were smaller in the medial cartilage than in the lateral cartilage. For the VW average models, peak contact stress, average contact stress and contact area were smaller in the PM region than in all other regions. Peak contact stress was larger in the AL region than in all other regions. Contact area in the SL region was larger than in all medial and both posterior regions. Contact area in the AL region was larger than in both posterior regions and the AM region. Contact area in the SM region was larger than in the AM region and both posterior regions. Average contact stress in the AL and SL regions was larger than in all medial regions. Although significant results varied slightly between the VW average models and the other two cartilage representations, the trends were similar.

Discussion

Qualitative and quantitative comparisons between FE and experimental results indicate that the quality of validation for contact stress is relatively insensitive to the choice of cartilage constitutive model. Further, the lack of difference in model predictions between analyses with specimen-specific material coefficients and analyses

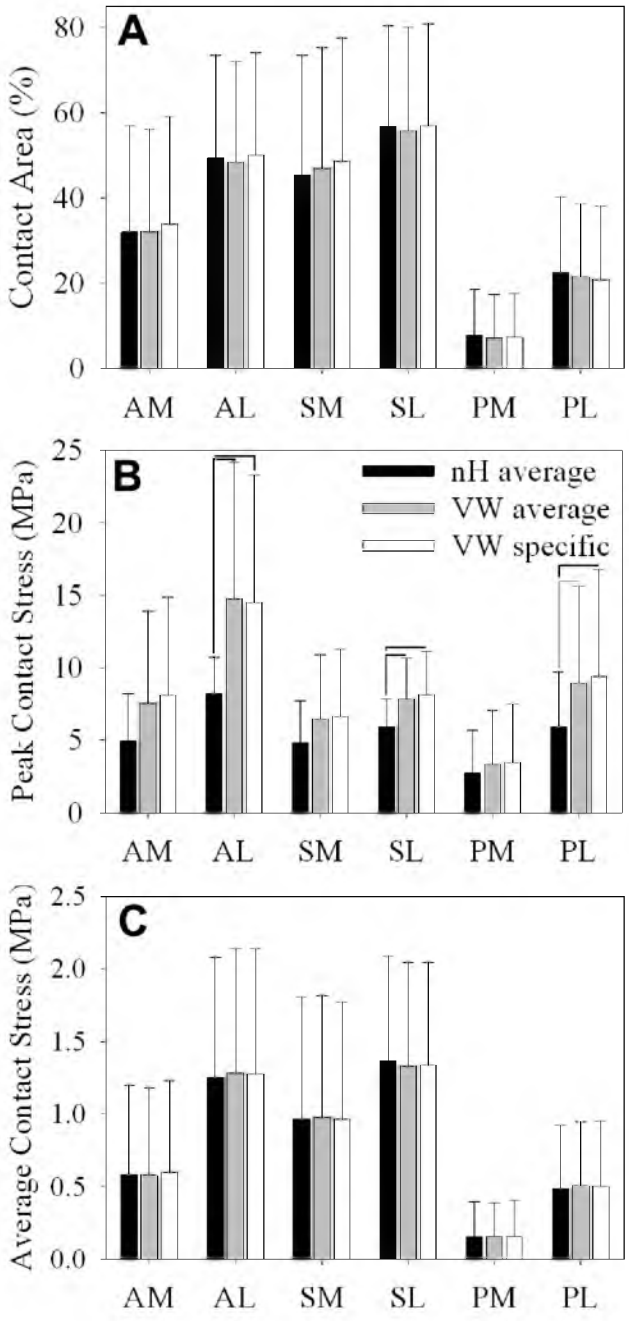

Figure 3.8: Contact area and contact stress for all constitutive models, by anatomical region. A – contact area. B – peak contact stress. C – average contact stress. Error bars = standard deviation. Black lines = significant differences ($p \leq 0.05$) and gray lines = nearly significant differences ($0.05 < p \leq 0.1$). The only significant differences were in peak contact stress in the lateral regions.

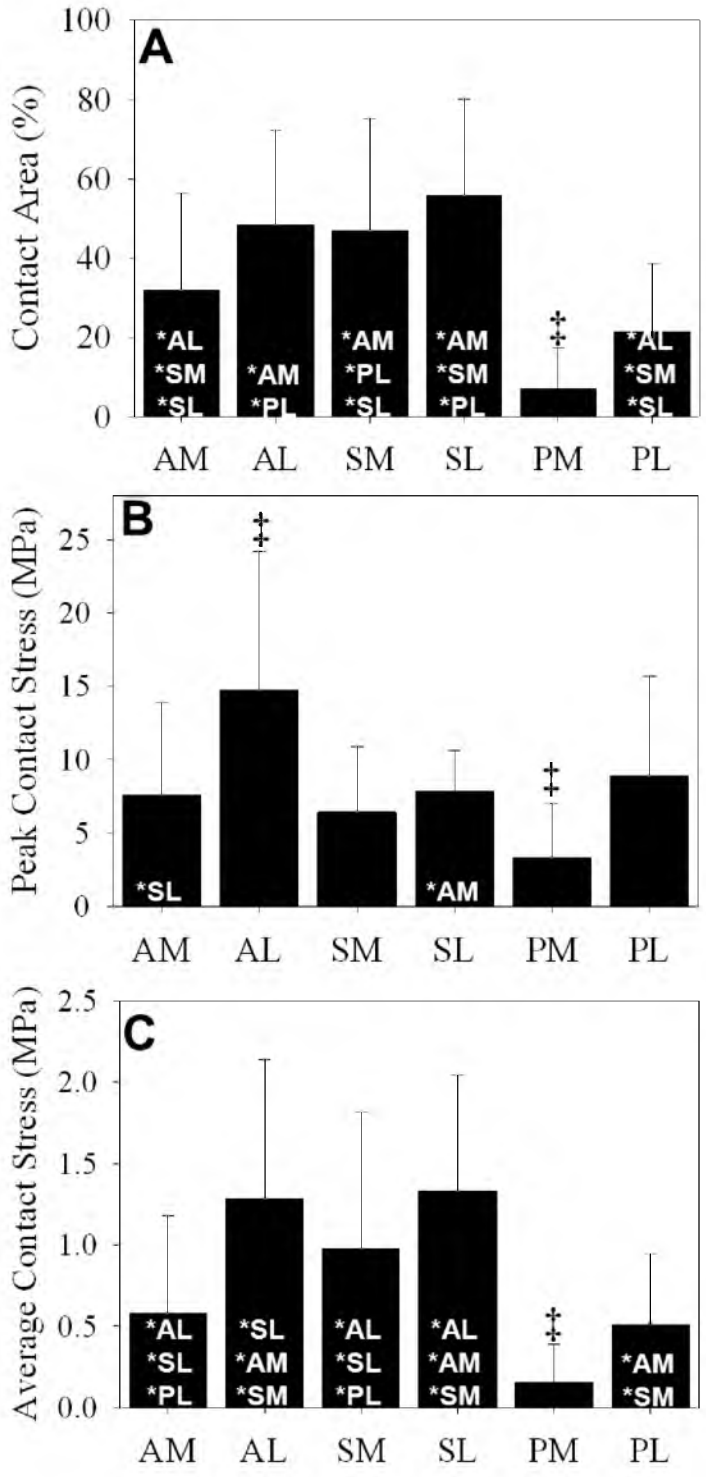

Figure 3.9: Contact area and contact stress VW average models. A – contact area. B – peak contact stress. C – average contact stress. Error bars = standard deviation. ‡ indicates $p \leq 0.05$ against all other regions. * indicates $p \leq 0.05$ against listed region. Results were generally larger in the lateral regions and were the smallest in the PM region.

with averaged material coefficients suggests that predictions of hip contact stress and contact area are insensitive to regional variations in material coefficients in hips with healthy articular cartilage (Figure 3.8). These results are consistent with previous analyses in the hip, wherein contact stress patterns resulted primarily from model geometry [12, 15], and in the knee, which reported that contact stress predictions were insensitive to variations in cartilage anisotropy [25]. The influence of model geometry also reiterates previous findings of intersubject variability in contact stress patterns in a population of normal hips [15]. The relative insensitivity of contact pattern to cartilage representation and the relative importance of model geometry can be explained by the fact that contact stress as measured by pressure-sensitive film is primarily a measure of the interstitial fluid pressure on the surface when the cartilage is loaded quickly [58].

This is the first study to characterize the instantaneous regional material behavior of healthy human hip cartilage. These data demonstrate distinct regional differences, including the finding that lateral cartilage is stiffer than medial cartilage. Previous studies have suggested that regional variations in cartilage properties result from adaptation to loading, with stiffer properties in areas of frequent loadbearing [27, 59-62]. Indeed, in the present study, the stiffer lateral regions of the acetabulum experienced larger peak contact stress, average contact stress and contact area than medial regions. Since walking accounts for most of the time wherein cartilage undergoes fast loading [63], these data suggest that the instantaneous material properties of healthy human hip cartilage may result from adaptation to the loading distribution.

The regional variations in instantaneous material behavior in this study are different than previously reported variations in the biphasic material behavior of cartilage.

Athanasiou et al. demonstrated that the linear biphasic aggregate moduli were larger in the medial acetabulum and femur than in the lateral acetabulum and femur, but there were no differences in aggregate modulus between the pooled femoral cartilage and the pooled acetabular cartilage [37]. In contrast, we found that lateral cartilage was stiffer than medial cartilage under fast loading rates, and pooled acetabular cartilage was stiffer than pooled femoral cartilage. Our findings do not necessarily contradict the results reported by Athanasiou et al.; the aggregate modulus is a measure of equilibrium behavior of the solid matrix, while μ and E_0 are measures of solid-fluid interactions. Further, the linear biphasic representation is valid for small strains, while the hyperelastic representations used in the present study are valid for arbitrarily large deformations. Therefore, these coefficients reflect different mechanisms and provide unique information regarding the ways in which cartilage responds to load.

The neo-Hookean constitutive model overpredicted the experimental stress-strain curve at small strain magnitudes and underpredicted stress at large strain magnitudes, which affected the FE predictions of contact stress. At large strain magnitudes, FE models with nH average cartilage underpredicted peak contact stress in comparison to both FE models with VW cartilage and experimental results (Figures 3.6B and 3.8B). However, when the results were evaluated over the entire range of strains, average contact stress, contact area and qualitative contact patterns were indistinguishable between cartilage representations (Figures 3.5, 3.8A and 3.8C). Therefore, a simple neo-Hookean constitutive model is sufficient to provide predictions of average contact stress on the articular surface and contact area that in reasonable agreement with experimental measurements. This is consistent with the findings reported in previous FE studies, as

well as the ability of discrete element analysis to accurately predict contact mechanics in the human hip [11, 64-66].

The experimental and computational results of this study for contact stress and contact patterns compare well with previous studies. In vitro peak contact stresses measured using pizeoelectric pressure sensors, pressure-sensitive film and transducers range between ~5 to ~10 MPa [11, 67-71]. An instrumented prosthesis measured peak pressures of up to ~10 MPa in vivo during activities of daily living [72]. In the present study, pressure sensitive film measured peak contact stress at 13.8 ± 2.8 MPa and FE models with VW average cartilage predicted peak contact stress at 16.4 ± 7.8 MPa. While the peak contact stresses in the present study are somewhat larger than previously published values, some of the previous studies were limited by upper thresholds on the pressure-sensing devices or by the use of spherical implants, which results in lower predictions of contact stress [12]. Qualitatively, the nonuniform and specimen-specific contact patterns in the present study are consistent with previous observations in experimental studies of hip contact [11, 67-71, 73, 74].

There were several limitations in this study. The primary dependent variables in this study, contact stress and contact area, were chosen because they can be measured experimentally, allowing direct validation against experimental measurements in the cadaveric hips, and because they have been suggested as important variables in the pathogenesis of OA [18, 30-33]. However, these variables only reflect the state of stress on the articular surface. Other variables, such as maximum shear stress and the first principal (most tensile) strain, or variables at other locations such as at the osteochondral interface, are likely to be even more important for predicting cartilage damage and

delamination [25, 31, 75]. While average contact stress and contact area were more sensitive to geometry than to cartilage constitutive model in the present study, the selected constitutive model may be more important in the evaluation of other variables. For example, a previous FE model of the knee demonstrated that a constitutive model that took into account spatial variance in the split line directions did not affect contact stress predictions but did affect other variables, including first principal strain [25]. A detailed investigation of the sensitivity of model predictions to other variables such as first principal strain and maximum shear stress will require further analysis of the strain and stress fields through the thickness, necessitating more refined experimental measurements, constitutive representations and new mesh convergence studies.

Although the cartilage constitutive behavior in these models captured material nonlinearity and spatial inhomogeneity, the constitutive models included several simplifying assumptions. Cartilage behavior was assumed to be nearly-incompressible and hyperelastic. While this assumption is justified by both theoretical analysis and experimental data for the loading rates and activities that were considered in this study [22, 23], it may have a minor effect on model results and will limit the interpretation of the results of this study to activities that occur at relatively high loading rates. The inclusion of cartilage tension-compression nonlinearity, wherein the modulus in tension is one to two orders of magnitude stiffer than that in compression, could also affect the FE model predictions [76]. Other characteristics of cartilage material behavior, such as depth-dependent variation in properties and material anisotropy, are considered to be higher order effects when compared to material nonlinearity and tension-compression nonlinearity, and would therefore be expected to have less pronounced effects on model

predictions [31, 77-82]. In addition to the limitations of the selected constitutive models, it is possible that freezing the cartilage samples prior to testing affected the material properties. While freezing was necessary due to the lengthy experimental protocol, literature suggests that this procedure has either no effect on cartilage stiffness or decreases cartilage stiffness up to 31% [83-86]. In either case, since all samples were frozen, there was no bias in the comparisons between groups.

Finally, there are limitations associated with the use of pressure-sensitive film for model validation. We used pressure-sensitive film because of its high spatial resolution (5-15 μm) (Fuji Prescale® Brochure, Sensor Products, Inc., NJ) and broad use in studies of joint contact mechanics [87]. A previous study demonstrated that the peak contact stress measured by pressure sensitive film may differ from that in a native joint by 10-26% for a plane-strain analysis of a surrogate contact mechanics problem (R_1 = 20 mm, R_2 = 30 mm or larger, cartilage thickness = 0.6 mm) [88]. Because hip cartilage is thicker and the hip joint is more congruent than in the model problem described above, we constructed and analyzed similar FE models using dimensions from spherical fits to the articular surfaces of one of our specimens (R_1 = 25 mm, R_2 = 27 mm, cartilage thickness = 2.0 mm). These models predicted differences in peak contact stress of less than 1% between the models with and without film. Independent of errors induced by the presence of film between the articular layers, pressure-sensitive film has an error of 10-15% when measuring contact stress [89]. This error may contribute to the large tolerance intervals in the Bland-Altman analysis (Figure 3.6).

In summary, this study provides a validated modeling protocol for a series of cadaveric specimens that supports the use of average cartilage material coefficients in

predicting specimen-specific hip contact stress and contact area. This protocol can be used in vivo to understand how abnormal hip contact stress and contact area lead to OA. The Veronda Westmann constitutive model with average material coefficients accurately predicted peak contact stress, average contact stress, contact area and contact patterns. The use of subject- and region-specific material coefficients did not increase the accuracy of FE model predictions with the Veronda Westmann constitutive model. The neo-Hookean constitutive model accurately predicted average contact stress, contact area and contact patterns, but underpredicted peak contact stress in areas of high stress. Therefore, the Veronda Westmann constitutive model with average material coefficients is preferred for future predictions of hip contact mechanics. The use of average material coefficients simplifies subject-specific modeling in vivo because subject-specific material coefficients are difficult to obtain. This protocol can be used for hips with healthy articular cartilage, but should be applied with caution to joints with degenerated cartilage. The equilibrium tensile modulus of osteoarthritic cartilage can be up to 15 times smaller than that of healthy cartilage [90], which is much larger than the largest interregion differences in the present study (up to four times in E_0). Additionally, the structural changes associated with OA cause decreased stiffness and increased permeability in human hip cartilage with increased matrix disruption [91]. Finally, this is the first report of the regional instantaneous material behavior of healthy cartilage in the hip, providing the necessary inputs for future computational studies investigating cartilage mechanics other than contact stress and area in the human hip.

References

[1] Murphy, L. B., Helmick, C. G., Schwartz, T. A., Renner, J. B., Tudor, G., Koch, G. G., Dragomir, A. D., Kalsbeek, W. D., Luta, G., and Jordan, J. M., 2010, "One in Four People May Develop Symptomatic Hip Osteoarthritis in His or Her Lifetime," Osteoarthritis Cartilage, **18**(11), pp. 1372-1379.

[2] Carter, D. R., Beaupre, G. S., Wong, M., Smith, R. L., andriacchi, T. p., and Schurman, D. J., 2004, "The Mechanobiology of Articular Cartilage Development and Degeneration," Clin Orthop Relat Res (427 Suppl), pp. S69-77.

[3] Guilak, F., Fermor, B., Keefe, F. J., Kraus, V. B., Olson, S. A., Pisetsky, D. S., Setton, L. A., and Weinberg, J. B., 2004, "The Role of Biomechanics and Inflammation in Cartilage Injury and Repair," Clin Orthop Relat Res(423), pp. 17-26.

[4] Wilson, W., Van Donkelaar, C. C., Van Rietbergen, R., and Huiskes, R., 2005, "The Role of Computational Models in the Search for the Mechanical Behavior and Damage Mechanisms of Articular Cartilage," Med Eng Phys, **27**(10), pp. 810-826.

[5] Guilak, F., and Hung, C. T., 2005, "Physical Regulation of Cartilage Metabolism," *Basic Orthopaedic Biomechanics and Mechano-Biology*, V. C. Mow, and R. Huiskes, Eds., Lippincott Williams & Wilkins, Philadephia.

[6] Atkinson, p. J., and Haut, R. C., 1995, "Subfracture Insult to the Human Cadaver Patellofemoral Joint Produces Occult Injury," J Orthop Res, **13**(6), pp. 936-944.

[7] Haut, R. C., Ide, T. M., and De Camp, C. E., 1995, "Mechanical Responses of the Rabbit Patello-Femoral Joint to Blunt Impact," J Biomech Eng, **117**(4), pp. 402-408.

[8] Li, X., Haut, R. C., and Altiero, N. J., 1995, "An Analytical Model to Study Blunt Impact Response of the Rabbit P-F Joint," J Biomech Eng, **117**(4), pp. 485-491.

[9] Newberry, W. N., Garcia, J. J., Mackenzie, C. D., Decamp, C. E., and Haut, R. C., 1998, "Analysis of Acute Mechanical Insult in an Animal Model of Posttraumatic Osteoarthrosis," J Biomech Eng, **120**(6), pp. 704-709.

[10] Silyn-Roberts, H., and Broom, N. D., 1990, "Fracture Behaviour of Cartilage-on-Bone in Response to Repeated Impact Loading," Connect Tissue Res, **24**(2), pp. 143-156.

[11] Anderson, A. E., Ellis, B. J., Maas, S. A., Peters, C. L., and Weiss, J. A., 2008, "Validation of Finite Element Predictions of Cartilage Contact Pressure in the Human Hip Joint," J Biomech Eng, **130**(5), pp. 051008-051008.

[12] Anderson, A. E., Ellis, B. J., Maas, S. A., and Weiss, J. A., 2010, "Effects of Idealized Joint Geometry On Finite Element Predictions of Cartilage Contact Stresses in the Hip," J Biomech, **43**(7), pp. 1351-1357.

[13] Brown, T. D., and DiGioia, A. M., 3rd, 1984, "A Contact-Coupled Finite Element Analysis of the Natural Adult Hip," J Biomech, **17**(6), pp. 437-448.

[14] Chegini, S., Beck, M., and Ferguson, S. J., 2009, "The Effects of Impingement and Dysplasia on Stress Distributions in the Hip Joint During Sitting and Walking: A Finite Element Analysis," J Orthop Res, **27**(2), pp. 195-201.

[15] Harris, M. D., Anderson, A. E., Henak, C. R., Ellis, B. J., Peters, C. L., and Weiss, J. A., 2012, "Finite Element Prediction of Cartilage Contact Stresses in Normal Human Hips," J Orthop Res, **30**(7), pp. 1133-1139.

[16] Henak, C. R., Ellis, B. J., Harris, M. D., Anderson, A. E., Peters, C. L., and Weiss, J. A., 2011, "Role of the Acetabular Labrum in Load Support Across the Hip Joint," J Biomech, **44**(12), pp. 2201-2206.

[17] Rapperport, D. J., Carter, D. R., and Schurman, D. J., 1985, "Contact Finite Element Stress Analysis of the Hip Joint," J Orthop Res, **3**(4), pp. 435-446.

[18] Russell, M. E., Shivanna, K. H., Grosland, N. M., and Pedersen, D. R., 2006, "Cartilage Contact Pressure Elevations in Dysplastic Hips: A Chronic Overload Model," J Orthop Surg Res, **1**, pp. 6-6.

[19] 2006, "ASME V&V 10-2006 Guide for Verification and Validation in Computational Solid Mechanics," ASME Standards.

[20] Anderson, A. E., Ellis, B. J., and Weiss, J. A., 2007, "Verification, Validation and Sensitivity Studies in Computational Biomechanics," Comput Methods Biomech Biomed Engin, **10**(3), pp. 171-184.

[21] Henninger, H. B., Reese, S. p., Anderson, A. E., and Weiss, J. A., 2010, "Validation of Computational Models in Biomechanics," Proc inst Mech Eng H, **224**(7), pp. 801-812.

[22] Ateshian, G. A., Ellis, B. J., and Weiss, J. A., 2007, "Equivalence Between Short-Time Biphasic and Incompressible Elastic Material Responses," J Biomech Eng, **129**(3), pp. 405-412.

[23] Wong, M., Ponticiello, M., Kovanen, V., and Jurvelin, J. S., 2000, "Volumetric Changes of Articular Cartilage During Stress Relaxation in Unconfined Compression," J Biomech, **33**(9), pp. 1049-1054.

[24] Gu, K. B., and Li, L. p., 2011, "A Human Knee Joint Model Considering Fluid Pressure and Fiber Orientation in Cartilages and Menisci," Med Eng Phys, **33**(4), pp. 497-503.

[25] Mononen, M. E., Mikkola, M. T., Julkunen, p., Ojala, R., Nieminen, M. T., Jurvelin, J. S., and Korhonen, R. K., 2012, "Effect of Superficial Collagen Patterns and

Fibrillation of Femoral Articular Cartilage on Knee Joint Mechanics-a Three-Dimensional Finite Element Analysis," J Biomech, **45**(3), pp. 579-587.

[26] Athanasiou, K. A., Agarwal, A., Muffoletto, A., Dzida, F. J., Constantinides, G., and Clem, M., 1995, "Biomechanical Properties of Hip Cartilage in Experimental Animal Models," Clin Orthop Relat Res (316), pp. 254-266.

[27] Shepherd, D. E., and Seedhom, B. B., 1999, "The 'Instantaneous' Compressive Modulus of Human Articular Cartilage in Joints of the Lower Limb," Rheumatology (Oxford), **38**(2), pp. 124-132.

[28] Taylor, S. D., Tsiridis, E., ingham, E., Jin, Z., Fisher, J., and Williams, S., 2012, "Comparison of Human and Animal Femoral Head Chondral Properties and Geometries," Proc inst Mech Eng H, **226**(1), pp. 55-62.

[29] Treppo, S., Koepp, H., Quan, E. C., Cole, A. A., Kuettner, K. E., and Grodzinsky, A. J., 2000, "Comparison of Biomechanical and Biochemical Properties of Cartilage From Human Knee and Ankle Pairs," J Orthop Res, **18**(5), pp. 739-748.

[30] Creamer, p., and Hochberg, M. C., 1997, "Osteoarthritis," Lancet, **350**(9076), pp. 503-508.

[31] Henak, C. R., Anderson, A. E., and Weiss, J. A., 2013, "Subject-Specific Analysis of Joint Contact Mechanics: Application to the Study of Osteoarthritis and Surgical Planning," J Biomech Eng, **135**(2), p. 021003.

[32] Segal, N. A., Anderson, D. D., Iyer, K. S., Baker, J., Torner, J. C., Lynch, J. A., Felson, D. T., Lewis, C. E., and Brown, T. D., 2009, "Baseline Articular Contact Stress Levels Predict incident Symptomatic Knee Osteoarthritis Development in the MOST Cohort," J Orthop Res, **27**(12), pp. 1562-1568.

[33] Segal, N. A., Kern, A. M., Anderson, D. D., Niu, J., Lynch, J., Guermazi, A., Torner, J. C., Brown, T. D., and Nevitt, M., 2012, "Elevated Tibiofemoral Articular Contact Stress Predicts Risk for Bone Marrow Lesions and Cartilage Damage At 30 Months," Osteoarthritis Cartilage, **20**(10), pp. 1120-1126.

[34] Fischer, K. J., Manson, T. T., Pfaeffle, H. J., Tomaino, M. M., and Woo, S. L., 2001, "A Method For Measuring Joint Kinematics Designed for Accurate Registration of Kinematic Data to Models Constructed from CT Data," J Biomech, **34**(3), pp. 377-383.

[35] Anderson, A. E., Ellis, B. J., Peters, C. L., and Weiss, J. A., 2008, "Cartilage Thickness: Factors influencing Multidetector CT Measurements in a Phantom Study," Radiology, **246**(1), pp. 133-141.

[36] Bergmann, G., Deuretzbacher, G., Heller, M., Graichen, F., Rohlmann, A., Strauss, J., and Duda, G. N., 2001, "Hip Contact Forces and Gait Patterns from Routine Activities," J Biomech, **34**(7), pp. 859-871.

[37] Athanasiou, K. A., Agarwal, A., and Dzida, F. J., 1994, "Comparative Study of the Intrinsic Mechanical Properties of the Human Acetabular and Femoral Head Cartilage," J Orthop Res, **12**(3), pp. 340-349.

[38] Huang, C. Y., Soltz, M. A., Kopacz, M., Mow, V. C., and Ateshian, G. A., 2003, "Experimental Verification of the Roles of Intrinsic Matrix Viscoelasticity and Tension-Compression Nonlinearity in the Biphasic Response of Cartilage," J Biomech Eng, **125**(1), pp. 84-93.

[39] Krishnan, R., Park, S., Eckstein, F., and Ateshian, G. A., 2003, "Inhomogeneous Cartilage Properties Enhance Superficial Interstitial Fluid Support and Frictional Properties, but do not Provide a Homogeneous State of Stress," J Biomech Eng, **125**(5), pp. 569-577.

[40] Park, S., Hung, C. T., and Ateshian, G. A., 2004, "Mechanical Response of Bovine Articular Cartilage Under Dynamic Unconfined Compression Loading At Physiological Stress Levels," Osteoarthritis Cartilage, **12**(1), pp. 65-73.

[41] Soltz, M. A., and Ateshian, G. A., 2000, "A Conewise Linear Elasticity Mixture Model For the Analysis of Tension-Compression Nonlinearity in Articular Cartilage," J Biomech Eng, **122**(6), pp. 576-586.

[42] Veronda, D. R., and Westmann, R. A., 1970, "Mechanical Characterization of Skin-Finite Deformations," J Biomech, B(1), pp. 111-124.

[43] Maas, S., Rawlins, D., Weiss, J., and Ateshian, G., 2011, "FEBio: Theory Manual," Musculoskeletal Reserach Laboratories.

[44] Quapp, K. M., and Weiss, J. A., 1998, "Material Characterization of Human Medial Collateral Ligament," J Biomech Eng, **120**(6), pp. 757-763.

[45] Anderson, A. E., Peters, C. L., Tuttle, B. D., and Weiss, J. A., 2005, "Subject-Specific Finite Element Model of the Pelvis: Development, Validation and Sensitivity Studies," J Biomech Eng, **127**(3), pp. 364-373.

[46] Dalstra, M., and Huiskes, R., 1995, "Load Transfer Across the Pelvic Bone," J Biomech, **28**(6), pp. 715-724.

[47] Puso, M. A., 2000, "A Highly Efficient Enhanced Assumed Strain Physically Stabilized Hexahedral Element," int J Numer Meth Eng, **49**(8), pp. 1029-1064.

[48] Puso, M. A., and Laursen, T. A., 2004, "A Mortar Segment-to-Segment Contact Method for Large Deformation Solid Mechanics," Comput Method Appl M, **193**(6-8), pp. 601-629.

[49] Puso, M. A., Maker, B. N., Ferencz, R. M., and Hallquist, J. O., 2007, "NIKE3D: A Nonlinear, Implicit, Three-Dimensional Finite Element Code For Solid and Structural Mechanics," User's Manual.

[50] Press, W. H., Teukolsky, S. A., Vetterling, W. T., and Flannery, B. p., 2007, "Interpolation and Extrapolation," *Numerical Recipes: The Art of Scientific Computing*, Cambridge University Press, New York.

[51] Chapra, S. C., and Canale, R. p., 2002, "Finite Difference: Elliptic Equations," *Numerical Methods For Engineers*, McGraw-Hill Higher Education, New York.

[52] Maas, S. A., Ellis, B. J., Ateshian, G. A., and Weiss, J. A., 2012, "FEBio: Finite Elements For Biomechanics," J Biomech Eng, **134**(1), p. 011005.

[53] Maas, S., Rawlins, D., and Weiss, J., 2012, "PostView: Finite Element Postprocessing," Musculoskeletal Research Laboratories, p. http://mrl.sci.utah.edu/software/postview.

[54] Allen, B. C., Peters, C. L., Brown, N. A., and Anderson, A. E., 2010, "Acetabular Cartilage Thickness: Accuracy of Three-Dimensional Reconstructions From Multidetector CT Arthrograms in A Cadaver Study," Radiology, **255**(2), pp. 544-552.

[55] Bland, J. M., and Altman, D. G., 1999, "Measuring Agreement in Method Comparison Studies," Stat Methods Med Res, **8**(2), pp. 135-160.

[56] McCarthy, W. F., and Thompson, D. R., 2007, "The Analysis of Pixel intensity (Myocardial Signal Density) Data: The Quantification of Myocardial Perfusion By Imaging Methods.," COBRA Preprint Series, Working Paper 23.

[57] Finner, H., 1993, "On A Monotonicity Problem in Step-Down Multiple Test Procedures," J Am Stat Assoc, **88**(423), pp. 920-923.

[58] Ateshian, G. A., Lai, W. M., Zhu, W. B., and Mow, V. C., 1994, "An Asymptotic Solution For the Contact of Two Biphasic Cartilage Layers," J Biomech, **27**(11), pp. 1347-1360.

[59] Seedhom, B. B., Takeda, T., Tsubuku, M., and Wright, V., 1979, "Mechanical Factors and Patellofemoral Osteoarthrosis," Ann Rheum Dis, **38**(4), pp. 307-316.

[60] Swann, A. C., and Seedhom, B. B., 1993, "The Stiffness of Normal Articular Cartilage and the Predominant Acting Stress Levels: Implications for the Aetiology of Osteoarthrosis," Br J Rheumatol, **32**(1), pp. 16-25.

[61] Yao, J. Q., and Seedhom, B. B., 1993, "Mechanical Conditioning of Articular Cartilage to Prevalent Stresses," Br J Rheumatol, **32**(11), pp. 956-965.

[62] Athanasiou, K. A., Rosenwasser, M. p., Buckwalter, J. A., Malinin, T. I., and Mow, V. C., 1991, "Interspecies Comparisons of In Situ Intrinsic Mechanical Properties of Distal Femoral Cartilage," J Orthop Res, **9**(3), pp. 330-340.

[63] Vissers, M. M., Bussmann, J. B., De Groot, I. B., Verhaar, J. A., and Reijman, M., 2011, "Walking and Chair Rising Performed in the Daily Life Situation Before and After Total Hip Arthroplasty," Osteoarthritis Cartilage, **19**(9), pp. 1102-1107.

[64] Anderson, D. D., Goldsworthy, J. K., Li, W., James Rudert, M., Tochigi, Y., and Brown, T. D., 2007, "Physical Validation of A Patient-Specific Contact Finite Element Model of the Ankle," J Biomech, **40**(8), pp. 1662-1669.

[65] Donahue, T. L., Hull, M. L., Rashid, M. M., and Jacobs, C. R., 2002, "A Finite Element Model of the Human Knee Joint For the Study of Tibio-Femoral Contact," J Biomech Eng, **124**(3), pp. 273-280.

[66] Abraham, C. L., Maas, S. A., Weiss, J. A., Ellis, B. J., Peters, C. L., and Anderson, A. E., 2013, "A New Discrete Element Analysis Method For Predicting Hip Joint Contact Stresses," J Biomech, **46**(6), pp. 1121-1127.

[67] Adams, D., and Swanson, S. A., 1985, "Direct Measurement of Local Pressures in the Cadaveric Human Hip Joint During Simulated Level Walking," Ann Rheum Dis, **44**(10), pp. 658-666.

[68] Afoke, N. Y., Byers, p. D., and Hutton, W. C., 1987, "Contact Pressures in the Human Hip Joint," J Bone Joint Surg Br, **69**(4), pp. 536-541.

[69] Brown, T. D., and Shaw, D. T., 1983, "In Vitro Contact Stress Distributions in the Natural Human Hip," J Biomech, **16**(6), pp. 373-384.

[70] von Eisenhart, R., Adam, C., Steinlechner, M., Muller-Gerbl, M., and Eckstein, F., 1999, "Quantitative Determination of Joint Incongruity and Pressure Distribution During Simulated Gait and Cartilage Thickness in the Human Hip Joint," J Orthop Res, **17**(4), pp. 532-539.

[71] von Eisenhart-Rothe, R., Eckstein, F., Muller-Gerbl, M., Landgraf, J., Rock, C., and Putz, R., 1997, "Direct Comparison of Contact Areas, Contact Stress and Subchondral Mineralization in Human Hip Joint Specimens," Anat Embryol (Berl), **195**(3), pp. 279-288.

[72] Hodge, W. A., Carlson, K. L., Fijan, R. S., Burgess, R. G., Riley, p. O., Harris, W. H., and Mann, R. W., 1989, "Contact Pressures from an Instrumented Hip Endoprosthesis," J Bone Joint Surg Am, **71**(9), pp. 1378-1386.

[73] Rushfeldt, p. D., Mann, R. W., and Harris, W. H., 1981, "Improved Techniques For Measuring In Vitro the Geometry and Pressure Distribution in the Human Acetabulum. II Instrumented Endoprosthesis Measurement of Articular Surface Pressure Distribution," J Biomech, **14**(5), pp. 315-323.

[74] Bay, B. K., Hamel, A. J., Olson, S. A., and Sharkey, N. A., 1997, "Statically Equivalent Load and Support Conditions Produce Different Hip Joint Contact Pressures and Periacetabular Strains," J Biomech, **30**(2), pp. 193-196.

[75] Brand, R. A., 2005, "Joint Contact Stress: A Reasonable Surrogate for Biological Processes?," Iowa Orthop J, **25**, pp. 82-94.

[76] Huang, C. Y., Stankiewicz, A., Ateshian, G. A., and Mow, V. C., 2005, "Anisotropy, Inhomogeneity, and Tension-Compression Nonlinearity of Human Glenohumeral Cartilage in Finite Deformation," J Biomech, **38**(4), pp. 799-809.

[77] Buckley, M. R., Gleghorn, J. p., Bonassar, L. J., and Cohen, I., 2008, "Mapping the Depth Dependence of Shear Properties in Articular Cartilage," J Biomech, **41**(11), pp. 2430-2437.

[78] Chen, A. C., Bae, W. C., Schinagl, R. M., and Sah, R. L., 2001, "Depth- and Strain-Dependent Mechanical and Electromechanical Properties of Full-Thickness Bovine Articular Cartilage in Confined Compression," J Biomech, **34**(1), pp. 1-12.

[79] Maroudas, A., Bayliss, M. T., and Venn, M. F., 1980, "Further Studies on the Composition of Human Femoral Head Cartilage," Ann Rheum Dis, **39**(5), pp. 514-523.

[80] Mow, V. C., and Guo, X. E., 2002, "Mechano-Electrochemical Properties of Articular Cartilage: Their Inhomogeneities and Anisotropies," Annu Rev Biomed Eng, **4**(1), pp. 175-209.

[81] Schinagl, R. M., Gurskis, D., Chen, A. C., and Sah, R. L., 1997, "Depth-Dependent Confined Compression Modulus of Full-Thickness Bovine Articular Cartilage," J Orthop Res, **15**(4), pp. 499-506.

[82] Setton, L. A., Zhu, W., and Mow, V. C., 1993, "The Biphasic Poroviscoelastic Behavior of Articular Cartilage: Role of the Surface Zone in Governing the Compressive Behavior," J Biomech, **26**(4-5), pp. 581-592.

[83] Changoor, A., Fereydoonzad, L., Yaroshinsky, A., and Buschmann, M. D., 2010, "Effects of Refrigeration and Freezing on the Electromechanical and Biomechanical Properties of Articular Cartilage," J Biomech Eng, **132**(6), p. 064502.

[84] Kennedy, E. A., Tordonado, D. S., and Duma, S. M., 2007, "Effects of Freezing on the Mechanical Properties of Articular Cartilage," Biomed Sci Instrum, **43**, pp. 342-347.

[85] Szarko, M., Muldrew, K., and Bertram, J. E., 2010, "Freeze-Thaw Treatment Effects on the Dynamic Mechanical Properties of Articular Cartilage," BMC Musculoskelet Disord, **11**, p. 231.

[86] Willett, T. L., Whiteside, R., Wild, p. M., Wyss, U. p., and Anastassiades, T., 2005, "Artefacts in the Mechanical Characterization of Porcine Articular Cartilage Due to Freezing," Proc inst Mech Eng H, **219**(1), pp. 23-29.

[87] Brown, T. D., Rudert, M. J., and Grosland, N. M., 2004, "New Methods for Assessing Cartilage Contact Stress After Articular Fracture," Clin Orthop Relat Res (423), pp. 52-58.

[88] Wu, J. Z., Herzog, W., and Epstein, M., 1998, "Effects of Inserting a Pressensor Film into Articular Joints on the Actual Contact Mechanics," J Biomech Eng, **120**(5), pp. 655-659.

[89] Hale, J. E., and Brown, T. D., 1992, "Contact Stress Gradient Detection Limits of Pressensor Film," J Biomech Eng, **114**(3), pp. 352-357.

[90] Akizuki, S., Mow, V. C., Muller, F., Pita, J. C., Howell, D. S., and Manicourt, D. H., 1986, "Tensile Properties of Human Knee Joint Cartilage: I. Influence of Ionic Conditions, Weight Bearing, and Fibrillation on the Tensile Modulus," J Orthop Res, **4**(4), pp. 379-392.

[91] Makela, J. T., Huttu, M. R., and Korhonen, R. K., 2012, "Structure-Function Relationships in Osteoarthritic Human Hip Joint Articular Cartilage," Osteoarthritis Cartilage.

CHAPTER 4[1]

ROLE OF THE ACETABULAR LABRUM IN LOAD SUPPORT ACROSS THE HIP JOINT

Abstract

The relatively high incidence of labral tears among patients presenting with hip pain suggests that the acetabular labrum is often subjected to injurious loading in vivo. However, it is unclear whether the labrum participates in load transfer across the joint during activities of daily living. This study examined the role of the acetabular labrum in load transfer for hips with normal acetabular geometry and acetabular dysplasia using subject-specific finite element analysis. Models were generated from volumetric CT data and analyzed with and without the labrum during activities of daily living. The labrum in the dysplastic model supported 4-11% of the total load transferred across the joint, while the labrum in the normal model supported only 1-2% of the total load. Despite the increased load transferred to the acetabular cartilage in simulations without the labrum, there were minimal differences in cartilage contact stresses. This was because the load supported by the cartilage correlated to the cartilage contact area. A higher percentage of load was transferred to the labrum in the dysplastic model because the femoral head achieved equilibrium near the lateral edge of the acetabulum. The results of this study

[1]Reprinted from *Journal of Biomechanics*, Vol. 44, Issue 12. Henak CR, Ellis BJ, Harris MD, Anderson AE, Peters CL, Weiss JA, "Role of the acetabular labrum in load support across the hip joint", pp: 2201-2206, with permission from ELSEVIER.

suggest that the labrum plays a larger role in load transfer and joint stability in hips with acetabular dysplasia than in hips with normal acetabular geometry.

Introduction

The labrum is a fibrocartilagenous ring surrounding the acetabulum in the hip. It is triangular in cross-section, approximately 4.7 mm wide at the bony attachment by approximately 5.5 mm tall [1]. The labrum is primarily composed of circumferential type I collagen fibers [2]. The extent of the labrum medial to the acetabular rim varies by subject and location in the acetabulum [1, 3].

Labral tears are often diagnosed in a clinical setting, suggesting that the labrum can be subjected to substantial loads in vivo [1, 4-13]. There is an increased incidence of labral tears, labral hypertrophy, and labral calcification in hips that exhibit acetabular dysplasia [7-9, 14-17], which suggests that the geometry of the dysplastic hip results in increased loads on the labrum in comparison to the normal hip.

Several studies have investigated the function of the labrum, but have not clearly determined the mechanical role of the labrum in the normal and dysplastic hip [18-24]. In a cadaveric study of normal hips, removal of the labrum had no effect on contact stresses on the acetabular cartilage [23]. However, only the midstance of walking was simulated and the magnitude of the loads that were used in the study were about half of previously measured values for walking [25]. Other studies reported that the labrum acts as a fluid seal on the joint during slow loading over longer periods of time [18, 20-22, 26]. It remains unclear whether the labrum contributes to joint stability and load transfer across the hip joint during activities of daily living.

The contribution of a structure to the mechanical function of a joint can be characterized by the percent of load supported by the structure across the joint. The aim of this study was to determine the load supported by the labrum and the cartilage contact stresses for a representative normal hip and a representative hip with acetabular dysplasia using subject-specific finite element modeling. Parametric studies examined how assumptions regarding the location of the boundary between acetabular cartilage and labrum and the assumed constitutive model for the labrum affected model predictions.

Methods

Two human subjects were selected from a series of six patients with traditional acetabular dysplasia and 18 normal volunteers that were recruited as part of a separate study. All subjects gave informed consent and were included following IRB approval. Patients with symptomatic acetabular dysplasia were screened with anteroposterior (A-P) radiographs. Those with lateral center-edge angles less than 20° were identified as having traditional acetabular dysplasia. Normal volunteers had no history of hip pathology or pain.

A subject with representative acetabular geometry was selected from each population. The patient (female, 35 years old, 66 kg) had a 17° center-edge angle and 19° acetabular index, which approximately matched the median values for the patient population. The shallow acetabulum and lateral under-coverage seen in dysplastic patients are characterized by center-edge angles below 25° and acetabular indices above 10° [27]. Similarly, a normal subject (male, 30 years old, 87 kg) was selected that approximately matched the median center-edge angle and acetabular index of the population of normal volunteers (32° center-edge angle, 9° acetabular index).

Volumetric image data were acquired using CT arthrography (Figure 4.1). Approximately 20 ml of a 2:1 mixture of 1% lidocaine hydrochloride to iohexol (Omnipaque 350, GE Healthcare, Princeton, NJ) was injected into the joint space. CT images were acquired with a field of view encompassing the entire pelvis and both femurs (342 mm for the dysplastic patient, and 331 mm for the normal volunteer), 512×512 acquisition matrix, and 1 mm slice thickness. Subjects were imaged under traction to increase the joint space and thus improve contrast between the acetabular and femoral cartilage [28].

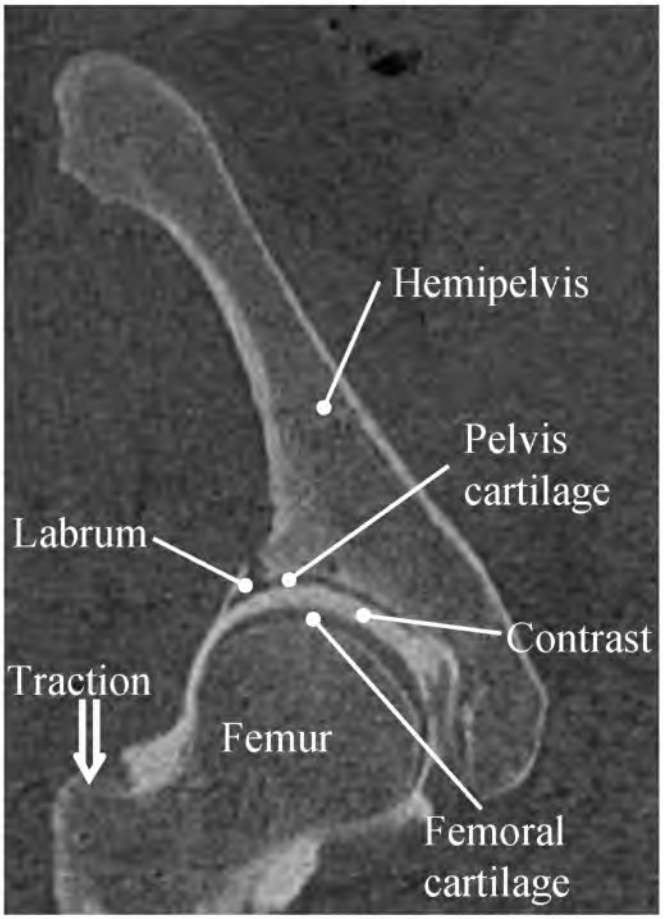

Figure 4.1: Coronal CT slice of the dysplasia patient. Structures of interest are highlighted.

Segmentation of volumetric CT data was performed with a combination of thresholding and manual techniques, using the Amira software (Visage Imaging, Inc., San Diego, CA). Because the resolution of the segmentation mask was tied to voxel size, images were resampled to a higher resolution prior to segmentation (1536×1536 matrix, 0.23×0.23x0.33 mm^3 effective voxel size in the dysplastic patient and 0.22×0.22×0.33 mm^3 effective voxel size in the normal subject). The boundary between the cartilage and labrum was not visible in CT image data, so the initial boundary was defined where the concave acetabulum transitioned into the convex acetabular rim (Figure 4.2). A previous investigation demonstrated that the extent of the labrum on the medial side of the acetabular rim is variable [3]. Therefore, a second boundary was placed approximately 2 mm medial to the baseline boundary to assess the effects of the labrum extending medial to the acetabular rim (Figure 4.2).

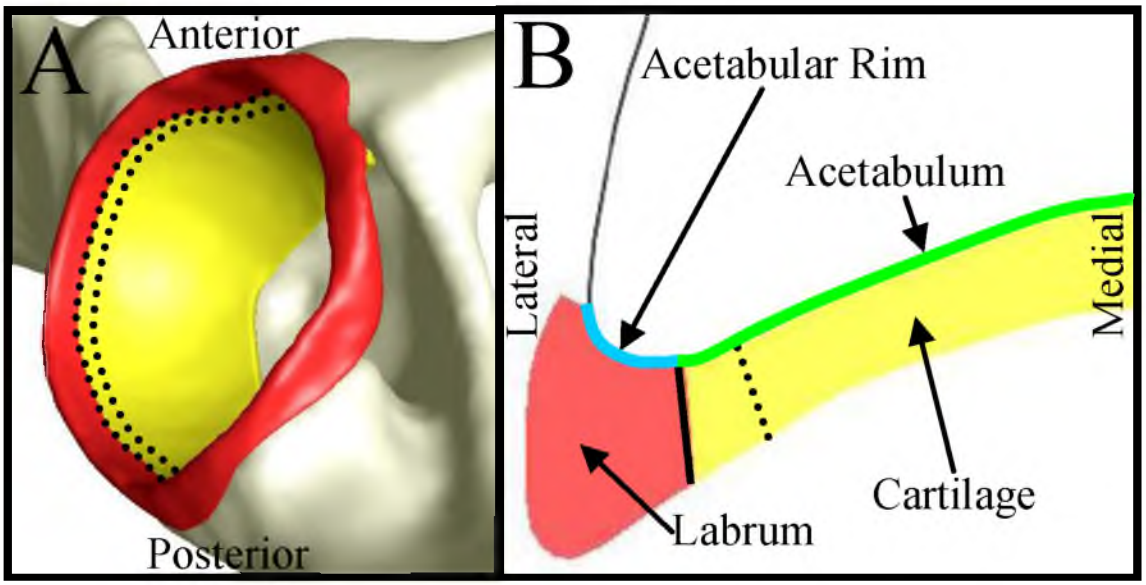

Figure 4.2: Boundaries between the cartilage and labrum that were used in the model of the normal hip. The solid black line indicates the baseline boundary, while the dotted black line indicates the medial boundary, as described in the text. A – superior view, B – cross-sectional view through the superior portion of the acetabulum. The convex acetabular rim is outlined in cyan, and the concave acetabulum is outlined in green.

Element formulations and mesh densities for bones and cartilage were based on our previous study [29] (Figure 4.3). Cortical bone was represented with shell elements [30], with a position-dependent thickness [31]. Cartilage and labrum were represented with hexahedral elements [32, 33]. Hexahedral meshes for the cartilage and labrum were generated from the segmented surfaces using TrueGrid (XYZ Scientific, Livermore, CA). All meshes were generated directly from the segmented surfaces, with no assumptions regarding the geometry of the articular surfaces. A mesh convergence study was performed for the labrum.

Constitutive models for bone and cartilage were identical to those in our previous study [29]. Cortical bone was represented as isotropic linear elastic (E = 17 GPa, ν = 0.29) [34]. Cartilage was represented as neo-Hookean hyperelastic (G = 13.6 MPa, K = 1359 MPa) [35]. The labrum was represented as transversely isotropic hyperelastic [36]. The matrix strain energy was chosen to yield the neo-Hookean constitutive model with shear modulus C_1. The equations describing the material behavior of the fibers included material coefficients that scaled the exponential stress (C_3), specified the rate of collagen uncrimping (C_4), specified the modulus of straightened collagen fibers (C_5), and specified the stretch at which the collagen was straightened (λ^*).

Labrum material coefficients were determined by fitting the constitutive equation to an experimentally-derived expression for uniaxial stress-strain behavior along the fiber direction (C_1 = 1.4 MPa, C_3 = 0.05 MPa, C_4 = 36, C_5 = 66 MPa, λ^* = 1.103) [19]. Material incompressibility was assumed when determining material coefficients because labrum is less permeable than cartilage [19, 37, 38] and cartilage has been demonstrated to behave as an incompressible elastic material over the loading frequencies in activities

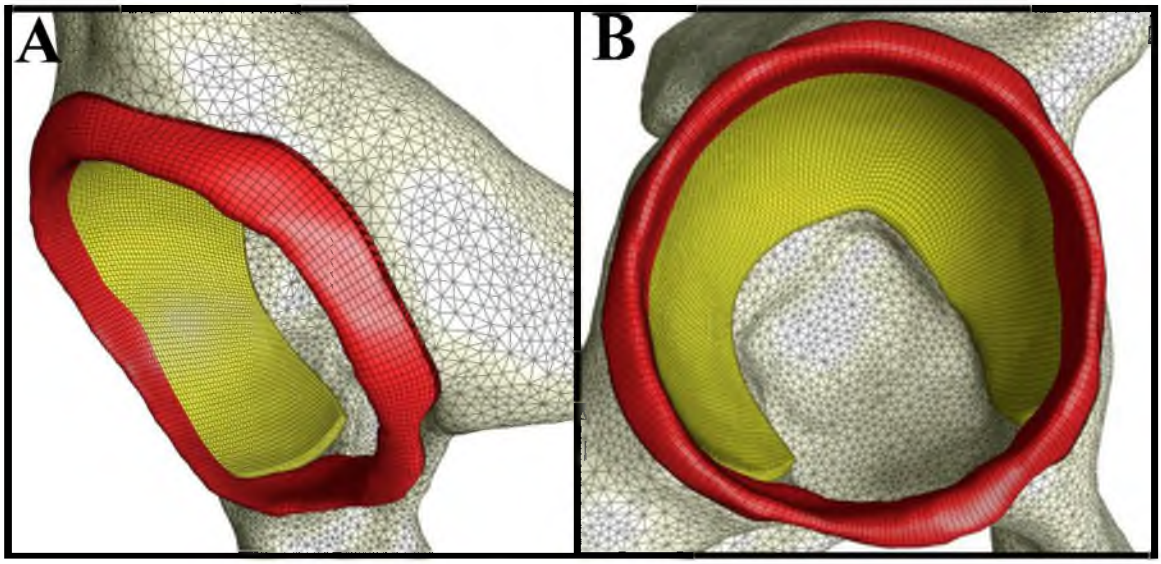

Figure 4.3: Discretized hemipelvis (white), acetabular cartilage (yellow), and labrum (red) in the normal model. A – oblique view of shell and hexahedral meshes. B – medial view of shell and hexahedral meshes.

of daily living [39]. To yield nearly incompressible material behavior, the bulk modulus was specified to be three orders of magnitude greater than C_1. The primary fiber direction was oriented circumferentially [2].

Boundary conditions were chosen to simulate heel strike during walking (WHS, 233% body weight), midstance during walking (WMS, 203% body weight), heel strike while ascending stairs (AHS, 252% body weight) and heel strike while descending stairs (DHS, 261% body weight). Neutral pelvic and femoral orientation was established using anatomical landmarks [25]. The orientation of the applied load and the femur relative to the pelvis were based on instrumented implant and gait data [25]. The magnitude of applied load was scaled by subject body weight [25]. The pubis and sacro-iliac joints were fixed rigidly in space [29]. Motion was applied superiorly to the distal femur. The femur was allowed to move in the medial-lateral and anterior-posterior directions to achieve equilibrium in the acetabulum. Four springs (k = 1 MPa) were used at the distal

femur to remove rigid-body modes from the simulation. Tied and sliding contact algorithms based on the mortar method were used [40, 41]. One sliding interface was defined between the femoral and acetabular cartilage, while a second interface was defined between the femoral cartilage and labrum. Models were analyzed with and without the labrum. Frictionless contact was assumed for all contact interfaces. The friction coefficient between articulating cartilage surfaces is very low, on the order of 0.01-0.02 in the presence of synovial fluid [42-44]. Therefore, it is reasonable to neglect frictional shear stresses between contacting articular surfaces. Models were preprocessed using PreView (http://mrl.sci.utah.edu/software.php), analyzed using the nonlinear implicit solver NIKE3D [45], and postprocessed using PostView (http://mrl.sci.utah.edu/software.php).

Parameter studies were completed to assess the effects of modeling assumptions. To assess the effect of material assumptions, a neo-Hookean constitutive model matched to that used for the simulated cartilage was substituted for the transversely isotropic constitutive model. Additionally, the labrum fiber stiffness was changed ±50% in the transversely isotropic constitutive model. To examine the effect of anatomical angles, the anatomical adduction angle was changed ±3° (approximately 1 standard deviation [25]) in all loading scenarios. Finally, the applied load was changed ±30% (approximately 1 standard deviation [25]) in WHS in the dysplastic model.

Percent load supported by the labrum, average contact stress on the articular cartilage, contact area on the articular cartilage, and deflection of the labrum were determined. Percent load was calculated from the ratio of contact interface force to applied load. Cartilage contact stress was sampled on the surface of the acetabular

cartilage. Cartilage contact area was calculated by summing the surface area of each element in the acetabular cartilage that was in contact with the femoral cartilage. Total deflection of the labrum was sampled through the thickness and maximum values were obtained.

Results

The labrum in the normal model supported 1-2% of the applied load, and the labrum in the dysplastic model supported 4-11% (Figure 4.4). The femoral head in the normal model achieved equilibrium in the center of the acetabulum, while the femoral head in the dysplastic model achieved equilibrium near the lateral edge of the acetabulum (Figure 4.5). When the cartilage-labrum boundary was moved medially, the percent load on the labrum increased 2- to 9-fold (Figure 4.6).

Changing the constitutive model from transversely isotropic to isotropic increased the load supported by the labrum 2-11% (Figure 4.7) and decreased the maximum deflection of the labrum 0-0.1 mm. The maximum deflection of the labrum occurred primarily in the radial direction and in approximately the same posterior-superior portion of the labrum for all loading scenarios (Figure 4.5C, asterisk). In the transversely isotropic labrum, the maximum deflection was 1.3 mm in WHS and WMS, and 1.5 mm in AHS and DHS. The maximum deflection of the labrum was 0.1 mm smaller in the isotropic labrum in WHS, WMS and AHS, but did not change in DHS.

Cartilage contact areas demonstrated small increases in most simulations without the labrum and correlated to the load supported by the cartilage (Figure 4.7), while average and peak cartilage contact stresses demonstrated minimal changes. Average cartilage contact stress in the normal model with the labrum was 1.1, 0.9, 1.3, and 1.0

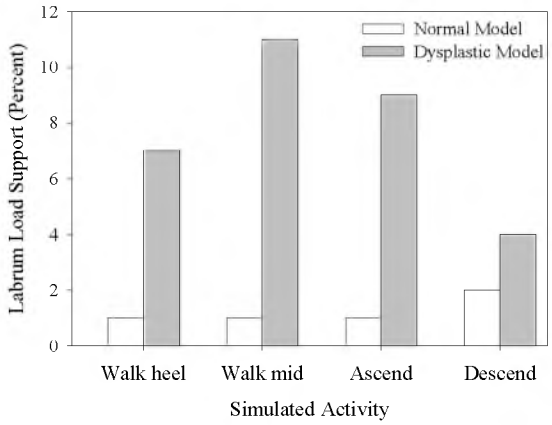

Figure 4.4: Percent load on the labrum for the normal model and the dysplastic model. The labrum in the dysplastic model supported a higher percentage of load across the joint in all scenarios.

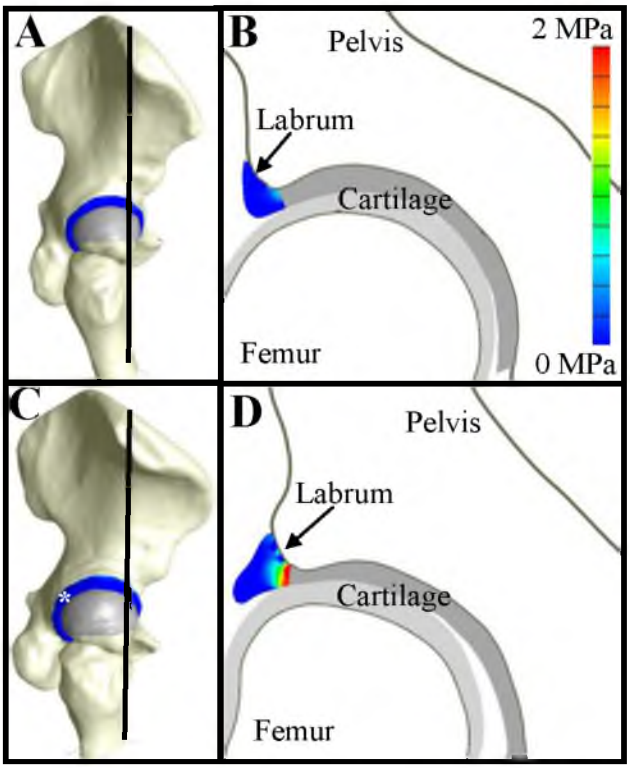

Figure 4.5: Coronal cross-sectional views of contact stress on the anterosuperior labrum during walking heel strike. A – the black line indicates the slice location in the normal model. B – labrum contact stress in the normal model. C – the black line indicates the slice location in the dysplastic model. *The approximate location of maximum deflection in the labrum. D – labrum contact stress in the dysplastic model. The labrum in the dysplastic model was subjected to larger contact stress than the labrum in the normal model because the femoral head achieved equilibrium near the lateral acetabulum. Note the elliptical shape of the femoral head in the dysplastic model as described by [46].

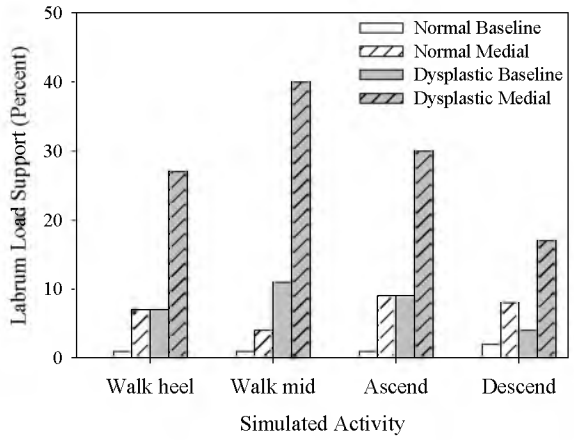

Figure 4.6: Percent load supported by the labrum with baseline and medial cartilage-labrum boundaries. The medial boundary simulations demonstrated higher labrum load support for both subjects in all loading scenarios.

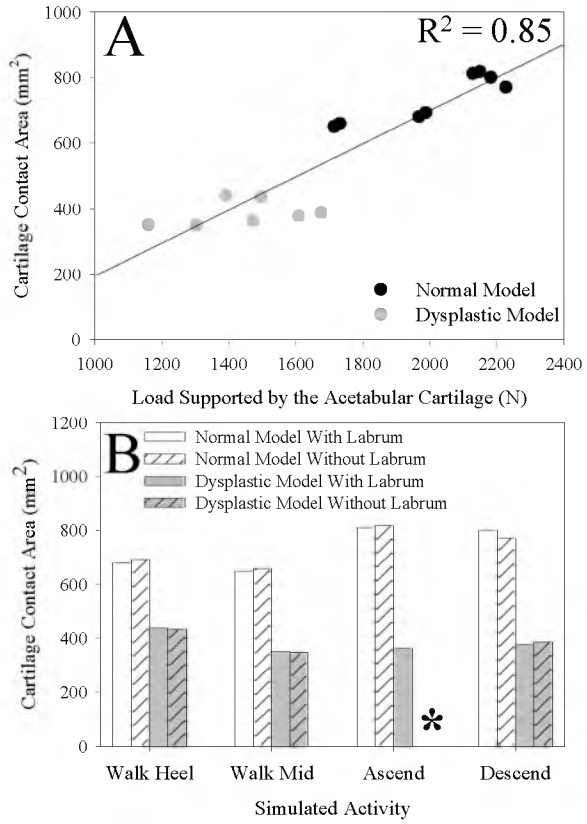

Figure 4.7: Cartilage contact area. A – cartilage contact area correlated well with the force supported by the acetabular cartilage. B – cartilage contact area increased without the labrum in most loading scenarios. Cartilage contact area in the dysplastic model was lower than in the normal model. *When the dysplastic model was used to simulate AHS without the labrum, the femoral head dislocated from the acetabulum.

MPa in WHS, WMS, AHS, and DHS, respectively. Average cartilage contact stress in the normal model without the labrum was 1.1, 0.9, 1.2, and 1.0 MPa in WHS, WMS, AHS, and DHS, respectively. Average cartilage contact stress in the dysplastic model with the labrum was 0.8, 0.8, 0.5, and 1.2 MPa in WHS, WMS, AHS, and DHS, respectively. Average cartilage contact stress in the dysplastic model without the labrum was 0.8, 0.8, and 1.1 MPa in WHS, WMS, and DHS, respectively. When the dysplastic model was used to simulate AHS without the labrum, the femoral head dislocated from the acetabulum, precluding calculation of average pressures. Peak cartilage contact stresses were between 6 MPa and 14 MPa for all simulations.

Altering fiber stiffness ±50% in the transversely isotropic constitutive model only changed the labrum load support 0-1%. Changes of ±3° in anatomical adduction angle only changed labrum load support 0-1%. Changing the applied force ±30% did not alter labrum load support.

Discussion

The purpose of this study was to examine the role of the acetabular labrum in load transfer for hips with normal acetabular geometry and acetabular dysplasia. The load supported by the labrum of the dysplastic hip was substantially larger than that of the normal hip for all simulated activities. This was due to the shallow acetabulum in the dysplastic model, which caused the femoral head to achieve equilibrium near the lateral edge of the acetabulum. Since the dysplastic model exhibited lateral under-coverage, scenarios with loading vectors that were oriented more laterally (e.g., WMS) caused the labrum to support the highest loads. In contrast, the femoral head in the normal model

achieved equilibrium near the center of the acetabulum, resulting in relatively low loads on the labrum.

Cartilage contact stresses were only slightly altered when the labrum was removed, despite the increased force on the acetabular cartilage. Contact area on the articular cartilage correlated to the load supported by the cartilage, therefore there were minimal changes in stress with and without the labrum (Figure 4.7). This is consistent with the results of a previous experimental study, which reported that removal of the labrum had no significant effect on cartilage contact stresses in cadaveric hips [23]. Taken together, these results suggest that the labrum functions to stabilize the joint, rather than to decrease cartilage contact stresses, during activities of daily living.

Average contact stresses on the acetabular cartilage were slightly lower than those reported in previous studies [23, 29, 47]. However, average stresses must be compared with caution because a threshold is often used when reporting experimental measurements of contact stress, based on the minimum stress that can be detected (e.g., pressure-sensitive film ranges, 2.4 MPa and 1.7 MPa [23, 29]). When results for average contact stress in this study were recalculated with thresholds matching experimental studies, the average stresses were in better agreement with the results of the studies referenced above. Peak contact stresses compared well to results from previous in vitro studies [29, 47-50] and computational studies that used nonidealized geometry [29, 51].

The labrum supported more load when it was represented with an isotropic constitutive model than when it was represented with a transversely isotropic constitutive model. This result may seem counterintuitive at first glance, since the fiber stiffness (C_5) in the transversely isotropic constitutive model was larger than the shear modulus (C_1) in

the isotropic constitutive model. Therefore, the transversely isotropic labrum could be expected to support greater loads and exhibit less deflection. However, the fibers were rarely loaded in tension during the simulations. Thus, the shear modulus (C_1) governed the material response of the labrum in simulations using both constitutive models. This also explains why changes to the fiber stiffness had a minimal effect. Many fiber-reinforced soft tissues are subjected to in situ stress (e.g., [52]), which results in a stiffer material response for a given applied load. If in situ stresses were considered in these simulations, the fibers would support more load, thus yielding the expected result of increased load support with the addition of fiber reinforcement. However, given the current limitations in the literature, the constitutive model derived from bovine labrum data is expected to yield the most accurate model predictions.

Assumptions regarding the multiaxial material behavior of the labrum were necessary in this study because previous characterization of the material behavior of the labrum only performed material testing along the fiber direction. Two studies have reported material properties of human labrum. One tested pathologic tissue [53], and one reported only linear tensile and compressive moduli [54]. The most complete characterization was performed using bovine labrum [19]. From these data, the toe region along the fiber direction was assumed to represent the matrix response in all directions since multiaxial testing was not performed. In addition to uncertainty about the material behavior of the normal labrum, labra in dysplastic hips may have altered material properties due to effects such as hypertrophy and calcification [8, 9, 17].

Parameter studies quantified the sensitivity of the simulations to assumed inputs. Large changes in load supported by the labrum with different boundaries between labrum

and cartilage indicate that this boundary should be considered carefully in future modeling studies. This is particularly true when the models are generated from image data, in which the boundary is not visible. While these differences highlight the impact of this parameter on model results, the parameter study was not intended to address the possible clinical consequences of the boundary between cartilage and labrum. Changes in the magnitude of joint reaction force had no effect on the percent load supported by the labrum. Thus, the absolute load supported by the labrum scaled linearly with the joint reaction force, and the differences in kinematics between activities dictated any differences in percent load supported by the labrum. Since changes to adduction angle had minimal effect on percent load supported by the labrum, the direction of the applied load was more important than the anatomical orientation of the joint. This result is further demonstrated when comparing WHS and WMS. In WMS, the adduction angle of the load vector is larger than for WHS, and the labrum in the dysplastic model supported more load. This result is consistent with the findings of previous studies, which reported that the orientation of the abductor force affected predictions of stress in the acetabular cartilage, especially in simulations with small center-edge angles [55, 56].

This study did not examine the possible effects of the sealing role of the labrum on predicted cartilage stresses and load support. Previous modeling and experimental studies suggest that the sealing role of the labrum may influence various aspects of hip biomechanics [18, 20-22, 26]. However, there is no direct evidence in the literature that the sealing role of the labrum influences loadsharing between the articular cartilage and labrum or contract pressure distributions during activities of daily living. The differences in loading conditions and frequency in the previous studies make it difficult to predict

how the results could be interpreted in light of the present study. Activities of daily living such as walking primarily involve compressive forces across the joint, with a frequency of about 1 second [25]. Based on the permeability of the labrum and articular cartilage, there should be minimal fluid exudation from these tissues during a cyclic loading over 1 second [19, 39]. While it may be possible to extend the present model to assess the influence of a labral seal, this was beyond the scope of the present study.

The normal subject and patient that were analyzed in this study were chosen because their acetabular geometries were representative of the means of their parent populations. Due to variance of geometry in the parent populations, it is possible that selection of different subjects from the parent populations would lead to different conclusions. Nevertheless, the results of this study strongly suggest that the labrum plays a larger role in load transfer and joint stability in hips with acetabular dysplasia than in hips with normal acetabular geometry.

References

[1] Seldes, R. M., Tan, V., Hunt, J., Katz, M., Winiarsky, R., and Fitzgerald, R. H., Jr., 2001, "Anatomy, Histologic Features, and Vascularity of the Adult Acetabular Labrum," Clin Orthop Relat Res (382), pp. 232-240.

[2] Petersen, W., Petersen, F., and Tillmann, B., 2003, "Structure and Vascularization of the Acetabular Labrum with Regard to the Pathogenesis and Healing of Labral Lesions," Arch Orthop Trauma Surg, **123**(6), pp. 283-288.

[3] Won, Y.-Y., Chung, I.-H., Chung, N.-S., and Song, K.-H., 2003, "Morphological Study on the Acetabular Labrum," Yonsei Medical Journal, **44**(5), pp. 855-862.

[4] Blankenbaker, D. G., De Smet, A. A., Keene, J. S., and Fine, J. p., 2007, "Classification and Localization of Acetabular Labral Tears," Skeletal Radiology, **36**(5), pp. 391-397.

[5] Burnett, R. S. J., Della Rocca, G. J., Prather, H., Curry, M., Maloney, W. J., and Clohisy, J. C., 2006, "Clinical Presentation of Patients with Tears of the Acetabular Labrum," J Bone Joint Surg Am, **88**(7), pp. 1448-1457.

[6] Fitzgerald, R. H., Jr., 1995, "Acetabular Labrum Tears. Diagnosis and Treatment," Clin Orthop Rel Res (311), pp. 60-68.

[7] Guevara, C. J., Pietrobon, R., Carothers, J. T., Olson, S. A., and Vail, T. p., 2006, "Comprehensive Morphologic Evaluation of the Hip in Patients with Symptomatic Labral Tear," Clin Orthop Rel Res (453), pp. 277-285.

[8] Leunig, M., Podeszwa, D., Beck, M., Werlen, S., and Ganz, R., 2004, "Magnetic Resonance Arthrography of Labral Disorders in Hips with Dysplasia and Impingement," Clin Orthop Rel Res (418), pp. 74-80.

[9] Leunig, M., Werlen, S., Ungersbock, A., Ito, K., and Ganz, R., 1997, "Evaluation of the Acetabular Labrum By MR Arthrography," J Bone Joint Surg Br, **79**(2), pp. 230-234.

[10] McCarthy, J. C., and Lee, J.-A., 2002, "Acetabular Dysplasia: A Paradigm of Arthroscopic Examination of Chondral Injuries," Clin Orthop Rel Res (405), pp. 122-128.

[11] McCarthy, J. C., Noble, p. C., Schuck, M. R., Wright, J., and Lee, J., 2001, "The Otto E. Aufranc Award: The Role of Labral Lesions to Development of Early Degenerative Hip Disease," Clin Orthop Rel Res (393), pp. 25-37.

[12] Neumann, G., Mendicuti, A. D., Zou, K. H., Minas, T., Coblyn, J., Winalski, C. S., and Lang, p., 2007, "Prevalence of Labral Tears and Cartilage Loss in Patients with Mechanical Symptoms of the Hip: Evaluation Using MR Arthrography," Osteoarthritis Cartilage, **15**(8), pp. 909-917.

[13] Wenger, D. E., Kendell, K. R., Miner, M. R., and Trousdale, R. T., 2004, "Acetabular Labral Tears Rarely Occur in the Absence of Bony Abnormalities," Clin Orthop Rel Res (426), pp. 145-150.

[14] Dorrell, J. H., and Catterall, A., 1986, "The Torn Acetabular Labrum," J Bone Joint Surg Br, **68**(3), pp. 400-403.

[15] Groh, M. M., and Herrera, J., 2009, "A Comprehensive Review of Hip Labral Tears," Current Reviews in Musculoskeletal Medicine, **2**(2), pp. 105-117.

[16] Haene, R. A., Bradley, M., and Villar, R. N., 2007, "Hip Dysplasia and the Torn Acetabular Labrum: An Inexact Relationship," J Bone Joint Surg Br, **89**(10), pp. 1289-1292.

[17] Klaue, K., Durnin, C. W., and Ganz, R., 1991, "The Acetabular Rim Syndrome. A Clinical Presentation of Dysplasia of the Hip," J Bone Joint Surg Br, **73**(3), pp. 423-429.

[18] Adeeb, S. M., Sayed Ahmed, E. Y., Matyas, J., Hart, D. A., Frank, C. B., and Shrive, N. G., 2004, "Congruency Effects on Load Bearing in Diarthrodial Joints," Comput Methods Biomech Biomed Engin, **7**(3), pp. 147-157.

[19] Ferguson, S. J., Bryant, J.T., Ito, K., 2001, "The Material Properties of the Bovine Acetabular Labrum," J Orthop Res, **19**(5), p. 887.

[20] Ferguson, S. J., Bryant, J. T., Ganz, R., and Ito, K., 2000, "The Acetabular Labrum Seal: A Poroelastic Finite Element Model," Clin Biomech, **15**(6), pp. 463-468.

[21] Ferguson, S. J., Bryant, J. T., Ganz, R., and Ito, K., 2000, "The Influence of the Acetabular Labrum on Hip Joint Cartilage Consolidation: A Poroelastic Finite Element Model," J Biomech, **33**(8), pp. 953-960.

[22] Hlavacek, M., 2002, "The Influence of the Acetabular Labrum Seal, Intact Articular Superficial Zone and Synovial Fluid Thixotropy on Squeeze-Film Lubrication of A Spherical Synovial Joint," J Biomech, **35**(10), pp. 1325-1335.

[23] Konrath, G. A., Hamel, A. J., Olson, S. A., Bay, B., and Sharkey, N. A., 1998, "The Role of the Acetabular Labrum and the Transverse Acetabular Ligament in Load Transmission in the Hip," J Bone Joint Surg Am, **80**(12), pp. 1781-1788.

[24] Miozzari, H. H., Clark, J. M., Jacob, H. A., Von Rechenberg, B., and Notzli, H. p., 2004, "Effects of Removal of the Acetabular Labrum in a Sheep Hip Model," Osteoarthritis Cartilage, **12**(5), pp. 419-430.

[25] Bergmann, G., Deuretzbacher, G., Heller, M., Graichen, F., Rohlmann, A., Strauss, J., and Duda, G. N., 2001, "Hip Contact Forces and Gait Patterns from Routine Activities," J Biomech, **34**(7), pp. 859-871.

[26] Ferguson, S. J., Bryant, J. T., Ganz, R., and Ito, K., 2003, "An In Vitro Investigation of the Acetabular Labral Seal in Hip Joint Mechanics," J Biomech, **36**(2), pp. 171-178.

[27] Clohisy, J. C., Carlisle, J. C., Beaule, p. E., Kim, Y.-J., Trousdale, R. T., Sierra, R. J., Leunig, M., Schoenecker, p. L., and Millis, M. B., 2008, "A Systematic Approach to the Plain Radiographic Evaluation of the Young Adult Hip," J Bone Joint Surg Am, **90** Suppl 4, pp. 47-66.

[28] Anderson, A. E., Ellis, B. J., Peters, C. L., and Weiss, J. A., 2008, "Cartilage Thickness: Factors Influencing Multidetector CT Measurements in a Phantom Study," Radiology, **246**(1), pp. 133-141.

[29] Anderson, A. E., Ellis, B. J., Maas, S. A., Peters, C. L., and Weiss, J. A., 2008, "Validation of Finite Element Predictions of Cartilage Contact Pressure in the Human Hip Joint," J Biomech Eng, **130**(5), pp. 051008-051008.

[30] Hughes, T. J. R., and Liu, W. K., 1981, "Nonlinear Finite Element Analysis of Shells. I. Three-Dimensionalal Shells," Comput Method Appl M, **26**(3), pp. 331-362.

[31] Anderson, A. E., Peters, C. L., Tuttle, B. D., and Weiss, J. A., 2005, "Subject-Specific Finite Element Model of the Pelvis: Development, Validation and Sensitivity Studies," J Biomech Eng, **127**(3), pp. 364-373.

[32] Puso, M. A., 2000, "A Highly Efficient Enhanced Assumed Strain Physically Stabilized Hexahedral Element," int J Numer Meth Eng, **49**(8), pp. 1029-1064.

[33] Simo, J. C., and Taylor, R. L., 1991, "Quasi-Incompressible Finite Elasticity in Principal Stretches. Continuum Basis and Numerical Algorithms," Comput Method Appl M, **85**(3), pp. 273-310.

[34] Dalstra, M., and Huiskes, R., 1995, "Load Transfer Across the Pelvic Bone," J Biomech, **28**(6), pp. 715-724.

[35] Park, S., Hung, C. T., and Ateshian, G. A., 2004, "Mechanical Response of Bovine Articular Cartilage Under Dynamic Unconfined Compression Loading At Physiological Stress Levels," Osteoarthritis Cartilage, **12**(1), pp. 65-73.

[36] Quapp, K. M., and Weiss, J. A., 1998, "Material Characterization of Human Medial Collateral Ligament," J Biomech Eng, **120**(6), pp. 757-763.

[37] Athanasiou, K. A., Agarwal, A., Muffoletto, A., Dzida, F. J., Constantinides, G., and Clem, M., 1995, "Biomechanical Properties of Hip Cartilage in Experimental Animal Models," Clin Orthop Relat Res (316), pp. 254-266.

[38] Mow, V. C., Kuei, S. C., Lai, W. M., and Armstrong, C. G., 1980, "Biphasic Creep and Stress Relaxation of Articular Cartilage in Compression? Theory and Experiments," J Biomech Eng, **102**(1), pp. 73-84.

[39] Ateshian, G. A., Ellis, B. J., and Weiss, J. A., 2007, "Equivalence between Short-Time Biphasic and Incompressible Elastic Material Responses," J Biomech Eng, **129**(3), pp. 405-412.

[40] Puso, M. A., 2004, "A Three-Dimensionalal Mortar Method for Solid Mechanics," int J Numer Meth Eng, **59**(3), pp. 315-336.

[41] Puso, M. A., and Laursen, T. A., 2004, "A Mortar Segment-to-Segment Contact Method for Large Deformation Solid Mechanics," Comput Method Appl M, **193**(6-8), pp. 601-629.

[42] Caligaris, M., and Ateshian, G. A., 2008, "Effects of Sustained Interstitial Fluid Pressurization Under Migrating Contact Area, and Boundary Lubrication by Synovial Fluid, on Cartilage Friction," Osteoarthritis Cartilage, **16**(10), pp. 1220-1227.

[43] Charnley, J., 1960, "The Lubrication of Animal Joints in Relation to Surgical Reconstruction by Arthroplasty," Annals of the Rheumatic Diseases, **19**, pp. 10-19.

[44] Schmidt, T. A., and Sah, R. L., 2007, "Effect of Synovial Fluid on Boundary Lubrication of Articular Cartilage," Osteoarthritis Cartilage, **15**(1), pp. 35-47.

[45] Puso, M. A., Maker, Bradley N., Ferencz, Robert M., Hallquist, John O., 2007, "NIKE3D: A Nonlinear, Implicit, Three-Dimensional Finite Element Code for Solid and Structural Mechanics," User's Manual.

[46] Steppacher, S., Tannast, M., Werlen, S., and Siebenrock, K., 2008, "Femoral Morphology Differs between Deficient and Excessive Acetabular Coverage," Clin Orthop Rel Res, **466**(4), pp. 782-790.

[47] Brown, T. D., and Shaw, D. T., 1983, "In Vitro Contact Stress Distributions in the Natural Human Hip," J Biomech, **16**(6), pp. 373-384.

[48] Afoke, N. Y., Byers, p. D., and Hutton, W. C., 1987, "Contact Pressures in the Human Hip Joint," J Bone Joint Surg Br, **69**(4), pp. 536-541.

[49] von Eisenhart, R., Adam, C., Steinlechner, M., Muller-Gerbl, M., and Eckstein, F., 1999, "Quantitative Determination of Joint Incongruity and Pressure Distribution During Simulated Gait and Cartilage Thickness in the Human Hip Joint," J Orthop Res, **17**(4), pp. 532-539.

[50] Adams, D., and Swanson, S. A., 1985, "Direct Measurement of Local Pressures in the Cadaveric Human Hip Joint During Simulated Level Walking," Ann Rheum Dis, **44**(10), pp. 658-666.

[51] Brown, T. D., and DiGioia, A. M., 3rd, 1984, "A Contact-Coupled Finite Element Analysis of the Natural Adult Hip," J Biomech, **17**(6), pp. 437-448.

[52] Gardiner, J. C., and Weiss, J. A., 2003, "Subject-Specific Finite Element Analysis of the Human Medial Collateral Ligament During Valgus Knee Loading," J Orthop Res, **21**(6), pp. 1098-1106.

[53] Ishiko, T., Naito, M., and Moriyama, S., 2005, "Tensile Properties of the Human Acetabular Labrum-the First Report," J Orthop Res, **23**(6), pp. 1448-1453.

[54] Smith, C. D., Masouros, S., Hill, A. M., Amis, A. A., and Bull, A. M. J., 2009, "A Biomechanical Basis for Tears of the Human Acetabular Labrum," Br J Sports Med, **43**(8), pp. 574-578.

[55] Armand, M., Lepisto, J., Tallroth, K., Elias, J., and Chao, E., 2005, "Outcome of Periacetabular Osteotomy: Joint Contact Pressure Calculation Using Standing AP Radiographs, 12 Patients Followed for Average 2 Years," Acta Orthopaedica, **76**(3), pp. 303-313.

[56] Genda, E., Iwasaki, N., Li, G., MacWilliams, B. A., Barrance, p. J., and Chao, E. Y., 2001, "Normal Hip Joint Contact Pressure Distribution in Single-Leg Standing--Effect of Gender and Anatomic Parameters," J Biomech, **34**(7), pp. 895-905.

CHAPTER 5

FINITE ELEMENT PREDICTIONS OF LABRUM AND CARTILAGE CONTACT MECHANICS IN DYSPLASTIC HUMAN HIPS

Abstract

Most osteoarthritis (OA) of the hip is secondary to bony pathomorphology, such as acetabular dysplasia. The link between pathomorphology and OA is thought to be mechanical, but has not been systematically established. Because mechanics cannot be measured in vivo, finite element (FE) modeling can be used to predict mechanics in the dysplastic hip in order to provide insight into the pathogenesis of hip OA. Therefore, the objective of this study was to evaluate cartilage and labrum contact mechanics in dysplastic hips in comparison to normal hips. Twenty subjects were recruited and imaged: ten with normal hip morphology and ten with acetabular dysplasia. Subject-specific FE models were generated from CT arthrogram data to evaluate cartilage and labrum contact mechanics. The acetabular labrum supported significantly more load in the dysplastic hips than in the normal hips. Additionally, the superior region of the acetabular labrum had significantly higher contact areas in the dysplastic hip than in the normal hip. Conversely, there were relatively few differences in cartilage mechanics. This is because the load supported by the acetabular labrum in dysplastic hips

compensated for the shallow acetabula and thus prevented elevated cartilage stresses. Overall, this study quantitatively demonstrates the mechanical role of the acetabular labrum in the dysplastic hip, which suggests that the labrum may be important in the pathogenesis of OA in the dysplastic hip.

Introduction

The majority of osteoarthritis (OA) of the hip is secondary to subtle bony pathomorphology [1, 2]. One such pathomophology is acetabular dysplasia, which is responsible for approximately 20% of hip OA [3]. Acetabular dysplasia is characterized by a shallow acetabulum, and is often diagnosed using the center-edge angle and the acetabular index on plain film radiographs [4, 5]. The center-edge angle measures the lateral coverage of the femoral head by the acetabulum. The acetabular index measures the inclination of the acetabular sourcil. Current clinical opinion is that elevated cartilage stresses are the main cause of OA in hips with acetabular dysplasia [6-10]. Clinical observation of hypertrophic or torn labra suggests that the acetabular labrum also experiences an altered mechanical environment in the dysplastic hip [10-17]. However, the specific alterations in the mechanics of the dysplastic hip that lead to OA are not well understood. Since mechanics cannot be measured directly in vivo, finite element (FE) modeling can be used to predict them.

While previous FE studies have provided insight into the mechanics of the human hip, there are many remaining questions regarding the pathogenesis of OA in the dysplastic hip that FE analysis is suited to address. It has been demonstrated that subject-specific geometry is an important feature of FE models in order to accurately predict contact mechanics [18]. Additionally, it has been suggested that the acetabular labrum is

an important feature of models of the dysplastic hip [19]. Two previous studies have evaluated contact mechanics in the dysplastic hip. In one study, idealized geometry was assumed [20]. In a second study, the acetabular labrum was omitted from subject-specific models [21].

Therefore, the aim of this study was to evaluate cartilage and labrum contact mechanics in dysplastic hips in comparison to normal hips using a validated approach to subject-specific FE modeling.

Methods

Twenty subjects were recruited and imaged with IRB approval. Ten healthy control subjects with normal center edge angles (CEA) and no history of hip pain were drawn from a previous study (five male, BMI 23.0 ± 3.9 kg·m-2, age 26 ± 4 years, CEA 33.5 ± 5.4°) [22]. Ten patients with CEA less than 25° that were being seen in our clinic for pain secondary to acetabular dysplasia were analyzed for the current study (three male, BMI 23.4 ± 5.9 kg·m-2, age 26 ± 6 years, CEA 14.8 ± 4.6°).

Subject-specific geometry was acquired using CT arthrography. CT image data were segmented semi-automatically to generate subject-specific FE models (Figure 5.1) [19, 22, 23]. Cortical bone was discretized into triangular shell elements with position-dependent thickness [19, 22-24]. Cortical bone was represented as linear isotropic elastic (E = 17 GPa, ν = 0.29) [19, 22, 25, 26]. Cartilage and labrum were discretized into hexahedral elements [19, 22, 25]. Cartilage was represented as neo-Hookean hyperelastic (G = 13.6 MPa, K = 1359 MPa) [19, 22, 25, 27]. Labrum was represented as transversely isotropic hyperelastic (C_1 = 1.4 MPa, C_3 = 0.05 MPa, C_4 = 36, C_5 = 66 MPa, λ^* = 1.103) [19, 28, 29].

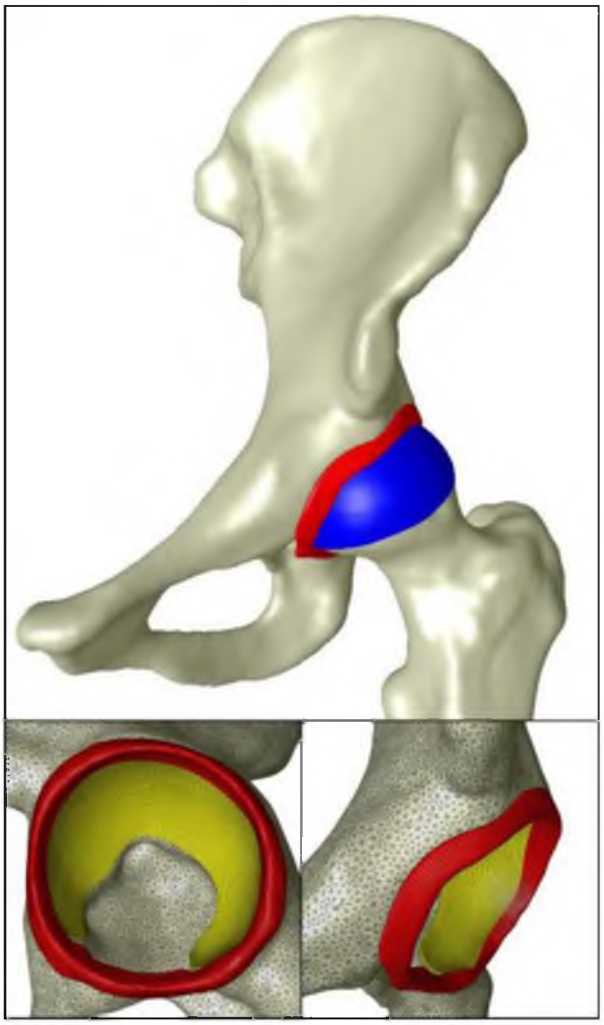

Figure 5.1: Example of a subject-specific finite element model. Top – the whole model, including the hemipelvis, the proximal femur, cartilage and labrum. The bone is shown in white, the femoral cartilage is shown in blue and the acetabular labrum is shown in red. Bottom left – medial view of the acetabulum, with mesh lines visible. The acetabular cartilage is shown in yellow. Bottom right – oblique view of the acetabulum, with mesh lines visible.

Four loading scenarios were analyzed to capture a range of anatomical orientations and loads. Average kinematics were derived from instrumented implant and gait data [30]. The load applied during each scenario was scaled by subject body weight. Heel strike during walking (WH, 233% BW), midstance during walking (WM, 203% BW), heel strike during stair descent (DH, 261% BW) and heel strike during stair ascent (AH, 252% BW) were simulated [30]. All models were analyzed in NIKE3D [31].

Cartilage and labrum contact mechanics were evaluated [19]. Labrum contact area and peak contact stress were evaluated in the anterior, superior and posterior regions. The percent of the total load transferred across the hip joint that was supported by the labrum was evaluated. Cartilage contact area, average contact stress and peak contact stress were evaluated in the anteromedial, anterolateral, superomedial, superolateral, posteromedial and posterolateral regions of the acetabulum. Cartilage contact area was normalized to the total area of each region. Model results were extracted using PostView [32].

Differences between groups within region and loading scenario were compared using t-tests. Significance was set at $p \leq 0.05$.

Results

The labrum supported significantly more load in dysplastic hips than in normal hips in all loading scenarios (Figure 5.2). Approximately 10% of the total load transferred across the dysplastic hip was transferred through the acetabular labrum (range 2-23%). Conversely, only ~2% of the total load transferred across the normal hip was transferred through the acetabular labrum (range 0-8%).

Contact area on the superior labrum was significantly larger in dysplastic hips than in normal hips for all loading scenarios (Figure 5.3A). However, there were no significant differences in contact area on the anterior or posterior labrum (Figure 5.3B,C). There were also no significant differences in the peak labral contact stress between the two groups in any region.

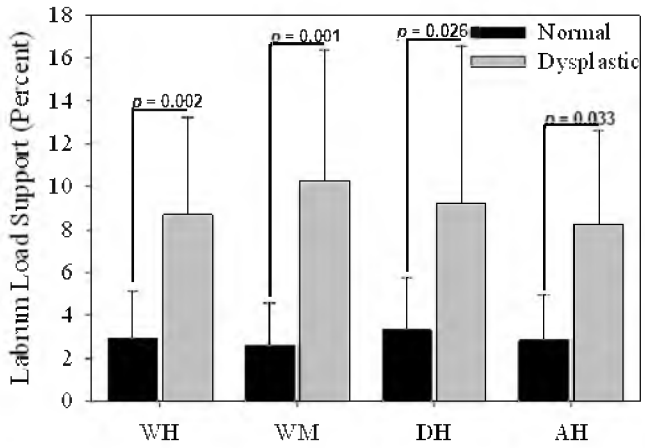

Figure 5.2: Load supported by the labrum as a percentage of the total load transferred across the joint. *P*-values are shown for each loading scenarios. The labrum in the dysplastic hip supported significantly more load than the labrum in the normal hip for all activities.

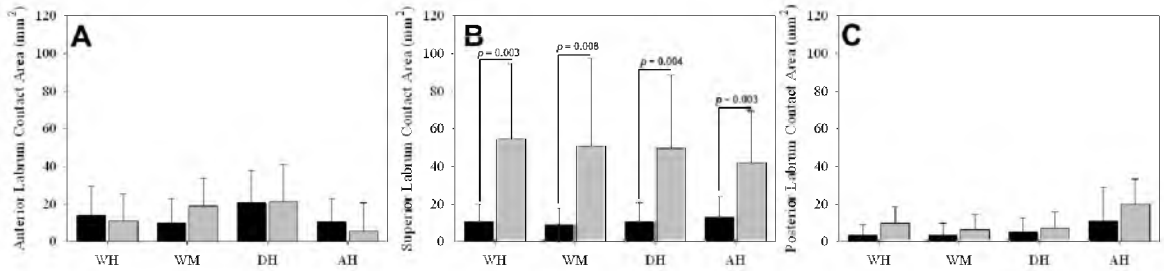

Figure 5.3: Contact area on the acetabular labrum. A – anterior region. B – superior region. The labrum in the dysplastic hip had significantly larger contact area in the superior region than the labrum in the normal hip. *P*-values are shown for each loading scenario. C – posterior region.

Qualitatively, there was a lateral shift in the contact pattern in the dysplastic hips in comparison to a more distributed contact pattern in the normal hips (Figures 5.4 and 5.5). However, there were few quantitative differences in cartilage contact stress and cartilage contact area between the two groups. For those regions that did have significant differences, the normal hips had larger contact stress or contact area than the dysplastic hips. In particular, the peak contact stress was larger in the normal hips than in the dysplastic hips during WM in the anteromedial region and during AH in the posteromedial region. Average contact stress was larger in the normal hips than in the

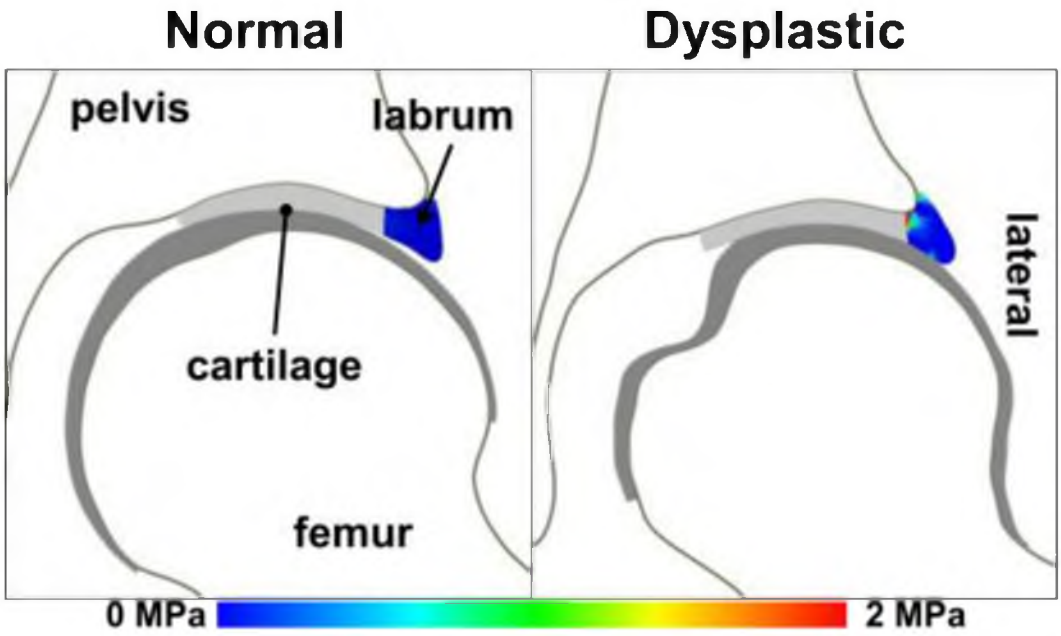

Figure 5.4: Coronal cross-sectional image of a representative normal subject (left) and a representative dysplastic subject (right). Pressure on the acetabular labrum is shown in the fringe plot. These images demonstrate the lateral contact in the dysplastic hip, which resulted in larger pressures on the labrum in the dysplastic hip.

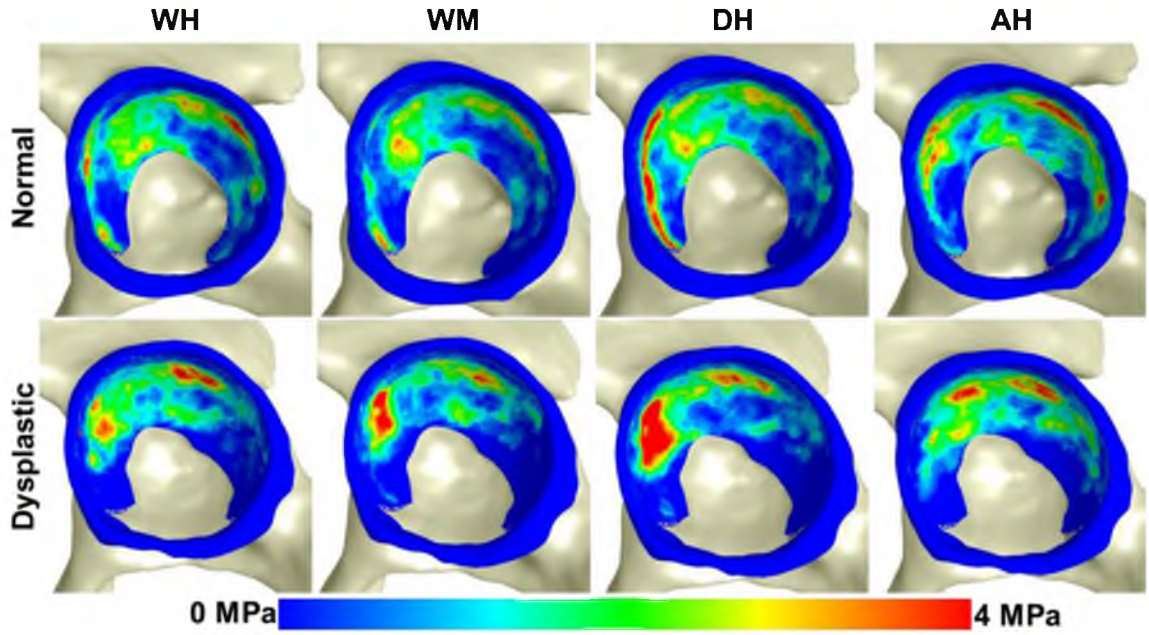

Figure 5.5: Average contact stress plots for each of the four loading scenarios across all subjects. Plots were generated by mapping the nodal results from all ten subjects in each group onto the mesh for one subject. Top row – normal hips. Bottom row – dysplastic hips. The dysplastic hips exhibited more lateral contact than the normal hips, resulting in elevated load support by the acetabular labrum.

dysplastic hips during AH in the anterolateral and posterolateral regions, during WM in the posterolateral and anteromedial regions and during DH in the superomedial region. Cartilage contact area was larger in the normal hips than in the dysplastic hips during AH in the anterolateral and posteromedial regions, during WM in the posterlateral and anteromedial regions, and during DH in the superomedial region.

Discussion

This study demonstrated the distinct role of the acetabular labrum as a load-bearing structure in the dysplastic hip. While the labrum is known to provide additional contact area and volume to the human hip, it has been assumed to be relatively unimportant to the mechanics of the hip [33]. This concept is supported by mechanical analysis in the normal hip. In a sheep model, removal of the labrum was insufficient to cause hip OA when evaluated for the same time frame that results in knee OA following removal of the meniscus [34]. In vitro testing with pressure-sensitive film in the joint space indicated that the labrum had a minimal mechanical role in the normal hip [35]. These previous results are consistent with the present study, and together provide strong evidence that the labrum has a minimal role in the normal hip. However, the labrum in the dysplastic hip provides significant mechanical support. These results are also consistent with clinical findings of hypertrophy in the dysplastic hip, which suggests remodeling in response to an altered mechanical environment [11, 13-16].

The differences in cartilage mechanics in the present study contradict the findings of previous FE and mathematical studies of the dysplastic hip. In subject-specific FE models without the labrum, dysplastic hips had larger contact stresses than the normal hip [21]. In another study with idealized models with the acetabular labrum, dysplastic hips

had high stresses on the acetabular rim [20]. Additionally, several mathematical studies have found elevated contact stress in the dysplastic hip in comparison to the normal hip [36-38]. However, both the present study and previous studies are consistent in the finding that contact shifts towards the lateral acetabular rim in the dysplastic hip. In the present study, the acetabular labrum was able to provide additional contact area and thereby prevent elevated cartilage stresses in the dysplastic hips.

The location of differences in labral contact area between the two groups may have important implications. In particular, only the superior region exhibited significantly different labral contact areas. This suggests that, during activities of daily living, the superior labrum is loaded more than other portions of the acetabular labrum. This may explain the global hypertrophy observed in the dysplastic hip, but does not explain the prominent locations of labral tears in the dysplastic hip. Labral tears in the dysplastic hip have been reported in the anterior labrum in 66% of patients in one study [17], and in the anterosuperior region in 72% of patients in another study [11]. Therefore, it may be expected that the differences in labral mechanics would have been in the anterior labrum, which was not the case in the present study. It is therefore possible that other activities are the main cause of labral tears. Alternatively, the variables selected in the present study may be insufficient for predicting the onset of labral tears. For example, shear stress at the chondrolabral boundary may be more relevant for labral tears.

There are several limitations in this study that warrant discussion. Subject groups were based solely off of two criteria: center-edge angle and the presence of hip pain. However, hip pathomorphology is three-dimensional, and these criteria may not have

provided homogeneous populations. For example, the dysplastic hip is often considered less congruent than the normal hip, but the extent of incongruity may vary by subject [39]. Therefore, differences in bony morphology within group may have confounded the results of the present study. However, even with these potential confounding factors in subject morphology, distinct differences were found between the two patient populations. Future work could evaluate subject groups with more narrow morphological characteristics, which could provide more detailed insight into the mechanics of the dysplastic hip. In addition to potential differences within group in the hip morphology, there were more females than males in the patient population. This is consistent with the higher prevalence of acetabular dysplasia in females than in males [40, 41].

The assumptions made in the FE models are also a limitation of the present study. Both the cartilage and the labrum constitutive descriptions were derived from literature data from bovine joints [27, 28]. This is primarily due to the lack of data regarding the material behavior of human hip cartilage and the human acetabular labrum in the literature. Additionally, the cartilage was described as neo-Hookean hyperelastic. While this is a gross simplification of actual cartilage behavior, previous studies justify its use for predictions of contact mechanics [25, 42]. The cartilage and labrum constitutive behavior was also assumed to be identical between dysplastic and normal subjects. While the dysplastic subjects were selected based on having healthy cartilage as diagnosed using radiographic and CT image data, it is possible that minor changes may have occurred. It is also possible that the acetabular labrum in the dysplastic hip, which is often hypertrophic, has stiffer material behavior than the acetabular labrum in the normal hip. Again, the literature does not provide data regarding changes in the material

behavior of the acetabular labrum in the dysplastic hip. Finally, both dysplastic and normal hips were placed into identical anatomical positions for loading [30]. The literature suggests that hip pathomophology results in altered gait [43-45], although there are no data available regarding gait alterations in young patients with acetabular dysplasia before corrective surgery.

In conclusion, this study quantitatively demonstrates the mechanical role of the acetabular labrum in the dysplastic hip, which suggests that the labrum may also be important in the pathogenesis of OA in the dysplastic hip.

References

[1] Harris-Hayes, M., and Royer, N. K., 2011, "Relationship of Acetabular Dysplasia and Femoroacetabular Impingement to Hip Osteoarthritis: A Focused Review," PM R, **3**(11), pp. 1055-1067 E1051.

[2] Murray, R. O., 1965, "The Aetiology of Primary Osteoarthritis of the Hip," Brit J Radiol, **38**(455), pp. 810-824.

[3] Solomon, L., 1976, "Patterns of Osteoarthritis of the Hip," J Bone Joint Surg Br, **58**(2), pp. 176-183.

[4] Bittersohl, B., Hosalkar, H. S., and Wenger, D. R., 2012, "Surgical Treatment of Hip Dysplasia in Children and Adolescents," Orthop Clin North Am, **43**(3), pp. 301-315.

[5] Wiberg, G., 1953, "Shelf Operation in Congenital Dysplasia of the Acetabulum and in Subluxation and Dislocation of the Hip," J Bone Joint Surg Am, **35-A**(1), pp. 65-80.

[6] Ganz, R., Klaue, K., Vinh, T. S., and Mast, J. W., 1988, "A New Periacetabular Osteotomy for the Treatment of Hip Dysplasias. Technique and Preliminary Results," Clin Orthop Relat Res (232), pp. 26-36.

[7] Leunig, M., and Ganz, R., 2011, "Evolution of Technique and Indications for the Bernese Periacetabular Osteotomy," Bull NYU Hosp Jt Dis, **69** Suppl 1, pp. S42-46.

[8] Millis, M. B., and Kim, Y. J., 2002, "Rationale of Osteotomy and Related Procedures for Hip Preservation: A Review," Clin Orthop Relat Res (405), pp. 108-121.

[9] Murphy, S. B., Millis, M. B., and Hall, J. E., 1999, "Surgical Correction of Acetabular Dysplasia in the Adult. A Boston Experience," Clin Orthop Relat Res (363), pp. 38-44.

[10] Peters, C. L., and Erickson, J., 2006, "The Etiology and Treatment of Hip Pain in the Young Adult," J Bone Joint Surg Am, **88** Suppl 4, pp. 20-26.

[11] Fujii, M., Nakashima, Y., Jingushi, S., Yamamoto, T., Noguchi, Y., Suenaga, E., and Iwamoto, Y., 2009, "Intraarticular Findings in Symptomatic Developmental Dysplasia of the Hip," J Pediatr Orthop, **29**(1), pp. 9-13.

[12] Guevara, C. J., Pietrobon, R., Carothers, J. T., Olson, S. A., and Vail, T. p., 2006, "Comprehensive Morphologic Evaluation of the Hip in Patients with Symptomatic Labral Tear," Clin Orthop Relat Res, **453**, pp. 277-285.

[13] Leunig, M., Podeszwa, D., Beck, M., Werlen, S., and Ganz, R., 2004, "Magnetic Resonance Arthrography of Labral Disorders in Hips with Dysplasia and Impingement," Clin Orthop Relat Res (418), pp. 74-80.

[14] Leunig, M., Werlen, S., Ungersbock, A., Ito, K., and Ganz, R., 1997, "Evaluation of the Acetabular Labrum By MR Arthrography," J Bone Joint Surg Br, **79**(2), pp. 230-234.

[15] McCarthy, J., Noble, p., Aluisio, F. V., Schuck, M., Wright, J., and Lee, J. A., 2003, "Anatomy, Pathologic Features, and Treatment of Acetabular Labral Tears," Clin Orthop Relat Res (406), pp. 38-47.

[16] Peelle, M. W., Della Rocca, G. J., Maloney, W. J., Curry, M. C., and Clohisy, J. C., 2005, "Acetabular and Femoral Radiographic Abnormalities Associated with Labral Tears," Clin Orthop Relat Res, **441**, pp. 327-333.

[17] McCarthy, J. C., and Lee, J. A., 2002, "Acetabular Dysplasia: A Paradigm of Arthroscopic Examination of Chondral Injuries," Clin Orthop Relat Res (405), pp. 122-128.

[18] Anderson, A. E., Ellis, B. J., Maas, S. A., and Weiss, J. A., 2010, "Effects of Idealized Joint Geometry on Finite Element Predictions of Cartilage Contact Stresses in the Hip," J Biomech, **43**(7), pp. 1351-1357.

[19] Henak, C. R., Ellis, B. J., Harris, M. D., Anderson, A. E., Peters, C. L., and Weiss, J. A., 2011, "Role of the Acetabular Labrum in Load Support Across the Hip Joint," J Biomech, **44**(12), pp. 2201-2206.

[20] Chegini, S., Beck, M., and Ferguson, S. J., 2009, "The Effects of Impingement and Dysplasia on Stress Distributions in the Hip Joint During Sitting and Walking: A Finite Element Analysis," J Orthop Res, **27**(2), pp. 195-201.

[21] Russell, M. E., Shivanna, K. H., Grosland, N. M., and Pedersen, D. R., 2006, "Cartilage Contact Pressure Elevations in Dysplastic Hips: A Chronic Overload Model," J Orthop Surg Res, **1**, pp. 6-6.

[22] Harris, M. D., Anderson, A. E., Henak, C. R., Ellis, B. J., Peters, C. L., and Weiss, J. A., 2012, "Finite Element Prediction of Cartilage Contact Stresses in Normal Human Hips," J Orthop Res, **30**(7), pp. 1133-1139.

[23] Anderson, A. E., Ellis, B. J., Peters, C. L., and Weiss, J. A., 2008, "Cartilage Thickness: Factors Influencing Multidetector CT Measurements in A Phantom Study," Radiology, **246**(1), pp. 133-141.

[24] Anderson, A. E., Peters, C. L., Tuttle, B. D., and Weiss, J. A., 2005, "Subject-Specific Finite Element Model of the Pelvis: Development, Validation and Sensitivity Studies," J Biomech Eng, **127**(3), pp. 364-373.

[25] Anderson, A. E., Ellis, B. J., Maas, S. A., Peters, C. L., and Weiss, J. A., 2008, "Validation of Finite Element Predictions of Cartilage Contact Pressure in the Human Hip Joint," J Biomech Eng, **130**(5), pp. 051008-051008.

[26] Dalstra, M., and Huiskes, R., 1995, "Load Transfer Across the Pelvic Bone," J Biomech, **28**(6), pp. 715-724.

[27] Park, S., Hung, C. T., and Ateshian, G. A., 2004, "Mechanical Response of Bovine Articular Cartilage Under Dynamic Unconfined Compression Loading at Physiological Stress Levels," Osteoarthritis Cartilage, **12**(1), pp. 65-73.

[28] Ferguson, S. J., Bryant, J. T., and Ito, K., 2001, "The Material Properties of the Bovine Acetabular Labrum," J Orthop Res, **19**(5), pp. 887-896.

[29] Quapp, K. M., and Weiss, J. A., 1998, "Material Characterization of Human Medial Collateral Ligament," J Biomech Eng, **120**(6), pp. 757-763.

[30] Bergmann, G., Deuretzbacher, G., Heller, M., Graichen, F., Rohlmann, A., Strauss, J., and Duda, G. N., 2001, "Hip Contact Forces and Gait Patterns from Routine Activities," J Biomech, **34**(7), pp. 859-871.

[31] Puso, M. A., Maker, Bradley N., Ferencz, Robert M., Hallquist, John O., 2007, "NIKE3D: A Nonlinear, Implicit, Three-Dimensional Finite Element Code for Solid and Structural Mechanics," User's Manual.

[32] Maas, S. A., 2012, "PostView Version 1.4: User's Manual."

[33] Tan, V., Seldes, R. M., Katz, M. A., Freedhand, A. M., Klimkiewicz, J. J., and Fitzgerald, R. H., Jr., 2001, "Contribution of Acetabular Labrum to Articulating Surface Area and Femoral Head Coverage in Adult Hip Joints: An Anatomic Study in Cadavera," Am J Orthop (Belle Mead NJ), **30**(11), pp. 809-812.

[34] Miozzari, H. H., Clark, J. M., Jacob, H. A., Von Rechenberg, B., and Notzli, H. p., 2004, "Effects of Removal of the Acetabular Labrum in a Sheep Hip Model," Osteoarthritis Cartilage, **12**(5), pp. 419-430.

[35] Konrath, G. A., Hamel, A. J., Olson, S. A., Bay, B., and Sharkey, N. A., 1998, "The Role of the Acetabular Labrum and the Transverse Acetabular Ligament in Load Transmission in the Hip," J Bone Joint Surg Am, **80**(12), pp. 1781-1788.

[36] Iglič, A., Kralj-Iglič, V., Daniel, M., and Maček-Lebar, A., 2002, "Computer Determination of Contact Stress Distribution and Size of Weight Bearing Area in the Human Hip Joint," Comput Methods Biomech Biomed Engin, **5**(2), pp. 185-192.

[37] Mavcic, B., Iglic, A., Kralj-Iglic, V., Brand, R. A., and Vengust, R., 2008, "Cumulative Hip Contact Stress Predicts Osteoarthritis in DDH," Clin Orthop Relat Res, **466**(4), pp. 884-891.

[38] Mavčič, B., Pompe, B., Antolič, V., Daniel, M., Iglič, A., and Kralj-Iglič, V., 2002, "Mathematical Estimation of Stress Distribution in Normal and Dysplastic Human Hips," J Orthop Res, **20**(5), pp. 1025-1030.

[39] Larson, A. N., Rabenhorst, B., De La Rocha, A., and Sucato, D. J., 2012, "Limited Intraobserver and Interobserver Reliability for the Common Measures of Hip Joint Congruency Used in Dysplasia," Clin Orthop Relat Res, **470**(5), pp. 1414-1420.

[40] de Hundt, M., Vlemmix, F., Bais, J. M., Hutton, E. K., De Groot, C. J., Mol, B. W., and Kok, M., 2012, "Risk Factors for Developmental Dysplasia of the Hip: A Meta-analysis," Eur J Obstet Gynecol Reprod Biol, **165**(1), pp. 8-17.

[41] Dezateux, C., and Rosendahl, K., 2007, "Developmental Dysplasia of the Hip," Lancet, **369**(9572), pp. 1541-1552.

[42] Anderson, D. D., Goldsworthy, J. K., Li, W., James Rudert, M., tochigi, Y., and Brown, T. D., 2007, "Physical Validation of a Patient-Specific Contact Finite Element Model of the Ankle," J Biomech, **40**(8), pp. 1662-1669.

[43] Endo, H., Mitani, S., Senda, M., Kawai, A., McCown, C., Umeda, M., Miyakawa, T., and inoue, H., 2003, "Three-Dimensionalal Gait Analysis of Adults with Hip Dysplasia after Rotational Acetabular Osteotomy," J Orthop Sci, **8**(6), pp. 762-771.

[44] Kennedy, M. J., Lamontagne, M., and Beaule, p. E., 2009, "Femoroacetabular Impingement Alters Hip and Pelvic Biomechanics During Gait Walking Biomechanics of FAI," Gait Posture, **30**(1), pp. 41-44.

[45] Marangoz, S., Atilla, B., Gok, H., Yavuzer, G., Ergin, S., tokgozoglu, A. M., and Alpaslan, M., 2010, "Gait Analysis in Adults with Severe Hip Dysplasia Before and After Total Hip Arthroplasty," Hip int, **20**(4), pp. 466-472.

CHAPTER 6[1]

FINITE ELEMENT PREDICITONS OF CARTILAGE CONTACT MECHANICS IN HIPS WITH RETROVERTED ACETABULA

Abstract

A contributory factor to hip osteoarthritis (OA) is abnormal cartilage mechanics. Acetabular retroversion, a version deformity of the acetabulum, has been postulated to cause OA via decreased posterior contact area and increased posterior contact stress. Although cartilage mechanics cannot be measured directly in vivo to evaluate the causes of OA, they can be predicted using finite element (FE) modeling.

The objective of this study was to compare cartilage contact mechanics between hips with normal and retroverted acetabula using subject-specific FE modeling.

Twenty subjects were recruited and imaged: ten with normal acetabula and ten with retroverted acetabula. FE models were constructed using a validated protocol. Walking, stair ascent, stair descent and rising from a chair were simulated. Acetabular cartilage contact stress and contact area were compared between groups.

Retroverted acetabula had superomedial cartilage contact patterns, while normal acetabula had widely distributed cartilage contact patterns. In the posterolateral

[1]Accepted for publication in *Osteoarthritis and Cartilage*, Henak CR, Carruth ED, Anderson AE, Harris MD, Ellis BJ, Weiss JA, "Finite Element Predictions of Cartilage Contact Mechanics in Hips with Retroverted Acetabula", June 2013.

acetabulum, average contact stress and contact area during walking and stair descent were 2.6 to 7.6 times larger in normal than retroverted acetabula ($p \leq 0.017$). Conversely, in the superomedial acetabulum, peak contact stress during walking was 1.2 to 1.6 times larger in retroverted than normal acetabula ($p \leq 0.044$). Further differences varied by region and activity.

This study demonstrated superomedial contact patterns in retroverted acetabula versus widely distributed contact patterns in normal acetabula. Smaller posterolateral contact stress in retroverted acetabula than in normal acetabula suggests that increased posterior contact stress may not be the link between retroversion and OA.

Introduction

Hip osteoarthritis (OA) occurs in approximately 9.5% of the male population and 11.2% of the female population [1]. OA is thought to be initiated by mechanical factors and advanced by a combination of mechanical and metabolic factors [2-4]. For example, elevated or prolonged cartilage stresses can cause permanently altered levels of aggrecan synthesis [3]. Also, impact trauma resulting in high contact stress can cause fissuring [5]. Thus, deleterious cartilage contact stresses are of interest as a potential mechanical initiator of OA at the cartilage level.

At the joint level, bony pathologies including acetabular retroversion have been linked to increased rates of hip OA [6-8]. Acetabular retroversion is defined as the acetabulum opening more posterolaterally than normal. This is recognized on anteroposterior radiographs by the presence of a crossover sign, which indicates a prominent anterior acetabular wall, a deficient posterior acetabular wall, or both (Figure 6.1) [9]. There is a higher incidence of acetabular retroversion among osteoarthritic hips

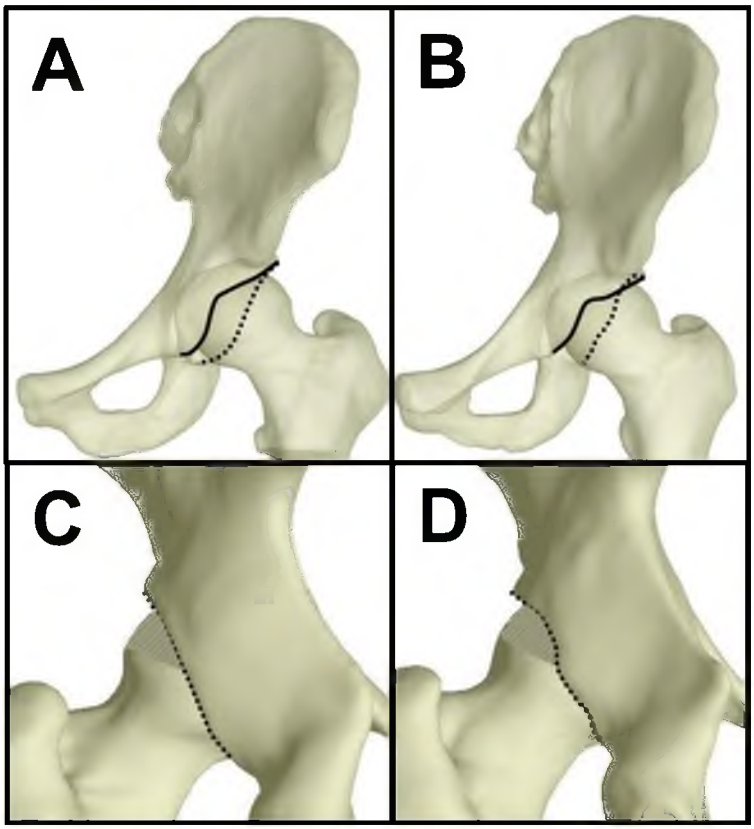

Figure 6.1: Anterior views of hips with A – normal anatomy and B – acetabular retroversion. The anterior acetabular rim is outlined in solid back and the posterior acetabular wall is outlined in dashed black. While the posterior acetabular wall lies lateral to the anterior acetabulum over the whole joint in the normal hip, the posterior acetabular wall lies medial to the anterior acetabulum in the superior portion of the retroverted hip. As the lines progress distally, the anterior and posterior lines outlining the acetabulum cross each other, creating the crossover sign. Posterior views of hips with C – normal anatomy and D – acetabular retroversion. The relative undercoverage of the femoral head in the hip with acetabular retroversion near the superior portion of the hip is highlighted.

than among healthy hips [6, 8, 9]. Specifically, in a series of anteroposterior radiographs, only 6% of the subjects without OA had a crossover sign, while 20% of the subjects with OA had a crossover sign. The presence of the crossover sign resulted in a significantly greater likelihood of OA [6]. In another study, subjects with acetabular retroversion had significantly narrower mean joint space than those without retroversion [8].

While clinical data suggest a link between acetabular retroversion and OA, the nature of that link remains unclear due to complications in the diagnosis of acetabular

retroversion and the lack of methodical evaluations of the mechanics of the retroverted acetabulum. There is controversy regarding the precise definition of acetabular retroversion. Diagnosis based on the crossover sign from clinical radiographs has been questioned because of the effect of pelvic inclination on the crossover sign [10, 11]. In addition, it is unclear whether altered mechanics result from relative posterior undercoverage of the femoral head or from anterior femoroacetabular impingement. Evaluations of hip morphology have demonstrated decreased posterior coverage of the femoral head in hips with retroverted acetabula compared to normal hips [12, 13]. This could cause OA from decreased contact area and the resulting increased contact stress on the posterior acetabulum [7, 12-15]. Alternatively, an acetabulum with normal posterior coverage but increased anterior coverage may also present as the crossover sign. Increased anterior coverage has caused retroversion to be associated with the diagnosis of pincer-type femoroacetabular impingement [16, 17]. In the case of impingement, OA may result from a combination of anterior labral damage caused by impingement and posterior cartilage damage caused by the countercoup lesion [18-20]. Because the pathomechanics of acetabular retroversion are not fully understood, comparison of the contact mechanics between hips with retroverted and normal acetabula may provide insight into the link between retroversion and OA. Specifically, regions of altered cartilage contact mechanics could indicate whether posterior undercoverage results in decreased posterior contact area and increased posterior contact stress in hips with retroverted acetabula compared to hips with normal acetabula.

Subject-specific finite element (FE) models can be used to predict cartilage contact mechanics that cannot be measured in vivo. Previous FE analysis has demonstrated the

variability in cartilage contact mechanics in the normal population, as well as altered cartilage contact mechanics in hips with acetabular dysplasia and acetabular overcoverage [21-24]. FE predictions of cartilage contact mechanics in retroverted hips have not been made but could lend valuable insight into mechanisms that lead to OA in this patient population. Therefore, the objective of this study was to compare cartilage contact mechanics between hips with normal bony anatomy and hips with acetabular retroversion during activities of daily living using a validated approach to subject-specific FE modeling [25].

Methods

Twenty subjects were recruited. All subjects gave informed consent to participate in the study and were recruited following IRB approval (University of Utah IRB #10983; the procedures followed were also in accordance with the Helsinki Declaration). Ten healthy control subjects with normal center edge angles and no history of hip pain were drawn from a previous study (five male, BMI 23.0 ± 3.9 $kg \cdot m^{-2}$, age 26 ± 4 years) [22]. Ten patients with a radiographic crossover sign on standardized radiographs, pain and clinical exams consistent with acetabular retroversion, and who subsequently received treatment for symptomatic acetabular retroversion were analyzed for the current study (nine male, BMI 24.1 ± 2.7 $kg \cdot m^{-2}$, age 24 ± 7 years). To quantify the morphology of the hips, standard radiographic measurements were made. The lateral center edge angle measures the coverage of the femoral head by the acetabulum [26]. Sharp's angle measures the acetabular inclination of the entire acetabulum, while the acetabular index measures the inclination of the acetabular roof [27, 28]. The alpha angle is a two-dimensional measure of femoral asphericity, and it was measured in the Dunn view with

external rotation because it provides the best correlation with three-dimensional measurements of asphericity [29]. The bony and articular surfaces were fit to spheres in order to evaluate the ratio of the acetabular to femoral head diameters.

Subject-specific geometry was acquired using CT arthrography [22, 23]. Approximately 15-25 mL of contrast agent was injected under fluoroscopic guidance. Contrast was a 2:1 mixture of xylocaine to Isovue 300. Manual traction was applied following the arthrography injection. CT images were acquired under constant traction applied via a hare-traction splint [22]. The CT field of view was adjusted to capture both hips (range: 331-500 mm). All images were acquired with 1 mm slice intervals and a 512 x 512 acquisition matrix.

CT images were segmented semi-automatically. Initial segmentation was done by thresholding, followed by manual segmentation to delineate regions that were visible but could not be captured using automated methods. All image data were resampled to three times the original resolution in all planes to facilitate smooth three-dimensional reconstructions [22]. Cortical bone, trabecular bone and cartilage were segmented for the hemipelvis and proximal femur.

Segmented surfaces were discretized and represented using constitutive models from the literature (Figure 6.2). Cortical bone was discretized into triangular shell elements with position-dependent thickness [25]. Cartilage was discretized into hexahedral elements. Element densities were based on previous mesh convergence analyses [25]. Bone was represented as isotropic linear elastic (E = 17 GPa, ν = 0.29) [30]. Cartilage

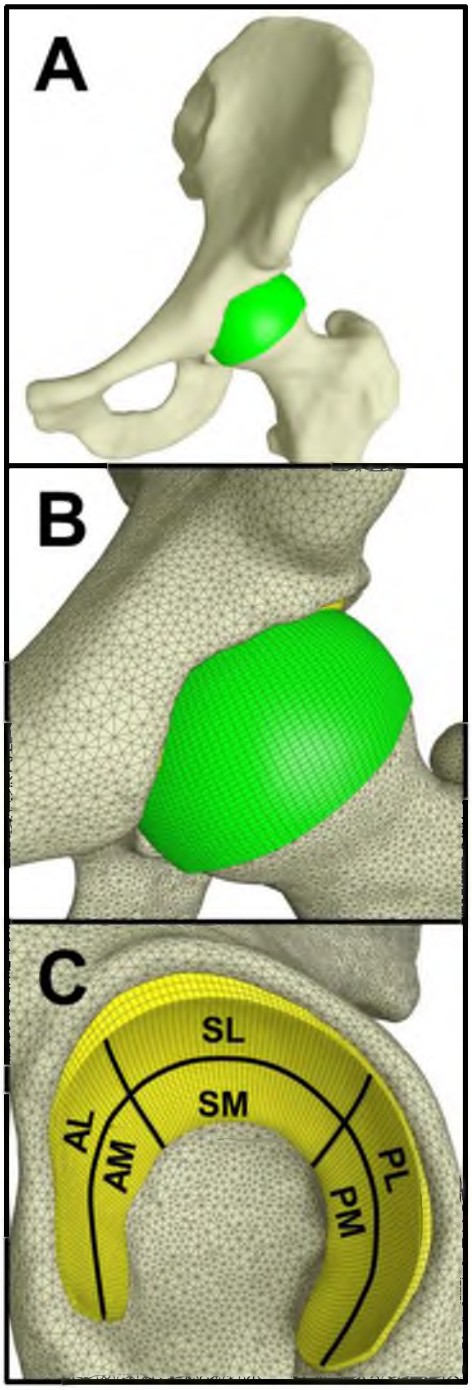

Figure 6.2: Subject-specific FE models were generated from CT data. A – anteroposterior view of a subject-specific FE model showing the bones (white) and femoral cartilage (green). B – anteroposterior view of the joint space showing discretization of the bone into triangular shell elements and the femoral cartilage into hexahedral elements. C – lateral view showing discretization of the acetabular cartilage (yellow) into hexahedral elements and the six anatomical regions on the acetabulum used for analysis of the results (AL = anterolateral, AM = anteromedial, SL = superolateral, SM = superomedial, PL = posterolateral, PM = posteromedial).

was represented as neo-Hookean hyperelastic (G = 13.6 MPa, K = 1359 MPa) [25, 31].

Boundary conditions from instrumented implant and gait data were applied to simulate average kinematics and kinetics [32]. Activities were chosen to cover a range of loads and anatomical positions. While kinematic joint angles were identical for all subjects, the applied load was scaled by subject body weight (BW). Five points through the stance phase of walking were simulated: heel strike (referred to as walking heel, 233% BW), between heel strike and midstance (referred to as walking heel-mid, 215% BW), midstance (referred to as walking mid, 203% BW), between midstance and toe-off (referred to as walking midtoe, 204% BW) and toe-off (referred to as walking toe, 205% BW). Heel strike during descending stairs (referred to as descending stairs, 261% BW) and ascending stairs (referred to as ascending stairs, 252% BW) were also simulated. Maximum flexion during chair rise (referred to as chair rise, 135% BW) was simulated primarily due to the posteriorly directed load, which focused loading on the posterior acetabulum. All models were analyzed with NIKE3D [33] and postprocessed using PostView [34].

Cartilage contact stress and contact area were evaluated on six anatomical regions of the acetabular cartilage surface: anterolateral, anteromedial, superolateral, superomedial, posterolateral and posteromedial (Figure 6.2C) [35]. Contact stress is the normal stress acting on the articular surface. Contact area was normalized to the total surface area in each region [22]. For each region and activity, statistical analysis between groups was completed using t-tests when data were normally distributed or Mann-Whitney Rank Sum tests when data were not normally distributed. Normality was tested using the Shapiro-Wilk test. For each region and group, statistical analysis between activities was

completed using paired t-tests. Statistical analysis was completed in SigmaPlot (Version 11.0, Systat Software, Inc., San Jose, CA). Significance was set at $p \leq 0.05$.

Results

Morphological differences in addition to acetabular retroversion were present, with significant differences in the lateral center-edge angle and the alpha angle between the groups. The lateral center-edge angle, Sharp's angle and acetabular index were 33.5 ± 5.4°, 40.0 ± 3.4° and 4.5 ± 3.3° in normal hips and 27.8 ± 5.5°, 37.4 ± 3.5° and 4.6 ± 4.7° in retroverted hips, respectively (p = 0.028, 0.104 and 0.965, respectively). The alpha angle was 44.0 ± 4.0° in normal hips and 61.7 ± 13.0° in retroverted hips ($p < 0.001$). The ratios of the acetabular to femoral head diameters were 1.09 ± 0.02 and 1.07 ± 0.02 at the bony surfaces and 0.95 ± 0.02 and 0.96 ± 0.02 at the articular surfaces in the normal and retroverted hips, respectively (p = 0.354 and 0.455, respectively).

The location of contact in retroverted subjects tended to be focused more medially and superiorly than in normal subjects, while contact in normal subjects was more widely distributed (Figure 6.3). Contact patterns also shifted due to loading scenario, with a shift towards more posterior loading in both groups during chair rise (Figure 6.4). However, trends of concentrated contact patterns in retroverted hips and widely distributed contact patterns in normal hips remained consistent across loading scenarios. Similar to previous findings, there was greater consistency between scenarios within each subject than between subjects within each scenario, indicating the importance of subject-specific geometry on contact pattern [22].

There were significant differences between the two groups in peak contact stress in the superomedial and posterolateral regions (Figure 6.5A). Peak contact stress in the

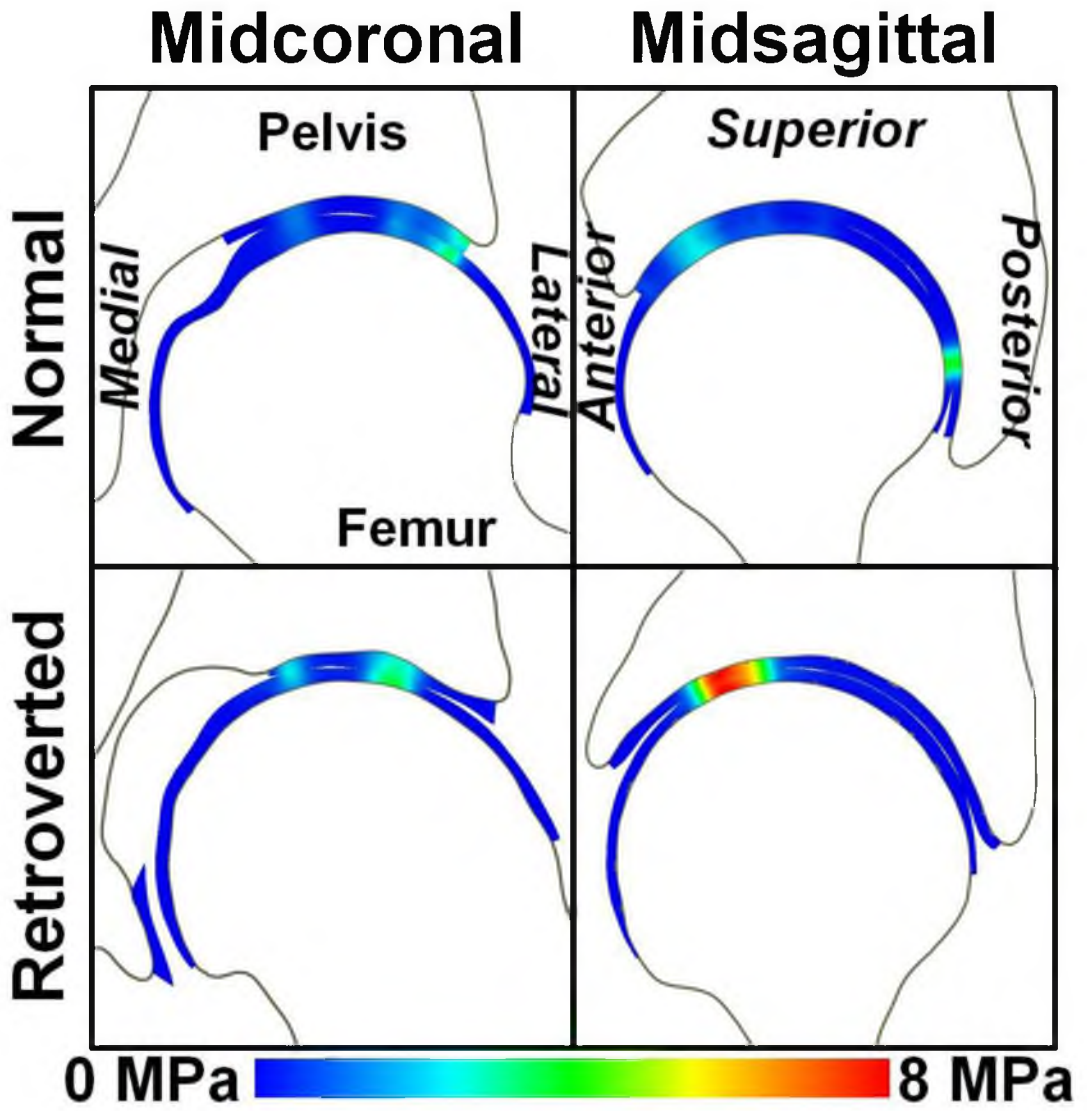

Figure 6.3: Cross sectional images of cartilage pressure during walk mid in the coronal (left column) and sagittal (right column) planes of representative normal and retroverted hips. The contact pattern was localized medially and superiorly in retroverted hips (bottom row), while normal hips had contact patterns that were more widely distributed over the articular surface (top row).

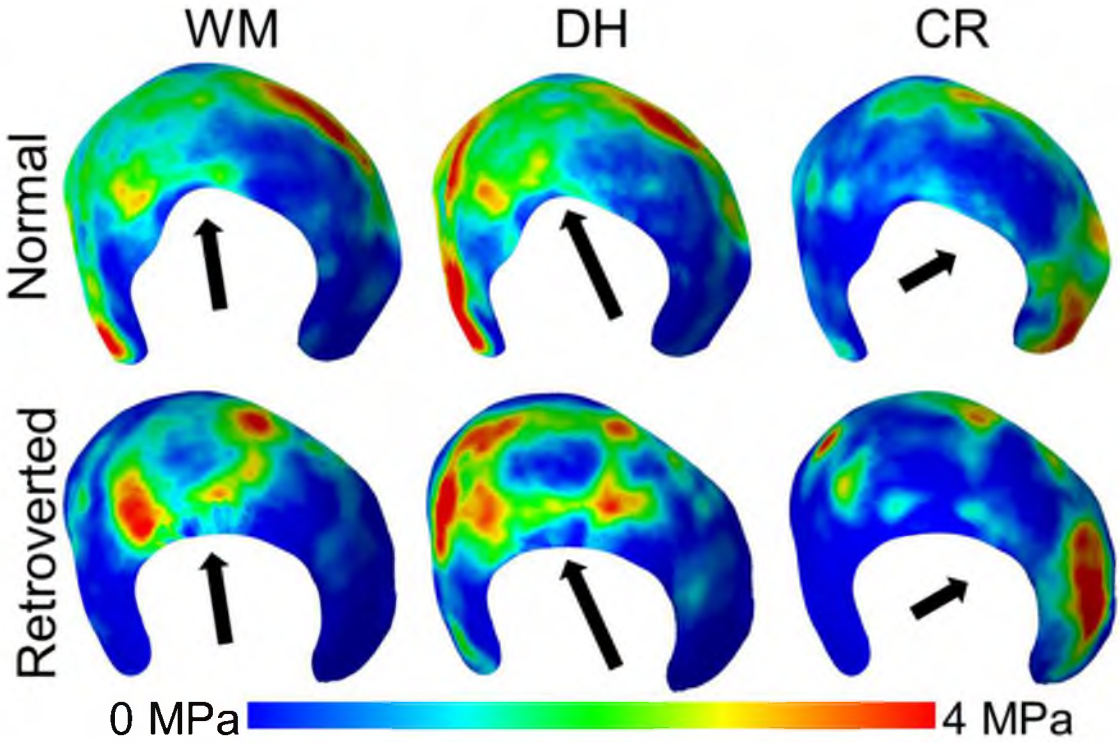

Figure 6.4: Contact stress patterns averaged across all normal hips (top row) and across all retroverted hips (bottom row) during three activities. The arrows indicate the approximate direction and relative magnitude of the load during each activity. Both the direction of the applied load and the subject group influenced contact pattern. When the load was directed superiorly during walk mid, the contact patterns in both groups were primarily in the superior acetabulum. When the load was directed slightly anteriorly during descend heel, the contact patterns were more anterior than during walk mid in both groups. When the load was directed posteriorly during CR, the contact patterns were primarily in the posterior acetabulum in both groups.

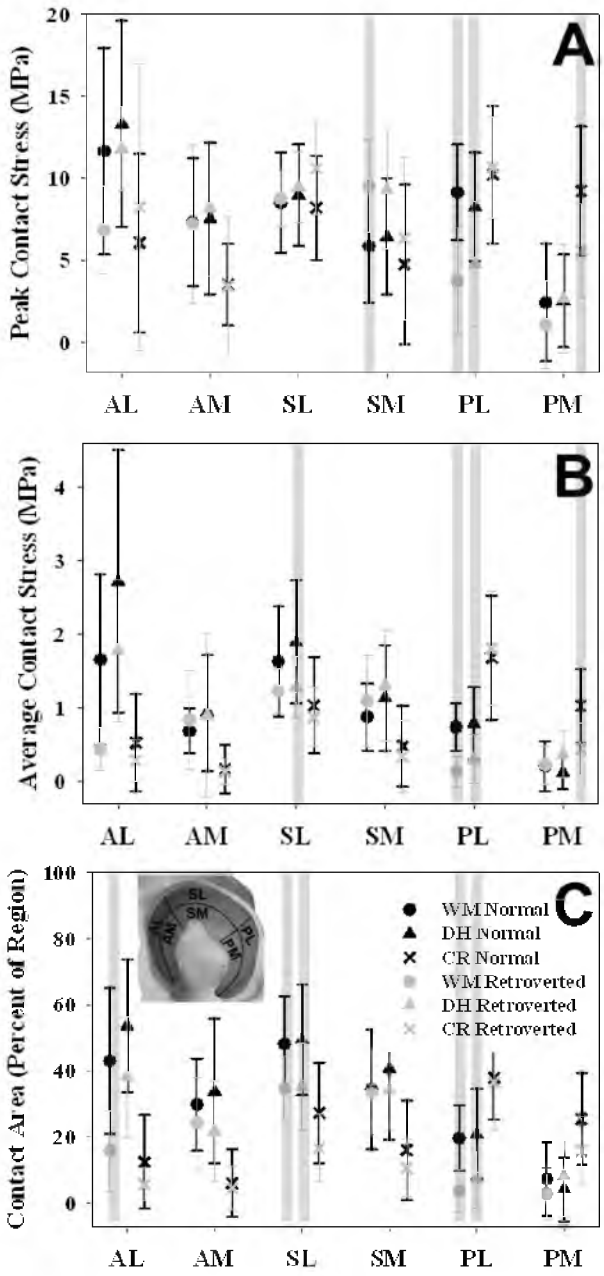

Figure 6.5: Contact stress and area results for walk mid, descend heel and chair rise loading scenarios in both groups (n = 10 in each group). Results are shown by anatomical region (AL = anterolateral, AM = anteromedial, SL = superolateral, SM = superomedial, PL = posterolateral, PM = posteromedial). A – peak contact stress. B – average contact stress. C – contact area. Peak contact stress in the superomedial region was larger in the retroverted hips than in the normal hips during walk mid. For all other significant differences, results were larger in the normal hips than in the retroverted hips. This included larger peak contact stress, average contact stress and contact area in the posterolateral region during walk mid and descend heel, as well as larger peak and average contact stress in the posteromedial region during chair rise in the normal hips than in the retroverted hips. Gray highlights indicate $p \leq 0.05$. Error bars show 95% confidence intervals.

posterolateral region was significantly larger in normal hips than in retroverted hips during walking heel-mid, walking mid, walking midtoe, walking toe and descending stairs (p = 0.022, 0.006, 0.002, 0.002 and 0.042, respectively). Conversely, peak contact stress in the superomedial region was significantly larger in retroverted hips than normal hips during all walking scenarios (p = 0.038, 0.044, 0.003, 0.044 and 0.009 for walking heel, walking heel-mid, walking mid, walking midtoe and walking toe, respectively). When the posterior acetabulum was loaded during chair rise, peak contact stress in the posteromedial region was significantly larger in normal hips than in retroverted hips (p = 0.029).

Average contact stress was significantly larger in normal hips than in retroverted hips in several activities in the lateral and posterior regions (Figure 6.5B). Specifically, average contact stress was significantly larger in normal hips than in retroverted hips in the posterolateral region during all walking activities and descending stairs (p = 0.003 for walking heel, $p \leq 0.001$ for all other walking activities, p = 0.013 for descending stairs). Average contact stress in the anterolateral region was significantly larger in normal hips than in retroverted hips in walking mid, walking midtoe and walking toe (p = 0.026, 0.017 and 0.014, respectively). As with peak contact stress, average contact stress in the posteromedial region during chair rise was significantly larger in normal hips than in retroverted hips (p = 0.006). While average contact stress in the superomedial region tended to be larger in retroverted hips than in normal hips, the only significant difference was during walking heel (p = 0.028).

Contact area as a percentage of each region tended to be smaller in retroverted hips than in normal hips (Figure 6.5C). Percent contact area in the superolateral and

posterolateral regions was significantly smaller in retroverted hips than in normal hips during all walking scenarios and descending stairs (in the superolateral region $p = 0.035$, 0.035, 0.025, 0.018, 0.021 and 0.048, respectively for walking heel, walking heel-mid, walking mid, walking midtoe, walking toe and descending stairs; in the posterolateral region $p = 0.005$, 0.007, 0.002, <0.001, <0.001 and 0.017, respectively). Percent contact area in the anterolateral region was significantly smaller in retroverted hips than in normal hips during walking heel-mid, walking mid, walking midtoe, walking toe and ascending stairs ($p = 0.009$, 0.003, 0.003, 0.003 and 0.044, respectively). There were no significant differences in percent contact area in the medial regions.

Regional peak contact stress, average contact stress and contact area varied by loading scenario within each group. Many of the regional differences were between chair rise, which had a posteriorly directed load, and the other activities. Contact stress and contact area in the anterior and superior regions tended to be smaller during chair rise than during other activities, but contact stress and contact area in the posterior regions tended to be larger in chair rise than during other activities. In the normal hips, peak contact stress, average contact stress and contact area during chair rise were significantly smaller than during all other activities in the anterolateral region, but significantly larger than during all other activities in the posteromedial region (in the anterolateral region for peak contact stress $p = 0.006$, 0.012, 0.012, 0.004, 0.009, <0.001 and 0.001, for average contact stress $p = 0.005$, 0.003, 0.003, 0.003, 0.002, <0.001 and 0.002 against walking heel, walking heel-mid, walking mid, walking midtoe, walking toe, descending stairs and ascending stairs, respectively, for contact area $p = 0.002$ against walking heel and $p < 0.001$ against all other activities; in the posteromedial region for peak contact stress $p =$

0.018 against ascending stairs and $p < 0.001$ against all other activities, for average contact stress $p = 0.002$ against walking heel and $p \leq 0.001$ against all other activites, for contact area $p = 0.020$, 0.002, 0.006, 0.005, 0.005, 0.001 and 0.007 against walking heel, walking heel-mid, walking mid, walking midtoe, walking toe, descending stairs and ascending stairs, respectively). Average contact stress in the posterolateral region was significantly larger during both ascending stairs and chair rise than during all walking activities and descending stairs (for ascending stairs $p = 0.004$, 0.001, 0.002, 0.001, 0.001 and <0.001, for chair rise $p = 0.013$, 0.002, 0.001, 0.001, <0.001 and 0.002 against walking heel, walking heel-mid, walking mid, walking midtoe, walking toe and descending stairs, respectively). Average contact stress in the anteromedial region was significantly smaller during chair rise than during all walking activities and descending stairs ($p = 0.019$, 0.02, 0.01, 0.009, 0.01, and 0.021 against walking heel, walking heel-mid, walking mid, walking midtoe, walking toe and descending stairs, respectively). Contact area in the superolateral, anteromedial, and superomedial regions was significantly smaller during chair rise than during all other activities (in the superolateral region $p = 0.002$ against descending stairs and $p < 0.001$ against all other activities; in the anteromedial region $p = 0.006$, 0.006, 0.002, 0.001, 0.002, 0.004 and 0.031; in the superomedial region $p = 0.001$, 0.003, 0.011, 0.020, 0.025, 0.005 and 0.005 against walking heel, walking heel-mid, walking mid, walking midtoe, walking toe, descending stairs and ascending stairs, respectively). Contact area in the posterolateral region was significantly larger in chair rise than during all activities except walking heel and ascending stairs ($p = 0.003$ against walking heel, $p < 0.001$ against walking mid, walking midtoe and walking toe, $p = 0.015$ against descending stairs). In the retroverted subjects,

peak contact stress in the posterolateral region during chair rise was significantly larger than during all walking scenarios and descending stairs ($p = 0.012$ against walking heel, $p = 0.002$ against descending stairs and $p < 0.001$ against all others). Average contact stress was significantly smaller during chair rise in the anterolateral and superomedial regions than during all other activities and was larger during chair rise than during all other activities in the posterolateral region (in the anterolateral region $p = 0.036$, 0.012 0.004 0.003 0.001, <0.001 and 0.015; in the superomedial region $p = <0.001$, <0.001, 0.006, 0.013, 0.027, 0.006 and 0.002 against walking heel, walking heel-mid, walking mid, walking midtoe, walking toe, descending stairs and ascending stairs, respectively; in the posterolateral region $p < 0.001$ against all activities). Contact area during chair rise was significantly smaller than during all other activities in the anterolateral and superolateral regions (in the anterolateral region $p = 0.003$, 0.005, 0.004, 0.004, 0.002, <0.001 and 0.008; in the superolateral region $p = 0.002$, 0.002, 0.003, 0.002, 0.004, 0.004 and 0.002 against walking heel, walking heel-mid, walking mid, walking midtoe, walking toe, descending stairs and ascending stairs, respectively). Contact area during chair rise was significantly larger than during all other activities in the posterolateral region ($p = 0.002$ against ascending stairs, $p < 0.001$ against all other activities).

Discussion

Unique contact patterns in the two groups affected the predicted contact stress and contact area. In many regions, both contact stress and percent contact area were lower in the retroverted hips than in the normal hips. Since force can be interpreted as stress integrated over a contact area, these results may seem counterintuitive. However, if the location of contact area and direction of the applied load are considered, the results are

clearer. Contact area has an associated direction, normal to the articular surface at each point. In the retroverted hips, contact tended to be in the superior and medial regions of the acetabulum during walking, ascending stairs and descending stairs. Conversely, in the normal hips, contact tended to be distributed across the entire acetabulum. During chair rise, contact in both groups was primarily in the posterior acetabulum, although it was more widely distributed in the normal hips than in the retroverted hips. The load was directed approximately superiorly during walking activities, ascending stairs and descending stairs, while the load was directed posteriorly during chair rise. These directions were more aligned with the surface normals of the contact area in the retroverted hips than in the normal hips. Therefore, the retroverted hips were able to sustain the applied load with lower contact stress and lower contact area than the normal hips as a result of a less distributed contact area that was aligned with the approximate direction of the applied load.

Differences in contact stress and contact area in the posterior regions may have important implications regarding the mechanisms of damage in retroverted hips and the preferred clinical treatment. Hips with retroversion often experience damage in the posterior acetabulum, which has been postulated to result from one of two mechanisms [36]. The first mechanism to consider is decreased contact area and a resulting elevated contact stress in the posterior acetabulum [7, 14, 15]. The preferred treatment for this mechanism of damage is periacetabular osteotomy [14, 37]. Previous studies demonstrated decreased posterior coverage in retroverted hips, suggesting that retroverted hips have a smaller posterior contact area [12, 13]. However, the results of the present study suggest that elevated posterior stresses may not be the mechanism of damage in

retroverted hips. Specifically, contact stresses were not elevated in the posterior acetabulum of retroverted subjects, which suggests that periacetabular osteotomy may not be warranted or beneficial in subjects with retroversion from the point of view of reducing contact stress. The second mechanism that has been proposed is anterior femoroacetabular impingement, where damage is caused by collision of the femoral head-neck region against an abnormally prominent anterior acetabular rim [18-20]. The alternative treatment for this mechanism of damage is resection of the prominent anterior acetabular rim [14]. The present study did not evaluate the possible effects of impingement in normal subjects or retroverted patients, and this is a topic that warrants further investigation in the future. In particular, other activities that will be more likely to produce impingement should be investigated.

Differences in predictions of contact stress between activities within each group illustrate the effects of the focused contact patterns in retroverted hips compared to the widely distributed contact patterns in normal hips (Figure 6.4). This can be seen by comparing chair rise, where the load was directed posteriorly, to all other activities. Peak contact stress in the posterolateral region was larger during chair rise than during all other activities in retroverted hips, but this was not the case for normal hips. When the load was directed posteriorly during chair rise, the focused contact pattern in the retroverted hips caused higher peak stresses in the posterolateral region. However, the contact pattern was distributed across more of the acetabulum in the normal hips in all loading scenarios. Therefore, the posterior direction of the load during chair rise did not cause higher peak contact stresses during chair rise in the normal hips.

Several limitations in the present study warrant discussion. Because of the lack of a widely accepted morphological definition of acetabular retroversion, the spectrum of the morphological variation associated with the disease could have confounding effects on the results of this study. Acetabular retroversion is most often diagnosed using the crossover sign. Although the crossover sign is sensitive to the orientation of the pelvis with respect to the imaging plane, we controlled for pelvic inclination in the present study, which improves sensitivity of the crossover sign for diagnosis of retroversion to 96% [12, 38]. It is worth noting that neither the Sharp's angle nor the acetabular index were significantly different between the two populations. Thus, it appears unlikely that abnormal acetabular inclination was the cause of medial contact in retroverted hips.

Similarly, this study did not evaluate femoral deformities as part of the patient selection criteria. Because femoral version in normal hips is correlated with acetabular version [39], abnormal femoral version in the retroverted hips may have influenced results. The retroverted hips in this study had larger alpha angles than the normal hips, suggesting a higher prevalence of cam-type deformities on the femur. With the possible exception of chair rise, the activities that were simulated in this study would not be expected to cause impingement even in hips with cam-type deformities. Nevertheless, confounding effects from the larger alpha angles in the retroverted group cannot be ruled out. In addition to the effects of isolated acetabular or femoral pathoanatomy, other differences in joint anatomy that were not quantified as part of the patient classification could have affected contact patterns.

The results of this study must be interpreted in light of the assumptions made in the FE models. Although cartilage material behavior is complex, it was represented as

spatially homogeneous, isotropic and nearly-linear hyperelastic [40]. These assumptions were justified because previous validation studies showed that FE predictions of contact stress and contact area using isotropic linear elastic and nearly-linear hyperelastic cartilage constitutive models were in good agreement with experimental measurements [25, 41]. A second limitation was the use of identical material coefficients for both groups. While there were no clinical or radiographic signs of cartilage degeneration in patients in the retroverted group, minor changes in cartilage material behavior may have occurred. Similarly, there is evidence that hips with abnormal bony anatomy exhibit abnormal gait patterns [42, 43]. Identical loading scenarios were used for all subjects in this study because of the lack of literature data on gait in subjects with acetabular retroversion. This study was limited to predictions of contact stress and contact area. A large body of literature points to these variables as important in the pathogenesis of OA (e.g., [24, 44, 45]). However, other mechanical variables, such as the maximum shear stress, may be more important for predicting cartilage damage [46-48]. The modeling requirements for accurate predictions of contact stress and contact area in the human hip have been established [25], but predicting other mechanical variables may require increased mesh resolution or more advanced constitutive models. Finally, the patient population used in this study was predominantly male. This bias is to be expected since the crossover sign and lower acetabular anteversion occur more frequently in men than in women [49, 50].

In conclusion, this study demonstrated that hips with acetabular retroversion exhibit superomedial cartilage contact patterns during simulations of activities of daily living, while hips with normal bony anatomy exhibit widely distributed cartilage contact

patterns. Further, the results suggest that elevated posterior stresses may not be the mechanism of damage in hips with retroverted acetabula.

References

[1] Gosvig, K. K., Jacobsen, S., Sonne-Holm, S., Palm, H., and Troelsen, A., 2010, "Prevalence of Malformations of the Hip Joint and their Relationship to Sex, Groin Pain, and Risk of Osteoarthritis: A Population-Based Survey," J Bone Joint Surg Am, **92**(5), pp. 1162-1169.

[2] Carter, D. R., Beaupre, G. S., Wong, M., Smith, R. L., andriacchi, T. p., and Schurman, D. J., 2004, "The Mechanobiology of Articular Cartilage Development and Degeneration," Clin Orthop Relat Res (427 Suppl), pp. S69-77.

[3] Guilak, F., and Hung, C. T., 2005, "Physical Regulation of Cartilage Metabolism," *Basic Orthopaedic Biomechanics and Mechano-Biology*, V. C. Mow, and R. Huiskes, Eds., Lippincott Williams & Wilkins, Philadephia.

[4] Wilson, W., Van Donkelaar, C. C., Van Rietbergen, R., and Huiskes, R., 2005, "The Role of Computational Models in the Search for the Mechanical Behavior and Damage Mechanisms of Articular Cartilage," Med Eng Phys, **27**(10), pp. 810-826.

[5] Scott, C. C., and Athanasiou, K. A., 2006, "Mechanical Impact and Articular Cartilage," Crit Rev Biomed Eng, **34**(5), pp. 347-378.

[6] Ezoe, M., Naito, M., and inoue, T., 2006, "The Prevalence of Acetabular Retroversion Among Various Disorders of the Hip," J Bone Joint Surg Am, **88**(2), pp. 372-379.

[7] Giori, N. J., and Trousdale, R. T., 2003, "Acetabular Retroversion is Associated with Osteoarthritis of the Hip," Clin Orthop Relat Res (417), pp. 263-269.

[8] Kim, W. Y., Hutchinson, C. E., andrew, J. G., and Allen, p. D., 2006, "The Relationship Between Acetabular Retroversion and Osteoarthritis of the Hip," J Bone Joint Surg Br, **88**(6), pp. 727-729.

[9] Reynolds, D., Lucas, J., and Klaue, K., 1999, "Retroversion of the Acetabulum. A Cause of Hip Pain," J Bone Joint Surg Br, **81**(2), pp. 281-288.

[10] Bircher, M. D., 1999, "Retroversion of the Acetabulum," J Bone Joint Surg Br, **81**(4), pp. 743-744.

[11] Siebenrock, K. A., Kalbermatten, D. F., and Ganz, R., 2003, "Effect of Pelvic Tilt on Acetabular Retroversion: A Study of Pelves from Cadavers," Clin Orthop Relat Res (407), pp. 241-248.

[12] Dandachli, W., Islam, S. U., Liu, M., Richards, R., Hall-Craggs, M., and Witt, J., 2009, "Three-Dimensional CT Analysis to Determine Acetabular Retroversion and the Implications for the Management of Femoro-Acetabular Impingement," J Bone Joint Surg Br, **91**(8), pp. 1031-1036.

[13] Hansen, B. J., Harris, M. D., Anderson, L. A., Peters, C. L., Weiss, J. A., and Anderson, A. E., 2012, "Correlation between Radiographic Measures of Acetabular Morphology with Three-Dimensional Femoral Head Coverage in Patients with Acetabular Retroversion," Acta Orthop, **83**(3), pp. 233-239.

[14] Peters, C. L., Anderson, L. A., Erickson, J. A., Anderson, A. E., and Weiss, J. A., 2011, "An Algorithmic Approach to Surgical Decision Making in Acetabular Retroversion," Orthopedics, **34**(1), p. 10.

[15] Tonnis, D., and Heinecke, A., 1999, "Acetabular and Femoral Anteversion: Relationship with Osteoarthritis of the Hip," J Bone Joint Surg Am, **81**(12), pp. 1747-1770.

[16] Cobb, J., Logishetty, K., Davda, K., and Iranpour, F., 2010, "Cams and Pincer Impingement are Distinct, not Mixed: The Acetabular Pathomorphology of Femoroacetabular Impingement," Clin Orthop Relat Res, **468**(8), pp. 2143-2151.

[17] Tannast, M., Siebenrock, K. A., and Anderson, S. E., 2007, "Femoroacetabular Impingement: Radiographic Diagnosis--What the Radiologist Should Know," Am J Roentgenol, **188**(6), pp. 1540-1552.

[18] Ganz, R., Leunig, M., Leunig-Ganz, K., and Harris, W. H., 2008, "The Etiology of Osteoarthritis of the Hip: An integrated Mechanical Concept," Clin Orthop Relat Res, **466**(2), pp. 264-272.

[19] Larson, C. M., 2010, "Arthroscopic Management of Pincer-type Impingement," Sports Med Arthrosc, **18**(2), pp. 100-107.

[20] Beck, M., Kalhor, M., Leunig, M., and Ganz, R., 2005, "Hip Morphology Influences the Pattern of Damage to the Acetabular Cartilage: Femoroacetabular Impingement as a Cause of Early Osteoarthritis of the Hip," J Bone Joint Surg Br, **87**(7), pp. 1012-1018.

[21] Chegini, S., Beck, M., and Ferguson, S. J., 2009, "The Effects of Impingement and Dysplasia on Stress Distributions in the Hip Joint During Sitting and Walking: A Finite Element Analysis," J Orthop Res, **27**(2), pp. 195-201.

[22] Harris, M. D., Anderson, A. E., Henak, C. R., Ellis, B. J., Peters, C. L., and Weiss, J. A., 2012, "Finite Element Prediction of Cartilage Contact Stresses in Normal Human Hips," J Orthop Res, **30**(7), pp. 1133-1139.

[23] Henak, C. R., Ellis, B. J., Harris, M. D., Anderson, A. E., Peters, C. L., and Weiss, J. A., 2011, "Role of the Acetabular Labrum in Load Support Across the Hip Joint," J Biomech, **44**(12), pp. 2201-2206.

[24] Russell, M. E., Shivanna, K. H., Grosland, N. M., and Pedersen, D. R., 2006, "Cartilage Contact Pressure Elevations in Dysplastic Hips: A Chronic Overload Model," J Orthop Surg Res, 1, pp. 6-6.

[25] Anderson, A. E., Ellis, B. J., Maas, S. A., Peters, C. L., and Weiss, J. A., 2008, "Validation of Finite Element Predictions of Cartilage Contact Pressure in the Human Hip Joint," J Biomech Eng, **130**(5), p. 051008.

[26] Wiberg, G., 1953, "Shelf Operation in Congenital Dysplasia of the Acetabulum and in Subluxation and Dislocation of the Hip," J Bone Joint Surg Am, **35-A**(1), pp. 65-80.

[27] Sharp, I. K., 1961, "Acetabular Dysplasia the Acetabular Angle," J Bone Joint Surg Br, **43**(2), pp. 268-272.

[28] Bittersohl, B., Hosalkar, H. S., and Wenger, D. R., 2012, "Surgical Treatment of Hip Dysplasia in Children and Adolescents," Orthop Clin N Am, **43**(3), p. 301.

[29] Harris, M. D., 2013, "The Geometry and Biomechanics of Normal and Pathomorphologic Human Hips," University of Utah, Salt Lake City.

[30] Dalstra, M., and Huiskes, R., 1995, "Load Transfer Across the Pelvic Bone," J Biomech, **28**(6), pp. 715-724.

[31] Park, S., Hung, C. T., and Ateshian, G. A., 2004, "Mechanical Response of Bovine Articular Cartilage Under Dynamic Unconfined Compression Loading at Physiological Stress Levels," Osteoarthritis Cartilage, **12**(1), pp. 65-73.

[32] Bergmann, G., Deuretzbacher, G., Heller, M., Graichen, F., Rohlmann, A., Strauss, J., and Duda, G. N., 2001, "Hip Contact Forces and Gait Patterns from Routine Activities," J Biomech, **34**(7), pp. 859-871.

[33] Puso, M. A., Maker, Bradley N., Ferencz, Robert M., Hallquist, John O., 2007, "NIKE3D: A Nonlinear, Implicit, Three-Dimensional Finite Element Code for Solid and Structural Mechanics," User's Manual.

[34] Maas, S. A., 2012, "PostView Version 1.4: User's Manual."

[35] Athanasiou, K. A., Agarwal, A., and Dzida, F. J., 1994, "Comparative Study of the Intrinsic Mechanical Properties of the Human Acetabular and Femoral Head Cartilage," J Orthop Res, **12**(3), pp. 340-349.

[36] Pfirrmann, C. W. A., Mengiardi, B., Dora, C., Kalberer, F., Zanetti, M., and Hodler, J., 2006, "Cam and Pincer Femoroacetabular Impingement: Characteristic MR Arthrographic Findings in 50 Patients," Radiology, **240**(3), pp. 778-785.

[37] Siebenrock, K. A., Schoeniger, R., and Ganz, R., 2003, "Anterior Femoro-acetabular Impingement Due to Acetabular Retroversion. Treatment with Periacetabular Osteotomy," J Bone Joint Surg Am, **85-A**(2), pp. 278-286.

[38] Jamali, A. A., Mladenov, K., Meyer, D. C., Martinez, A., Beck, M., Ganz, R., and Leunig, M., 2007, "Anteroposterior Pelvic Radiographs to Assess Acetabular Retroversion: High Validity of the "Cross-Over-Sign"," J Orthop Res, **25**(6), pp. 758-765.

[39] Buller, L. T., Rosneck, J., Monaco, F. M., Butler, R., Smith, T., and Barsoum, W. K., 2012, "Relationship Between Proximal Femoral and Acetabular Alignment in Normal Hip Joints Using 3-Dimensional Computed Tomography," Am J Sport Med, **40**(2), pp. 367-375.

[40] Mow, V., Gu, W., and Chen, F., 2005, "Structure and Function of Articular Cartilage and Meniscus," *Basic Orthopaedic Biomechanics and Mechano-Biology*, V. Mow, and R. Huiskes, Eds., Lippincott, Philadephia, pp. 181-258.

[41] Anderson, D. D., Goldsworthy, J. K., Li, W., James Rudert, M., tochigi, Y., and Brown, T. D., 2007, "Physical Validation of a Patient-Specific Contact Finite Element Model of the Ankle," J Biomech, **40**(8), pp. 1662-1669.

[42] Brisson, N., Lamontagne, M., Kennedy, M. J., and Beaule, p. E., 2012, "The Effects of Cam Femoroacetabular Impingement Corrective Surgery on Lower-Extremity Gait Biomechanics," Gait Posture.

[43] Kennedy, M. J., Lamontagne, M., and Beaule, p. E., 2009, "Femoroacetabular Impingement Alters Hip and Pelvic Biomechanics During Gait Walking Biomechanics of FAI," Gait Posture, **30**(1), pp. 41-44.

[44] Haut, R. C., Ide, T. M., and De Camp, C. E., 1995, "Mechanical Responses of the Rabbit Patello-femoral Joint to Blunt Impact," J Biomech Eng, **117**(4), pp. 402-408.

[45] Segal, N. A., Anderson, D. D., Iyer, K. S., Baker, J., Torner, J. C., Lynch, J. A., Felson, D. T., Lewis, C. E., and Brown, T. D., 2009, "Baseline Articular Contact Stress Levels Predict Incident Symptomatic Knee Osteoarthritis Development in the MOST Cohort," J Orthop Res, **27**(12), pp. 1562-1568.

[46] Guilak, F., Fermor, B., Keefe, F. J., Kraus, V. B., Olson, S. A., Pisetsky, D. S., Setton, L. A., and Weinberg, J. B., 2004, "The Role of Biomechanics and Inflammation in Cartilage Injury and Repair," Clin Orthop Relat Res (423), pp. 17-26.

[47] Atkinson, T. S., Haut, R. C., and Altiero, N. J., 1998, "Impact-Induced Fissuring of Articular Cartilage: An Investigation of Failure Criteria," J Biomech Eng, 120(2), pp. 181-187.

[48] Brand, R. A., 2005, "Joint Contact Stress: A Reasonable Surrogate for Biological Processes?," Iowa Orthop J, **25**, pp. 82-94.

[49] Laborie, L. B., Lehmann, T. G., Engesaeter, I. O., Eastwood, D. M., Engesaeter, L. B., and Rosendahl, K., 2011, "Prevalence of Radiographic Findings Thought to be Associated with Femoroacetabular Impingement in a Population-Based Cohort of 2081 Healthy Young Adults," Radiology, **260**(2), pp. 494-502.

[50] Perreira, A. C., Hunter, J. C., Laird, T., and Jamali, A. A., 2011, "Multilevel Measurement of Acetabular Version Using 3-D CT-generated Models: Implications For Hip Preservation Surgery," Clin Orthop Relat Res, **469**(2), pp. 552-561.

CHAPTER 7

EFFECTS OF CONSTITUTIVE MODEL ASSUMPTIONS ON TRANSCHONDRAL MAXIMUM SHEAR STRESS AND FIRST PRINCIPAL STRAIN IN THE HUMAN HIP

Abstract

Hip osteoarthritis (OA) affects approximately 10% of the population and may be caused by abnormal cartilage mechanics. Surface fibrillation, which may be caused by elevated first principal (most tensile) strain, and cartilage delamination, which may be caused by elevated shear stress, are early aspects of cartilage degeneration in OA. Although transchondral mechanics cannot be measured in vivo, they can be predicted using finite element (FE) modeling. However, the required mesh resolution and cartilage constitutive model for accurately predicting transchondral mechanics in the human hip are unknown. The objectives of this study were to use a population of validated FE models to evaluate the mesh resolution required to predict transchondral mechanics; to assess cartilage mechanics at the articular surface, the osteochondral surface and transchondrally; and to assess the effects of cartilage constitutive assumptions on predictions of cartilage mechanics by comparing predictions from FE models with linear, nonlinear and tension-compression nonlinear cartilage constitutive models. Five validated, specimen-specific FE models of normal human hips were evaluated with

nearly-linear neo-Hookean, nonlinear Veronda Westmann and tension-compression nonlinear ellipsoidal fiber distribution cartilage constitutive models. Transchondral predictions of maximum shear stress and first principal strain were compared between FE models with different cartilage constitutive models. Mesh convergence analysis demonstrated that five elements were required through the depth of the cartilage for accurate predictions of transchondral maximum shear stress and first principal strain. At large magnitudes of stress and strain, the ellipsoidal fiber distribution model had the stiffest response, which caused this model to predict the largest peak stresses and the smallest peak strains. Conversely, the neo-Hookean model predicted the smallest peak stresses and the largest peak strains. Models with neo-Hookean cartilage predicted smaller maximum shear stress transchondral gradients than models with Veronda Westmann and ellipsoidal fiber distribution cartilage predicted. For all constitutive models, transchondral first principal strain peaked below the articular surface of the femur. In conclusion, this study suggests that tension-compression nonlinearity and/or strain induced anisotropy are important features for predicting accurate transchondral maximum shear stress and first principal strain in the human hip. Additionally, this study indicates that five elements through the cartilage thickness are required mesh for converged predictions of maximum shear stress and first principal strain.

Introduction

Abnormal cartilage mechanics are thought to initiate and advance osteoarthritis (OA) through the combination of damage to the cartilage matrix and altered cartilage metabolism [1, 2]. For example, contact stress and maximum shear stress predict cartilage fissuring under impact loads [3, 4], while compressive, tensile and shear

deformation alter the cartilage matrix and cartilage metabolism of explants in a dose- and location-dependent manner [2, 5-7]. In the context of OA, early signs of cartilage damage include fibrillation and fissuring of the articular surface and cartilage delamination from the bone [3, 4, 8-11]. Fibrillation may be caused by elevated tensile strains near the articular surface and cartilage delamination may be caused by elevated shear stress at the osteochondral interface [12-16]. Therefore, understanding tensile strain and shear stress at the articular surface, at the osteochondral interface and transchondrally (through the cartilage thickness), would provide insight into OA at the tissue level.

The mechanics of articular cartilage in the normal and pre-arthritic hip are still poorly understood. Hip OA affects 9.5% of men and 11.2% of women [17], and an improved understanding of tissue level cartilage mechanics could guide the development of strategies to prevent or delay the onset of hip OA. Cartilage mechanics are difficult to directly measure in the hip, but can be predicted with finite element (FE) analysis. FE analysis has been used to primarily to study contact stress and contact area in the human hip [18-26]. Parametric studies have demonstrated that predictions of contact stress and contact area are sensitive to subject-specific geometry and the material properties of cortical bone, but are relatively insensitive to cartilage constitutive model [18, 19, 27, 28]. In a recent series of directly validated, specimen-specific FE models, we demonstrated that contact stress and area were relatively insensitive to material nonlinearity and spatial inhomogeneity in the cartilage constitutive model, and also determined the required mesh resolution for accurate predictions of these variables [28]. While previous studies elucidate model requirements for predicting contact stress and

area, these variables are only a small subset of the stress- and strain-dependent variables that are relevant to the initiation and progression of OA. Therefore, the next logical step in the application of FE modeling for understanding hip OA is to expand the predictive capability of subject-specific FE models to additional mechanical variables. This requires re-evaluating modeling strategies, since those that are sufficient to predict contact stress and contact area may be inadequate for accurate predictions of other variables.

Two aspects of the modeling strategy that are likely to affect predictions of transchondral cartilage mechanics in the hip are the cartilage constitutive model and the resolution of the cartilage discretization. Cartilage exhibits rate- and time-dependent behavior, material nonlinearity, tension-compression nonlinearity and transchondral variation in properties [29-36]. Nearly-incompressible elastic behavior is an appropriate assumption for predictions during activities wherein the loading occurs quickly, which removes the need to include rate- and time-dependent behavior [37, 38]. Even with this simplification, the effects of other features of cartilage behavior on FE model predictions may influence the predictions of cartilage mechanics at the articular surface, transchondrally and at the osteochondral interface. Additionally, mesh resolution is an important aspect of FE modeling strategy, since the accuracy of the solution is directly linked to the density of the mesh [39, 40]. While the mesh resolution required to predict contact stress and contact area has been established [28], the required mesh resolution for accurate predictions of transchondral mechanics is unknown. Therefore, the objectives of this study were to use a population of validated FE models to evaluate the mesh resolution required to predict transchondral mechanics; to assess cartilage mechanics at

the articular surface, the osteochondral surface and transchondrally; and to assess the effects of cartilage constitutive assumptions on predictions of cartilage mechanics by comparing predictions from FE models with linear, nonlinear and tension-compression nonlinear cartilage constitutive models [28].

Methods

Five male specimens were used for this study (40 ± 14 years old, weight 63 ± 14 kg, height 177 ± 9 cm). Specimen-specific FE models were generated and underwent direct validation of contact stress and contact area as part of a previous study [28] (Figure 7.1). Briefly, specimens were dissected free of soft tissue and volumetric image data were acquired (Siemens Somatom Emotion, 0.7 mm slice thickness, 512 × 512 acquisition matrix, 276-420 mm field of view). Image data were segmented and the segmented data were used to create polygonal surfaces (Amira version 5.3, Visage Imaging, San Diego, CA) [18, 22, 23, 41]. Cortical bone was discretized into triangular shell elements with position dependent thickness [18, 42]. Cartilage surfaces were discretized into hexahedral elements using TrueGrid (XYZ Scientific, Livermore, CA).

Four activities of daily living were simulated based off of instrumented implant and gait data, and matched to loading scenarios achieved during experimental loading for the previous study: heel strike during walking (WH), mid stance during walking (WM), heel strike during stair descent (DH) and heel strike during stair descent (AH) [28, 43]. Rigid boundary conditions were assumed at the pubis and sacroiliac joints on the pelvis, and on the femur below the lesser trochanter [18]. Mortar tied contact was used between cartilage and bone, and mortar sliding contact was used between acetabular and femoral cartilage [44, 45]. All FE models were analyzed in NIKE3D and postprocessed in

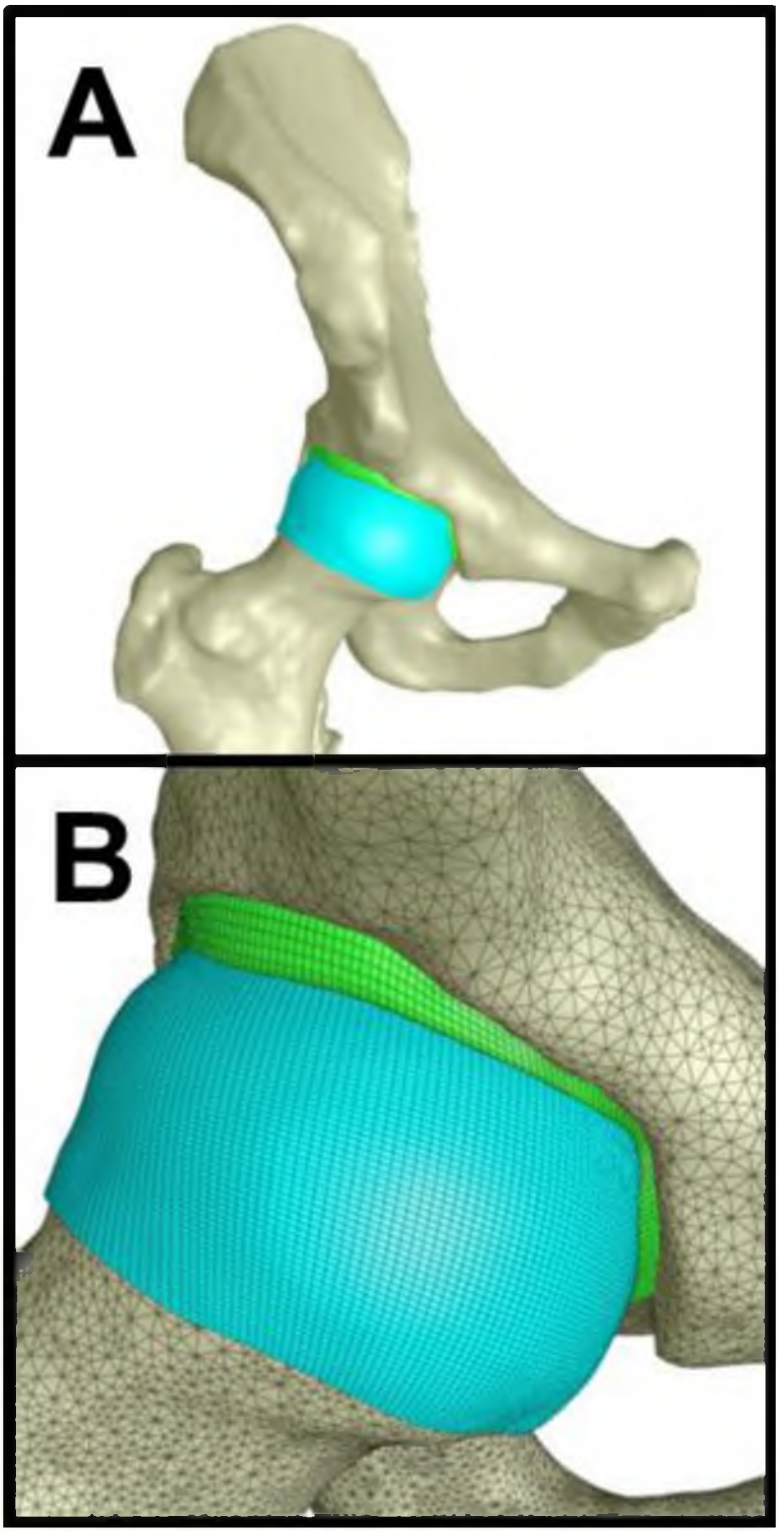

Figure 7.1: Representative FE model. A – subject-specific FE model, showing the bones in white, the acetabular cartilage in green and the femoral cartilage in blue. B – close up view of the joint space with lines showing discretization.

PostView [46, 47].

Cartilage mesh convergence was evaluated by analyzing models with four different mesh densities for all loading scenarios in one specimen. Meshes for both the femoral and acetabular cartilage were generated with three, four, five and six transchondral elements (Figure 7.2). Mesh density was increased while maintaining the approximate element Jacobian, thus resulting in a simultaneous refinement of the mesh density on the articular surfaces. The resulting models of the cartilage layers consisted of 39,300, 108,972, 185,020 and 303,804 hexahedral elements for meshes with three, four, five and six transchondral elements, respectively. All models for mesh convergence analysis used a Veronda Westmann constitutive model for cartilage. Mesh convergence was achieved when the change in first principal strain and maximum shear stress between subsequent meshes was less than 10%. As per our previous studies [18, 23, 28], all models used trilinear hexahdral elements with a single gauss point based on the enhanced strain element formulation [46, 48]. We have found that the trilinear hexahedron with a single integration point and hourglass control is sometimes more robust than the fully integrated trilinear hexahedral element for simulations that involve large compressive contact strains.

The nearly-incompressible material behavior of human hip cartilage was characterized by testing cartilage samples from the contralateral joint of each specimen in unconfined compression [28]. Three hyperelastic constitutive models were fit to experimental data (Figure 7.3). The simplest constitutive model was an uncoupled version of the isotropic, hyperelastic neo-Hookean model [49], with strain energy W :

$$W = \frac{1}{2}\mu(\tilde{I}_1 - 3) + \frac{1}{2}K(\ln(J))^2 \quad (7.1)$$

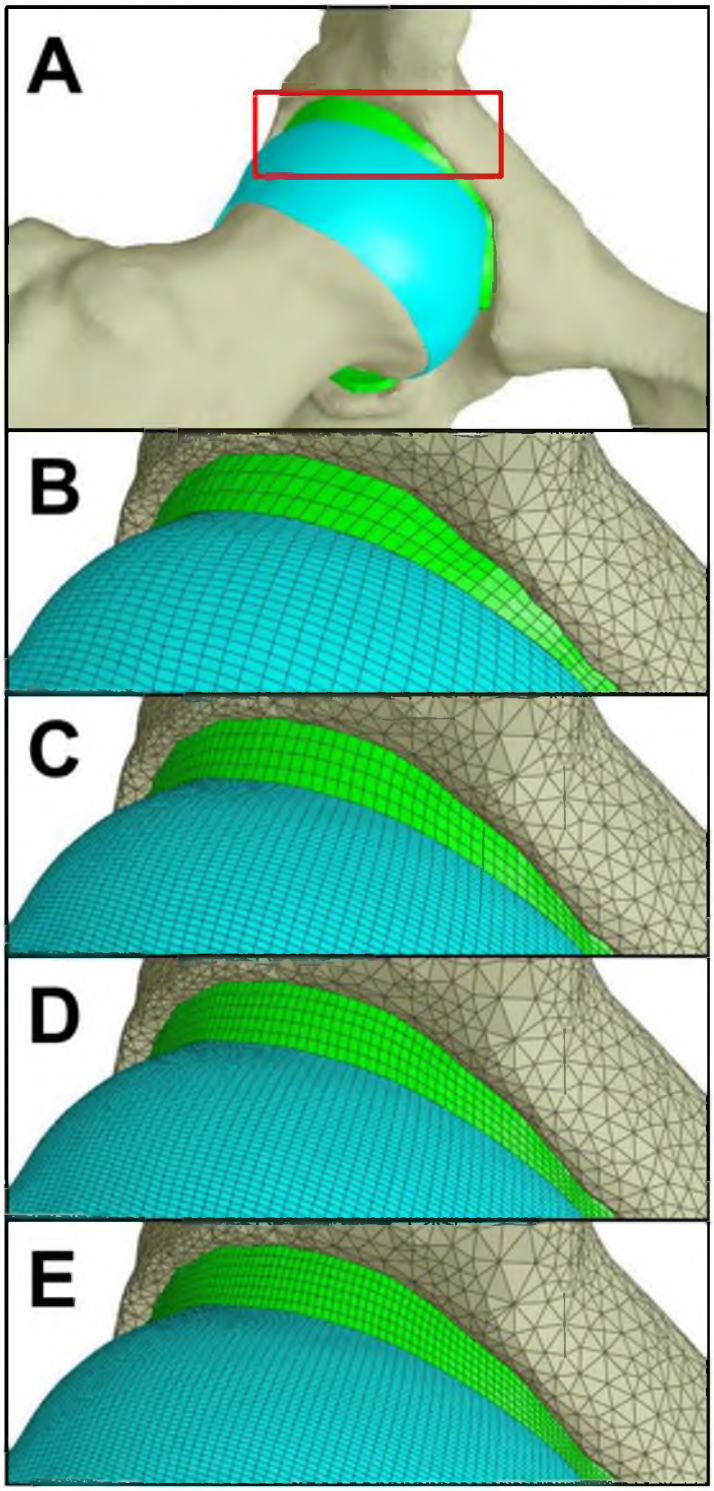

Figure 7.2: Mesh convergence analysis. A – view of the whole joint. The red box indicates the region where the remaining images focus on. B – FE model with three elements through the cartilage thickness. C – FE model with four elements through the cartilage thickness. D – FE model with five elements through the cartilage thickness (this was the converged density). E – FE model with six elements through the cartilage thickness.

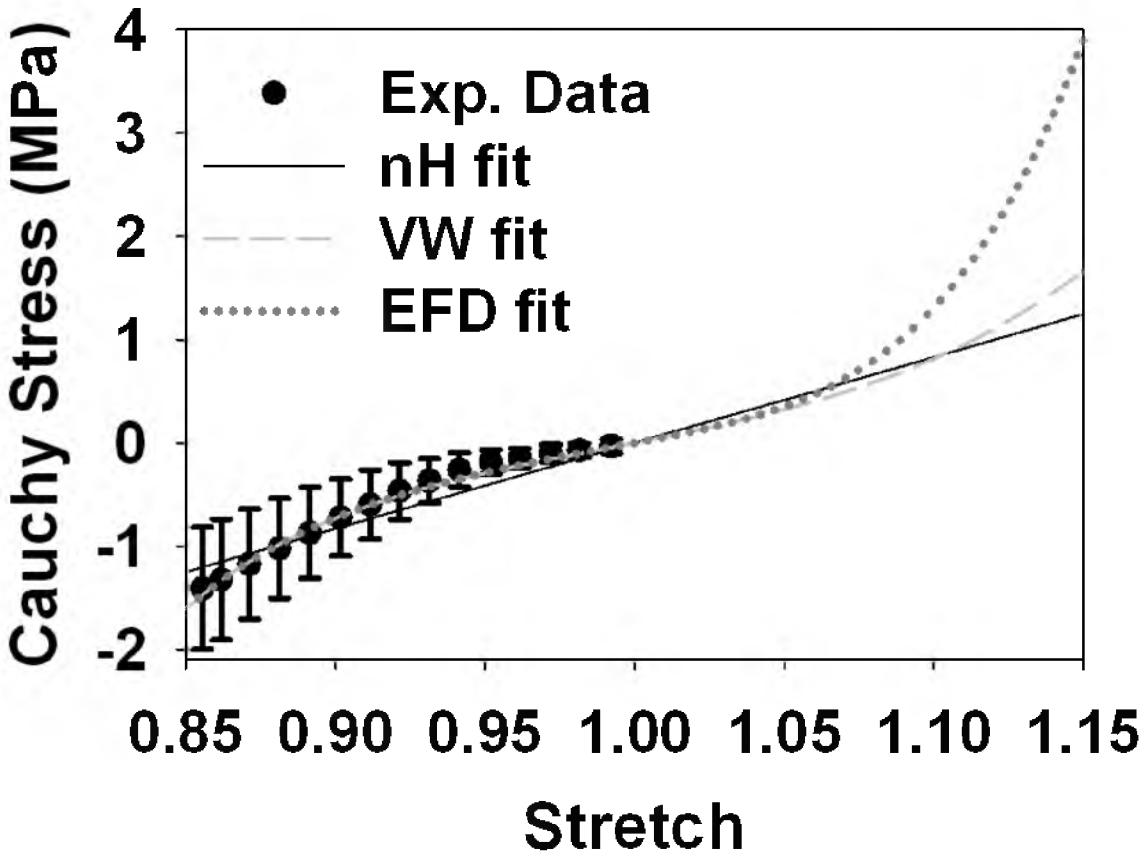

Figure 7.3: Unaixal stress response of the three constitutive models. Experimental data are shown. At small strains (near stretch values of 1), there were minimal differences between the three models. At larger tensile strains, there were drastic differences. The EFD model was the stiffest at higher levels of stretch due to the fiber contribution to the response, likely resulting in both the higher τmax and lower E1 at large magnitudes (Figure 7.5). In compression (stretch values less than 1), the EFD and VW constitutive models predicted nearly identical responses.

In this expression, $\tilde{I}_1$ is the first deviatoric invariant of the right Cauchy deformation tensor, J is the Jacobian, μ is the shear modulus in the limit of small deformations and K is the bulk modulus. This model was selected as a baseline constitutive model, both because of its simple quasilinear stress-stretch relationship and because it has been used previously in FE models of the human hip joint [18-25]. The second constitutive model was an uncoupled version of the isotropic, hyperelastic Veronda Westmann (VW) model [49, 50]:

$$W = C_1 C_2 (\exp[C_2(\tilde{I}_1 - 3)] - 1) - \frac{C_1 C_2}{2}(\tilde{I}_2 - 3) + \frac{1}{2}K(\ln(J))^2 \quad (7.2)$$

Here, is the second deviatoric invariant of the right Cauchy deformation tensor, the coefficient C_1 scales the overall response, the coefficient C_2 controls the exponential response and K is the bulk modulus. Although the VW model is isotropic, it captures strain-dependent material nonlinearity [50]. The final constitutive model was an uncoupled version of the ellipsoidal fiber distribution (EFD) model, with a neo-Hookean ground matrix [49, 51, 52]. The fiber strain energy W_f for the EFD model was in the form [49, 51, 52]:

$$W_f = \xi(\boldsymbol{n})(\tilde{I}_n - 1)^{\beta(\boldsymbol{n})} \quad (7.3)$$

Here, is the square of the deviatoric fiber stretch and $\boldsymbol{n}$ is the unit vector along the fiber direction in the current configuration. The material coefficient ξ scales the fiber response and β controls the nonlinearity of the fibers. An initially isotropic fiber distribution was assumed. For this case, the fiber material coefficients are equal in all directions, such that $\xi_1 = \xi_2 = \xi_3 = \xi(\boldsymbol{n})$ and $\beta_1 = \beta_2 = \beta_3 = \beta(\boldsymbol{n})$. The total strain energy was the sum of the fiber strain energy in Equation (7.3) and the neo-Hookean strain energy in Equation (7.1) [49]. This constitutive model captures tension-compression nonlinearity via the nonlinear stress-strain behavior of the fibers since they only resist tensile deformation [52]. Further, the model simulates the strain-induced anisotropy of articular cartilage [51].

Material coefficients for each of the constitutive models were determined fitting the experimental stress-stretch curves using a constrained nonlinear least squares method (SigmaPlot 11.0, Systat Software Inc., San Jose, CA). To determine average coefficients

for all cartilage samples, experimental data from all samples were fit simultaneously to the incompressible stress-stretch expressions given in Equations (7.4), (7.5) and (7.6). This method is different from the method used in our previous study, where experimental data from each sample was fit individually and then material coefficients were averaged [53]. For an incompressible material subjected to unconfined compression by a stretch ratio of λ, the neo-Hookean Cauchy stress along the loading axis is:

$$\sigma = \frac{1}{2}\mu(\lambda^2 - \frac{1}{\lambda}) \tag{7.4}$$

For an incompressible material subjected to unconfined compression by a stretch ratio of λ, the VW Cauchy stress along the loading axis is:

$$\sigma = C_1 C_2[(2\lambda^2 - \frac{2}{\lambda})\exp[C_2(\lambda^2 + \frac{2}{\lambda} - 3)] - \lambda + \frac{1}{\lambda^2}] \tag{7.5}$$

For an incompressible material subjected to unconfined compression by a stretch ratio of λ, the EFD Cauchy stress along the loading axis is:

$$\sigma = \frac{1}{2}\mu(\lambda^2 - \frac{1}{\lambda}) - \frac{256\pi\xi(8\lambda - 15\lambda^2 + 6\lambda^3 - 10\lambda^4 + 24\lambda^5 - 15\lambda^6 - 2\lambda^7)}{315\lambda^5(1 + \lambda + \lambda^2)^{3/2}} \tag{7.6}$$

The value of the material coefficient β was set to 4.0 in order to obtain an analytical solution that could be fit. Preliminary data demonstrated that the least squares fit was relatively insensitive to the choice of β for integer values above 2.0. For all constitutive models, the uniqueness of the best-fit material coefficients was verified by perturbing initial guesses.

To evaluate the effects of cartilage constitutive model on FE predictions, FE models of all specimens and loading scenarios were analyzed with the cartilage represented by each of the three constitutive models. For all analyses, cortical bone was represented as

isotropic linear elastic (E = 17 GPa, v = 0.29) [54]. The representation of the cortical shell was based off of our previous analyses, which demonstrated the importance of deformable cortical bone in predictions of cartilage contact mechanics [18, 42]. Average neo-Hookean cartilage coefficients were μ = 5.52 MPa and K = 550 MPa. Average VW cartilage coefficients were C_1 = 0.34 MPa, C_2 = 5.57 and K = 1,178 MPa. Average EFD cartilage coefficients were μ = 1.82 MPa, ξ = 9.19 MPa, β = 4 and K = 1,860 MPa. The bulk modulus values were selected for each cartilage constitutive model to ensure near-incompressibility. This was confirmed by examining the Jacobian field in the articular cartilage for each simulation. In all cases, the change in volume at all locations in the finite element meshes was less than 4%.

Green-Lagrange first principal strain (E_1) and Cauchy maximum shear stress (τ_{max}) were evaluated in each FE model. E_1 is the first eigenvalue of the strain tensor, and is the largest tensile strain at each point. E_1 was sampled at the articular surfaces and transchondrally at the location of the articular surface peak. τ_{max} is the maximum shear stress at each point. τ_{max} was evaluated at the osteochondral interface and transchondrally at the location of the osteochondral peak. Results were analyzed on the femoral head and in six anatomical regions on the acetabulum (Figure 7.4A).

FE predictions from the three difference constitutive models were compared. Differences between acetabular results were compared within region and activity using repeated measures ANOVAs on ranks with Tukey posthoc analysis. Differences in transchondral mechanics on the femur were compared using repeated t-tests within activity and location. Significance was set at $p \leq 0.05$.

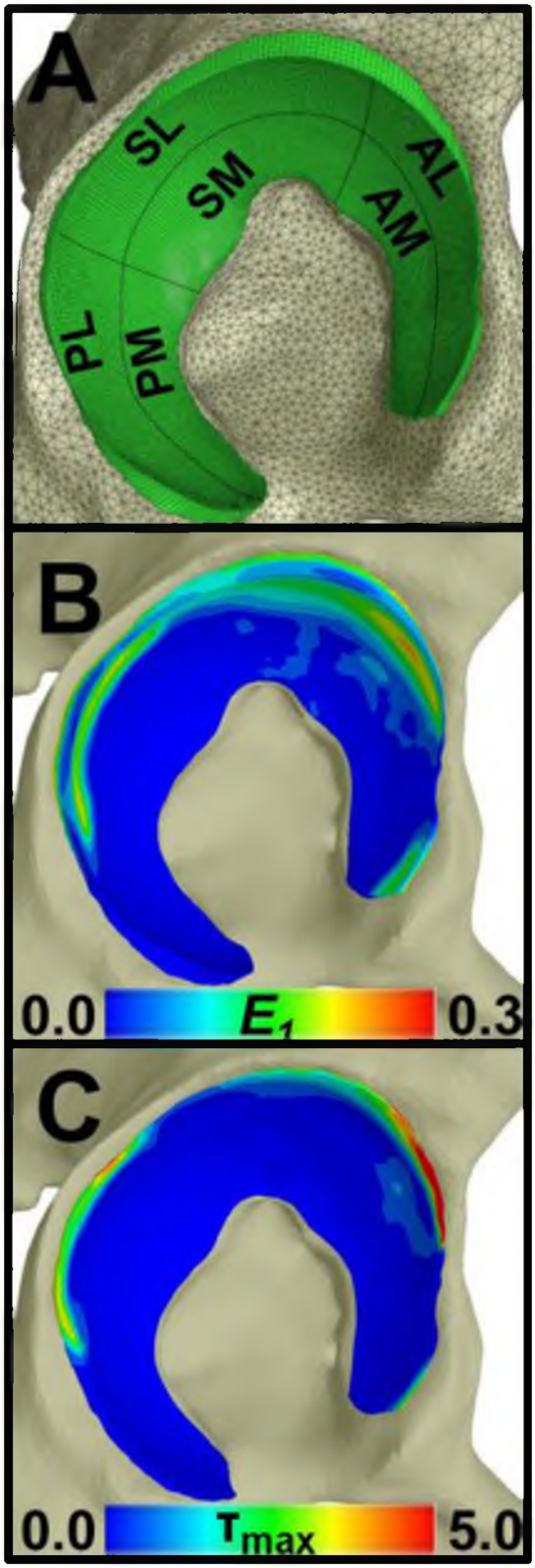

Figure 7.4: E_1 and τ_{max} results on the acetabulum in the EFD models of one specimen. A – lateral view of the acetabulum with the six anatomic regions used for analysis. B – E_1 at the articular surface. C – τ_{max} near the osteochondral interface.

Results

Mesh convergence analysis demonstrated that meshes with five elements through the cartilage thickness were converged, predicting results less than 10% different than meshes with six elements through the thickness predicted. E_1 achieved convergence at a lower mesh resolution than τ_{max}. Model run times were 1.4 ± 0.3 hours, 5.0 ± 1.6 hours, 8.3 ± 1.3 hours and 24.3 ± 10.8 hours for meshes with three, four, five and six transchondral elements, respectively. The change in peak E_1 at the articular surface was ≤ 16%, ≤ 3% and <1% between models with three versus four, four versus five and five versus six transchondral elements, respectively. Therefore, models with four elements through the cartilage thickness would have been appropriate for predicting E_1 alone. Convergence in τ_{max} was evaluated for peak osteochondral values away from the edge of the acetabular cartilage. The change in peak τ_{max} was ≤ 37%, ≤ 13% and <10% between models with three versus four, four versus five and five versus six transchondral elements, respectively. Comparisons of transchondral predicitons demonstrated that models with three transchondral elements missed features of the depth-wise gradients, which were captured at all other mesh resolutions. There were only minor differences between the transchondral predictions from models with five and six transchondral elements, confirming that meshes with five transchondral elements were adequate for the variables of interest.

Differences in the three constitutive models are apparent in the uniaxial stress response of the at the approximate strain levels predicted in the FE models (Figure 7.3). The most dramatic differences are in tension. The stiffest tensile stress response was in the EFD constitutive model, due to the fibers creating the tension-compression nonlinear

behavior. The material nonlinearity in the VW model predicted the next highest stresses in uniaxial tension. The tensile response of the neo-Hookean constitutive model was smaller than the other two models at large stretch values. In compression, the response of the VW and EFD constitutive models were nearly identical and reflected the nonlinearity measured during experimental unconfined compression testing. The nearly-linear behavior of the neo-Hookean constitutive model resulted in overpredictions of compressive stress magnitudes at stretch values near unity and underpredictions of compressive stress magnitudes at stretch values near 0.85.

The choice of cartilage constitutive model significantly affected predictions of τ_{max} at the osteochondral interface and E_1 at the articular surface of the acetabulum (Figures 7.4 and 7.5). Generally, the EFD model predicted larger stresses, while the neo-Hookean model predicted larger strains. Specifically, at locations of high peak values, use of the EFD constitutive model resulted in significantly larger predictions of peak τ_{max} than the other two constitutive models (Figure 7.5A, AL, SL and PL regions). In contrast, at locations with lower peak values, there were minimal or no differences in peak τ_{max}. VW cartilage predicted significantly smaller average τ_{max} than neo-Hookean cartilage in all regions (Figure 7.5B). The VW constitutive model also predicted significantly smaller average τ_{max} than the EFD model in two regions. Trends in E_1 were approximately opposite those in τ_{max} (Figure 7.5C, D). At large strain values, peak E_1 was significantly larger in neo-Hookean models than in the other two models (Figure 7.5C, AL and SL regions). At low strain values, peak E_1 was significantly larger when the neo-Hookean constitutive model was used than in the other two models (Figure 7.5C, AM, SM and PM regions). Average E_1 at large values was significantly larger in VW models than in the

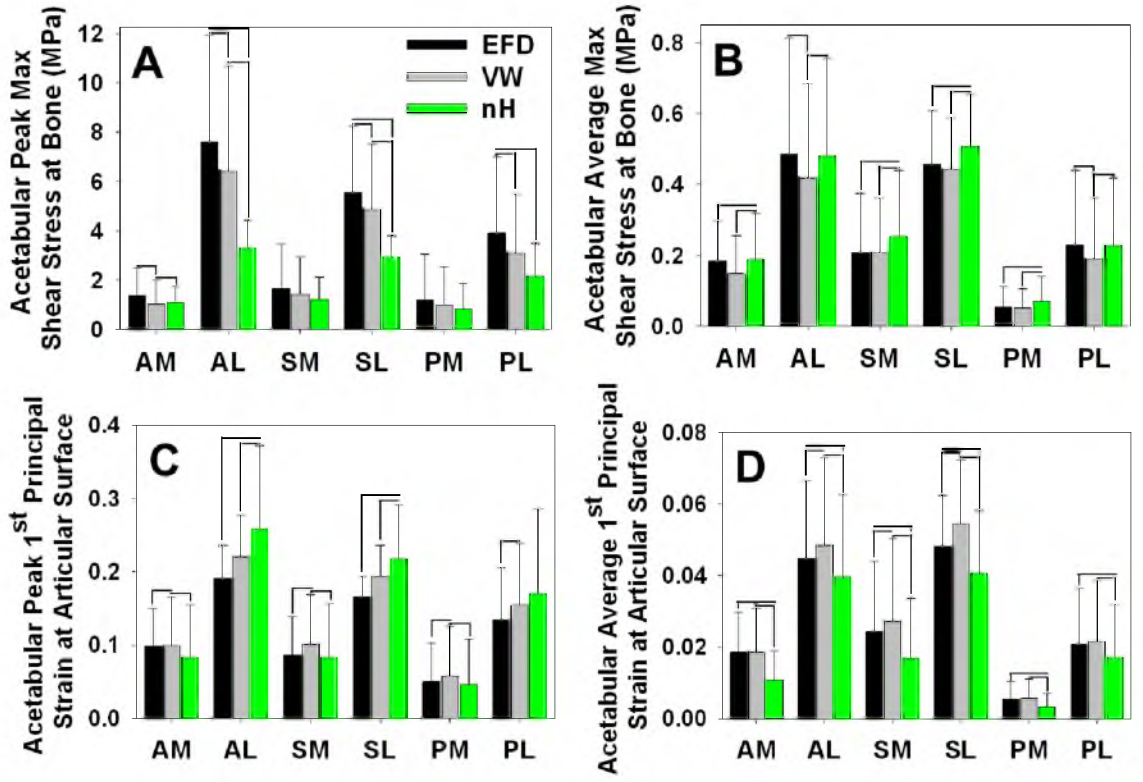

Figure 7.5: Results in six anatomical regions on the acetabular cartilage. A – peak τ_{max} at the osteochondral interface. B – average τ_{max} at the osteochondral interface. C – peak E_1 at the articular surface. D – average E_1 at the articular surface. At high stress values, the EFD models predicted the largest stresses. A high strain values, the neo-Hookean models predicted the largest strains.

other two models (Figure 7.5D, AL, SL and SM regions). At low average E_1, results were significantly smaller when the neo-Hookean constitutive model was used than in the other two models (Figure 7.5D, AM, PM and PL regions).

There were significant differences in predictions of transchondral τ_{max} and E_1 between the three constitutive models (Figure 7.6). Consistent with the acetabular results, peak τ_{max} at the femoral osteochondral interface was significantly larger in the EFD models than in the other two models (Figure 7.5A). These differences persisted partway through the cartilage thickness from the osteochondral interface. However, at the articular surface corresponding to the location of peak τ_{max} at the osteochondral interface, there were

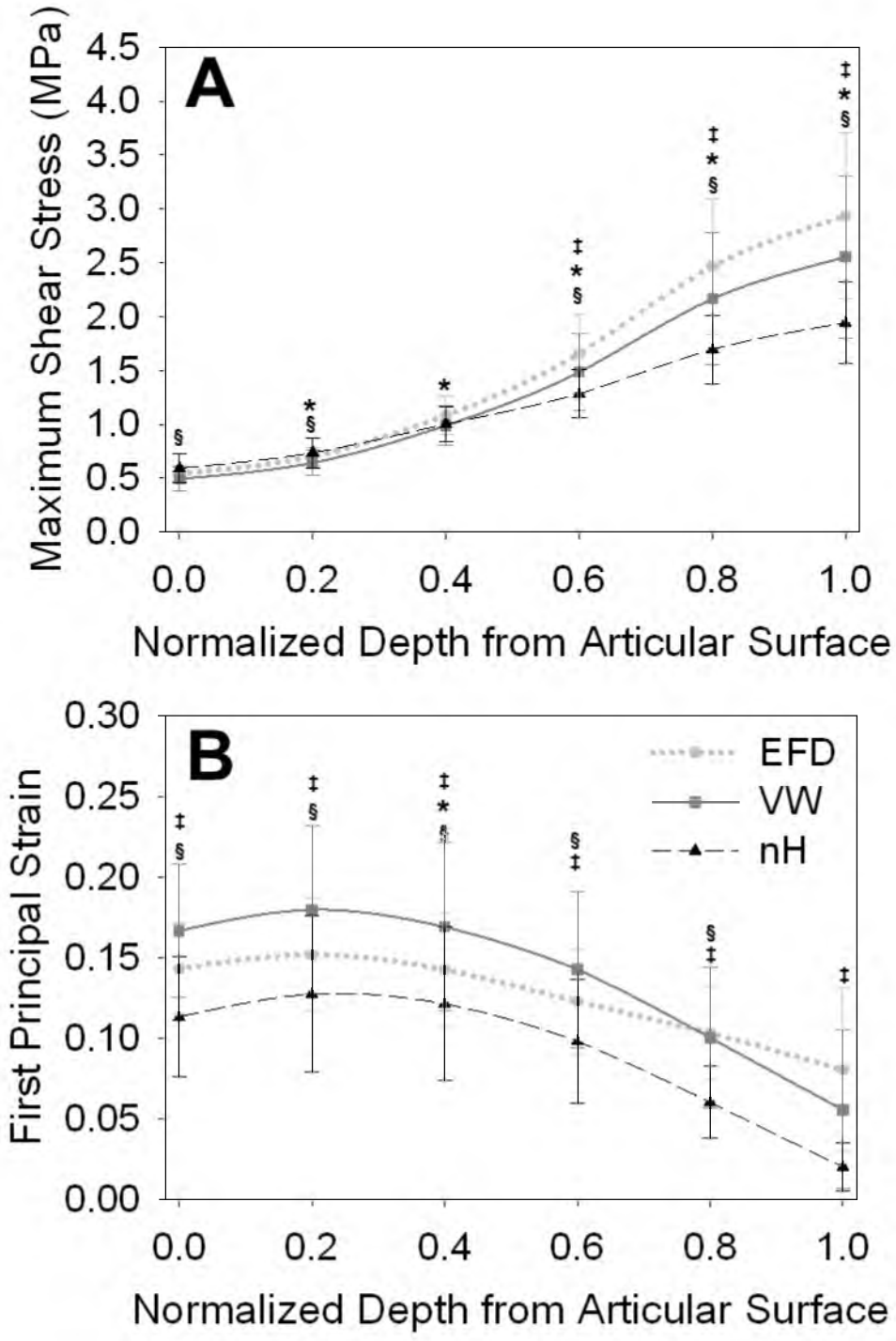

Figure 7.6: Results through the depth of the femoral cartilage during AH. A – τ_{max} at the location of the osteochondral peak. B – E_1 at the location of the articular peak. While τ_{max} near the osteochondral interface was larger in the EFD model, it was larger in the nH models near the articular surface. For all constitutive models, E_1 peaked just below the articular surface. * indicates differences between EFD and VW, ‡ indicates differences between EFD and nH, and § indicates differences between VW and nH.

trends toward higher τ_{max} for the neo-Hookean models. This indicated a smaller depth-wise gradient in τ_{max} for the neo-Hookean models than for the other two models. There was a peak in transchondral E_1 just below the articular surface for all constitutive models in the femoral cartilage (Figures 7.6B and 7.7). While this result occurred consistently across specimens and loading scenarios in the femoral cartilage, it was not seen in the acetabular cartilage (Figure 7.7).

Discussion

This study focused on two aspects of the three-dimensional stress and strain fields, τ_{max} and E_1. These variables were selected because they may be important in the pathogenesis of OA, especially in the human hip [12, 15, 16, 55, 56]. Cartilage delamination, which is thought to be caused by high levels of osteochondral τ_{max}, occurs frequently in patients with cam femoroacetabular impingement [12, 15]. Thus, τ_{max} is a relevant variable to predict in patient populations at risk for early onset hip OA. Cartilage fibrillation, which may be caused by elevated articular E_1, occurs early in the OA process in most joints [9-11]. Thus, accurate predictions of E_1 may be able to predict the early stages of hip OA.

The nearly-linear, nonlinear and tension-compression nonlinear constitutive models affected FE predictions of τ_{max} and E_1 in a manner consistent with the key features of the constitutive models. The nearly-linear behavior of the neo-Hookean constitutive model resulted in lower FE predictions of τ_{max} and higher FE predictions of E_1, especially at large magnitudes. This can be explained by the fact that the neo-Hookean constitutive model underpredicts the behavior of cartilage away from the limits of small deformation (Figure 7.3). Thus, the neo-Hookean constitutive model resulted in an effectively softer

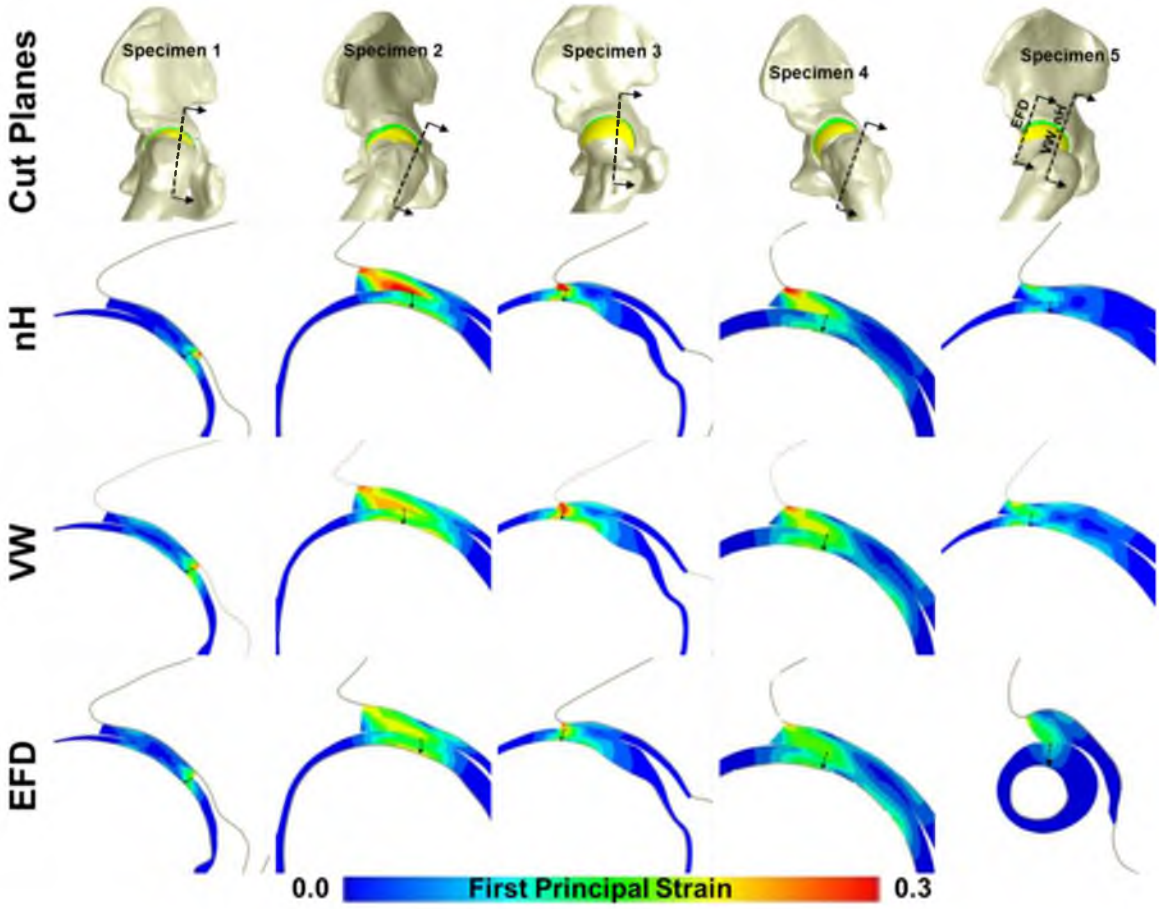

Figure 7.7: Cut planes for femoral E_1 as reported in Figure 4B. Each column is for one specimen. The top row indicates the location of the cut planes. The next three rows are the nH, VW and EFD model results, respectively. The arrows in each cut figure indicate the location and direction of sampling. The increase in E_1 just below the femoral articular surface is visible.

tangent modulus than the other two constitutive models at larger magnitudes of stress and strain. Conversely, the EFD constitutive model resulted in the highest values of τ_{max} and the lowest values of E_1. This was due to the stiffening of the fibers in the EFD model in tension.

Differences in the gradient of τ_{max} between the constitutive models demonstrates the role of tension-compression nonlinearity in predictions of cartilage mechanics. Although the influence of the gradient in τ_{max} on cartilage damage has not been evaluated,

experimental measurements of impact damage indicate that gradients in stress or strain may be more relevant than the magnitudes in the pathogenesis of OA. As an example, the gradient of contact stress on the joint surface was a better predictor of failure than the magnitude of contact stress as measured by pressure-sensitive film in an impact model of a rabbit joint [4]. In the present study, the largest gradients in transchondral τ_{max} were in the EFD models, whereas the neo-Hookean models predicted drastically smaller gradients. Because the EFD constitutive model most accurately describes cartilage material behavior, these results suggest that it is necessary to represent tension-compression nonlinearity and/or strain-induced anisotropy to accurately predict transchondral τ_{max} in the human hip.

Although the magnitudes of transchondral E_1 were affected by cartilage constitutive model, all models predicted a peak in E_1 below the articular surface of the femur. This suggests that cartilage mechanics below the articular surface may be important in the pathogenesis of OA in the hip. Assuming that elevated E_1 can predict damage to the cartilage matrix, these results suggest that damage may be initiated slightly below the articular surface, rather than at the articular surface. Cadaveric studies have found fibrillation on the femoral head at younger ages than in the acetabulum [57-60]. In these studies, some of the fibrillation occurred in regions that are unloaded, but fibrillation also occurred in the superior region of the femur where loading is frequent [57-59]. Thus, the high values of E_1 below the articular surface of the femoral cartilage may be relevant in the fibrillation of the femoral head that occurs in early degenerative changes in the human hip.

While there has been limited use of advanced constitutive models in FE analysis of the human hip, the results of the present study can be compared to FE analysis in the knee completed with more advanced constitutive models. In the knee, parametric FE studies have been performed to examine the influence of fiber orientation and transchondral variation in properties on predictions of cartilage stress and strain [61-65]. The collagen fiber orientation affects predictions of transchondral mechanics in the knee. Including the highly aligned superficial zone fibers decreased strains at the articular surface by up to approximately 30% [62-65]. Using an arcade-like transchondral fiber orientation decreased the transchondral von Mises stress and increased the transchondral axial strains when compared to predictions with all fibers aligned parallel to the articular surface [62]. Consistent with the present study, these findings highlight the effects of anisotropy and tension-compression nonlinearity on transchondral predictions of cartilage stress and deformation. These findings also indicate that transchondral variation in fiber orientation influences predictions of cartilage mechanics. In the present study, a homogeneous and initially isotropic distribution of fiber orientation was assumed. This provides a reasonable representation of the middle zone, but it is likely less applicable to the fiber topography of the superficial and deep zones of the articular cartilage in the hip. Experimental studies are needed to quantify transchondral fiber orientation in the articular cartilage of the hip, as data are not yet available in the literature. Unlike variation in the fiber orientation, transchondral variation in the matrix elastic modulus had no appreciable effect on cartilage mechanics [62]. This provides confidence in the use of depth-averaged matrix properties in the present study.

Previous FE models provide insight into the effects of constitutive assumptions and model geometry on predictions of τ_{max}. Plane strain analysis of biphasic cartilage has shown similar patterns in transchondral τ_{max} to those seen in the present study, where the peak values occurred at the osteochondral interface away from the center of contact [13, 14]. In a plane strain FE model of impact loading, the location of highest τ_{max} varied with the assumed cartilage constitutive model [66]. Specifically, peak τ_{max} occurred at the articular surface when cartilage was modeled as transversely isotropic, but occurred at the osteochondral interface when the cartilage was modeled as isotropic. In an FE study of knee mechanics, peak τ_{max} was predicted at the osteochondral interface when the meniscus was modeled, but peak τ_{max} was predicted at the articular surface without the meniscus modeled [67]. These studies demonstrate that both constitutive model and local geometry affect predictions of τ_{max}. The results of the present study are consistent with the conclusion that the constitutive model affects predictions of peak τ_{max}.

In contrast to previous studies that demonstrated the insensitivity of contact stress and contact area to the cartilage constitutive model, τ_{max} and E_1 are fairly sensitive to the cartilage constitutive model [18, 28]. Previously, we have demonstrated that predictions of contact stress and contact area are relatively insensitive to variations in the material nonlinearity, spatial inhomogeneity and material coefficients of the cartilage constitutive model [18, 28]. Cartilage contact mechanics under fast loading are the result of the total load supported by the cartilage, which is largely supported by the fluid phase [13, 37, 38, 68]. Therefore, it is logical that cartilage contact mechanics are insensitive to cartilage representation. In fact, if cartilage contact mechanics are the extent of the results of interest, discrete element analysis can be used for accurate predictions in a fraction of the

time required for FE analysis [69]. Conversely, predictions of τ_{max} and E_1 represent the deviatoric response of hydrated tissue under fast loading, and it is therefore logical that they are sensitive to the cartilage constitutive model.

The required mesh resolution to accurately predict transchondral τ_{max} is more refined than the mesh resolution that has been used in previous FE models of live subjects [22, 25]. Thus, more time will be required in future research to generate subject-specific FE models for predicting transchondral mechanics than was required for predicting contact stress and contact area in patient populations. Because transchondral E_1 and τ_{max} are pertinent to the pathogenesis of hip OA, the mesh density and constitutive model requirements found in this study are directly applicable to ongoing use of FE of the human hip.

There are several limitations in this study that warrant discussion. While these models have undergone direct validation of contact stress and contact area at the articular surface, neither E_1 nor τ_{max} was directly validated [28]. The magnitudes of E_1 in the present study are consistent with those measured experimentally in the human patellofemoral joint [70]. Because τ_{max} cannot be measured experimentally, confidence in predictions of this variable comes from the combination of directly validated FE models with accurate cartilage constitutive models.

Although the cartilage constitutive assumptions in the present study are more complex than in previous hip FE analysis, the models still make use of a number of simplifying assumptions that warrant discussion. The material properties of cartilage vary transchondrally, but this variation was not represented in this study. It has been established that the variation between tensile and compressive moduli is larger than

transchondral variation in cartilage moduli [29, 32, 36]. In the context of FE analysis, transchondral variation in elastic modulus had a minimal effect on predictions of three-dimensional knee cartilage mechanics [62] and a minimal effect on predictions of transchondral stress and strain in a axisymmetric indentation analysis [71]. Therefore, the decision to omit transchondral variation in cartilage behavior is justified in the present study. Cartilage behavior is also biphasic and viscoelastic [31, 33, 35]. Because of the loading rates in this study, the omission of rate-dependent behavior is reasonable [28, 37, 38, 53]. This omission is also supported by biphasic analysis of an idealized hip joint [72]. However, if other loading rates or regimes are considered in future studies, then the rate-dependence of cartilage mechanics may become important for accurate predictions.

The lateral edge of the acetabular cartilage and the chondrolabral boundary may have confounding effects of the results of this study. The acetabular labrum was omitted from the present models. This modeling strategy is consistent with previous FE analyses [18, 25, 28], as well as with studies that suggest limited loading on the labrum in the normal hip [23, 73, 74]. However, this omission may explain why there was a peak in E_1 below the surface of the femoral cartilage, but not below the surface of the acetabular cartilage. Unfortunately, the material properties of the human labrum and chondrolabrum that would be required for FE modeling are not available in the literature. The behavior of bovine labrum has been characterized, and there is a small amount of data on the averaged behavior of human labrum [75-77], but neither the full material behavior of the human labrum nor the behavior of the chondrolabral transition have been evaluated. Therefore, ongoing experimental work is required in order to accurately model the labrum and chondrolabrum in the human hip.

In conclusion, this study suggests that tension-compression nonlinearity and/or strain induced anisotropy are important features for predicting accurate transchondral τ_{max} and E_1 in the human hip. Further, this study indicates that five elements through the cartilage thickness are required for converged predictions of E_1 and τ_{max}. In addition to the technical aspects evaluated in this study, the peak in E_1 below the articular surface of the femur is an intriguing finding that can be further explored in patient populations related to the pathogenesis of hip OA. There are other mechanical variables that may be important predictors of the onset and progression of cartilage damage, and further experimental studies are needed to determine the variables that are most predictive of cartilage damage at the tissue and joint levels. The approach highlighted in this study can be used to evaluate these additional mechanical variables in the human hip, and their potential role in the pathogenesis of OA.

References

[1] Carter, D. R., Beaupré, G. S., Wong, M., Smith, R. L., andriacchi, T. p., and Schurman, D. J., 2004, "The Mechanobiology of Articular Cartilage Development and Degeneration," Clin Orthop Relat Res (427 Suppl), pp. S69-S77.

[2] Guilak, F., Fermor, B., Keefe, F. J., Kraus, V. B., Olson, S. A., Pisetsky, D. S., Setton, L. A., and Weinberg, J. B., 2004, "The Role of Biomechanics and Inflammation in Cartilage Injury and Repair," Clin Orthop Relat Res (423), pp. 17-26.

[3] Atkinson, T. S., Haut, R. C., and Altiero, N. J., 1998, "Impact-Induced Fissuring of Articular Cartilage: An Investigation of Failure Criteria," J Biomech Eng, **120**(2), pp. 181-187.

[4] Haut, R. C., Ide, T. M., and De Camp, C. E., 1995, "Mechanical Responses of the Rabbit Patello-Femoral Joint to Blunt Impact," J Biomech Eng, **117**(4), pp. 402-408.

[5] Bader, D. L., Salter, D. M., and Chowdhury, T. T., 2011, "Biomechanical influence of Cartilage Homeostasis in Health and Disease," Arthritis, 2011, p. 979032.

[6] Grodzinsky, A. J., Levenston, M. E., Jin, M., and Frank, E. H., 2000, "Cartilage Tissue Remodeling in Response to Mechanical Forces," Annu Rev Biomed Eng, **2**, pp. 691-713.

[7] Guilak, F., 2011, "Biomechanical Factors in Osteoarthritis," Best Pract Res Clin Rheumatol, **25**(6), pp. 815-823.

[8] Atkinson, p. J., and Haut, R. C., 2001, "Impact Responses of the Flexed Human Knee Using a Deformable Impact Interface," J Biomech Eng, **123**(3), pp. 205-211.

[9] Wilson, W., Van Burken, C., Van Donkelaar, C., Buma, p., Van Rietbergen, B., and Huiskes, R., 2006, "Causes of Mechanically Induced Collagen Damage in Articular Cartilage," J Orthop Res, **24**(2), pp. 220-228.

[10] Maniwa, S., Nishikori, T., Furukawa, S., Kajitani, K., and Ochi, M., 2001, "Alteration of Collagen Network and Negative Charge of Articular Cartilage Surface in the Early Stage of Experimental Osteoarthritis," Arch Orthop Trauma Surg, **121**(4), pp. 181-185.

[11] Arokoski, J. p., Jurvelin, J. S., Vaatainen, U., and Helminen, H. J., 2000, "Normal and Pathological Adaptations of Articular Cartilage to Joint Loading," Scand J Med Sci Sports, **10**(4), pp. 186-198.

[12] Anderson, L. A., Peters, C. L., Park, B. B., Stoddard, G. J., Erickson, J. A., and Crim, J. R., 2009, "Acetabular Cartilage Delamination in Femoroacetabular Impingement. Risk Factors and Magnetic Resonance Imaging Diagnosis," J Bone Joint Surg Am, **91**(2), pp. 305-313.

[13] Ateshian, G. A., Lai, W. M., Zhu, W. B., and Mow, V. C., 1994, "An Asymptotic Solution for the Contact of Two Biphasic Cartilage Layers," J Biomech, **27**(11), pp. 1347-1360.

[14] Ateshian, G. A., and Wang, H., 1995, "A Theoretical Solution for the Frictionless Rolling Contact of Cylindrical Biphasic Articular Cartilage Layers," J Biomech, **28**(11), pp. 1341-1355.

[15] Beck, M., Kalhor, M., Leunig, M., and Ganz, R., 2005, "Hip Morphology Influences the Pattern of Damage to the Acetabular Cartilage: Femoroacetabular Impingement as a Cause of Early Osteoarthritis of the Hip," J Bone Joint Surg Br, **87**(7), pp. 1012-1018.

[16] Askew, M., and Mow, V., 1978, "The Biomechanical Function of the Collagen Fibril Ultrastructure of Articular Cartilage," J Biomech Eng, **100**, p. 105.

[17] Gosvig, K. K., Jacobsen, S., Sonne-Holm, S., Palm, H., and Troelsen, A., 2010, "Prevalence of Malformations of the Hip Joint and their Relationship to Sex, Groin Pain, and Risk of Osteoarthritis: A Population-Based Survey," J Bone Joint Surg Am, **92**(5), pp. 1162-1169.

[18] Anderson, A. E., Ellis, B. J., Maas, S. A., Peters, C. L., and Weiss, J. A., 2008, "Validation of Finite Element Predictions of Cartilage Contact Pressure in the Human Hip Joint," J Biomech Eng, **130**(5), pp. 051008-051008.

[19] Anderson, A. E., Ellis, B. J., Maas, S. A., and Weiss, J. A., 2010, "Effects of Idealized Joint Geometry on Finite Element Predictions of Cartilage Contact Stresses in the Hip," J Biomech, **43**(7), pp. 1351-1357.

[20] Brown, T. D., and DiGioia, A. M., 3rd, 1984, "A Contact-Coupled Finite Element Analysis of the Natural Adult Hip," J Biomech, **17**(6), pp. 437-448.

[21] Chegini, S., Beck, M., and Ferguson, S. J., 2009, "The Effects of Impingement and Dysplasia on Stress Distributions in the Hip Joint During Sitting and Walking: A Finite Element Analysis," J Orthop Res, **27**(2), pp. 195-201.

[22] Harris, M. D., Anderson, A. E., Henak, C. R., Ellis, B. J., Peters, C. L., and Weiss, J. A., 2012, "Finite Element Prediction of Cartilage Contact Stresses in Normal Human Hips," J Orthop Res, **30**(7), pp. 1133-1139.

[23] Henak, C. R., Ellis, B. J., Harris, M. D., Anderson, A. E., Peters, C. L., and Weiss, J. A., 2011, "Role of the Acetabular Labrum in Load Support Across the Hip Joint," J Biomech, **44**(12), pp. 2201-2206.

[24] Rapperport, D. J., Carter, D. R., and Schurman, D. J., 1985, "Contact Finite Element Stress Analysis of the Hip Joint," J Orthop Res, **3**(4), pp. 435-446.

[25] Russell, M. E., Shivanna, K. H., Grosland, N. M., and Pedersen, D. R., 2006, "Cartilage Contact Pressure Elevations in Dysplastic Hips: A Chronic Overload Model," J Orthop Surg Res, **1**, pp. 6-6.

[26] Wei, H. W., Sun, S. S., Jao, S. H., Yeh, C. R., and Cheng, C. K., 2005, "The Influence of Mechanical Properties of Subchondral Plate, Femoral Head and Neck on Dynamic Stress Distribution of the Articular Cartilage," Med Eng Phys, **27**(4), pp. 295-304.

[27] Gu, D. Y., Hu, F., Wei, J. H., Dai, K. R., and Chen, Y. Z., 2011, "Contributions of Non-Spherical Hip Joint Cartilage Surface to Hip Joint Contact Stress," Conf Proc IEEE Eng Med Biol Soc, 2011, pp. 8166-8169.

[28] Henak, C. R., Kapron, A. L., Anderson, A. E., Ellis, B. J., Maas, S. A., and Weiss, J. A., 2013, "Specimen-Specific Predictions of Contact Stress in the Human Hip: Validation and Sensitivity Studies," Biomech Model Mechanobiol.

[29] Buckley, M. R., Gleghorn, J. p., Bonassar, L. J., and Cohen, I., 2008, "Mapping the Depth Dependence of Shear Properties in Articular Cartilage," J Biomech, **41**(11), pp. 2430-2437.

[30] Chen, A. C., Bae, W. C., Schinagl, R. M., and Sah, R. L., 2001, "Depth- and Strain-Dependent Mechanical and Electromechanical Properties of Full-Thickness Bovine Articular Cartilage in Confined Compression," J Biomech, **34**(1), pp. 1-12.

[31] Huang, C. Y., Soltz, M. A., Kopacz, M., Mow, V. C., and Ateshian, G. A., 2003, "Experimental Verification of the Roles of Intrinsic Matrix Viscoelasticity and Tension-compression Nonlinearity in the Biphasic Response of Cartilage," J Biomech Eng, **125**(1), pp. 84-93.

[32] Huang, C. Y., Stankiewicz, A., Ateshian, G. A., and Mow, V. C., 2005, "Anisotropy, Inhomogeneity, and Tension-Compression Nonlinearity of Human Glenohumeral Cartilage in Finite Deformation," J Biomech, **38**(4), pp. 799-809.

[33] Mak, A. F., 1986, "The Apparent Viscoelastic Behavior of Articular Cartilage--The Contributions from the Intrinsic Matrix Viscoelasticity and Interstitial Fluid Flows," J Biomech Eng, **108**(2), pp. 123-130.

[34] Mow, V. C., and Guo, X. E., 2002, "Mechano-Electrochemical Properties of Articular Cartilage: Their Inhomogeneities and Anisotropies," Annu Rev Biomed Eng, **4**(1), pp. 175-209.

[35] Mow, V. C., Kuei, S. C., Lai, W. M., and Armstrong, C. G., 1980, "Biphasic Creep and Stress Relaxation of Articular Cartilage in Compression? Theory and Experiments," J Biomech Eng, **102**(1), pp. 73-84.

[36] Schinagl, R. M., Gurskis, D., Chen, A. C., and Sah, R. L., 1997, "Depth-Dependent Confined Compression Modulus of Full-Thickness Bovine Articular Cartilage," J Orthop Res, **15**(4), pp. 499-506.

[37] Ateshian, G. A., Ellis, B. J., and Weiss, J. A., 2007, "Equivalence Between Short-Time Biphasic and Incompressible Elastic Material Responses," J Biomech Eng, **129**(3), pp. 405-412.

[38] Wong, M., Ponticiello, M., Kovanen, V., and Jurvelin, J. S., 2000, "Volumetric Changes of Articular Cartilage During Stress Relaxation in Unconfined Compression," J Biomech, **33**(9), pp. 1049-1054.

[39] Anderson, A. E., Ellis, B. J., and Weiss, J. A., 2007, "Verification, Validation and Sensitivity Studies in Computational Biomechanics," Comput Methods Biomech Biomed Engin, **10**(3), pp. 171-184.

[40] Henninger, H. B., Reese, S. p., Anderson, A. E., and Weiss, J. A., 2010, "Validation of Computational Models in Biomechanics," Proc inst Mech Eng H, **224**(7), pp. 801-812.

[41] Anderson, A. E., Ellis, B. J., Peters, C. L., and Weiss, J. A., 2008, "Cartilage Thickness: Factors Influencing Multidetector CT Measurements in a Phantom Study," Radiology, **246**(1), pp. 133-141.

[42] Anderson, A. E., Peters, C. L., Tuttle, B. D., and Weiss, J. A., 2005, "Subject-Specific Finite Element Model of the Pelvis: Development, Validation and Sensitivity Studies," J Biomech Eng, **127**(3), pp. 364-373.

[43] Bergmann, G., Deuretzbacher, G., Heller, M., Graichen, F., Rohlmann, A., Strauss, J., and Duda, G. N., 2001, "Hip Contact Forces and Gait Patterns from Routine Activities," J Biomech, **34**(7), pp. 859-871.

[44] Puso, M. A., 2004, "A Three-Dimensionalal Mortar Method for Solid Mechanics," int J Numer Meth Eng, **59**(3), pp. 315-336.

[45] Puso, M. A., and Laursen, T. A., 2004, "A Mortar Segment-to-Segment Contact Method for Large Deformation Solid Mechanics," Comput Method Appl M, **193**(6-8), pp. 601-629.

[46] Puso, M. A., Maker, B. N., Ferencz, R. M., and Hallquist, J. O., 2007, "NIKE3D: A Nonlinear, Implicit, Three-Dimensional Finite Element Code for Solid and Structural Mechanics," User's Manual.

[47] Maas, S., Rawlins, D., and Weiss, J., 2012, "PostView: Finite Element Postprocessing," Musculoskeletal Research Laboratories, p. http://mrl.sci.utah.edu/software/postview.

[48] Puso, M. A., 2000, "A Highly Efficient Enhanced Assumed Strain Physically Stabilized Hexahedral Element," int J Numer Meth Eng, **49**(8), pp. 1029-1064.

[49] Maas, S., Rawlins, D., Weiss, J., and Ateshian, G., 2011, "FEBio: Theory Manual," Musculoskeletal Reserach Laboratories.

[50] Veronda, D. R., and Westmann, R. A., 1970, "Mechanical Characterization of Skin-Finite Deformations," J Biomech, **3**(1), pp. 111-124.

[51] Ateshian, G. A., 2007, "Anisotropy of Fibrous Tissues in Relation to the Distribution of Tensed and Buckled Fibers," J Biomech Eng, **129**(2), pp. 240-249.

[52] Ateshian, G. A., Rajan, V., Chahine, N. O., Canal, C. E., and Hung, C. T., 2009, "Modeling the Matrix of Articular Cartilage Using a Continuous Fiber Angular Distribution Predicts Many Observed Phenomena," J Biomech Eng, **131**(6), p. 061003.

[53] Henak, C. R., Anderson, A. E., and Weiss, J. A., 2013, "Subject-Specific Analysis of Joint Contact Mechanics: Application to the Study of Osteoarthritis and Surgical Planning," J Biomech Eng, **135**(2), p. 021003.

[54] Dalstra, M., and Huiskes, R., 1995, "Load Transfer Across the Pelvic Bone," J Biomech, **28**(6), pp. 715-724.

[55] Athanasiou, K. A., Agarwal, A., and Dzida, F. J., 1994, "Comparative Study of the Intrinsic Mechanical Properties of the Human Acetabular and Femoral Head Cartilage," J Orthop Res, **12**(3), pp. 340-349.

[56] Athanasiou, K. A., Agarwal, A., Muffoletto, A., Dzida, F. J., Constantinides, G., and Clem, M., 1995, "Biomechanical Properties of Hip Cartilage in Experimental Animal Models," Clin Orthop Relat Res (316), pp. 254-266.

[57] Bullough, p., Goodfellow, J., and O'Conner, J., 1973, "The Relationship between Degenerative Changes and Load-Bearing in the Human Hip," J Bone Joint Surg Br, **55**(4), p. 746.

[58] Harrison, M., Schajowicz, F., and Trueta, J., 1953, "Osteoarthritis of the Hip: A Study of the Nature and Evolution of the Disease," J Bone Joint Surg Br, **35**(4), pp. 598-626.

[59] Byers, P. D., Contepomi, C. A., and Farkas, T. A., 1970, "A Post Mortem Study of the Hip Joint Including the Prevalence of the Features of the Right Side," Ann Rheum Dis, **29**(1), pp. 15-31.

[60] Byers, p. D., Contepomi, C. A., and Farkas, T. A., 1976, "Postmortem Study of the Hip Joint. II. Histological Basis for Limited and Progressive Cartilage Alterations," Ann Rheum Dis, **35**(2), pp. 114-121.

[61] Gu, K. B., and Li, L. p., 2011, "A Human Knee Joint Model Considering Fluid Pressure and Fiber Orientation in Cartilages and Menisci," Med Eng Phys, **33**(4), pp. 497-503.

[62] Halonen, K. S., Mononen, M. E., Jurvelin, J. S., Toyras, J., and Korhonen, R. K., 2013, "Importance of Depth-Wise Distribution of Collagen and Proteoglycans in Articular Cartilage--a Three-Dimensional Finite Element Study of Stresses and Strains in Human Knee Joint," J Biomech, **46**(6), pp. 1184-1192.

[63] Mononen, M. E., Mikkola, M. T., Julkunen, p., Ojala, R., Nieminen, M. T., Jurvelin, J. S., and Korhonen, R. K., 2012, "Effect of Superficial Collagen Patterns and Fibrillation of Femoral Articular Cartilage on Knee Joint Mechanics-A Three-Dimensional Finite Element Analysis," J Biomech, **45**(3), pp. 579-587.

[64] Rasanen, L. p., Mononen, M. E., Nieminen, M. T., Lammentausta, E., Jurvelin, J. S., and Korhonen, R. K., 2013, "Implementation of Subject-Specific Collagen Architecture of Cartilage into a 2D Computational Model of A Knee Joint--Data From the Osteoarthritis Initiative (OAI)," J Orthop Res, **31**(1), pp. 10-22.

[65] Shirazi, R., Shirazi-Adl, A., and Hurtig, M., 2008, "Role of Cartilage Collagen Fibrils Networks in Knee Joint Biomechanics Under Compression," J Biomech, **41**(16), pp. 3340-3348.

[66] Garcia, J. J., Altiero, N. J., and Haut, R. C., 1998, "An Approach for the Stress Analysis of Transversely Isotropic Biphasic Cartilage Under Impact Load," J Biomech Eng, **120**(5), pp. 608-613.

[67] Wilson, W., Van Rietbergen, B., Van Donkelaar, C. C., and Huiskes, R., 2003, "Pathways of Load-Induced Cartilage Damage Causing Cartilage Degeneration in the Knee After Meniscectomy," J Biomech, **36**(6), pp. 845-851.

[68] Krishnan, R., Kopacz, M., and Ateshian, G. A., 2004, "Experimental Verification of the Role of Interstitial Fluid Pressurization in Cartilage Lubrication," J Orthop Res, **22**(3), pp. 565-570.

[69] Abraham, C. L., Maas, S. A., Weiss, J. A., Ellis, B. J., Peters, C. L., and Anderson, A. E., 2013, "A New Discrete Element Analysis Method for Predicting Hip Joint Contact Stresses," J Biomech, **46**(6), pp. 1121-1127.

[70] Guterl, C. C., Gardner, T. R., Rajan, V., Ahmad, C. S., Hung, C. T., and Ateshian, G. A., 2009, "Two-Dimensionalal Strain Fields on the Cross-section of the Human Patellofemoral Joint Under Physiological Loading," J Biomech, **42**(9), pp. 1275-1281.

[71] Krishnan, R., Park, S., Eckstein, F., and Ateshian, G. A., 2003, "Inhomogeneous Cartilage Properties Enhance Superficial Interstitial Fluid Support and Frictional Properties, but do not Provide a Homogeneous State of Stress," J Biomech Eng, **125**(5), pp. 569-577.

[72] Li, J., Stewart, T. D., Jin, Z., Fisher, J., and Wilcox, R. K., 2013, "Application of Biphasic Cartilage to a Three-Dimensional Natural Hip Under Static and Dynamic Loads," Preceeding of the 2013 Computer Methods in Biomechanics and Biomedical Engineering 11.

[73] Miozzari, H. H., Clark, J. M., Jacob, H. A., Von Rechenberg, B., and Notzli, H. p., 2004, "Effects of Removal of the Acetabular Labrum in a Sheep Hip Model," Osteoarthritis Cartilage, **12**(5), pp. 419-430.

[74] Konrath, G. A., Hamel, A. J., Olson, S. A., Bay, B., and Sharkey, N. A., 1998, "The Role of the Acetabular Labrum and the Transverse Acetabular Ligament in Load Transmission in the Hip," J Bone Joint Surg Am, **80**(12), pp. 1781-1788.

[75] Ferguson, S. J., Bryant, J. T., and Ito, K., 2001, "The Material Properties of the Bovine Acetabular Labrum," J Orthop Res, **19**(5), pp. 887-896.

[76] Ishiko, T., Naito, M., and Moriyama, S., 2005, "Tensile Properties of the Human Acetabular Labrum-the First Report," J Orthop Res, **23**(6), pp. 1448-1453.

[77] Smith, C. D., Masouros, S., Hill, A. M., Amis, A. A., and Bull, A. M., 2009, "A Biomechanical Basis for Tears of the Human Acetabular Labrum," Br J Sports Med, **43**(8), pp. 574-578.

CHAPTER 8

DISCUSSION

Summary

The overall objectives of this dissertation were to assess model validation and the effects of modeling assumptions on subject-specific predictions of cartilage mechanics in the human hip, and to use the insights from validation and parameter studies to quantify the mechanics in two patient populations at risk for the development of osteoarthritis (OA). This research focused on contact mechanics, but also provides the technical background for predicting other mechanical variables in the human hip. Additionally, this dissertation provides data regarding the regional, nearly-incompressible, hyperelastic behavior of healthy human hip cartilage, which provides insight into cartilage behavior and can be used in finite element (FE) models. Direct validation of a series of specimen-specific FE models demonstrated good agreement between experimental and computational contact stress and contact area, as well as relative insensitivity of FE predictions of contact mechanics to the assumed cartilage constitutive model. The effects of modeling assumptions of the acetabular labrum were assessed in a normal and a dysplastic hip. The insights from these validation and parameter studies informed the prediction of contact mechanics in two populations with hip pathomorphology. Subject-specific FE models of hips with acetabular dysplasia and hips with acetabular

retroversion were generated for comparison against subject-specific FE models of hips with normal anatomy. The final study of this dissertation evaluated the effects of cartilage constitutive model assumptions on transchondral predictions of maximum shear stress (τ_{max}) and first principal strain (E_1) as a first step in evaluating mechanical variables aside from just contact mechanics that may be relevant to the pathogenesis of OA. The major findings of this dissertation include:

- Specimen-specific FE predictions of contact stress and contact area agreed with experimental results well. Further, specimen-specific predictions of cartilage contact area and contact stress were relatively insensitive to the assumed cartilage constitutive model. Material nonlinearity improved predictions of peak contact stress over nearly-linear material behavior, but had no discernible effect on average contact stress or contact area. There were no differences in peak contact stress, average contact stress or contact area between FE models with average material coefficients and those with region- and specimen-specific material coefficients. This study provides confidence in the use of average material coefficients for subject-specific FE predictions of cartilage contact stress and contact area.
- The material behavior of regional human hip cartilage was characterized. These data provide valuable inputs for ongoing research evaluating the effects of regional variations in behavior on FE predictions.
- Predictions of the load supported by the acetabular labrum in the normal and dysplastic hip are sensitive to the assumed labrum constitutive model and the location of the chondrolabral junction. These findings inform the use of a

conservative chondrolabral boundary and structurally-based labral constitutive model for FE modeling of the human hip with the acetabular labrum.

- The acetabular labrum in the dysplastic hip supports significantly more load than the acetabular labrum in the normal hip during activities of daily living.
- Hips with acetabular retroversion exhibit a distinct superomedial contact pattern in comparison to hips with normal bony morphology.
- FE predictions of transchondral τ_{max} and E_1 in the human hip were relatively sensitive to the assumed cartilage constitutive model. In particular, capturing the tension-compression nonlinear behavior of articular cartilage resulted in the largest peak values of τ_{max} and the smallest peak values of E_1. These results provide insight that can be used in future modeling studies to predict values of τ_{max} and E_1 in pathomorphologic populations.

The link between pathomorphology and OA, which affects approximately 10% of the population, is thought to be mechanical [1, 2]. However, the differences in mechanics between normal and pathomorphologic hips have not been fully established. Because mechanics cannot be measured directly in patients with hip pathomorphology, FE modeling can be used to predict them. Previous FE modeling of the human hip has provided many valuable insights [3-11]. On the technical side, a previous study completed direct validation and parameter studies for a single cadaveric specimen [3]. In this study, the insensitivity of predictions of contact stress and contact area to variations in the neo-Hookean hyperelastic cartilage material coefficients and the importance of representing cortical bone as a deformable shell were demonstrated [3]. Parameter studies have also indicated the importance of subject-specific geometry and the

inaccuracy of idealized geometry for predictions of hip joint cartilage mechanics [4, 12]. FE analysis has been used in a limited manner to evaluate the mechanics of the normal and pathomorphologic hip. Analysis on a population of hips with normal anatomy demonstrated the intersubject variation in contact patterns, even within a population of normal hips [8]. Subject-specific analysis on a population of dysplastic subjects who underwent correction at infancy demonstrated differences in contact pressure overload in hips with residual dysplasia in comparison to a normal hip [10]. FE analysis with idealized geometry was used to evaluate the effects of simulated pathomorphology ranging from an overcovered acetabular socket (impingement) to an undercovered acetabular socket (dysplasia). Distinct contact patterns were found, which depending on the gross pathomorphology [6]. For example, the idealized dysplastic hip had elevated stresses near the lateral acetabular rim [6].

Although these previous studies have provided many valuable insights relevant to the pathogenesis of hip OA, there are limitations from the previous research that this dissertation aimed to address. In particular, these previous studies were limited by single-specimen validation, linear elastic or nearly-linear hyperelastic cartilage constitutive behavior, the omission of the acetabular labrum from subject-specific analyses and a focus on contact mechanics.

Completing direct validation on a series of specimens allows the effects of modeling assumptions to be assessed statistically. Therefore, direct validation of contact stress and contact area was completed on a series of five cadaveric specimens (Chapter 3). This study provided novel insight regarding the sensitivity of model predictions to variations in the assumed cartilage constitutive model, as well as to average versus

region- and specimen-specific cartilage constitutive model coefficients. These results provide insight into the effects of modeling assumptions on predictions of contact mechanics, which is consistent with a previous validation study that demonstrated insensitivity in model predictions to variations in the nearly-linear hyperelastic material coefficients [3]. Complementary to the direct validation presented in Chapter 3, parameter studies in Chapter 4 suggested an appropriate modeling approach for including the acetabular labrum into subject-specific FE models.

The material behavior of articular cartilage in the human hip is not well characterized. Studies suggest that data from other joints or other species is may not provide an accurate representation of the material behavior of human hip cartilage [13]. Therefore, the study presented in Chapter 3 provided regional quantification of healthy human hip cartilage behavior under the physiologic loading rates associated with activities of daily living. These data provide novel insights into the nearly instantaneous behavior of human hip cartilage, including the discrepancy in stiffness between the medial and lateral cartilage, as well as between acetabular and femoral cartilage. These data can also be used in ongoing research as inputs to FE models.

Building from the research in Chapters 3 and 4, Chapters 5 and 6 presented FE predictions of joint contact mechanics in two pathomorphologic groups. Acetabular dysplasia accounts for an estimated 20% of all hip OA [14]. While dysplasia is a known risk factor for OA, the specific mechanical links between the two are unclear. To evaluate the mechanics in the dysplastic hip, FE models of ten subjects with acetabular dysplasia were compared to FE models of ten subjects with normal hip morphology. This study demonstrated that the acetabular labrum is an important load-bearing structure

in the dysplastic hip. These findings were consistent with clinical observations of labral hypertrophy in the dysplastic hip [16-18] but they provide a novel contribution in the quantification of the differences in labral mechanics between normal and dysplastic hips. Acetabular retroversion is not as well understood as acetabular dysplasia, having only been described in the native hip in the last 15 years [19]. However, there is strong evidence that acetabular retroversion causes OA [20-22]. This may be through one of two mechanisms: decreased posterior coverage leading to elevated posterior stresses or anterior impingement leading to the countercoup lesion [23-26]. In Chapter 6, the first possible mechanism of damage was evaluated in a series of ten hips with acetabular retroversion. This study demonstrated distinct superomedial contact patterns in the retroverted hip in comparison to the normal hip. However, the retroverted hips did not have elevated posterior stresses, suggesting that the first mechanism of damage is not the case in this patient population, or that contact stress may not be an accurate predictor of the location of damage in OA in the hip. Because acetabular retroversion is not well understood, the insight provided by this study may be important for the clinical treatment of retroverted hips.

Although contact stress has a long history of use in predicting the pathogenesis of OA, there may be other mechanical variables that are more relevant to cartilage damage [27]. Therefore, Chapter 7 presented research that shifts away from predictions of contact stress and contact area alone. In particular, the required mesh resolution and constitutive models to accurately predict transchondral τ_{max} and E_1 were evaluated. This research provides the groundwork for ongoing studies to evaluate the mechanics in pathomorphologic hips.

In conclusion, the research presented in this dissertation elucidated the technical requirements necessary for accurately predicting cartilage mechanics in the human hip, and applied the results to provide insight into the pathogenesis of hip OA in patient populations. These studies provide technical background for ongoing research into the pathogenesis of hip OA. Additionally, these studies provide quantitative insight into the mechanical role of the labrum in the dysplastic hip and the superomedial contact pattern in the retroverted hip.

Limitations

Although the research presented in this dissertation provides advances in FE modeling of the human hip and insights into patient populations, there are limitations that merit discussion. There are two broad categories of limitations in this dissertation: FE models necessarily involve assumptions related to discretization, physics and model inputs, and there are risks and limitations inherent to generating subject-specific models of live subjects.

Constitutive assumptions associated with the representation of articular cartilage and labrum are an important limitation to consider. Cartilage material behavior is complex, including rate- and time-dependent behavior, spatial variation in material coefficients, material nonlinearity and tension-compression nonlinearity [28-31]. For the research presented in this dissertation, cartilage material behavior was assumed to be nearly-incompressible hyperelastic and material coefficients were averaged through the depth of the cartilage. The assumption of near-incompressibility is justified for the loading rates that were simulated [32, 33]. However, the effects of transchondral variations in elastic behavior and fiber distribution were not assessed, although these

effects could also influence FE model predictions [34]. In addition to the cartilage constitutive model, the assumed labrum constitutive model may affect FE predictions. The behavior of healthy human acetabular labrum has not been fully characterized [35, 36]. Therefore, the constitutive assumptions in Chapters 4 and 5 were based on qualitative structural descriptions and bovine labrum behavior [37, 38]. Uncertainty in labrum material coefficients was evaluated in Chapter 4. However, the assumptions of the labrum constitutive behavior remain a limitation of the research presented in this dissertation.

Similarly, the kinematics and kinetics used for this dissertation were identical for all subjects. There is evidence that patients with pathomorphology exhibit different kinematics and kinetics than patients with normal hip anatomy, on average [39, 40]. Further, using subject-specific kinematics and kinetics may be the most appropriate method of evaluating hip soft tissue mechanics on a subject-specific basis. While these methods should be considered in future studies, the use of identical kinematics for all subjects in the present studies provides the advantage of eliminating one set of variables that could influence the results. Specifically, the use of identical kinematics and kinetics means that the differences in model results were due to the bony morphology of the joints.

The selected FE model outputs represent only a small subset of the mechanical variables that may be relevant to the pathogenesis of OA. Contact stress and area have a long history of use in the biomechanics community as variables that are relevant to OA [10, 41-44]. However, other mechanical variables may be more important [27]. In this dissertation, two alternative variables were evaluated, τ_{max} and E_J. Whether the variables

that were evaluated are the most relevant to the pathogenesis of OA has yet to be determined conclusively, but FE analysis could theoretically be used to predict any mechanical variable at any location in the continuum. Therefore, the limited number of mechanical variables evaluated in this dissertation represents a limitation of this research.

In addition to the relatively limited set of mechanical variables that were examined, τ_{max} and E_1 could not be measured directly in the experiments for validation. Contact stress and contact area were directly validated in specimen-specific models. Therefore, predictions of these variables in those models can be made with the greatest confidence. However, one of the roles of computational modeling is to predict mechanics that cannot be directly measured. This dissertation used this role of computational modeling in two ways. First, contact stress and contact area were predicted in live subjects, where direct validation was not an option because of the inability to directly measure contact mechanics in vivo. In this case, confidence in model predictions arose from the direct validation completed on specimen-specific models for the same outputs. Second, τ_{max} and E_1 were predicted in specimen-specific models. In this case, the magnitudes of E_1 were indirectly validated by comparison against experimental measurements made in the human patellofemoral joint [45]. However, direct validation with one-to-one comparisons of experimental measurements of E_1 in the human hip would have provided more rigorous validation for predictions of this variable. Unlike E_1, τ_{max} cannot be measured. Therefore, confidence in predictions of τ_{max} was created by the combination of validation for contact mechanics and parameter studies.

The second set of limitations involves modeling live subjects. The model geometry for Chapters 3, 4 and 5 came from CT arthrogram data. CT imaging has

ionizing radiation, which presents certain risks to the subjects [42]. Alternative approaches that reduce or eliminate the need for the exposure to ionizing radiation are needed for application of the patient-specific modeling pipeline to other populations such as children, or for the repeated imaging and modeling of individual subjects. Additionally, it is difficult to obtain subject-specific inputs for FE modeling, such as subject-specific cartilage and labrum material properties. While imaging sequences are emerging for the evaluation of subject-specific material properties, ongoing research is required for the accurate in vivo estimation of soft tissue properties [42].

Future Work and Preliminary Studies

This dissertation focused on specific aspects of cartilage and labrum mechanics in normal and pathomorphologic hips that are relevant to the pathogenesis of OA. Hips with acetabular dysplasia and acetabular retroversion exhibited different contact patterns than hips with normal bony morphology, as well as some statistically significant differences in contact stress, contact area and load supported by the labrum. However, it is unclear whether the statistically significant differences reflect clinically significant differences. Further, there may be differences in other aspects of articular soft tissue mechanics between pathomorphologic and normal hips that were not evaluated as part of this dissertation. Additionally, many of the limitations discussed above result from the limited availability of data in the literature. There is a clear need for additional experimental studies to better characterize the material behavior of soft tissues of the human hip, and to determine the mechanical thresholds or damage for articular cartilage and labrum.

FE Model Outputs

A logical extension of this research would be to apply the methods presented in Chapter 7 to the patient populations evaluated in Chapters 5 and 6. Some of this research will be fairly straightforward, although time consuming. For example, increasing the mesh resolution from three elements through the cartilage to five elements through the cartilage in the models in Chapter 6 should only be a matter of updating TrueGrid input files and repositioning models. Conversely, the complex structure of the acetabular labrum will make increasing the mesh density in models that include the acetabular labrum more challenging. As a preliminary study, one of the normal subject models with the acetabular labrum was remeshed with five elements through the acetabular cartilage thickness and evaluated in the neutral model position (Figure 8.1). Analysis of this model in NIKE3D took approximately 5 days with neo-Hookean cartilage and transversely isotropic hyperelastic labrum. This preliminary study demonstrates the feasibility of meshing the acetabular labrum with increased mesh density.

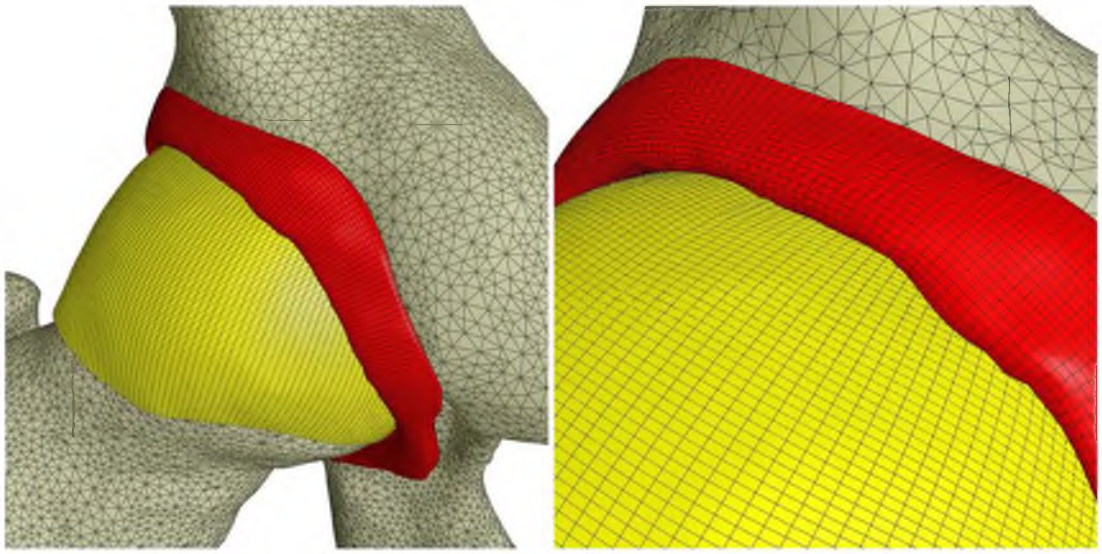

Figure 8.1: Model of a normal subject with increased mesh density. Left – view of the whole joint with the bones in white, the acetabular labrum in red and the femoral cartilage in yellow. Right – close-up view of the mesh.

FE Model Assumptions

In addition to the FE model outputs, there remain many FE model assumptions that could be probed further. Of particular relevance to predictions of cartilage and labrum mechanics are the assumed cartilage and labrum constitutive models. For example, the effects of transchondral variation or biphasic behavior on transchondral predictions of τ_{max} and E_1 could be evaluated. Because of the increasing complexity, and thus the need for increasing mesh density, there is a place for idealized models in the evaluation of some of these modeling assumptions [42]. As a preliminary study to further address the effects of cartilage constitutive model on predictions of transchondral mechanics, four plane strain models were analyzed (Figure 8.2). The model geometry was a cylinder contacting a plane (outer radius = 22 mm, thickness = 2 mm). The three constitutive models characterized in Chapter 7 were used: neo-Hookean, Veronda Westmann and ellipsoidal fiber distribution with neo-Hookean matrix, all with properties averaged through the cartilage thickness. An additional FE model was built with transchondral variation in neo-Hookean behavior based on data from the literature [46]. These models provide a first look at the potential qualitative effects of transchondral variations in cartilage constitutive behavior on predictions of transchondral mechanics. Specifically, all constitutive models predicted peaks in E_1 below the articular surface, which suggests that transchondral variation in material properties does not affect this finding of transchondral mechanics. However, the model with depth-variant properties did not predict the large E_1 at the deep surface that was predicted in models with depth-averaged properties. This suggests that future work should incorporate depth-variant properties for predictions of E_1 near the osteochondral interface.

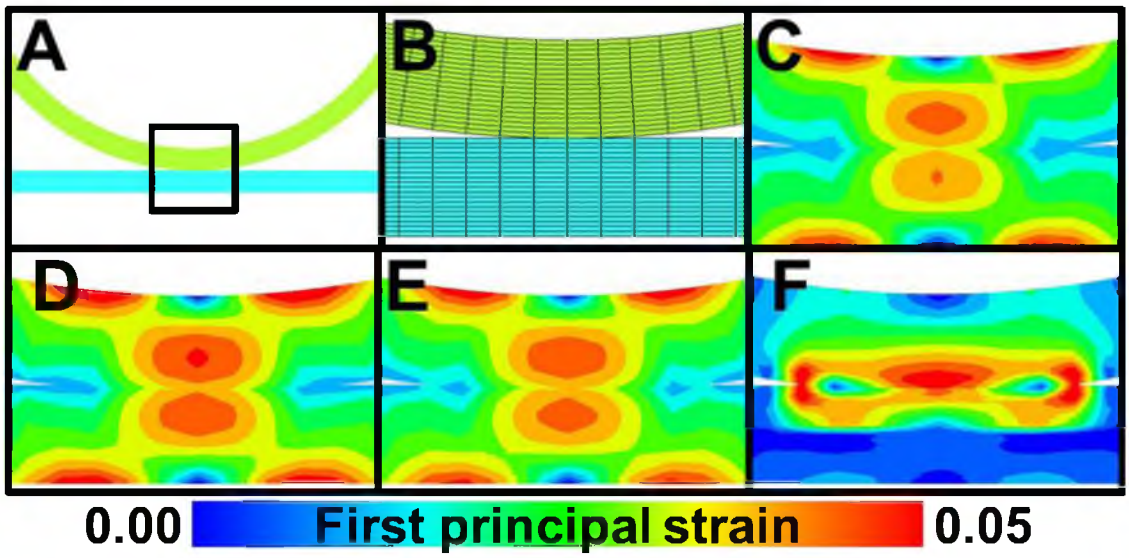

Figure 8.2: Plane strain models showing the effects of constitutive model on predicted transchondral E_1. A – view of a cylinder (outer radius 22 mm) contacting a plane. Both layers were 2 mm thick. The black box indicates the zoomed in view in the remainder of the panels. B – discretization of the plane strain models. C – neo-Hookean model with depth-averaged properties. D – Veronda Westmann model with depth-averaged properties. E – EFD model with depth-averaged properties. F – neo-Hookean model with depth-variant properties. All constitutive assumptions resulted in peak E_1 just below the contacting surface. However, the model with depth-variant properties did not exhibit the high values of E_1 at the deep surface that were seen in the models with depth-averaged properties.

Labrum Structure and Function

The structure of the labrum has been described qualitatively using microscopy and gross dissection [38, 47, 48]. However, quantitative measurements of the fiber orientation, which would be used as inputs to FE models, have not been completed. As a preliminary study, human labrum was evaluated using two-photon confocal imaging with second-harmonic generation in order to visualize collagen (Figure 8.3). Labrum was fixed overnight in paraformaldehyde. Serial 100 μm thick sections were obtained using a cryostat. Sections were oriented either parallel or perpendicular to the acetabular rim. Following sectioning, slices were places on slides in PBS, covered with a coverslip and sealed. Imaging was completed on an Olympus FV1000, with a 25× objective. Collagen

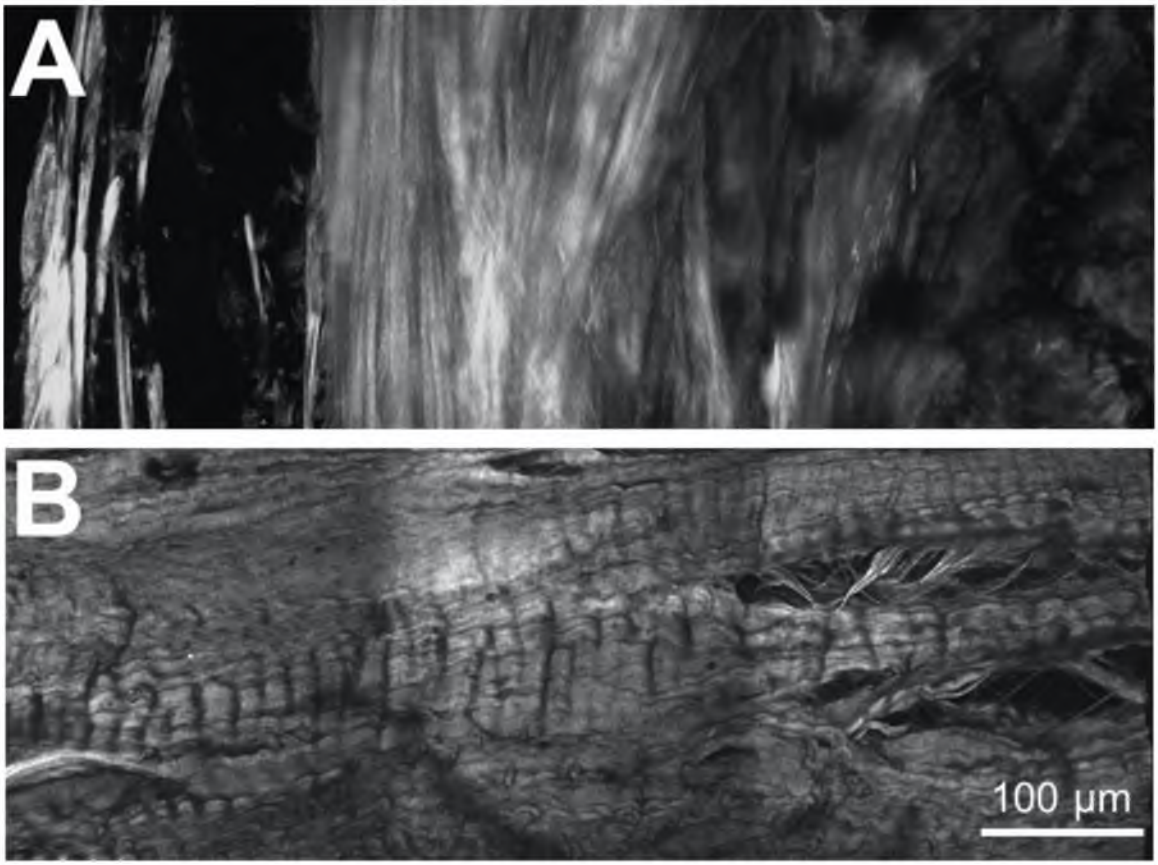

Figure 8.3: Confocal imaging of human labrum. A – stack of images perpendicular to the acetabular rim. The articular surface is at the left of the image and the bone is at the right. These images indicate an aligned region below the articular surface, which transitions to a more oblique orientation closer to the bone. B – stack of images parallel to the acetabular rim. These images demonstrate the aligned fibers in the midsubstance of the labrum.

was imaged using second-harmonic generation with an 860 nm excitation and both 420-460 nm and 570 nm filters. Building off of this image data, quantitative fiber orientation could be obtained via methods developed in the Musculoskeletal Research Laboratories [49].

The material behavior of the human acetabular labrum is also largely unknown. The mechanical behavior of the human acetabular labrum has been the subject of two studies. In one study, samples were removed from patients undergoing hip surgery and tested in tension [35]. In another study, cadaveric samples were tested in both tension

and compression [36]. Neither of these studies provide complete characterization of the normal acetabular labrum under loading rates relevant to activities of daily living. Further, additional test configurations may be needed to fully characterize the behavior of the labrum. In order to provide the inputs for FE models that evaluate hip mechanics under relatively fast loading, the nearly-incompressible behavior of the human labrum should be evaluated. Given the orientated nature of the labrum, this would likely require a minimum of two configurations tested in uniaxial tension plus a compression test. In order to fully evaluate the mechanical behavior of the labrum, the rate-dependent behavior should also be quantified. Finally, the changes in labral behavior through the disease process need to be evaluated. For example, the acetabular labrum is often hypertrophied in dysplastic hip. This is likely to alter the mechanical behavior. However, how the behavior is altered under these conditions is completely unknown.

Cartilage Material Behavior

Cartilage behavior in general has been evaluated extensively (reviewed in [50]). However, the material behavior differs between joints and species [13, 51-54] and the behavior of cartilage in the human hip is largely unknown. Therefore, future work should continue to build on our understanding of human hip cartilage, which can then be used to increase the accuracy of FE model predictions. In the nearly-incompressible hyperelastic domain, transchondral variation in properties should be determined. For a full understanding of the material behavior of human hip cartilage, rate-dependent behavior should also be evaluated.

Mechanical Thresholds of Damage

While the studies presented in Chapters 5 and 6 demonstrated statistical significance between normal and pathomorphologic hips, it is unclear whether statistical differences indicates clinical significance. In vitro studies on cartilage explants have demonstrated that the response of cartilage to loading is dose-dependent, however, there is no clear threshold for doses that are chondroprotective versus those that cause damage [55-58]. The types of tissue, specific loading regimes and methods used to evaluate changes in cartilage metabolism can affect the levels at which damage is observed. For example, dynamic compression has been evaluated in mouse cartilage in vivo, in immature bovine cartilage in vitro and in adult bovine cartilage in vitro [59-62]. In the mouse, physical damage to the cartilage matrix was induced at loads $\geq$ 4.5 N across the entire joint [60]. In immature bovine cartilage, a chondroprotective upregulation of protein and proteoglycans synthesis was seen at frequencies $\geq$ 0.01 Hz and strains of 1-5%, but no damage was induced at the strain levels evaluated [59, 62]. In adult bovine cartilage, a chondroprotective response was seen at frequencies $\geq$ 0.25 Hz and stresses of 0.5 – 1.0 MPa, but no damage was induced [61]. While these studies suggest that there are certain thresholds that cause a chondroprotective response and certain thresholds that cause damage, the studies are not directly comparable. This makes it is unclear whether the thresholds of damage are consistent across species and joints. In addition, it is possible that damage in the human hip is initiated in the labrum or at the chondrolabral junction, which suggests the need for evaluating thresholds of damage to the acetabular labrum. Therefore, studies of the damage thresholds for cartilage and labrum in the hip are needed to improve the use of FE modeling in predicting the pathogenesis of hip OA.

References

[1] Gosvig, K. K., Jacobsen, S., Sonne-Holm, S., Palm, H., and Troelsen, A., 2010, "Prevalence of Malformations of the Hip Joint and their Relationship to Sex, Groin Pain, and Risk of Osteoarthritis: A Population-Based Survey," J Bone Joint Surg Am, **92**(5), pp. 1162-1169.

[2] Harris-Hayes, M., and Royer, N. K., 2011, "Relationship of Acetabular Dysplasia and Femoroacetabular Impingement to Hip Osteoarthritis: A Focused Review," PM R, **3**(11), pp. 1055-1067 E1051.

[3] Anderson, A. E., Ellis, B. J., Maas, S. A., Peters, C. L., and Weiss, J. A., 2008, "Validation of Finite Element Predictions of Cartilage Contact Pressure in the Human Hip Joint," J Biomech Eng, **130**(5), pp. 051008-051008.

[4] Anderson, A. E., Ellis, B. J., Maas, S. A., and Weiss, J. A., 2010, "Effects of Idealized Joint Geometry on Finite Element Predictions of Cartilage Contact Stresses in the Hip," J Biomech, **43**(7), pp. 1351-1357.

[5] Brown, T. D., and DiGioia, A. M., 3rd, 1984, "A Contact-Coupled Finite Element Analysis of the Natural Adult Hip," J Biomech, **17**(6), pp. 437-448.

[6] Chegini, S., Beck, M., and Ferguson, S. J., 2009, "The Effects of Impingement and Dysplasia on Stress Distributions in the Hip Joint During Sitting and Walking: A Finite Element Analysis," J Orthop Res, **27**(2), pp. 195-201.

[7] Gu, D. Y., Hu, F., Wei, J. H., Dai, K. R., and Chen, Y. Z., 2011, "Contributions of Non-Spherical Hip Joint Cartilage Surface to Hip Joint Contact Stress," Conf Proc IEEE Eng Med Biol Soc, 2011, pp. 8166-8169.

[8] Harris, M. D., Anderson, A. E., Henak, C. R., Ellis, B. J., Peters, C. L., and Weiss, J. A., 2012, "Finite Element Prediction of Cartilage Contact Stresses in Normal Human Hips," J Orthop Res, **30**(7), pp. 1133-1139.

[9] Rapperport, D. J., Carter, D. R., and Schurman, D. J., 1985, "Contact Finite Element Stress Analysis of the Hip Joint," J Orthop Res, **3**(4), pp. 435-446.

[10] Russell, M. E., Shivanna, K. H., Grosland, N. M., and Pedersen, D. R., 2006, "Cartilage Contact Pressure Elevations in Dysplastic Hips: A Chronic Overload Model," J Orthop Surg Res, **1**, pp. 6-6.

[11] Wei, H. W., Sun, S. S., Jao, S. H., Yeh, C. R., and Cheng, C. K., 2005, "The Influence of Mechanical Properties of Subchondral Plate, Femoral Head and Neck on Dynamic Stress Distribution of the Articular Cartilage," Med Eng Phys, **27**(4), pp. 295-304.

[12] Gu, D. Y., Dai, K. R., Hu, F., and Chen, Y. Z., 2010, "The Shape of the Acetabular Cartilage Surface and Its Role in Hip Joint Contact Stress," Conf Proc IEEE Eng Med Biol Soc, 2010, pp. 3934-3937.

[13] Athanasiou, K. A., Agarwal, A., Muffoletto, A., Dzida, F. J., Constantinides, G., and Clem, M., 1995, "Biomechanical Properties of Hip Cartilage in Experimental Animal Models," Clin Orthop Relat Res (316), pp. 254-266.

[14] Solomon, L., 1976, "Patterns of Osteoarthritis of the Hip," J Bone Joint Surg Br, **58**(2), pp. 176-183.

[15] Klaue, K., Durnin, C. W., and Ganz, R., 1991, "The Acetabular Rim Syndrome. A Clinical Presentation of Dysplasia of the Hip," J Bone Joint Surg Br, **73**(3), pp. 423-429.

[16] Leunig, M., Podeszwa, D., Beck, M., Werlen, S., and Ganz, R., 2004, "Magnetic Resonance Arthrography of Labral Disorders in Hips with Dysplasia and Impingement," Clin Orthop Relat Res (418), pp. 74-80.

[17] Leunig, M., Werlen, S., Ungersbock, A., Ito, K., and Ganz, R., 1997, "Evaluation of the Acetabular Labrum By MR Arthrography," J Bone Joint Surg Br, **79**(2), pp. 230-234.

[18] Reynolds, D., Lucas, J., and Klaue, K., 1999, "Retroversion of the Acetabulum. A Cause of Hip Pain," J Bone Joint Surg Br, **81**(2), pp. 281-288.

[19] Ezoe, M., Naito, M., and inoue, T., 2006, "The Prevalence of Acetabular Retroversion Among Various Disorders of the Hip," J Bone Joint Surg Am, **88**(2), pp. 372-379.

[20] Giori, N. J., and Trousdale, R. T., 2003, "Acetabular Retroversion is Associated with Osteoarthritis of the Hip," Clin Orthop Relat Res (417), pp. 263-269.

[21] Kim, W. Y., Hutchinson, C. E., andrew, J. G., and Allen, p. D., 2006, "The Relationship Between Acetabular Retroversion and Osteoarthritis of the Hip," J Bone Joint Surg Br, **88**(6), pp. 727-729.

[22] Peters, C. L., Anderson, L. A., Erickson, J. A., Anderson, A. E., and Weiss, J. A., 2011, "An Algorithmic Approach to Surgical Decision Making in Acetabular Retroversion," Orthopedics, **34**(1), p. 10.

[23] Siebenrock, K. A., Schoeniger, R., and Ganz, R., 2003, "Anterior Femoro-acetabular Impingement Due to Acetabular Retroversion. Treatment With Periacetabular Osteotomy," J Bone Joint Surg Am, **85-A**(2), pp. 278-286.

[24] Sierra, R. J., 2013, "The Management of Acetabular Retroversion With Reverse Periacetabular Osteotomy," Instr Course Lect, **62**, pp. 305-313.

[25] Tonnis, D., and Heinecke, A., 1999, "Acetabular and Femoral Anteversion: Relationship with Osteoarthritis of the Hip," J Bone Joint Surg Am, **81**(12), pp. 1747-1770.

[26] Brand, R. A., 2005, "Joint Contact Stress: A Reasonable Surrogate for Biological Processes?," Iowa Orthop J, **25**, pp. 82-94.

[27] Huang, C. Y., Soltz, M. A., Kopacz, M., Mow, V. C., and Ateshian, G. A., 2003, "Experimental Verification of the Roles of Intrinsic Matrix Viscoelasticity and Tension-Compression Nonlinearity in the Biphasic Response of Cartilage," J Biomech Eng, **125**(1), pp. 84-93.

[28] Huang, C. Y., Stankiewicz, A., Ateshian, G. A., and Mow, V. C., 2005, "Anisotropy, Inhomogeneity, and Tension-Compression Nonlinearity of Human Glenohumeral Cartilage in Finite Deformation," J Biomech, **38**(4), pp. 799-809.

[29] Mak, A. F., 1986, "The Apparent Viscoelastic Behavior of Articular Cartilage--The Contributions from the Intrinsic Matrix Viscoelasticity and Interstitial Fluid Flows," J Biomech Eng, **108**(2), pp. 123-130.

[30] Mow, V. C., Kuei, S. C., Lai, W. M., and Armstrong, C. G., 1980, "Biphasic Creep and Stress Relaxation of Articular Cartilage in Compression? Theory and Experiments," J Biomech Eng, **102**(1), pp. 73-84.

[31] Ateshian, G. A., Ellis, B. J., and Weiss, J. A., 2007, "Equivalence Between Short-Time Biphasic and Incompressible Elastic Material Responses," J Biomech Eng, **129**(3), pp. 405-412.

[32] Wong, M., Ponticiello, M., Kovanen, V., and Jurvelin, J. S., 2000, "Volumetric Changes of Articular Cartilage During Stress Relaxation in Unconfined Compression," J Biomech, **33**(9), pp. 1049-1054.

[33] Halonen, K. S., Mononen, M. E., Jurvelin, J. S., Toyras, J., and Korhonen, R. K., 2013, "Importance of Depth-Wise Distribution of Collagen and Proteoglycans in Articular Cartilage--a Three-Dimensional Finite Element Study of Stresses and Strains in Human Knee Joint," J Biomech, **46**(6), pp. 1184-1192.

[34] Ishiko, T., Naito, M., and Moriyama, S., 2005, "Tensile Properties of the Human Acetabular Labrum-the First Report," J Orthop Res, **23**(6), pp. 1448-1453.

[35] Smith, C. D., Masouros, S., Hill, A. M., Amis, A. A., and Bull, A. M. J., 2009, "A Biomechanical Basis for Tears of the Human Acetabular Labrum," Br J Sports Med, **43**(8), pp. 574-578.

[36] Ferguson, S. J., Bryant, J. T., and Ito, K., 2001, "The Material Properties of the Bovine Acetabular Labrum," J Orthop Res, **19**(5), pp. 887-896.

[37] Petersen, W., Petersen, F., and Tillmann, B., 2003, "Structure and Vascularization of the Acetabular Labrum with Regard to the Pathogenesis and Healing of Labral Lesions," Arch Orthop Trauma Surg, **123**(6), pp. 283-288.

[38] Endo, H., Mitani, S., Senda, M., Kawai, A., McCown, C., Umeda, M., Miyakawa, T., and inoue, H., 2003, "Three-Dimensional Gait Analysis of Adults with Hip Dysplasia After Rotational Acetabular Osteotomy," J Orthop Sci, **8**(6), pp. 762-771.

[39] Kennedy, M. J., Lamontagne, M., and Beaule, p. E., 2009, "Femoroacetabular Impingement Alters Hip and Pelvic Biomechanics During Gait Walking Biomechanics of FAI," Gait Posture, **30**(1), pp. 41-44.

[40] Creamer, p., and Hochberg, M. C., 1997, "Osteoarthritis," Lancet, **350**(9076), pp. 503-508.

[41] Henak, C. R., Anderson, A. E., and Weiss, J. A., 2013, "Subject-Specific Analysis of Joint Contact Mechanics: Application to the Study of Osteoarthritis and Surgical Planning," J Biomech Eng, **135**(2), p. 021003.

[42] Segal, N. A., Anderson, D. D., Iyer, K. S., Baker, J., Torner, J. C., Lynch, J. A., Felson, D. T., Lewis, C. E., and Brown, T. D., 2009, "Baseline Articular Contact Stress Levels Predict Incident Symptomatic Knee Osteoarthritis Development in the MOST Cohort," J Orthop Res, **27**(12), pp. 1562-1568.

[43] Segal, N. A., Kern, A. M., Anderson, D. D., Niu, J., Lynch, J., Guermazi, A., Torner, J. C., Brown, T. D., and Nevitt, M., 2012, "Elevated Tibiofemoral Articular Contact Stress Predicts Risk for Bone Marrow Lesions and Cartilage Damage At 30 Months," Osteoarthritis Cartilage, **20**(10), pp. 1120-1126.

[44] Guterl, C. C., Gardner, T. R., Rajan, V., Ahmad, C. S., Hung, C. T., and Ateshian, G. A., 2009, "Two-Dimensionalal Strain Fields on the Cross-Section of the Human Patellofemoral Joint Under Physiological Loading," J Biomech, **42**(9), pp. 1275-1281.

[45] Buckley, M. R., Bergou, A. J., Fouchard, J., Bonassar, L. J., and Cohen, I., 2010, "High-Resolution Spatial Mapping of Shear Properties in Cartilage," J Biomech, **43**(4), pp. 796-800.

[46] Seldes, R. M., Tan, V., Hunt, J., Katz, M., Winiarsky, R., and Fitzgerald, R. H., Jr., 2001, "Anatomy, Histologic Features, and Vascularity of the Adult Acetabular Labrum," Clin Orthop Relat Res (382), pp. 232-240.

[47] Won, Y. Y., Chung, I. H., Chung, N. S., and Song, K. H., 2003, "Morphological Study on the Acetabular Labrum," Yonsei Med J, **44**(5), pp. 855-862.

[48] Edgar, L. T., Sibole, S. C., Underwood, C. J., Guilkey, J. E., and Weiss, J. A., 2012, "A Computational Model of In Vitro Angiogenesis Based on Extracellular Matrix Fibre Orientation," Comput Methods Biomech Biomed Engin.

[49] Mow, V., Gu, W., and Chen, F., 2005, "Structure and Function of Articular Cartilage and Meniscus," *Basic Orthopaedic Biomechanics and Mechano-Biology*, V. Mow, and R. Huiskes, Eds., Lippincott, Philadephia, pp. 181-258.

[50] Athanasiou, K. A., Agarwal, A., and Dzida, F. J., 1994, "Comparative Study of the Intrinsic Mechanical Properties of the Human Acetabular and Femoral Head Cartilage," J Orthop Res, **12**(3), pp. 340-349.

[51] Demarteau, O., Pillet, L., inaebnit, A., Borens, O., and Quinn, T. M., 2006, "Biomechanical Characterization and In Vitro Mechanical Injury of Elderly Human Femoral Head Cartilage: Comparison to Adult Bovine Humeral Head Cartilage," Osteoarthritis Cartilage, **14**(6), pp. 589-596.

[52] Shepherd, D. E., and Seedhom, B. B., 1999, "The 'Instantaneous' Compressive Modulus of Human Articular Cartilage in Joints of the Lower Limb," Rheumatology (Oxford), **38**(2), pp. 124-132.

[53] Treppo, S., Koepp, H., Quan, E. C., Cole, A. A., Kuettner, K. E., and Grodzinsky, A. J., 2000, "Comparison of Biomechanical and Biochemical Properties of Cartilage From Human Knee and Ankle Pairs," J Orthop Res, **18**(5), pp. 739-748.

[54] Grodzinsky, A. J., Levenston, M. E., Jin, M., and Frank, E. H., 2000, "Cartilage Tissue Remodeling in Response to Mechanical Forces," Annu Rev Biomed Eng, **2**, pp. 691-713.

[55] Guilak, F., 2011, "Biomechanical Factors in Osteoarthritis," Best Pract Res Clin Rheumatol, **25**(6), pp. 815-823.

[56] Guilak, F., Fermor, B., Keefe, F. J., Kraus, V. B., Olson, S. A., Pisetsky, D. S., Setton, L. A., and Weinberg, J. B., 2004, "The Role of Biomechanics and Inflammation in Cartilage Injury and Repair," Clin Orthop Relat Res (423), pp. 17-26.

[57] Guilak, F., and Hung, C. T., 2005, "Physical Regulation of Cartilage Metabolism," *Basic Orthopaedic Biomechanics and Mechano-Biology*, V. C. Mow, and R. Huiskes, Eds., Lippincott Williams & Wilkins, Philadephia.

[58] Fitzgerald, J. B., Jin, M., and Grodzinsky, A. J., 2006, "Shear and Compression Differentially Regulate Clusters of Functionally Related Temporal Transcription Patterns in Cartilage Tissue," J Biol Chem, **281**(34), pp. 24095-24103.

[59] Ko, F. C., Dragomir, C., Plumb, D. A., Goldring, S. R., Wright, T. M., Goldring, M. B., and Van Der Meulen, M. C., 2013, "In Vivo Cyclic Compression Causes Cartilage Degeneration and Subchondral Bone Changes in Mouse Tibiae," Arthritis Rheum.

[60] Parkkinen, J. J., Lammi, M. J., Helminen, H. J., and Tammi, M., 1992, "Local Stimulation of Proteoglycan Synthesis in Articular Cartilage Explants By Dynamic Compression In Vitro," J Orthop Res, **10**(5), pp. 610-620.

[61] Sah, R. L., Kim, Y. J., Doong, J. Y., Grodzinsky, A. J., Plaas, A. H., and Sandy, J. D., 1989, "Biosynthetic Response of Cartilage Explants to Dynamic Compression," J Orthop Res, 7(5), pp. 619-636.